FROM BLUE TO RED:
EMISSION COLOUR TUNING IN IRIDIUM(III) COMPLEXES WITH SULFUR-FUNCTIONALIZED LIGANDS FOR LEECS

Inauguraldissertation

zur
Erlangung der Würde eines Doktors der Philosophie
vorgelegt der
Philosophisch-Naturwissenschaftlichen Fakultät
der Universität Basel

von
Cathrin Delphine Ertl

aus Dornbirn, Österreich

Basel, 2016

Genehmigt von der Philosophisch-Naturwissenschaftlichen Fakultät
auf Antrag von

Prof. Dr. Catherine Housecroft und Prof. Dr. Marcel Mayor

Basel, den 23.02.2016

Prof. Dr. Jörg Schibler
Dekan

Darkness cannot drive out darkness; only light can do that.
Hate cannot drive out hate; only love can do that.

Martin Luther King Jr. (1957)

Für meine Urli

TABLE OF CONTENTS

ABSTRACT

Light-emitting electrochemical cells (LEECs) are a promising class of solid state lighting devices. Their working mechanism is based on the presence of mobile ionic species within the device, making them independent of the work function of the electrodes and layer thickness. Compared to multilayer organic light emitting diodes (OLEDs), the architecture and assembly is much simpler, resulting in reduced manufacturing costs.

Cationic iridium(III) complexes of the type $[Ir(C\hat{}N)_2(N\hat{}N)]^+$, where C^N is a cyclometallating ligand (*e.g.* 2-phenylpyridine (ppy)) and N^N is an ancillary ligand (*e.g.* 2,2'-bipyridine (bpy)), have been extensively used in LEECs due to their excellent properties. High quantum yields and stability make them well suited for application in light emitting devices. Furthermore, the emission colour can be tuned easily, spanning the whole visible region. The frontier orbitals are spatially separated in this type of complex and by careful design of the ligands, desired blue- or red-shifts in the emission maximum are possible.

In this thesis, the synthesis, characterization and LEEC performance of iridium(III) complexes containing sulfur-functionalized ligands are described. Thioether- and sulfone-based cyclometallating ligands are introduced in Chapter I, resulting in complexes with yellow to green emission. In Chapter II, the influence on photophysical, electrochemical and device properties of iridium complexes with regioisomeric cyclometallating ligands containing a methylsulfonyl group is investigated. Based on the results of the previous chapters, the combination of sulfone-substituted cyclometallating ligands with electron-rich ancillary ligands to obtain blue emitting complexes is described in Chapter III. Chapter IV summarizes a series of iridium complexes with benzothiazole-based ancillary ligands, yielding red emitters with exceptionally long LEEC lifetimes. Ongoing work in the field of glycosylated iridium complexes is reported in Chapter V.

Parts of this work have been published:

E. C. Constable, C. D. Ertl, C. E. Housecroft and J. A. Zampese, "Green-emitting iridium(III) complexes containing sulfanyl- or sulfone-functionalized cyclometallating 2-phenylpyridine ligands", *Dalton Trans.* 2014, **43**, 5343–5356.

C. D. Ertl, J. Cerdá, J. M. Junquera-Hernández, A. Pertegás, H. J. Bolink, E. C. Constable, M. Neuburger, E. Ortí and C. E. Housecroft, "Colour tuning by the ring roundabout: $[Ir(C\hat{}N)_2(N\hat{}N)]^+$ emitters with sulfonyl-substituted cyclometallating ligands", *RSC Adv.* 2015, **5**, 42815–42827.

C. D. Ertl, L. Gil-Escrig, J. Cerdá, A. Pertegás, H. J. Bolink, J. M. Junquera-Hernández, A. Prescimone, M. Neuburger, E. C. Constable, E. Ortí and C. E. Housecroft, "Regioisomerism in cationic sulfonyl-substituted $[Ir(C\hat{}N)_2(N\hat{}N)]^+$ complexes: its influence on photophysical properties and LEC performance", *Dalton Trans.* **2016**, *45*, 11668–11681.

ACKNOWLEDGEMENTS

First of all, I want to thank Prof. Dr. Catherine Housecroft and Prof. Dr. Edwin Constable for providing me with the opportunity to conduct research on such an exciting and relevant topic. They have always supported me with their knowledge and guidance throughout those four years I have spent working on my PhD project. It was an excellent experience to be able to develop my own ideas on how to reach a certain goal.

Prof. Dr. Marcel Mayor is thanked greatly for agreeing to be the co-examiner of my thesis.

For proof-reading my thesis I thank Prof. Dr. Catherine Housecroft, Dr. Markus Willgert and Dr. Manuel Scherer.

Very special thanks go to Dr. Henk Bolink and his team at the University of Valencia, namely Dr. Antonio Pertegás and María Cristina Momblona-Rincón, for without their expertise in the field of light emitting electrochemical cells my project would not have been half as fruitful. Furthermore, I thank Prof. Dr. Enrique Ortí and his co-workers, especially José M. Junquera-Hernández and Jesús Cerdá, for their calculations. They have helped us to gain a deeper understanding of the properties and experimental observations of my complexes.

I thank PD Dr. Daniel Häußinger and Yann Baumgartner for variable temperature NMR measurements. In addition, PD Dr. Daniel Häußinger, Dr. Heiko Gsellinger and Kaspar Zimmermann are thanked for providing the department with such excellent NMR support. I want to thank Dr. Jennifer Zampese, Dr. Markus Neuburger and Dr. Alessandro Prescimone for measuring and solving the crystal structures.

Beatrice Erismann is thanked for help with every problem or question I had. Dr. Bernhard Jung is thanked for IT support and the good times we had in the first-year Praktikum lab. I thank Markus Hauri for making everything work within the department, Roy Lips for material supply and the “Werkstatt team” for help with everything that needed fixing.

Dr. Gabriel Schneider, Dr. Collin Morris and Frederik Malzner are thanked for measuring (LC-)ESI-MS samples. Thanks go to Dr. Steffen Müller and Dr. Srboljub Vujović for MALDI-TOF mass spectra. I thank Sylvie Mittelheisser for elemental analysis and Heinz Nadig for high resolution ESI mass spectrometry.

Big thanks go to all present and former group members of the Constable/Housecroft research group; I especially thank Dr. Sven Brauchli, Dr. Andreas Bünzli, Annika Büttner, Dr. Sebastian Fürer, Dr. Nik Hostettler, Max Klein, Frederik Malzner, Dr. Colin Martin, Dr. Collin Morris, Dr. Steffen Müller, Dr. Gabriel Schneider, Dr. Ewald Schönhofer, Dr. Jonas Schönle, Dr. Roché Walliser, Dr. Markus Willgert, Cedric Wobill and Dr. Iain Wright for the great times we spent in- and particularly outside of the lab. Thanks go to Felix Brunner, Emanuel Kohler, Tatjana Kosmalski and Daniel Ris for the work they have done during their Wahlpraktikum and Master thesis projects.

Very special thanks go to my family for always supporting me, for without them I would not have been able to come this far. Thank you, Mama, Wolfgang and Lucas, for always believing in me and wanting the best for me. My brother Lucas is also thanked for his help in the lab when visiting me. It was so enjoyable to be able to show him my work.

I am very grateful to Manuel for putting up with my impatience, grumpiness, tempers and nervous breakdowns during the past couple of months. Thank you so much for helping me through this stressful time.

ABBREVIATIONS

°	degree
°C	degree Celsius
2-MeTHF	2-methyltetrahydrofuran
A	Ampère
Å	Ångström
AIE	aggregation-induced emission
ATP	adenosine triphosphate
au	atomic units
a.u.	arbitrary units
avg.	average
bbtz	2,2'-bibenzo[*d*]thiazole
biq	2,2'-biquinoline
[Bmim][PF_6]	3-butyl-1-methylimidazolium hexafluoridophosphate
Bn	benzyl
bozpy	2-(pyridin-2-yl)benzo[*d*]oxazole
bpy	2,2'-bipyridine
br	broad
btl	1,1'-benzyl-4,4'-bi-1*H*-1,2,3-triazole
btzpy	2-(pyridin-2-yl)benzo[*d*]thiazole
btzpybtz	2,6-bis(benzo[*d*]thiazol-2-yl)pyridine
BuLi	butyllithium
C^N	cyclometallating ligand
calc.	calculated
Cbz	carbazole
cd	candela
CFL	compact fluorescent lamp
CIE	Commission internationale de l'éclairage
cm	centimetre
cod	1,5-cyclooctadiene
coord.	coordinates

COSY	correlation spectroscopy
CT	charge transfer
δ	chemical shift
d	day; doublet
dd	doublet of doublets
ddd	doublet of doublets of doublets
dddd	doublet of doublets of doublets of doublets
dFphtl	1-benzyl-4-(2,4-difluorophenyl)-1*H*-1,2,3-triazole
DFT	density functional theory
dm	decimetre
DMAE	2-(dimethylamino)ethanol
DMF	*N*,*N*-dimethylformamide
dmpzpy	2-(3,5-dimethyl-1*H*-pyrazol-1-yl)pyridine
DMSO	dimethylsulfoxide
DNA	deoxyribonucleic acid
dppf	1,1'-bis(diphenylphosphino)ferrocene
dt	doublet of triplets
E	half-cell potential; energy
E_{pa}	anodic peak potential
E_{pc}	cathodic peak potential
ε	extinction coefficient
ECD	electrochemical doping
ED	electrodynamical
EDG	electron-donating group
EL	electroluminescence
EPESS	enhanced phosphorescence emission in the solid state
eq.	equivalent
EQE	external quantum efficiency
ESI	electrospray ionization
Et	ethyl
eV	electronvolt
EWG	electron-withdrawing group
EXSY	exchange spectroscopy
Fc	ferrocene

g	gram
GS	ground state
h	hour
HOMO	highest occupied molecular orbital
HMBC	heteronuclear multiple bond correlation
HMQC	heteronuclear multiple quantum coherence
Hz	Hertz
i	intrinsic
IL	ionic liquid
^{i}Pr	isopropyl
ir	irreversible
IR	infrared
ISC	intersystem crossing
iTMC	ionic transition metal complex
ITO	indium tin oxide
J	coupling constant
K	Kelvin
kHz	kilohertz
k_{nr}	non-radiative decay rate constant
k_{r}	radiative decay rate constant
λ	wavelength
λ_{exc}	excitation wavelength
λ_{em}^{max}	wavelength of emission maximum
λ_{EL}^{max}	wavelength of electroluminescence maximum
LC	ligand-centred; liquid chromatography
LED	light emitting diode
LEEC	light emitting electrochemical cell
LLCT	ligand-to-ligand charge transfer
lm	lumen
Lum_{max}	maximum luminance
LUMO	lowest unoccupied molecular orbital
m	metre; multiplet (NMR); medium (IR)
M	molarity
MALDI-TOF	matrix-assisted laser desorption ionization – time of flight

MC	metal-centred
MCPBA	*meta*-chloroperbenzoic acid
Me	methyl
Mes	mesityl
mg	milligram
µg	microgram
MHz	Megahertz
min	minute
mL	millilitre
µL	microlitre
MLCT	metal-to-ligand charge transfer
mmol	millimole
µmol	micromole
mol	mole
m.p.	melting point
MS	mass spectrometry
µs	microsecond
MW	microwave
m/z	mass to charge ratio
v	frequency
$\tilde{v}$	wavenumber
n	negative
N^N	ancillary ligand
nm	nanometre
NMP	*N*-methyl-2-pyrrolidone
NMR	nuclear magnetic resonance
NOESY	nuclear Overhauser effect spectroscopy
ns	nanosecond
OAc	acetate
p	positive
pbtz	2-phenylbenzo[*d*]thiazole
PCE	power conversion efficiency
PEDOT:PSS	poly(3,4-ethylenedioxythiophene):poly(styrenesulfonate)
Ph	phenyl

piq	1-phenylisoquinoline
PLQY	photoluminescence quantum yield
PMMA	poly(methyl methacrylate)
ppm	parts per million
ppy	2-phenylpyridine
ppybtz	2-(6-phenylpyridin-2-yl)benzo[*d*]thiazole
ppz	1-phenyl-1*H*-pyrazole
pzpy	2-(1*H*-pyrazol-1-yl)pyridine
qr	quasi-reversible
quant.	quantitative
rac	racemic
RNA	ribonucleic acid
ROESY	rotating frame nuclear Overhauser effect spectroscopy
σ_m	Hammett parameter (*meta*)
σ_p	Hammett parameter (*para*)
S_0	ground state
s	second; singlet (NMR); strong (IR)
sh	shoulder
τ	excited state lifetime
t	triplet
T_1	lowest-lying triplet state
$t_{1/2}$	half lifetime (time to reach half of the maximum luminance)
$TBAPF_6$	tetrabutylammonium hexafluorophosphate
t-BME	*tert*-butyl methyl ether
^{t}Bu	tertiary butyl
tert-butyl	tertiary butyl
td	triplet of doublets
TD	time-dependent
THF	tetrahydrofuran
t_{on}	turn-on time (time to reach the maximum luminance)
tppy	2-(3-(*tert*-butyl)phenyl)pyridine
tpy	2,2':6',2''-terpyridine
tpybtz	2-(4-(*tert*-butyl)pyridin-2-yl)benzo[*d*]thiazole
UV	ultraviolet

V	Volt
Vis	visible
w	weak (IR)
W	Watt
ζ	spin-orbit coupling constant

MATERIALS AND METHODS

Starting materials were obtained in reagent grade from Sigma-Aldrich, Alfa Aesar, Acros Organics, Fluorochem, Strem, Apollo Scientific, Oxkem or TCI and used as received. For boronic acids, the purity was determined by ^{1}H NMR spectroscopy. Dry solvents (crown cap or AcroSeal®) were purchased from Sigma-Aldrich or Acros Organics and used for reactions carried out under inert atmosphere. For all other reactions, solvents used were of reagent grade or distilled. HPLC grade solvents were used for analyses. Column chromatography was performed using Fluka silica gel 60 (0.040–0.063 mm) or Merck aluminium oxide 90 standardized. Microwave-assisted syntheses were carried out on a Biotage Initiator 8 reactor.

^{1}H, ^{13}C, ^{19}F, ^{11}B and ^{31}P NMR spectra were measured on Bruker Avance III-250 (250 MHz), III-400 (400 MHz) or III-500 (500 MHz) spectrometers. 2D experiments (COSY, NOESY, HMQC and HMBC) were used for complete assignment and carried out on a Bruker Avance III-500 spectrometer. Chemical shifts are referenced to residual solvent peaks with δ(TMS) = 0 ppm. Variable temperature experiments were performed by PD Dr. Daniel Häußinger and Yann Baumgartner on a Bruker Avance III-600 (600 MHz) spectrometer.

Electrospray ionization mass spectra were recorded by Dr. Gabriel Schneider, Dr. Collin Morris or Frederik Malzner on a Bruker esquire 3000^{plus} spectrometer. LC-ESI mass spectra were obtained by Dr. Collin Morris on a combination of Shimadzu (LC) and Bruker AmaZon X instruments. MALDI-TOF mass spectrometry was carried out on a Bruker Daltonics microflex instrument by Dr. Steffen Müller and Dr. Srboljub Vujović. Elemental analysis was performed by Sylvie Mittelheisser on an Elementar Vario Micro Cube instrument. High resolution ESI mass spectra were acquired on a Bruker maXis 4G QTOF spectrometer by Heinz Nadig.

FT-IR spectra were recorded on a Perkin Elmer Spectrum Two UATR instrument. Absorption spectra were measured on an Agilent 8453 spectrophotometer and solution emission spectra on a Shimadzu 5301PC spectrofluorophotometer. Solution and powder photoluminescence quantum yields were recorded on a Hamamatsu absolute PL quantum yield spectrometer C11347 Quantaurus QY. Emission spectra of powder samples as well as

solution and powder excited state lifetime measurements were carried out on a Hamamatsu Compact Fluorescence lifetime spectrometer C11367 Quantaurus Tau.

Electrochemical measurements were performed using cyclic and square wave voltammetry on a CH Instruments 900B potentiostat with glassy carbon or platinum working and platinum auxiliary electrodes; a silver wire was used as a pseudo-reference electrode. Dry, purified CH_3CN or CH_2Cl_2 was used as solvent and 0.1 M $TBAPF_6$ as supporting electrolyte. Ferrocene as internal reference was added at the end of each experiment.

Single crystal structure determination was carried out by Dr. Jennifer Zampese, Dr. Markus Neuburger and Dr. Alessandro Prescimone on a Bruker-Nonius KappaAPEX or a Bruker APEX-II diffractometer. Data reduction, solution and refinement used the programs APEX[1] and SHELXL97.[2] Structure analysis was done using Mercury v. 3.6.[3]

Density functional theory (DFT) calculations were performed by Prof. Dr. Enrique Ortí and his team at the University of Valencia with the D.01 revision of the Gaussian 09 program package[4] using Becke's three-parameter B3LYP exchange-correlation functional[5,6] together with the 6-31G** basis set for C, H, N, S and O[7] and the "double-ζ" quality LANL2DZ basis set for iridium.[8] The singlet ground state (S_0) and lowest-energy triplet state (T_1) geometries were fully optimized without any symmetry restriction. The T_1 geometry was calculated at the spin-unrestricted UB3LYP level with a spin multiplicity of three. Emission energies were assumed as the vertical difference between the energy minimum of T_1 and the energy of S_0. All calculations were carried out in the presence of acetonitrile solvent, considering the self-consistent reaction field theory using the polarized continuum model approach.[9–11] The 15 lowest lying triplets were estimated with time-dependent DFT (TD-DFT)[12–14] calculations at the minimum-energy geometry optimized for S_0 in the presence of acetonitrile.

Light emitting electrochemical cells were assembled and investigated by Dr. Henk Bolink and his team at the University of Valencia as follows: glass substrates with ITO contact layers (Naranjo Substrates) were washed and sonicated with soap, deionized water and isopropanol. They were further cleaned under a UV-O_3 lamp (Jelight 42-220) for 20 min. In order to increase the reproducibility and to avoid the formation of pinholes, an 80 nm thick

layer of poly(3,4-ethylenedioxythiophene):polystyrenesulfonate (PEDOT:PSS) (CLEVIOS™ P VP AI 4083, aqueous dispersion, 1.3–1.7% solid content, Heraeus) was spin-coated on the ITO substrates. Iridium complex and 1-butyl-3-methylimidazolium hexfluoridophosphate ([Bmim][PF_6]) (>98.5%, Sigma-Aldrich) were mixed in a 4:1 molar ratio in acetonitrile solution (20 mg mL^{-1}) and spin-coated onto the PEDOT:PSS layer to form a 100 nm transparent film. Thermal vapour deposition of the Al electrode (70 nm) was done using a shadow mask under vacuum (<1×10^{-6} mbar) with an Edwards Auto500 evaporator integrated in the glovebox (<0.1 ppm O_2 and H_2O, M. Braun). The device performance was investigated using pulsed current conditions (average current density 100 A m^{-2}, 50% duty cycle, 1 kHz, block wave). Current and luminance were measured over time using a True Colour Sensor MAZeT (MTCSiCT Sensor) with a Botest OLT OLED Lifetime-Test System. Electroluminescence spectra were obtained from an Avantes AvaSpec-2048 Fiber Optic spectrometer.

INTRODUCTION

1. A Story about Light

2015 was declared the "International Year of Light and Light-Based Technologies" by the United Nations to "raise awareness of how optical technologies promote sustainable development and provide solutions to worldwide challenges in energy, education, agriculture, communications and health".[15] But what is light and why is it so essential and fascinating to us? Physically speaking light is an electromagnetic wave of a certain wavelength (λ) and frequency (ν). At the same time it consists of particles, called photons (photon = quantum of light). This wave–particle duality of light was first described at the beginning of the 20th century by Max Planck and Albert Einstein.[16,17]

For humans, it is only possible to perceive light with wavelengths between 380 and 700 nm, thus called visible light (Fig. 1). Adjacent to the visible region lie the ultraviolet (UV, below 380 nm) and the infrared (IR, above 700 nm) regions.[17] The Sun's spectrum is at its most intense in the visible region and tails into the UV and IR range.[18] Sunlight is the source of all life on Earth. Through the mechanism of photosynthesis, plants are capable of using light to produce energy-rich carbohydrates from carbon dioxide with oxygen as by-product. This carbon dioxide fixation by photosynthesis is basically the storage of solar energy and is therefore extremely beneficial for mankind as energy source (*e.g.* wood and fossil fuels).[15] Indeed, animals or humans are not capable to perform photosynthesis but also need sunlight irradiation for some vital processes in the body, for example the production of vitamin D by a photochemical reaction.[19] Furthermore, light has a not negligible cultural aspect. For thousands of years, mankind was dependent on the daily light–dark cycle: when the sun went down, human activity stopped. This is why the development of artificial lighting became so crucial to mankind. First, fire was used not only as a light, but also as a heat source. Later, candles and simple lamps based on natural resources, such as fish oil and later petroleum, appeared. Due to the low energy conversion and poor sustainability, alternatives were needed. With the development of the incandescent light bulb by the work of Thomas Edison and Joseph Swan in 1879, the rise of electrical light sources began. The tungsten lamp was introduced in 1906, followed by the sodium vapour lamp in the 1930s, which is still used

today as street lighting in its high pressure form. Fluorescent tubes were developed in the 1940s, halogen lamps in the 1960s and compact fluorescent lamps in the 1980s. All of these light sources are still being applied nowadays.[20,21]

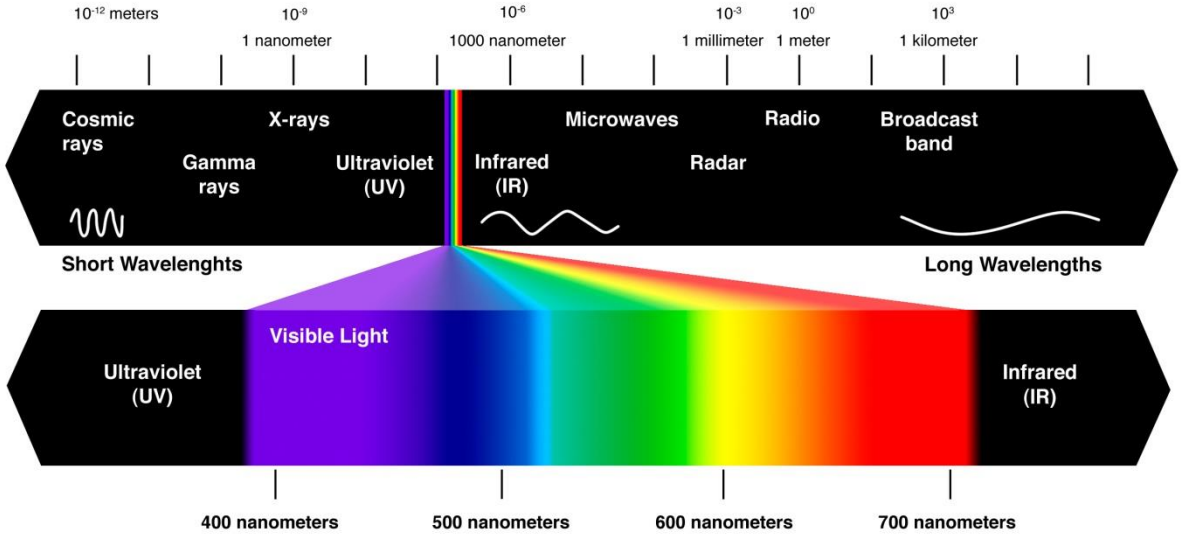

Fig. 1 The electromagnetic spectrum, highlighting the part visible to humans between 380 and 700 nm.[22]

The impressive power of electric light sources can be illustrated by the example of the "Centennial Bulb": In 1901, when Thomas Edison was still alive, a hand-blown light bulb based on a carbon filament was installed in the Fire Station in Livermore, California (Fig. 2a). It has since been shining with only short interruptions for 114 years – corresponding to an incredible lifetime of over one million hours – making it the longest lasting light bulb known. It is noteworthy to mention that its power has dropped significantly from an initial 60 W to today's 4 W during the 114 years.[23] Due to its outstanding stability, the "Centennial Bulb" became a problem for the industry at that time. To overcome this problem, the industrial leaders of the light industry started with the planned obsolescence of light bulbs in the 1920s.[24] Planned obsolescence describes the strategy of companies to design a product with limited lifetime in order to increase consumption. The lifetime reduction of light bulbs is one of the earliest examples of planned obsolescence. It was carried out by the Phoebus Cartel, an

association of the worldwide largest light bulb producers at the time, including for example Philips, Osram and General Electric. Before the agreement, light bulbs existed which could last around 2500 hours, but the Phoebus Cartel limited the lifetime to 1000 hours. The light bulbs of all member companies were regularly tested and in case that they lasted for more than 1000 hours, the manufacturing company had to pay a fine (Fig. 2b). This means that instead of conducting research focused on making the bulbs more stable and efficient, the goal was to create a product that was more fragile and had to be replaced more often than necessary.[24]

Planned obsolescence is now part of our consumer society; however, it is in no way compatible with sustainability. Therefore, it is of great importance that research is focused on creating the best, most stable and most efficient products possible.

a) **b)**

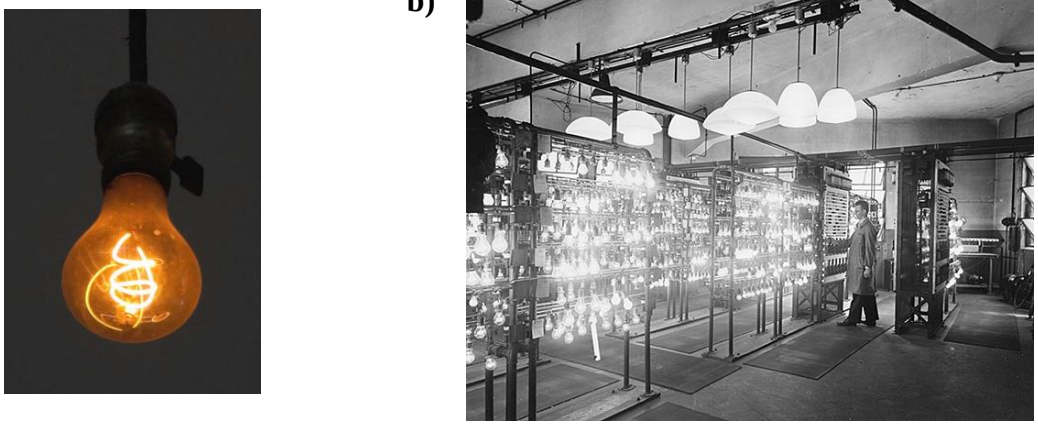

Fig. 2 a) Photograph of the "Centennial Bulb" at the Livermore Fire Station, 17th November 2013.[25] b) A Philips testing facility used to ensure standardized light bulb lifetimes of 1000 hours according to the Phoebus Cartel.[24] Copyright (2014) IEEE.

2. A Short History of Solid State Lighting

Nowadays, artificial lighting amounts to 14% of the total electricity consumption in the European Union and an even higher percentage of 19% worldwide.[26] In a time of expeditious climate change, the reduction of energy consumption accompanied with sustainable,

renewable energy sources is of ever growing importance. The potential of artificial lighting as an energy saver was therefore noted by the European Union[27] and many other countries, including Switzerland[28] and Canada.[29] They have already put a ban on the most inefficient incandescent light bulbs. This has paved the way for a shift towards more efficient and thus energy-saving lamps, *e.g.* compact fluorescent lamps (CFLs) or light emitting diodes (LEDs).

Since the first reports of red LEDs in 1962,[30,31] solid state lighting techniques have emerged as the promising new class of efficient lighting devices. LEDs consist of inorganic semiconductor materials and are now used for traffic lights, Christmas decorations, automotive lighting, display backlighting and in home illumination.[31] In 2014, the Nobel Prize in Physics was awarded to Isamu Akasaki, Hiroshi Amano and Shuji Nakamura "for the invention of efficient blue light-emitting diodes which has enabled bright and energy-saving white light sources".[32–35] This highlights the impact that LEDs have had on mankind since their first development. More recently, organic light emitting diodes (OLEDs) and light emitting electrochemical cells (LEECs) have attracted attention. The active layer in OLEDs and LEECs contains either polymers or small molecules as emissive materials. OLEDs already have made it into the market applied in displays of mobile phones, media players, digital cameras and televisions, to note just a few examples.[21]

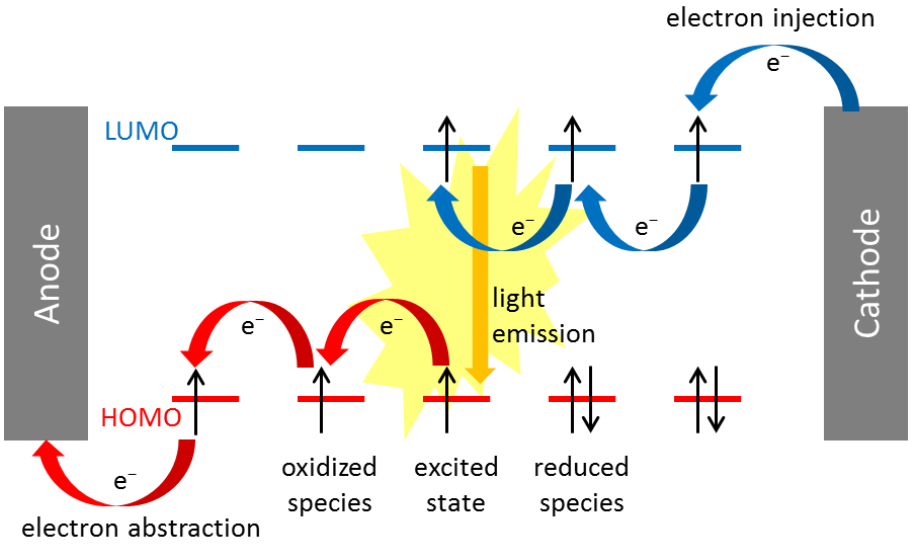

Fig. 3 Schematic representation of the principle of electroluminescence.

In comparison to traditional light sources, where light is only a by-product of discharging or heating processes, the principal output in solid state lighting applications is light itself, posing a huge advantage.[21] In all solid state lighting devices, light is generated by the mechanism of electroluminescence, shown schematically in Fig. 3. Upon applying a bias to the device, electrons are injected from the cathode into the active layer of the device, while electrons are abstracted at the anode (hole injection). In LEDs, electron injection takes place into the conduction band of the inorganic semiconductor material and electrons are abstracted from the valence band. In both OLEDs and LEECs, electrons are injected into the lowest unoccupied molecular orbital (LUMO) of the emissive material and electrons are abstracted from the highest occupied molecular orbital (HOMO), creating reduced and oxidized molecules within the active layer (Fig. 3). The electrons continue to travel through the device, from cathode to anode, until the recombination of an electron-hole pair yields an exciton. This excited state can then relax back to the ground state *via* emission of a photon, as happens for photoluminescence.[36–38]

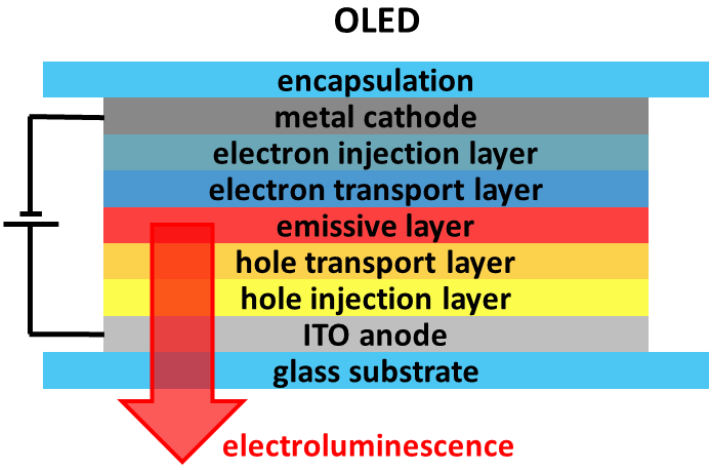

Fig. 4 Schematic representation of a multilayer OLED architecture.

The emissive material in an OLED consists either of a polymer, a fluorescent organic molecule or a phosphorescent transition metal complex. To avoid quenching effects, recombination should take place in the middle of the device. Therefore, multiple layers are required between the electrodes and the active layer to get a balanced charge injection. These

additional layers include finely tuned electron and hole injection and transport layers based on organic materials. Indium tin oxide (ITO) is widely used as transparent anode material and the cathode consists of air-sensitive, low work-function metals (*e.g.* Ca, Ba). The schematic device structure of a typical multilayer OLED is shown in Fig. 4. As a result of their complex architecture, the assembly of OLEDs involves many different steps. Layer after layer has to be vacuum-deposited, requiring materials that are stable under these conditions. In addition, the final device needs to be rigorously encapsulated, resulting in a costly manufacturing process.[21,36,37]

3. Light-Emitting Electrochemical Cells – the Future?

1995 marked the birth year of a new type of solid state lighting device, the light-emitting electrochemical cell (LEEC). While OLEDs typically contain uncharged emitters, LEECs are built up of ionic species. The first reported LEEC consisted of a fluorescent polymer as the emissive material, mixed with a conductive polymer to improve the ionic mobility and lithium trifluoromethanesulfonate as the ion source.[39] By choosing the appropriate emissive polymer, orange, green and blue LEECs were prepared.

One year later, the first LEECs based on ionic transition metal complexes (iTMCs) were described by Maness *et al*.[40] and Lee *et al*.[41] In both cases, the emissive material was a charged ruthenium(II) complex (compounds **A** and **B** in Scheme 1), resulting in orange-red electroluminescence. The first iTMC-LEECs were mostly based on ruthenium[42–48] with some examples of osmium complexes.[49,50] This changed completely with the introduction of an ionic biscyclometallated iridium(III) complex as the emissive material in a yellow LEEC in 2004 (compound **C** in Scheme 1).[51] Since then, the number of iridium emitters has continuously risen, replacing ruthenium complexes as the most used active materials.

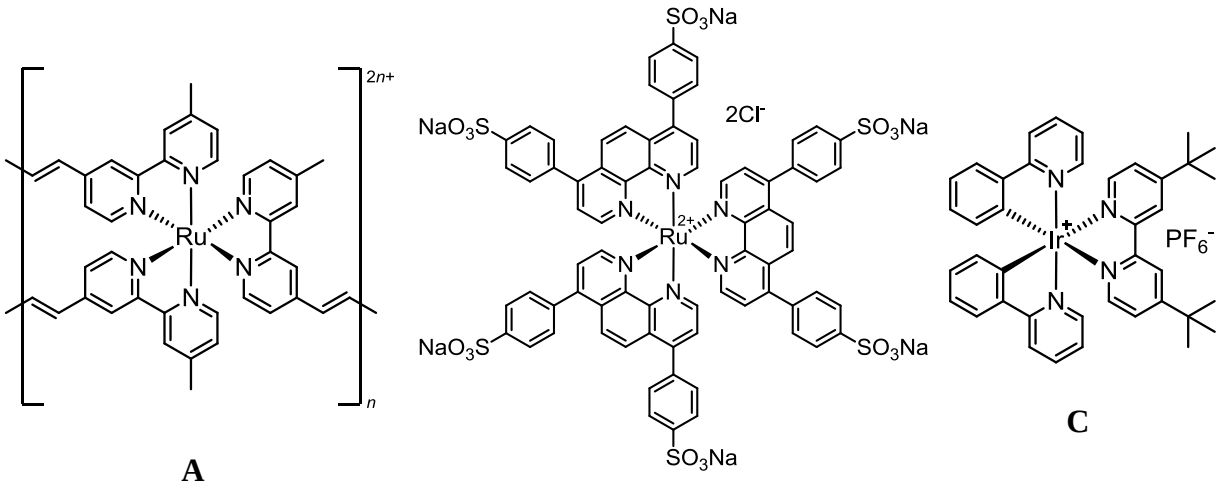

Scheme 1 Structures of the first iTMCs used in LEECs (ruthenium complexes **A** and **B**) and structure of the first charged iridium complex (**C**) used as emissive material.

The typical architecture of an iTMC-LEEC is shown in Fig. 5. ITO is commonly used as transparent anode material on a glass substrate. The anode is covered with a hole injection layer consisting of poly(3,4-ethylenedioxythiophene):poly(styrenesulfonate) (PEDOT:PSS) in order to smoothen the ITO surface, therefore enhancing the reproducibility of device preparation. A layer of the emissive material (*e.g.* an ionic biscyclometallated iridium complex), often diluted with ionic liquid, is spin-coated onto the polymer layer. Finally, the metal cathode (usually Au, Ag or Al) is thermally evaporated onto the active layer, yielding the finished device.[21]

Due to the presence of ionic species in the device, the working principle of a LEEC is different to that of an OLED. When a bias is applied to the device, the ions start to migrate to either the anode or cathode, leading to the build-up of electric double layers at the electrodes. The separation of cations and anions results in a facilitated charge injection from the electrodes. Two models exist to describe the operation mechanism of a LEEC, the electrodynamical (ED) and the electrochemical doping (ECD) model. Until now, it was not possible to exclude the occurrence of either one of these models. The ED model suggests that a large potential drop takes place at the electrodes, due to the formation of electric double

layers, but in the bulk material, the ions are not separated and emission occurs from there. In the ECD model, it is assumed that rearrangement of the ions leads to p- and n-doped regions (p = positive, n = negative) at the anode and cathode, respectively. These doped regions widen over time, giving rise to a p–i–n junction (i = intrinsic, undoped). Light emission is believed to take place in the undoped region in the middle of the device, where a continuous potential drop occurs.[21,52]

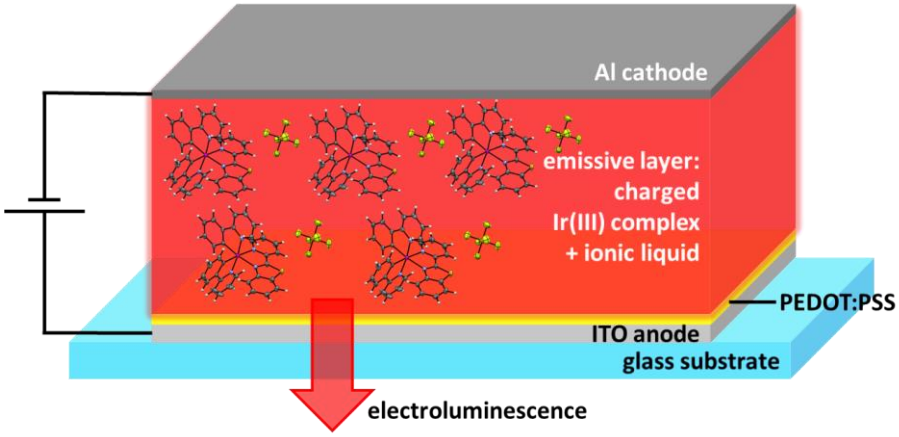

Fig. 5 Schematic representation of the typical architecture of an iTMC-LEEC. The active layer contains an emissive iridium complex mixed with ionic liquid, sandwiched between an ITO anode coated with PEDOT:PSS and an aluminium cathode.

As a result of their distinctive working mechanism based on the mobility of ionic species within the device, LEECs have several advantages with respect to OLEDs. Operation is independent of the thickness of the active layer and the work function of the electrodes; therefore, air-stable metals can be used as cathode material. There is also no need for a multi-layer structure, making solution processing possible. Rigorous encapsulation of the final device is not necessary either. All of these benefits lead to simple and cost-efficient device preparation.[21,52]

There are, however, still some intrinsic issues of LEECs which have to be addressed before commercialization becomes possible. Turn-on times (t_{on}, Fig. 6), defined as the time until reaching maximum luminance, are typically long and can range from a few seconds to

hundreds of hours. This feature is related to the ion separation taking place upon biasing the device, until charge injection starts. In contrast to OLEDs, which may be stable over thousands of hours, the lifetimes of LEECs are generally much shorter, ranging from a few minutes to several days.[21] The lifetime ($t_{1/2}$, Fig. 6) of a device is defined as the time to reach half of the maximum luminance. The poor stability of most LEECs is explained by both chemical degradation of the emissive material and the increase of the doped zones with time, leading to luminescence quenching effects. A correlation between turn-on time and lifetime is often observed for LEECs and can be traced back to the operation mechanism (formation of electric double layers and subsequent growth of the p- and n-doped regions).[21] Therefore, many of the improvements carried out in order to reduce the turn-on time generally lead to a decreased lifetime and *vice versa*.

In addition to turn-on time (t_{on}) and lifetime ($t_{1/2}$), there are several other important parameters used to determine the performance of a LEEC.[21] The luminance (black solid line in Fig. 6) is defined as the flux of light emitted by the device, measured in candela per surface unit (cd m^{-2}). In general, the maximum luminance (Lum_{max}) level reached is described for a LEEC. The current density corresponds to the flux of current through the device, determined in ampere per surface unit (A m^{-2}). The efficacy or current efficiency is the emitted light per electric flux, given in candela per ampere (cd A^{-1}). The flux of light per electric power input defines the power efficiency or power conversion efficiency (PCE), measured in lumen per watt (lm W^{-1}). The external quantum efficiency (EQE) is determined by the ratio of photons released from the device per electrons injected and given as percentage. For all efficiency measures, the maximum reached by the device is reported. Fig. 6 shows the typical evolution of luminance (black solid line) and average voltage (open red squares) over time of a LEEC driven under pulsed current conditions. When the average current density is kept constant, an initial high voltage is necessary, which quickly drops when the injection barriers are reduced due to rearrangement of the ionic species and then remains basically constant over time. The luminance shows a fast increase at the start until the maximum is reached (turn-on time), then slowly decreases due to quenching effects and chemical degradation.[21]

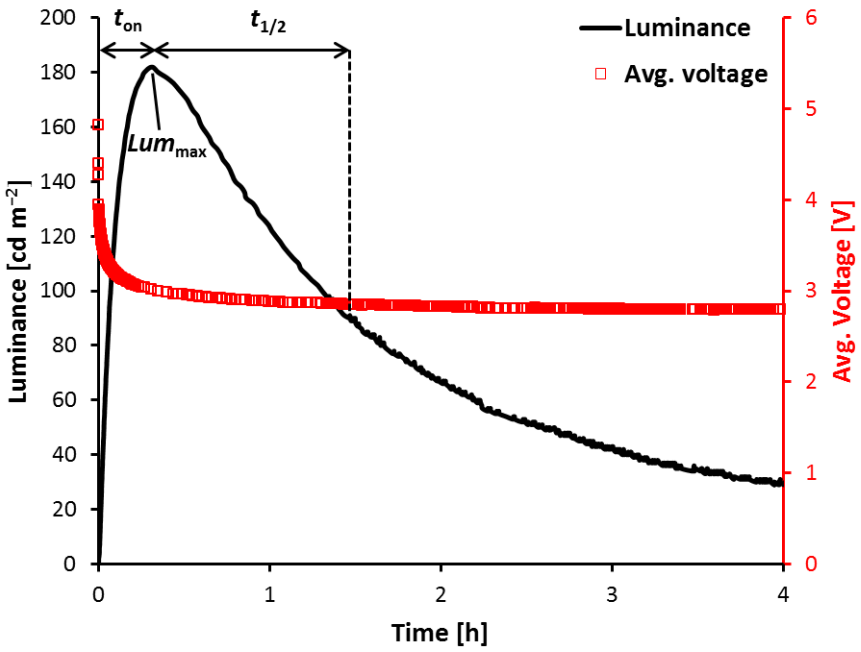

Fig. 6 Typical performance of a LEEC operated under pulsed driving conditions: Luminance (black solid line) and average voltage (open red squares) plotted against time. t_{on} = turn-on time, $t_{1/2}$ = lifetime, Lum_{max} = maximum luminance.

Chemical modifications employed to improve LEEC performance will be discussed in the following section, together with the properties of iridium-based emitters. An enhancement of the device performance can also be achieved by physical measures. For ruthenium-based LEECs, the beneficial effect of a high initial voltage[45] as well as a pulsed driving method[46] was reported. Combining these approaches and applying them to LEECs containing iridium complexes resulted in both drastically reduced turn-on times and increased stability.[53] Until the introduction of pulsed driving conditions at a constant current density, LEECs were run at a constant voltage. Another means of improving turn-on time, luminance and efficiency is the addition of ionic liquid, usually 3-butyl-1-methylimidazolium hexafluoridophosphate ([Bmim][PF_6]) to the active layer. The dilution of an emitter with ionic liquid leads to reduced intermolecular interactions and thus less self-quenching, thereby enhancing luminance and efficiency of a device. The turn-on time is reduced as a consequence of the increased number of small ionic species present.[21]

4. Why Iridium?

While mostly ruthenium(II) and a few osmium(II) complexes have been the used materials in the early days of iTMC-LEECs, biscyclometallated iridium(III) complexes have become popular choices. Few reports exist on LEECs using complexes based on other metal centres, such as rhenium(I),[54] silver(I)[55] and copper(I).[56–61] Recently, there have been two examples of charged organic small molecules used as fluorescent emitters in LEECs.[62,63]

Considering the price and scarcity of iridium, why are iridium-based complexes so extensively used as emissive material in both OLEDs and LEECs? Cyclometallated iridium compounds have excellent properties, well suited for the use in light emitting devices, such as high stability, high quantum yields and easy emission colour tunability. With this class of complexes, it is possible to obtain luminescence colours from blue to red, spanning the whole visible region.[21,64–67]

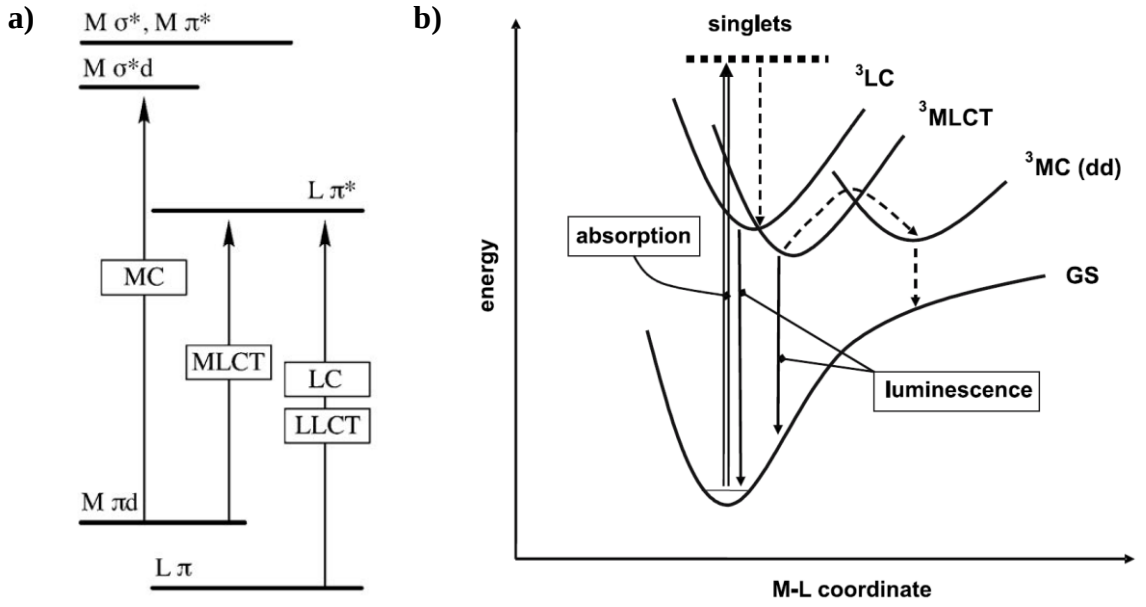

Fig. 7 Energy diagrams of iridium(III) complexes. a) Metal-centred (MC), ligand-centred (LC), metal-to-ligand charge transfer (MLCT) and ligand-to-ligand charge transfer (LLCT) transitions. Adapted with permission from *Angew. Chem. Int. Ed.*, 2012, **51**, 8178–8211.[21] Copyright (2012) Wiley-VCH. b) Absorption, luminescence and non-radiative relaxation mechanisms (dashed lines) occurring in iridium complexes. GS = ground state. Adapted with permission from *Top. Curr. Chem.*, 2007, **281**, 143–203.[68] Copyright (2007) Springer.

Iridium(III) is a $5d^6$ metal centre and in cyclometallated complexes of the type $[Ir(C\hat{}N)_2(N\hat{}N)]^+$ (C^N = cyclometallating ligand, *e.g.* the conjugate base of 2-phenylpyridine (Hppy), N^N = ancillary ligand, *e.g.* 2,2'-bipyridine (bpy)) the electron configuration is always low-spin, resulting in three filled t_{2g} and two empty e_g orbitals. Due to the strong ligand field splitting, the metal-centred (MC) states are high in energy, reducing the probability of degradation or non-radiative relaxation from these states (Fig. 7b).[21,68] Photon absorption leads to the electronic transitions shown in Fig. 7; these include mainly ligand-centred (LC), metal-to-ligand charge transfer (MLCT) and ligand-to-ligand charge transfer (LLCT) transitions.[21] As a result of the high spin-orbit coupling constant of iridium (ζ = 3909 cm^{-1}), direct excitation to the triplet excited states becomes possible, in addition to fast intersystem crossing (ISC) from the excited singlet to triplet states.[21,68] Emission takes place from a mixed triplet state of ^{3}LC, ^{3}MLCT and ^{3}LLCT transitions (Fig. 7). The extent of contribution from each of these states on the emission depends on the ligands in any individual iridium complex.[21]

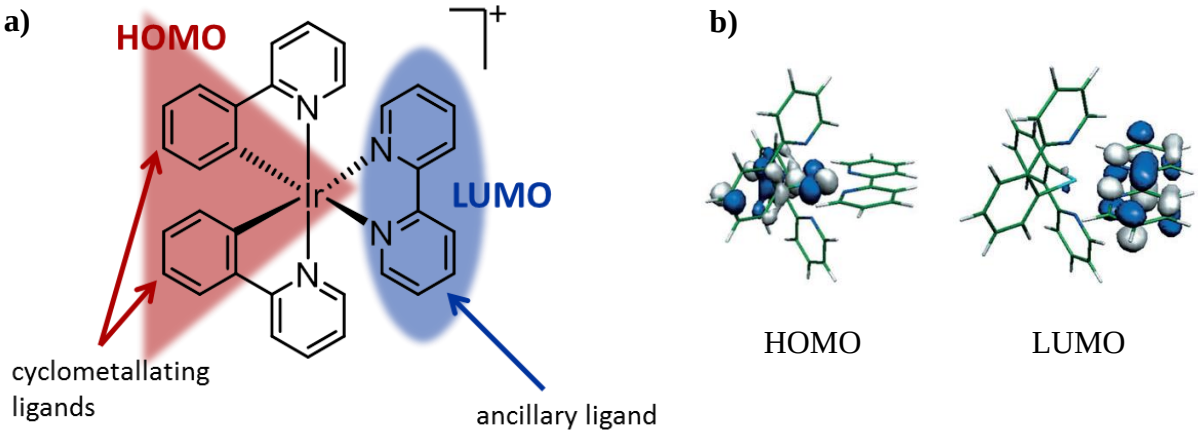

Fig. 8 a) Structure of the archetypal iridium complex $[Ir(ppy)_2(bpy)]^+$, indicating the typical position of the frontier orbitals. b) Electron density contours showing the location of the HOMO and LUMO in $[Ir(ppy)_2(bpy)]^+$. Adapted with permission from *Angew. Chem. Int. Ed.*, 2012, **51**, 8178–8211.[21] Copyright (2012) Wiley-VCH.

Typically, the frontier orbitals are spatially separated in $[Ir(C\hat{}N)_2(N\hat{}N)]^+$ complexes. The HOMO (red) usually resides on the iridium centre and the phenyl rings of the

cyclometallating ligands, whereas the LUMO (blue) is located on the ancillary ligand (shown in Fig. 8a for the simple complex $[Ir(ppy)_2(bpy)]^+$).[21,64,66,68] This is supported by density functional theory (DFT) calculations (see Fig. 8b) and corroborated by electrochemical measurements.[21,64] Because of the separation of the frontier orbitals, iridium complexes are such versatile materials in terms of emission colour tuning. Blue-shifts in the emission colour are possible by attaching electron-withdrawing groups (EWG) on the cyclometallating ligands and electron-donating groups (EDG) on the ancillary ligand. This leads to an enhanced HOMO-LUMO energy gap by stabilization of the HOMO and destabilization of the LUMO. Another possibility is the replacement of the standard 2,2'-bipyridine (bpy) ancillary ligand by more electron-rich ligands, for example 2-(1*H*-pyrazol-1-yl)pyridine (pzpy). Strong-field ancillary ligands such as CO, isocyanides or carbenes are also effective in shifting the emission towards the blue. Emission red-shifts can be achieved by using electron-releasing cyclometallating and electron-deficient ancillary ligands. Due to a destabilization of the HOMO and stabilization of the LUMO, the energy gap is reduced, resulting in a red-shifted emission. Another strategy is an increased delocalization of the π-system, using for example quinoline- or isoquinoline-based ligands, also leading to a red-shift in the emission maximum.[21,66]

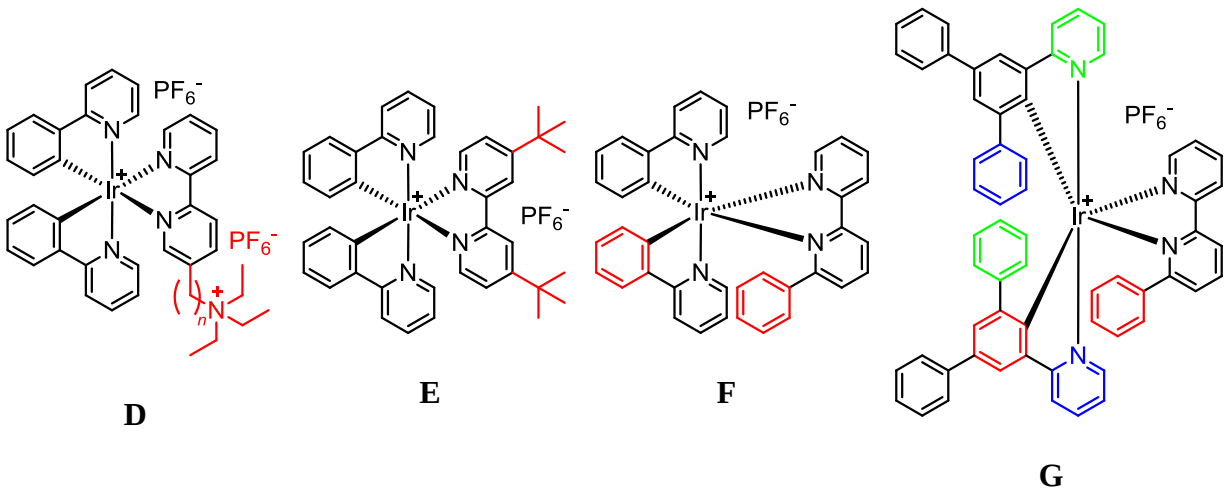

Scheme 2 Structure of iridium complexes designed to enhance LEEC performance: charged substituents (compound **D**), bulky groups (compound **E**) and one to three π-stacking interactions (compounds **F** and **G**, respectively). π-stacking occurs between rings of the same colour.

Not only can iridium complexes be chemically modified to tune the emission colour, but also to improve LEEC performance. The turn-on time of a device is reduced by changing the widely used $[PF_6]^-$ anion to a smaller counterion, for example $[BF_4]^-$ or $[ClO_4]^-$. However, this usually results also in a reduced lifetime of the device.[21] The addition of extra charge on the emissive compound has the same effect, as shown by Zysman-Colman *et al.*[69] for the introduction of triethylammonium hexafluoridophosphate substituents on the ancillary ligand (compound **D**, Scheme 2). It is possible to enhance the stability of LEECs by designing robust and hydrophobic iridium complexes. For that, bulky substituents such as *tert*-butyl groups can be introduced to the ligands (compound **E**, Scheme 2). This approach does not only exert a positive effect on the lifetime, but also the efficiency of a device by reducing the intermolecular interactions, resulting in less luminescence quenching.[21,66] Another strategy to increase the stability of a LEEC is the design of intramolecular π-stacking interactions, leading to robust iridium complexes and diminishing the probability of chemical degradation in the device. This was first demonstrated by adding a pendant phenyl ring to the bpy ancillary ligand which enables π-stacking with the phenyl ring of one of the cyclometallating ligands (compound **F**, Scheme 2).[70–72] The concept has since been extended to multiple intramolecular π-stacking interactions by careful design of the cyclometallating and ancillary ligands, leading to complexes with up to three of such π-π interactions (compound **G**, Scheme 2).[73,74] Interestingly, increasing the number of intramolecular interactions does not further enhance the LEEC lifetime.

While great progress has been made in the field of iTMC-LEECs since their first report in 2004, some issues still need to be resolved. Up to today, there is a lack of stable blue and green LEECs. In addition, there are no reports of efficient and stable red emitters for LEECs.[21,66] These drawbacks greatly limit practical application, as devices of all colours are required; *e.g.* for display applications, as well as for the development of white LEECs, which are commonly based on a mixture of active materials with different emission colours.[75–77]

CHAPTER I: YELLOW & GREEN EMITTERS – THIOETHER- AND SULFONE-SUBSTITUTED CYCLOMETALLATING LIGANDS

1. Introduction

Fluoro-substituted cyclometallating ligands have been extensively used in iridium complexes of the type $[Ir(C\hat{}N)_2(N\hat{}N)]^+$ in order to tune the emission colour to the blue region.[78–80] Introduction of electron-withdrawing fluorine substituents leads to a stabilization of the HOMO in $[Ir(C\hat{}N)_2(N\hat{}N)]^+$ complexes, which is located on the C^N ligands and the iridium metal centre. However, it has been shown that increasing the number of fluorine atoms leads to a decrease in device stability in both OLEDs[81] and LEECs.[82] The cause of this effect is assumed to be a hydrodehalogenation reaction occurring on the iridium complexes when operated in a device.[81] As a result, the design of fluorine-free blue emitting iridium complexes has become a challenging goal in recent years. Considering the Hammett parameters (σ_m = 0.60 and σ_p = 0.72 for SO_2Me; σ_m = 0.34 and σ_p = 0.06 for F[83,84]), sulfonyl moieties appear to be an interesting choice for the design of green and blue emitting iridium complexes: the higher the Hammett parameter, the larger the electron-withdrawing effect. Few examples of sulfone-substituted cyclometallating ligands in iridium complexes exist; most of them are used in neutral emitters, suited for OLEDs. These include 3-(pyridin-2-yl)dibenzo[*b*,*d*]thiophene 5,5-dioxide (**H**),[85] 2-(4-(phenylsulfonyl)phenyl)pyridine (**I**),[86–88] fluorinated 2-(4-(phenylsulfonyl)phenyl)pyridine (**J**),[89] regioisomeric benzylsulfonyl-substituted 2-phenylpyridine and fluorinated 2-(4-(benzylsulfonyl)phenyl)pyridine (**K**),[90] 2-(2,4-difluoro-3-tosylphenyl)pyridine (**L**)[91] and sulfonyl-functionalized 2-(4-methoxyphenyl)pyridine (**M**)[92] cyclometallating ligands (Scheme 3).

Our group has recently reported the use of 1-(4-(methylsulfonyl)phenyl)-1*H*-pyrazole (compound **N** in Scheme 3) as a cyclometallating ligand in iridium complexes for highly efficient green light emitting electrochemical cells.[93] Due to the promising device performances, the investigation of iridium complexes with sulfone-substituted phenylpyridines was started.[94] In this chapter, the synthesis and characterization of a series of sulfone- and thioether-substituted iridium complexes is presented. The influence of the

sulfone and thioether groups is investigated with respect to the reference compound containing 2-(4-fluorophenyl)pyridine as cyclometallating ligands. By comparing pairs of thioether and sulfonyl-substituted complexes, it is possible to study the influence of the sulfur oxidation state on photophysical and electrochemical properties. Furthermore, different alkyl groups bound to the sulfur atom were examined: from simple methyl to bulky *tert*-butyl and long-chain dodecyl substituents. Judging by their photophysical properties, the most promising candidates have been tested in LEECs.[95]

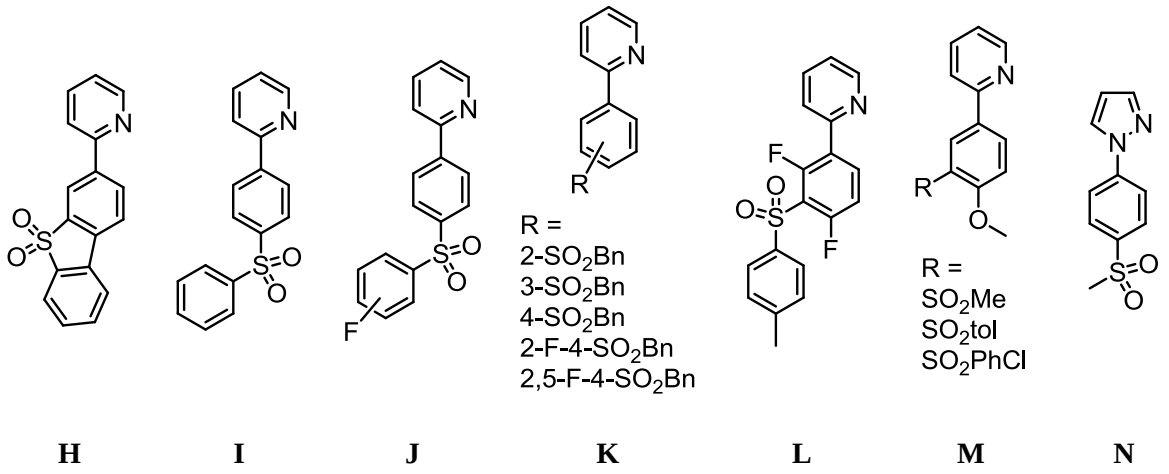

H **I** **J** **K** **L** **M** **N**

Scheme 3 Structures of sulfonyl-substituted cyclometallating ligands used in the literature for iridium complexes.

2. Synthesis and NMR Spectroscopic Characterization

2.1. Ligand synthesis

The synthetic route to ligands H**1**–H**7** is summarized in Scheme 4. Fluoro ligand H**1** was synthesized by a room temperature Suzuki coupling of 4-fluorophenylboronic acid and 2-bromopyridine in EtOH/H_2O with $PdCl_2$ as catalyst.[96] H**1** acts as a precursor for thioether compounds H**2**, H**4** and H**6**, which were formed *via* a nucleophilic substitution reaction with the appropriate thiolate. In the case of H**2**, commercially available NaSMe was reacted with H**1** in *N*-methyl-2-pyrrolidone (NMP) under microwave conditions, leading to a superior yield of 93% with respect to the Ullmann coupling reported in the literature.[97] For H**4** and H**6**, a

literature procedure was adapted:[98] The corresponding thiol (2-methyl-2-propanethiol and 1-dodecanethiol, respectively) was deprotonated *in situ* with sodium hydride before the fluoro precursor was added. Compounds H**4** and H**6** were obtained in quantitative and good yield, respectively. The desired sulfone ligands H**3**, H**5** and H**7** were prepared in excellent yields from the corresponding thioether compounds, using $H_2O_2/Na_2WO_4{\cdot}2H_2O$ as oxidizing agent.[99]

Previous to the synthesis of mono-sulfone cyclometallating ligands, the preparation of bis-sulfonyl phenylpyridines was investigated. Several conditions and reagents (H_2O_2, MCPBA, $KMnO_4$, oxone, $NaIO_4$, $H_2O_2/(NH_4)_6Mo_7O_{24}{\cdot}4H_2O$) were tested for the oxidation of 2-(2,4-bis(methylthio)phenyl)pyridine to the bis-sulfone compound. The combination of $H_2O_2/Na_2WO_4{\cdot}2H_2O$ in MeOH at room temperature proved to be the most effective and selective: the least side products (mixed sulfone-sulfoxide or pyridine *N*-oxide) were observed with this method. Therefore, this synthetic protocol was adapted for the oxidation of the mono-sulfone ligands.

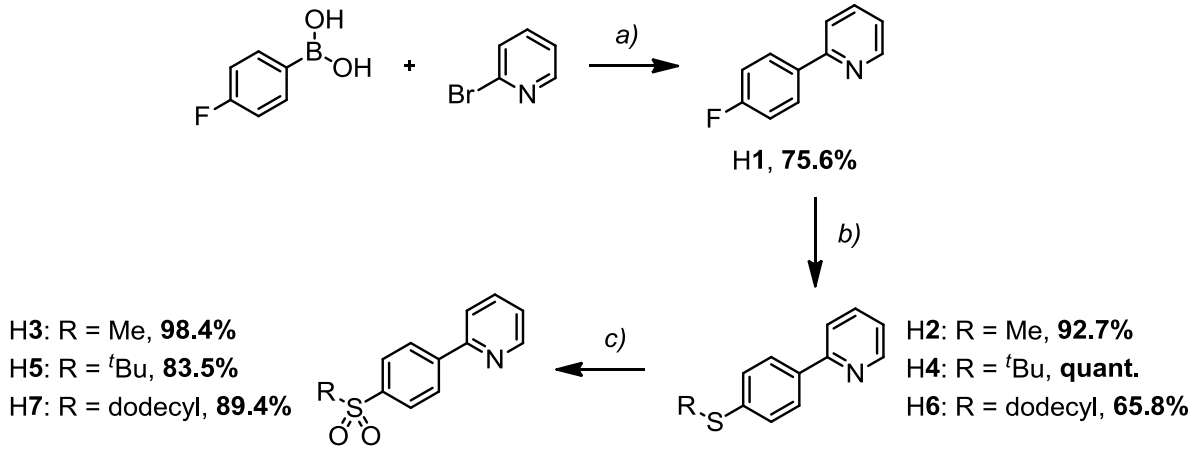

Scheme 4 Synthetic route to ligands H**1** and H**3**–H**7**. Reaction conditions: *a)* $PdCl_2$, K_2CO_3, EtOH/H_2O 1:1, room temperature, 3 d; *b)* for H**2**: NaSMe, NMP, MW, 80 °C, 1 h; for H**4** and H**6**: 2-methyl-2-propanethiol or 1-dodecanethiol, NaH (60%), DMF, 120 °C, 24 or 4 h, N_2; *c)* $Na_2WO_4{\cdot}2H_2O$, H_2O_2, MeOH, room temperature, overnight.

Compounds H**2**–H**7** were characterized by NMR and IR spectroscopies, mass spectrometry, elemental analysis and melting point analysis. ^{1}H and ^{13}C{^{1}H} NMR signals were fully assigned using 2D methods (COSY, HMQC, HMBC). For each of H**2**–H**5** and H**7**, the base peak in the ESI mass spectrum corresponds to the $[M+H]^+$ ion. No ESI peak was observed in the case of H**6**, however, $[M]^+$ could be detected at *m/z* 355.7 in the MALDI-TOF mass spectrum.

2.2. Synthesis of $[Ir(C\hat{}N)_2Cl]_2$ dimers

Chlorido-bridged dimers of the type $[Ir(C\hat{}N)_2Cl]_2$ are typically synthesized from iridium trichloride and the corresponding cyclometallating ligand under reflux conditions in a mixture of 2-ethoxyethanol and water.[100,101] This method was used in the case of ligands H**1**, H**5** and H**7** to obtain the iridium dimers in moderate to good yields (Scheme 5). For the preparation of $[Ir(C\hat{}N)_2Cl]_2$ dimers with C^N = **3** and **4**, however, the standard procedure did not prove successful as no product could be isolated. Reaction of H**3** and H**4** with $[Ir(cod)Cl]_2$ in 2-ethoxyethanol[102] either under reflux or microwave conditions as an alternative route finally gave the desired iridium dimers. Compounds $[Ir(C\hat{}N)_2Cl]_2$ with C^N = **3**–**5** and **7** were characterized by NMR spectroscopic methods and LC-ESI or MALDI-TOF mass spectrometry. Proton and ^{13}C NMR signals were fully assigned with the support of 2D experiments (COSY, HMQC, HMBC), except for $[Ir(\mathbf{4})_2Cl]_2$, where low solubility prevented the recording of a sufficiently resolved ^{13}C{^{1}H} NMR spectrum. For $[Ir(C\hat{}N)_2Cl]_2$ (C^N = **3**–**5**), observed peaks in the LC-ESI mass spectra correspond to $[Ir(C\hat{}N)_2]^+$, $[Ir(C\hat{}N)_2(CH_3CN)]^+$ and $[Ir(C\hat{}N)_2(CH_3CN)_2]^+$. The coordinating CH_3CN arises from the eluent of the LC column. $[Ir(\mathbf{7})_2Cl]_2$ did not give any peaks in the LC-ESI mass spectrum, however, the base peak in the MALDI-TOF mass spectrum is attributed to $[Ir(\mathbf{7})_2]^+$.

Complexation reactions with H**2** under different conditions did not yield the desired iridium dimer. A yellow insoluble solid was obtained which could not be characterized and gave only trace amounts of $[Ir(\mathbf{2})_2(bpy)]^+$ when treated with 2,2'-bipyridine under standard conditions. Treatment of $[Ir(cod)Cl]_2$ with H**6** to give $[Ir(\mathbf{6})_2Cl]_2$ was not successful either, only unreacted ligand could be isolated after the reaction.

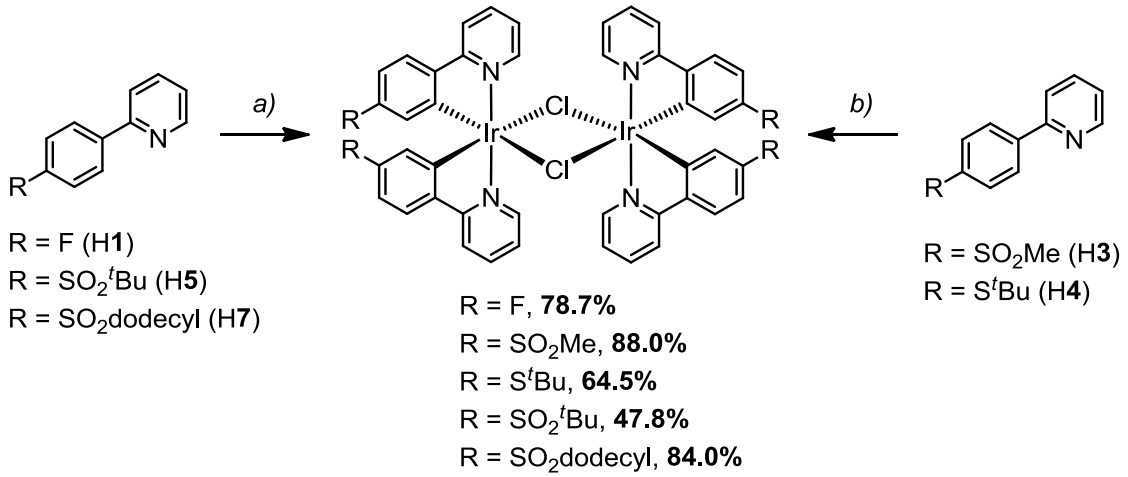

Scheme 5 Synthetic pathway to $[Ir(C\hat{}N)_2Cl]_2$ dimers with C^N = **1**, **3**–**5** and **7**. Reaction conditions: *a)* $IrCl_3 \cdot xH_2O$, 2-ethoxyethanol/H_2O 3:1, reflux, overnight, N_2; *b)* $[Ir(cod)Cl]_2$, 2-ethoxyethanol, reflux, overnight, Ar (for H**3**) or MW, 110 °C, 1.5 h, N_2 (for H**4**).

2.3. Synthesis of $[Ir(C\hat{}N)_2(bpy)][PF_6]$ complexes

To obtain the desired $[Ir(C\hat{}N)_2(bpy)][PF_6]$ complexes, dimers $[Ir(C\hat{}N)_2Cl]_2$ with C^N = **1**, **3**–**5** and **7** were treated with bpy according to standard literature procedures (Scheme 6).[93,103,104] The reactions proceeded smoothly in MeOH under reflux or microwave conditions, followed by anion exchange with an excess of solid NH_4PF_6. The complexes were obtained as yellow to dark yellow solids in moderate to good yields.

Since the iridium dimer $[Ir(\mathbf{6})_2Cl]_2$ could not be synthesized, an alternative route to $[Ir(\mathbf{6})_2(bpy)][PF_6]$ was developed. 1-Dodecanethiol was deprotonated with sodium hydride in DMF to produce the thiolate nucleophile which was subsequently reacted with fluoro-subtituted complex $[Ir(\mathbf{1})_2(bpy)][PF_6]$ in a nucleophilic aromatic substitution reaction, leading to the desired complex in good yield (Scheme 6). The base peak in the ESI mass spectrum of each complex corresponds to the $[M–PF_6]^+$ ion, exhibiting the typical iridium isotope pattern. ^1H and $^{13}C\{^1H\}$ signals were assigned for all complexes using 2D NMR spectroscopic measurements (COSY, HMQC, HMBC).

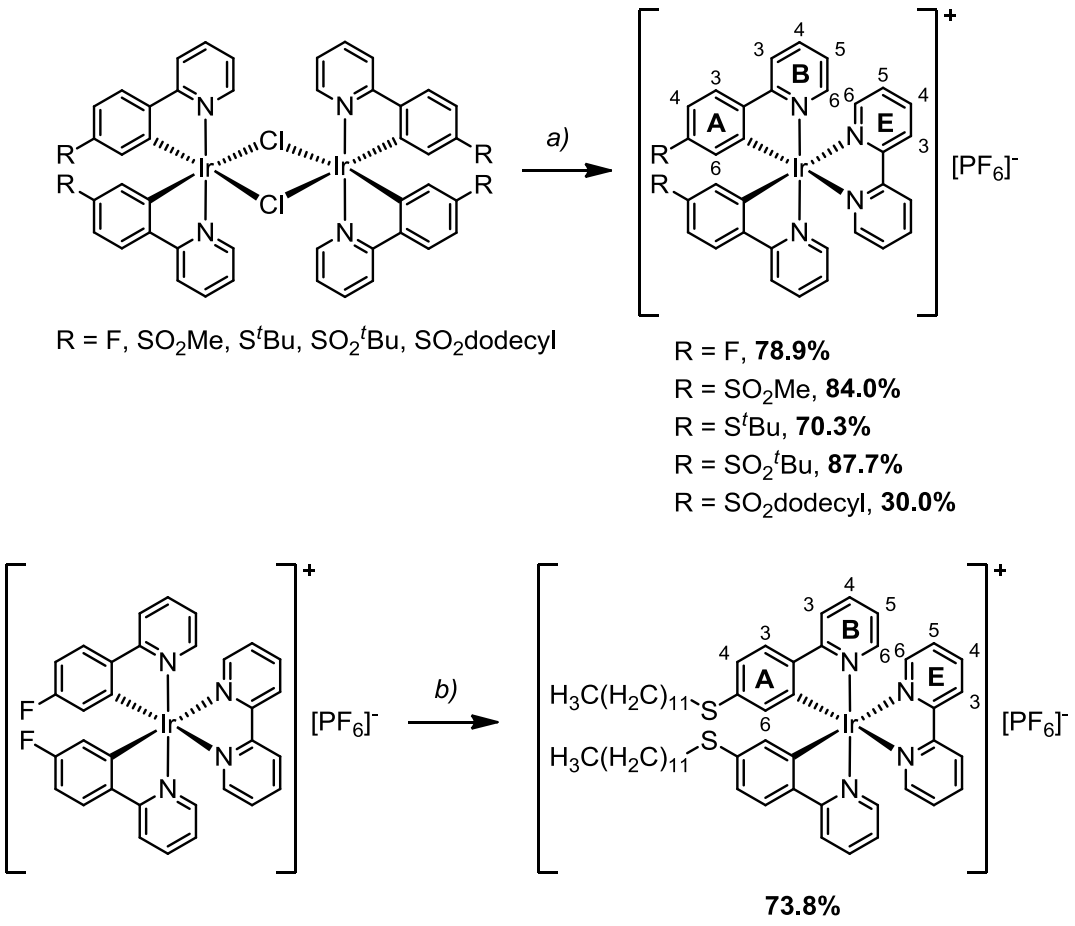

Scheme 6 Synthetic route to complexes $[Ir(C\hat{}N)_2(bpy)][PF_6]$ with C^N = **1**, **3**–**7**. Structures include numbering scheme used for NMR assignment. Reaction conditions: *a)* 2,2'-bipyridine, MeOH, MW, 120 °C, 1 h (for C^N = **3**) or reflux, overnight (for C^N = **1**, **4**, **5** and **7**); then NH_4PF_6; *b)* 1-dodecanethiol, NaH (60%), DMF, 120 °C, 1.5 h, N_2.

The aromatic region of the ^{1}H NMR spectra of complexes $[Ir(C\hat{}N)_2(bpy)][PF_6]$ with C^N = **1**, **3**–**7** is shown in Fig. 9 (numbering according to Scheme 6). Proton H^{A6} shows a range of chemical shift from δ 5.89 to 6.70 ppm and is affected the most by changing the substituent on the cyclometallating ligand. The second-largest chemical shift differences are seen for H^{A4} (ranges from δ 6.81 to 7.58 ppm) and to a lesser extent for H^{A3} and the B ring protons. Negligible shifts are observed for protons on the bpy ancillary ligand (E ring). In $[Ir(\mathbf{1})_2(bpy)][PF_6]$, protons H^{A4} (δ 6.81 ppm) and H^{A6} (δ 5.89 ppm) are observed at the lowest frequency within this series. Comparing the thioether and sulfone complexes, all A ring

protons are shifted downfield on going from the thioether to the sulfone compounds. These shifts are attributed to the de-shielding effect of the electron-withdrawing sulfone group. Chemical shifts of protons H^{tBu} move from δ 1.00 ppm in the thioether complex [Ir(**4**)$_2$(bpy)][PF$_6$] to δ 0.93 ppm in the sulfone complex [Ir(**5**)$_2$(bpy)][PF$_6$]. CH_2 protons of the dodecyl chains next to the thioether and sulfone moieties are shifted downfield on going from [Ir(**6**)$_2$(bpy)][PF$_6$] (δ 2.63 ppm) to [Ir(**7**)$_2$(bpy)][PF$_6$] (δ 2.87 ppm).

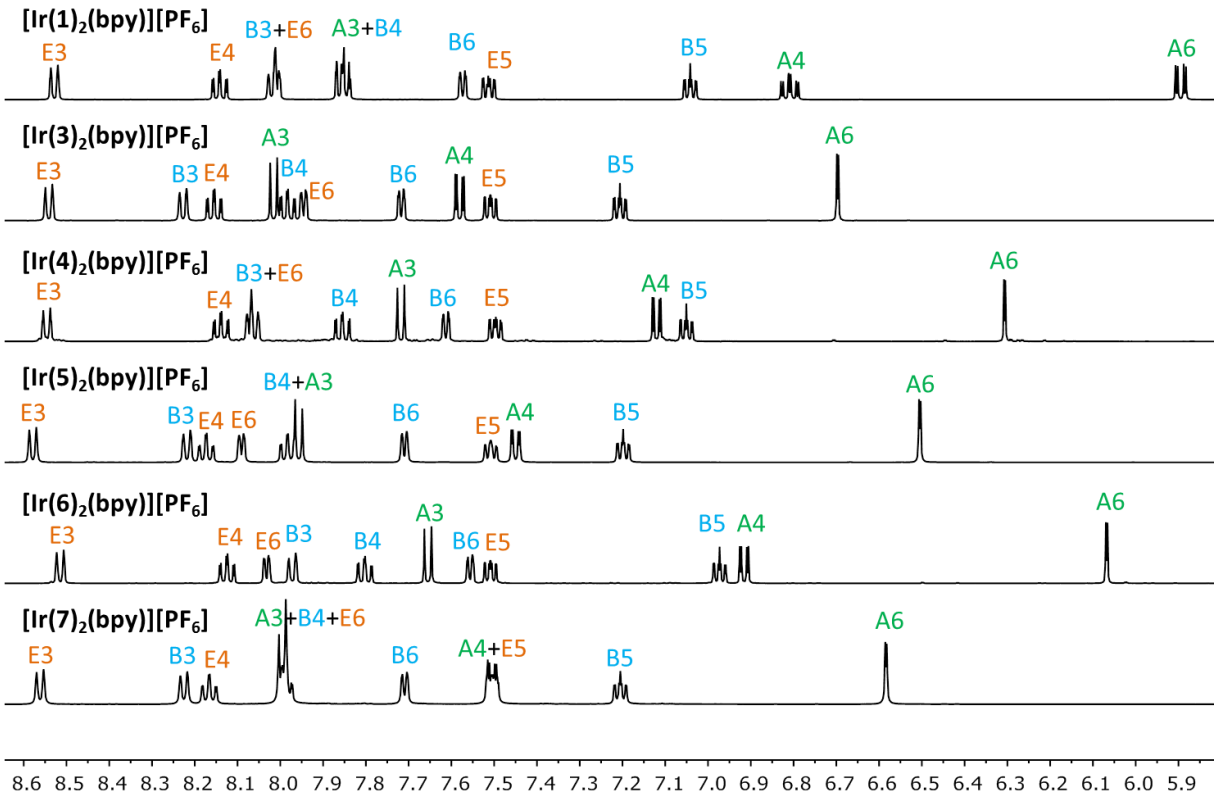

Fig. 9 Aromatic region of the 500 MHz ^{1}H NMR spectra of [Ir(C^N)$_2$(bpy)][PF$_6$] (C^N = **1**, **3**–**7**) in CD_3CN solution with assignments. Scale: δ/ppm.

3. Crystal Structures

X-ray quality single crystals of H**3** and H**5** were grown by overlaying $CHCl_3$ or CH_2Cl_2 solutions of the compounds, respectively, with *n*-hexane. Structures of both ligands are shown in Fig. 10, with selected bond lengths and angles given in the figure caption. Both H**3** and H**5** crystallize in the monoclinic space group *C*2/*c*. As observed in several aryl-aryl[105,106] and

aryl-alkyl sulfones,[105] the sulfone group is twisted with respect to the attached aromatic ring, leading to intramolecular CH···OS contacts. The dihedral angles O1–S1–C9–C10 and O2–S1–C9–C8 in H**3** are −25.0 and 28.2°, respectively, resulting in intramolecular interactions with distances of 2.60 (O1···H10A) and 2.64 Å (O2···H8A). In H**5**, the corresponding angles are −23.1 (O1–S1–C9–C8) and 24.6° (O2–S1–C9–C10), giving short intramolecular CH···OS contacts of 2.57 (O1···H8A) and 2.64 Å (O2···H10A). The phenyl and pyridine rings are twisted with respect to each other in both structures, with angles between the ring planes of 17.7° in H**3** and 37.7° in H**5**.

a) **b)**

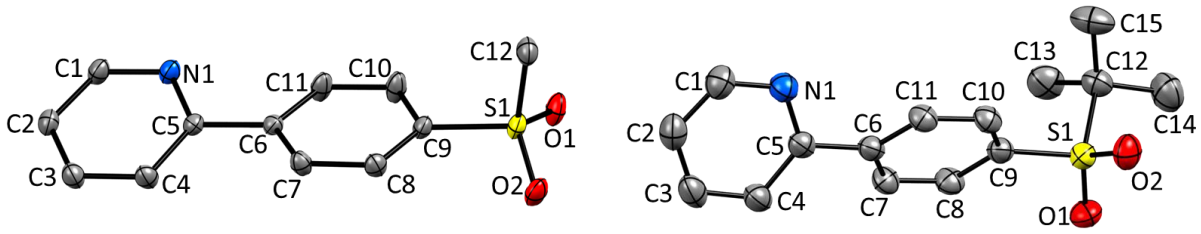

Fig. 10 Structures of ligands a) H**3** and b) H**5**, H atoms omitted and ellipsoids plotted at 40% probability level. Selected bond parameters: a) S1–O1 = 1.4434(10), S1–O2 = 1.4411(9), S1–C9 = 1.7575(11), S1–C12 = 1.7569(14) Å; O1–S1–O2 = 118.19(6), O1–S1–C9 = 108.45(6), O1–S1–C12 = 108.11(6), O2–S1–C9 = 109.20(6), O2–S1–C12 = 108.03(7), C9–S1–C12 = 103.93(6)°; b) S1–O1 = 1.4402(12), S1–O2 = 1.4378(12), S1–C9 = 1.7727(15), S1–C12 = 1.8190(16) Å; O1–S1–O2 = 118.85(8), O1–S1–C9 = 107.03(7), O1–S1–C12 = 107.50(8), O2–S1–C9 = 107.48(7), O2–S1–C12 = 108.05(8), C9–S1–C12 = 107.46(7)°.

Single crystals of $[Ir(\mathbf{3})_2Cl]_2 \cdot 2CH_2Cl_2$ were grown from a CH_2Cl_2 solution of the iridium dimer overlaid with Et_2O. The structure is shown in Fig. 11 with important bond lengths and angles stated in the figure caption. The compound crystallizes in the orthorhombic space group *Pbca* and the asymmetric unit contains the Λ,Λ-enantiomer; both Λ,Λ- and Δ,Δ-enantiomers are present in the lattice. One CH_2Cl_2 solvent molecule is disordered and has been modelled over two positions with fractional occupancies of 0.62 and 0.38. Two of the sulfone groups are again twisted with respect to the phenyl rings with dihedral angles O2–S2–C9–C10 = −20.5, O1–S2–C9–C8 = 30.9, O6–S3–C33–C34 = −17.4 and O5–S3–C33–C32 =

31.4°. These torsions give rise to short CH···OS contacts ranging from 2.56 to 2.66 Å. In the remaining two sulfone groups, torsion angles are −1.3 (O8–S4–C45–C44) and −53.8 (O7–S4–C45–C46) and −3.3 (O4–S1–C21–C20) and −58.1° (O3–S1–C21–C22). This leads to two shorter (2.47 and 2.49 Å) and two longer (2.96 and 2.99 Å) CH···OS interactions.

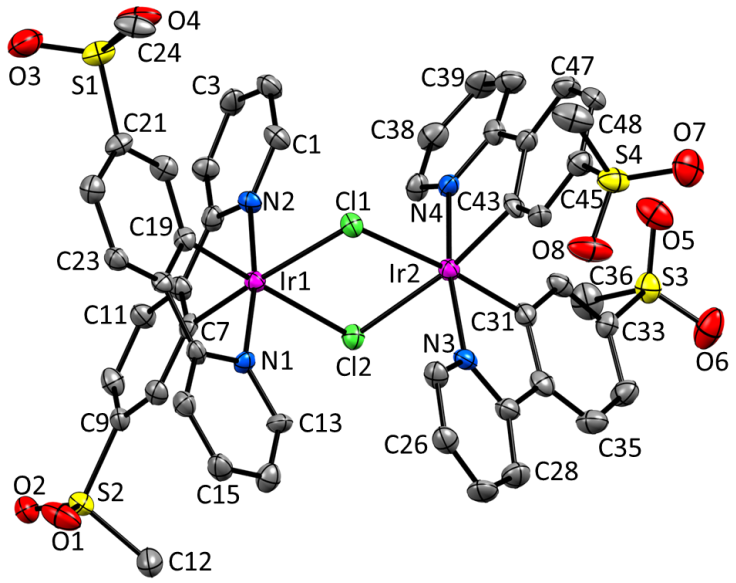

Fig. 11 Structure of [Ir(**3**)$_2$Cl]$_2$ in [Ir(**3**)$_2$Cl]$_2$·2CH$_2$Cl$_2$; H atoms and solvent molecules omitted and ellipsoids plotted at 40% probability level. Selected bond parameters: Ir1–Cl1 = 2.486(2), Ir1–Cl2 = 2.512(2), Ir1–N1 = 2.050(7), Ir1–N2 = 2.057(7), Ir1–C7 = 1.988(8), Ir1–C19 = 1.984(8), S1–O3 = 1.404(9), S1–O4 = 1.441(8), S2–O1 = 1.422(8), S2–O2 = 1.439(7), Ir2–Cl1 = 2.504(2), Ir2–Cl2 = 2.503(2), Ir2–N3 = 2.053(7), Ir2–N4 = 2.043(7), Ir2–C31 = 2.015(9), Ir2–C43 = 1.995(8), S3–O5 = 1.427(8), S3–O6 = 1.423(8), S4–O7 = 1.435(9), S4–O8 = 1.443(8) Å; N1–Ir1–C19 = 80.2(3), N2–Ir1–C7 = 80.9(3), Cl1–Ir1–Cl2 = 84.46(7), O1–S2–O2 = 117.0(5), O3–S1–O4 = 117.5(5), N3–Ir2–C31 = 80.7(3), N4–Ir2–C43 = 80.4(3), Cl1–Ir2–Cl2 = 84.30(6), O5–S3–O6 = 119.7(5), O7–S4–O8 = 117.1(6)°.

Crystals of [Ir(**1**)$_2$(bpy)][PF$_6$] were grown from CH$_3$CN or CH$_2$Cl$_2$ solutions of the complex layered with Et$_2$O and resulted in the resolution of two different structures, namely Δ-[Ir(**1**)$_2$(bpy)][PF$_6$] (Fig. 12) and *rac*-4{[Ir(**1**)$_2$(bpy)][PF$_6$]}·Et$_2$O·2CH$_2$Cl$_2$ (Fig. 13a). Important bond lengths and angles are similar in both structures and are given in the figure captions. Enantiomerically pure Δ-[Ir(**1**)$_2$(bpy)][PF$_6$] crystallizes in the trigonal space group $P3_12_1$. In *rac*-4{[Ir(**1**)$_2$(bpy)][PF$_6$]}·Et$_2$O·2CH$_2$Cl$_2$, two independent cations (Δ- and Λ-enantiomer) are

present in the asymmetric unit and the compound crystallizes in the triclinic space group *P*−1. The Et_2O solvent molecule in the asymmetric unit is half occupancy and the CH_2Cl_2 molecule is ordered. π-stacking interactions are observed between the two independent cations in the asymmetric unit and are displayed in Fig. 13b. Face-to-face π-stacking occurs between the bpy pyridyl ring containing N1B and the cyclometallating phenyl ring containing C28A with a distance of 4.24 Å between the two centroids and an angle of 12.4° between the ring planes. In addition, CH···π contacts are observed between proton H3BA and the phenyl ring containing C17A (H···centroid distance = 2.59 Å) and between H31A and the pyridyl ring with N4B (3.03 Å). No π-stacking is observed in Δ-[Ir(**1**)$_2$(bpy)][PF_6], where dominant packing motifs are CH···F interactions between aromatic protons and F from both $[PF_6]^-$ anions and cyclometallating ligands.

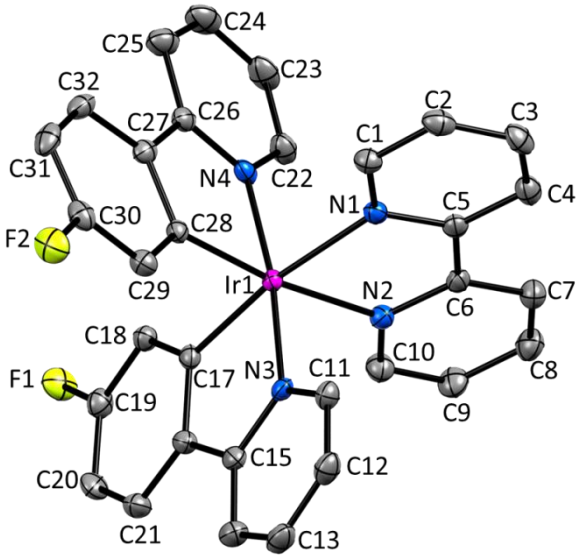

Fig. 12 Structure of the Δ-[Ir(**1**)$_2$(bpy)]$^+$ cation of Δ-[Ir(**1**)$_2$(bpy)][PF_6]; H atoms omitted for clarity and ellipsoids plotted at 40% probability level. Selected bond parameters: Ir1–N1 = 2.130(3), Ir1–N2 = 2.141(3), Ir1–N3 = 2.048(3), Ir1–N4 = 2.054(3), Ir1–C17 = 2.008(4), Ir1–C28 = 2.008(4), F1–C19 = 1.374(5), F2–C30 = 1.370(5) Å; N1–Ir1–N2 = 76.95(12), N3–Ir1–C17 = 80.17(14), N4–Ir1–C28 = 80.77(14), N1–Ir1–C17 = 170.94(13), N2–Ir1–C28 = 172.58(13), N3–Ir1–N4 = 172.38(12)°.

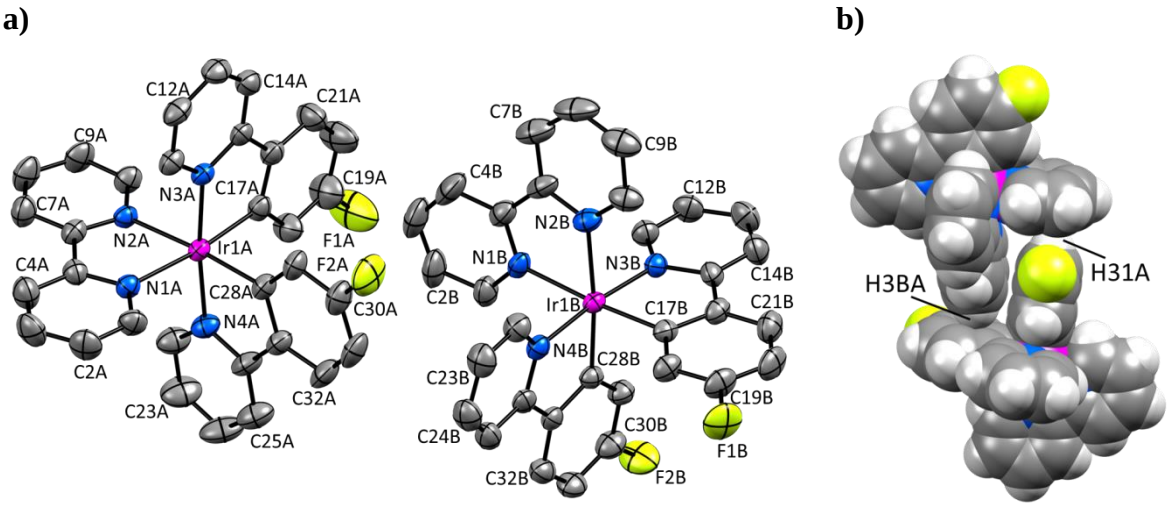

Fig. 13 Structures of the two independent Δ- and Λ-[Ir(**1**)$_2$(bpy)]$^+$ cations in *rac*-4{[Ir(**1**)$_2$(bpy)][PF$_6$]}·Et$_2$O·2CH$_2$Cl$_2$. a) H atoms and solvent molecules omitted and ellipsoids plotted at 40% probability level. Selected bond parameters: Ir1A–N1A = 2.136(4), Ir1A–N2A = 2.136(4), Ir1A–N3A = 2.050(4), Ir1A–N4A = 2.058(4), Ir1A–C17A = 2.007(5), Ir1A–C28A = 2.013(5), F1A–C19A = 1.356(8), F2A–C30A = 1.360(8), Ir1B–N1B = 2.144(4), Ir1B–N2B = 2.141(5), Ir1B–N3B = 2.044(4), Ir1B–N4B = 2.050(4), Ir1B–C17B = 2.011(5), Ir1B–C28B = 2.009(5), F1B–C19B = 1.367(7), F2B–C30B = 1.364(7) Å; N1A–Ir1A–N2A = 76.45(16), N3A–Ir1A–C17A = 80.2(2), N4A–Ir1A–C28A = 80.8(2), N1A–Ir1A–C17A = 173.29(17), N2A–Ir1A–C28A = 175.01(18), N3A–Ir1A–N4A = 173.46(18), N1B–Ir1B–N2B = 76.88(19), N3B–Ir1B–C17B = 80.0(2), N4B–Ir1B–C28B = 80.4(2), N1B–Ir1B–C17B = 175.15(17), N2B–Ir1B–C28B = 173.20(18), N3B–Ir1B–N4B = 173.52(16)°. b) Space-fill model showing the face-to-face and edge-to-face π-stacking interactions between the two independent cations.

4. Photophysical Properties

UV-Vis absorption spectra are similar for complexes [Ir(C^N)$_2$(bpy)][PF$_6$] with C^N = **1**, **3**–**5** and **7** and are pictured in Fig. 14. [Ir(**6**)$_2$(bpy)][PF$_6$] (brown line) exhibits a slightly different absorption spectrum with a less intense maximum in the UV region and more intense absorption bands above 320 nm compared to the other complexes in this series. Ligand-centred, spin-allowed π*←π transitions lead to the intense absorption maxima observed in the UV region, around 250–265 nm. Less intense absorption bands between 350 and 450 nm are attributed to spin-allowed charge transfer transitions (^{1}MLCT and ^{1}LLCT), whereas the very weak tails above 450 nm arise from spin-forbidden direct excitation to the triplet state (^{3}MLCT, ^{3}LLCT and ^{3}LC).[21]

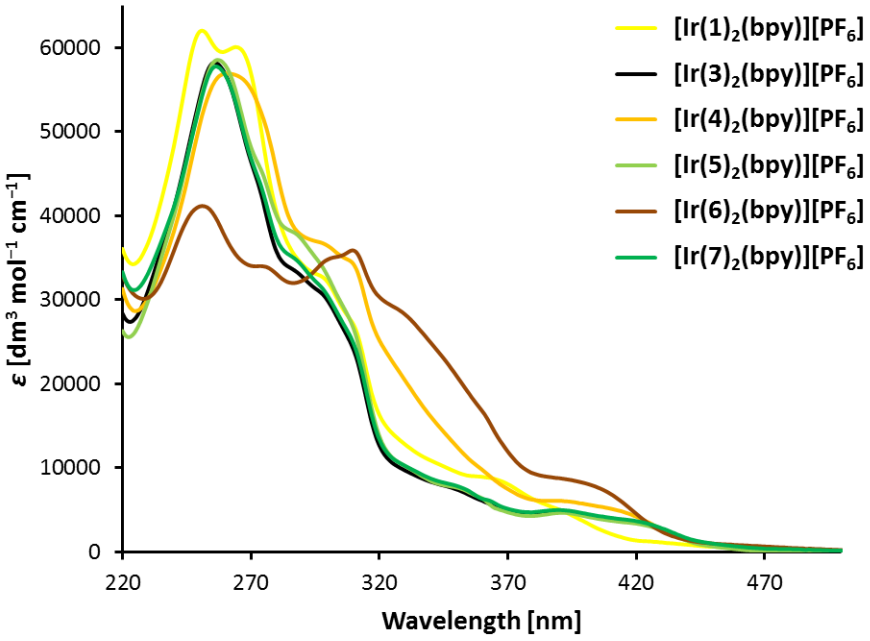

Fig. 14 UV-Vis absorption spectra in CH_3CN solution (1.0×10^{-5} M) of $[Ir(C\text{^}N)_2(bpy)][PF_6]$ complexes with C^N = **1**, **3**–**7**.

Excitation of CH_3CN solutions of complexes $[Ir(C\text{^}N)_2(bpy)][PF_6]$ with C^N = **1**, **3**–**7** leads to the photoluminescence spectra shown in Fig. 15. Emission profiles are independent of the excitation wavelength for all complexes. With respect to unsubstituted parent compound $[Ir(ppy)_2(bpy)][PF_6]$,[103] the emission maximum of fluoro complex $[Ir(\mathbf{1})_2(bpy)][PF_6]$ is blue-shifted by 28 nm in CH_3CN solution. This shift from 585 to 557 nm is attributed to the electron-withdrawing nature of the fluorine substituents, leading to a stabilization of the HOMO localized on the iridium centre and the phenyl rings of the cyclometallating ligands.

Introduction of a strongly electron-withdrawing sulfone group shifts the emission maximum significantly to the blue region, by 64 or even 92 nm when compared to reference compounds $[Ir(\mathbf{1})_2(bpy)][PF_6]$ and $[Ir(ppy)_2(bpy)][PF_6]$,[103] respectively. All three complexes containing a sulfone substituent are therefore green emitters and exhibit vibrational structure in their emission bands. No influence on the photoluminescence position was observed by changing the alkyl substituent on the sulfone group from methyl in $[Ir(\mathbf{3})_2(bpy)][PF_6]$ to sterically hindered *tert*-butyl in $[Ir(\mathbf{5})_2(bpy)][PF_6]$ and long-chain dodecyl in

[Ir(**7**)$_2$(bpy)][PF$_6$]. Only the relative intensities of the vibrational bands are affected slightly by changing the alkyl group (*cf.* Fig. 15).

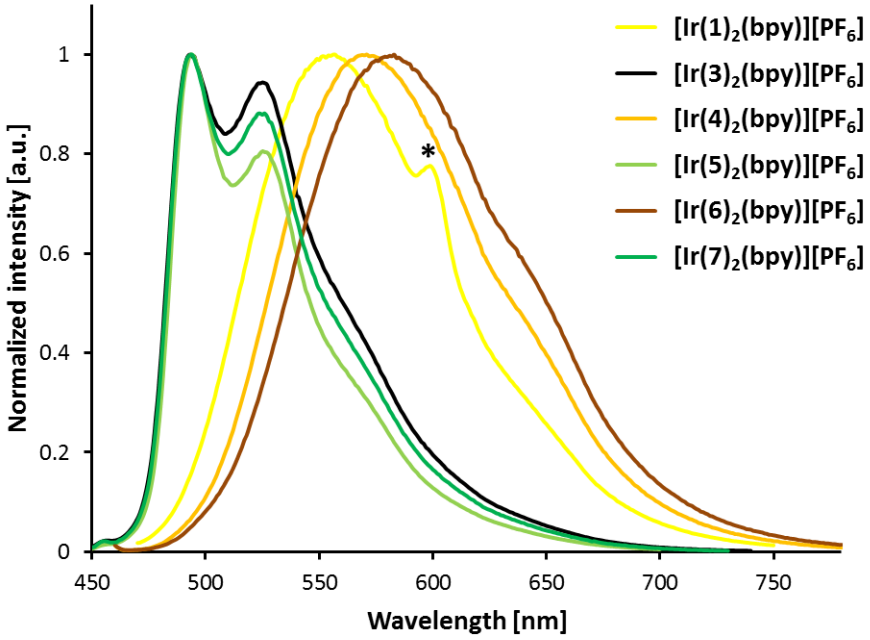

Fig. 15 Emission spectra of complexes [Ir(C^N)$_2$(bpy)][PF$_6$] with C^N = **1**, **3**–**7** in CH_3CN solution (1.0×10^{-5} M). λ_{exc} = 300 nm for [Ir(**1**)$_2$(bpy)][PF$_6$], 400 nm for [Ir(C^N)$_2$(bpy)][PF$_6$] (C^N = **3**–**7**). * = Harmonic (600 nm) of the excitation.

Replacing the fluoro- by thioether-substituents in [Ir(**4**)$_2$(bpy)][PF$_6$] and [Ir(**6**)$_2$(bpy)][PF$_6$] leads to small red-shifts in the emission maximum of 11 and 20 nm for *tert*-butyl- and dodecylthio-groups, respectively. Compared to [Ir(ppy)$_2$(bpy)][PF$_6$],[103] the emission is blue-shifted by 8–17 nm for both complexes, resulting from a weak electron-accepting nature of the thioether substituents. In contrast to the sulfone complexes, all three yellow emitters [Ir(C^N)$_2$(bpy)][PF$_6$] (C^N = **1**, **4** and **6**) have broad, unstructured emission bands. Such broad emission spectra indicate larger charge transfer contributions to the triplet emissive state, which is a mix of ^{3}MLCT, ^{3}LLCT and ^{3}LC excited states in this type of iridium complexes. Vibrational structure, however, as observed for sulfone complexes [Ir(C^N)$_2$(bpy)][PF$_6$] with C^N = **3**, **5** and **7**, suggests a larger ligand-centred character of the emissive state.[21]

Sulfone complexes $[Ir(\mathbf{3})_2(bpy)][PF_6]$, $[Ir(\mathbf{5})_2(bpy)][PF_6]$ and $[Ir(\mathbf{7})_2(bpy)][PF_6]$ exhibit high quantum yields in de-aerated CH_3CN solution of 64 and 74%, together with long excited state lifetimes in the range 2.33 to 3.36 µs (Table 1). These τ values are an order of magnitude longer than for the fluoro- and thioether-substituted analogues (0.224 to 0.528 µs). PLQYs are also substantially lower for $[Ir(C\text{^}N)_2(bpy)][PF_6]$ (C^N = **1**, **4** and **6**) with respect to the sulfone compounds, ranging from 15 to 36%. When solutions are not de-aerated, both quantum yield and excited state lifetime values are considerably lower due to strong oxygen quenching of the excited state.

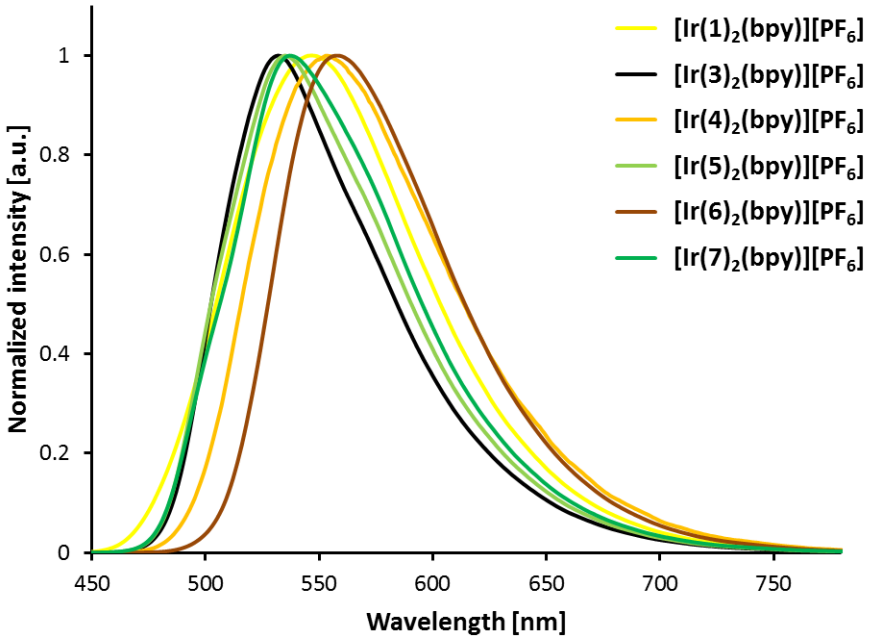

Fig. 16 Solid state emission spectra of powder samples of complexes $[Ir(C\text{^}N)_2(bpy)][PF_6]$ with C^N = **1**, **3**–**7**. λ_{exc} = 405 nm.

Solid state photoluminescence spectra shown in Fig. 16 were obtained upon excitation of powder samples of complexes $[Ir(C\text{^}N)_2(bpy)][PF_6]$ (C^N = **1**, **3**–**7**). Emission maxima and quantum yields are given in Table 1. In the solid state, all complexes are yellow emitters, with maxima ranging from 532 to 558 nm and broad, unstructured emission profiles. Small blue-shifts of 10 to 19 nm are observed on going from solution to powder samples for compounds with fluoro and thioether groups. The three sulfone complexes exhibit more pronounced

bathochromic shifts of roughly 40 nm, which can be attributed to strong intermolecular interactions, together with the loss of vibrational structure. Quantum yields are much lower in powder samples for most of the complexes (2.6 to 6.6%), suggesting strong quenching in the solid state. With 15 and 23%, [Ir(**5**)$_2$(bpy)][PF$_6$] and [Ir(**1**)$_2$(bpy)][PF$_6$] show significantly higher PLQYs than the other complexes. In the case of [Ir(**5**)$_2$(bpy)][PF$_6$], this observation can be assigned to a beneficial effect of the bulky *tert*-butyl substituents, leading to less excited state quenching due to intermolecular interactions.

Table 1 Photophysical properties of complexes [Ir(C^N)$_2$(bpy)][PF$_6$] (C^N = **1**, **3**–**7**) in CH$_3$CN solution and as powder samples.

Compound	**CH$_3$CN solution**				**Powder**	
	λ_{exc} **[nm]**	λ_{em}^{max} **[nm]**	**PLQY [%]**[a]	τ **[µs]** (χ)[a,b]	λ_{em}^{max} **[nm]**[c]	**PLQY [%]**
[Ir(**1**)$_2$(bpy)][PF$_6$]	269	557	36	0.224 (1.0)	547	23
[Ir(**3**)$_2$(bpy)][PF$_6$]	262	493, 525	74	2.33 (1.3)	532	6.6
[Ir(**4**)$_2$(bpy)][PF$_6$]	260	568	24	0.528 (1.0)	553	4.9
[Ir(**5**)$_2$(bpy)][PF$_6$]	262	493, 523	64	3.36 (1.3)	535	15
[Ir(**6**)$_2$(bpy)][PF$_6$]	252	577	15	0.369 (1.1)	558	2.6
[Ir(**7**)$_2$(bpy)][PF$_6$]	262	493, 524	64	3.21 (1.4)	537	4.2

[a] Measured in de-aerated solution. [b] λ_{exc} = 280 nm for [Ir(C^N)$_2$(bpy)][PF$_6$] with C^N = **3**, **5** and **7**; 340 nm for [Ir(C^N)$_2$(bpy)][PF$_6$] with C^N = **1**, **4** and **6**. [c] λ_{exc} = 405 nm.

5. Electrochemical Properties

Table 2 Cyclic voltammetric data of [Ir(C^N)$_2$(bpy)][PF$_6$] (C^N = **1**, **3**–**7**) measured in de-aerated CH$_3$CN solution with glassy carbon working, Pt counter and Ag pseudo-reference electrode, 0.1 M TBAPF$_6$ supporting electrolyte and a scan rate of 0.1 V s^{-1}. Referenced to Fc/Fc$^+$. qr = quasi-reversible, ir = irreversible.

Compound	$E_{1/2}^{ox}$ **[V]**	$E_{1/2}^{red}$ **[V]**	$\Delta E_{1/2}$ **[V]**
[Ir(**1**)$_2$(bpy)][PF$_6$]	+1.07^{qr}	−1.74, −2.41^{ir}, −2.54	2.81
[Ir(**3**)$_2$(bpy)][PF$_6$]	+1.18	−1.72, −2.16, −2.61^{ir}	2.90
[Ir(**4**)$_2$(bpy)][PF$_6$]	+1.04^{ir}	−1.75, −2.48^{ir}, −2.57^{ir}	2.79
[Ir(**5**)$_2$(bpy)][PF$_6$]	+1.19	−1.73, −2.18, −2.43	2.92
[Ir(**6**)$_2$(bpy)][PF$_6$]	+0.82^{ir}, +0.98^{ir}	−1.76, −2.55^{ir}	2.58
[Ir(**7**)$_2$(bpy)][PF$_6$]	+1.25	−1.71, −2.16, −2.39	2.96

Cyclic voltammetric data for $[Ir(C\hat{}N)_2(bpy)][PF_6]$ (C^N = **1**, **3**–**7**) in CH_3CN solution with respect to Fc/Fc^+ are summarized in Table 2 and cyclic voltammograms showing the oxidation and first reduction waves are given in Fig. 17. With values between −1.71 and −1.76 V, the first reduction potentials are similar for all complexes. This observation is in accordance with the assumption that the LUMO is localized on the ancillary ligand in $[Ir(C\hat{}N)_2(N\hat{}N)]^+$ complexes, which is the 2,2'-bipyridine ligand for all compounds in this series. The first reductions of all complexes are reversible and comparable to that of the parent complex $[Ir(ppy)_2(bpy)][PF_6]$ (−1.77 V *vs.* Fc/Fc^+ in DMF).[103] One or two more reduction waves are seen within the accessible solvent window for all complexes, but have not been investigated in detail.

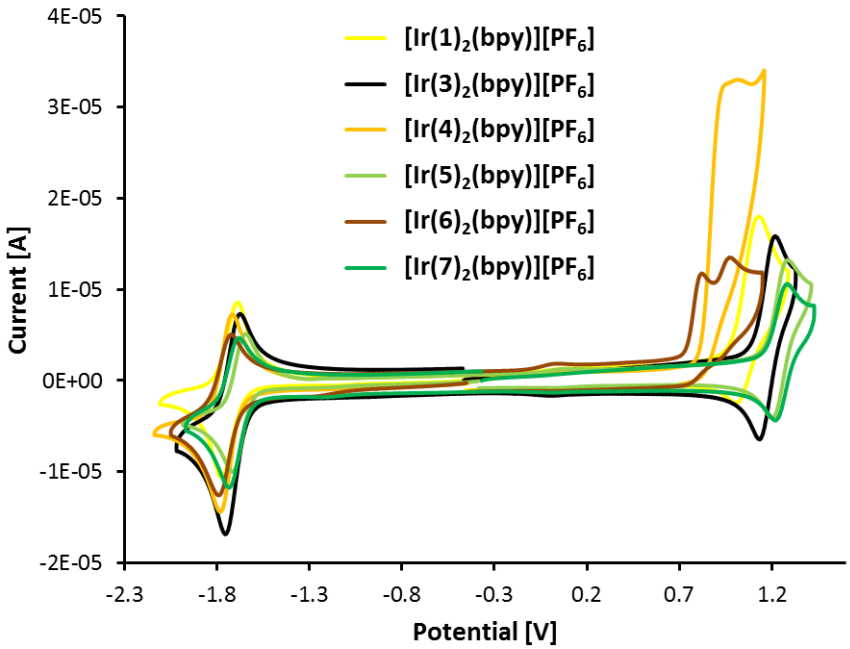

Fig. 17 Cyclic voltammograms of $[Ir(C\hat{}N)_2(bpy)][PF_6]$ (C^N = **1**, **3**–**7**) with respect to Fc/Fc^+ in de-aerated CH_3CN solution with glassy carbon working, Pt counter and Ag pseudo-reference electrode, 0.1 M $TBAPF_6$ supporting electrolyte, scan rate = 0.1 V s^{-1}.

Quasi-reversible to reversible oxidation waves are observed for complexes with strongly electron-withdrawing groups (fluoro and sulfonyl) and occur at higher potential than for unsubstituted $[Ir(ppy)_2(bpy)][PF_6]$ (+0.84 V). $[Ir(\mathbf{4})_2(bpy)][PF_6]$ (+1.04 V) and

[Ir(**6**)$_2$(bpy)][PF$_6$] (+0.82 and 0.98 V) exhibit irreversible oxidation waves at lower potentials than the remaining four complexes, in agreement with the introduction of weakly accepting thioether moieties on the cyclometallating ligands. The electrochemical HOMO-LUMO gap values, $\Delta E_{1/2}$, follow the same trend as the solution emission maxima (*vide supra*). With respect to [Ir(**1**)$_2$(bpy)][PF$_6$], the three sulfone-substituted complexes [Ir(C^N)$_2$(bpy)][PF$_6$] (C^N = **3**, **5**, **7**) exhibit a larger $\Delta E_{1/2}$, consistent with a blue-shifted emission. [Ir(**4**)$_2$(bpy)][PF$_6$] and [Ir(**6**)$_2$(bpy)][PF$_6$] have both a smaller electrochemical band gap and a photoluminescence maximum that is slightly red-shifted compared to [Ir(**1**)$_2$(bpy)][PF$_6$].

6. Electroluminescence and Device Data

Due to their promising photophysical properties in solution and powder, sulfone complexes [Ir(**3**)$_2$(bpy)][PF$_6$] and [Ir(**5**)$_2$(bpy)][PF$_6$] were tested in light emitting electrochemical cells by Dr. Henk Bolink and co-workers at the University of Valencia. Devices composed of ITO/PEDOT:PSS/[Ir(C^N)$_2$(bpy)][PF$_6$]:[Bmim][PF$_6$] 4:1/Al were measured under block-wave pulsed current conditions[21,93,107] with a frequency of 1 kHz, average current density of 100 A m^{-2} and 50% duty cycles. Both complexes show yellow-green electroluminescence in LEEC configuration (see Fig. 18 and Table 3) with electroluminescence maxima around 550 nm and a shoulder at 495 nm.

Table 3 Device parameters for LEECs containing complexes [Ir(**3**)$_2$(bpy)][PF$_6$] and [Ir(**5**)$_2$(bpy)][PF$_6$]. Configuration: ITO/PEDOT:PSS/[Ir(C^N)$_2$(bpy)][PF$_6$]:[Bmim][PF$_6$] 4:1/Al. Measured by applying a block-wave pulsed current of 100 A m^{-2} at a frequency of 1 kHz and duty cycles of 50%.[21,93,107]

Compound	t_{on} **[min]**	Lum_{max} **[cd m^{-2}]**	$t_{1/2}$ **[min]**	**PCE [lm W^{-1}]**	**EQE [%]**	λ_{EL}^{max} **[nm]**
[Ir(**3**)$_2$(bpy)][PF$_6$]	19	182	69	0.9	0.5	495 sh, 553
[Ir(**5**)$_2$(bpy)][PF$_6$]	17	71	25	0.3	0.2	495 sh, 548

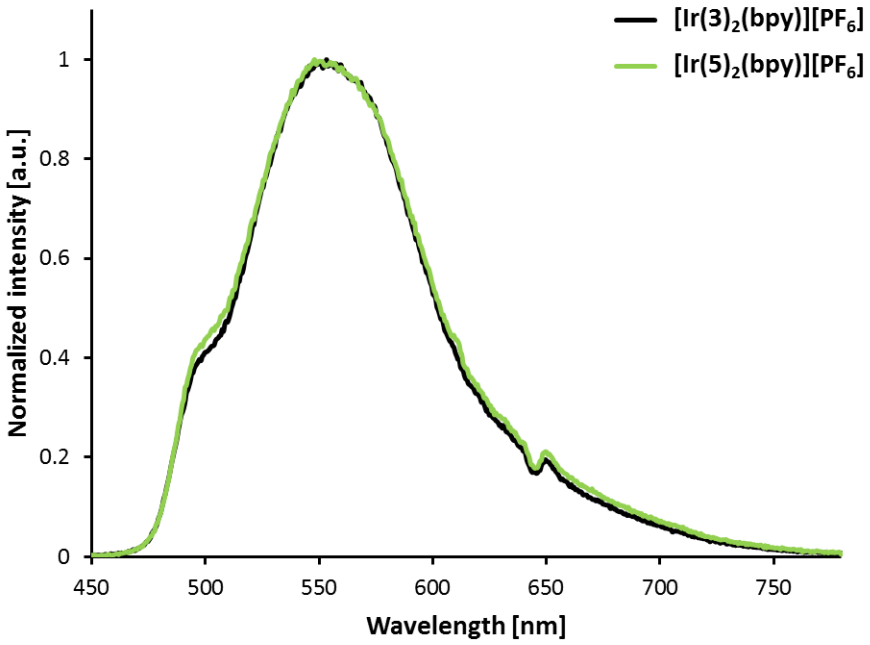

Fig. 18 Normalized electroluminescence spectra of sulfone complexes [Ir(**3**)$_2$(bpy)][PF$_6$] and [Ir(**5**)$_2$(bpy)][PF$_6$] applied in LEEC devices.

Performance parameters of LEEC devices with complexes [Ir(**3**)$_2$(bpy)][PF$_6$] and [Ir(**5**)$_2$(bpy)][PF$_6$] are given in Table 3. Luminance and average voltage curves *vs.* time are depicted in Fig. 19. Complex [Ir(**3**)$_2$(bpy)][PF$_6$] reaches a significantly higher maximum luminance level of 182 cd m^{-2} compared to [Ir(**5**)$_2$(bpy)][PF$_6$] (71 cd m^{-2}). Similarly, power conversion efficiency and external quantum efficiency values are more than two times higher for [Ir(**3**)$_2$(bpy)][PF$_6$] (0.9 lm W^{-1} and 0.5%) than for [Ir(**5**)$_2$(bpy)][PF$_6$] (0.3 lm W^{-1} and 0.2%). The turn-on time (defined as the time needed to reach maximum luminance) does not change considerably from methyl-substituted [Ir(**3**)$_2$(bpy)][PF$_6$] (19 min) to *tert*-butyl-substituted [Ir(**5**)$_2$(bpy)][PF$_6$] (17 min) and is relatively long in relation to the half lifetime exhibited by the LEECs. Turn-on times reported in the literature for green light emitting electrochemical cells range from less than five seconds[80,82,93,107] to several minutes[80,108] and more than one hour.[80,109] Device lifetimes ($t_{1/2}$, time to reach half of the luminance maximum) amount to 25 and 69 min, with [Ir(**3**)$_2$(bpy)][PF$_6$] exhibiting better device stability. These observed half lifetimes are relatively short, but similar to green LEECs reported in the literature, where lifetimes range from several minutes to a few hours.[80,93,107–110]

In general, methylsulfonyl-substituted complex [Ir(**3**)$_2$(bpy)][PF$_6$] shows superior device performance with respect to [Ir(**5**)$_2$(bpy)][PF$_6$]. Apparently, in this case, the bulky *tert*-butyl groups do not enhance LEEC performance. This observation is in contrast to the frequently reported improvement of device parameters such as efficiency, turn-on time, luminance and stability by the introduction of sterically hindered substituents.[21]

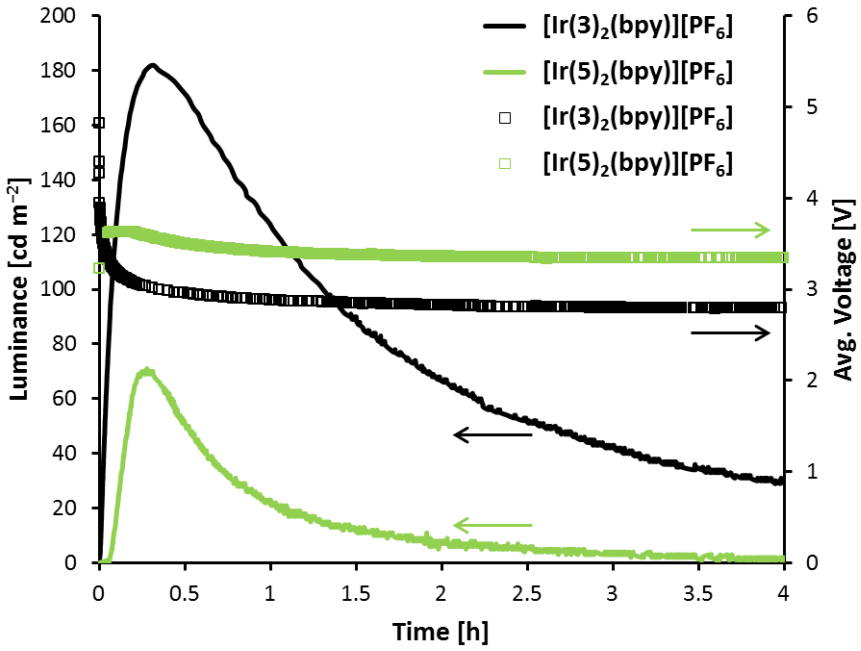

Fig. 19 Luminance and average voltage curves *vs.* time of LEECs containing [Ir(**3**)$_2$(bpy)][PF$_6$] (black) and [Ir(**5**)$_2$(bpy)][PF$_6$] (green). Device configuration: ITO/PEDOT:PSS/ [Ir(C^N)$_2$(bpy)][PF$_6$]:[Bmim][PF$_6$] 4:1/Al. Measured by applying a block-wave pulsed current of 100 A m^{-2} at a frequency of 1 kHz and duty cycles of 50%.[21,93,107]

7. Conclusions

Iridium complexes with thioether- and sulfone-substituted cyclometallating ligands have been prepared in order to investigate the influence of these groups on the photophysical and electrochemical properties. As expected, the strongly electron-withdrawing sulfone moieties lead to blue-shifted emission maxima. With respect to unsubstituted parent complex $[Ir(ppy)_2(bpy)]^+$, λ_{em}^{max} is hypsochromically shifted by 92 nm in CH_3CN solution, indicating the potential of the sulfone group to act as an alternative to the commonly used fluoro substituents for green and blue emission. Emission bands show vibrational structure, suggesting a pronounced ligand-centred (^{3}LC) character of the emissive triplet state. Only a negligible effect was observed upon changing the alkyl group on the sulfone from methyl to sterically hindered *tert*-butyl and long-chain dodecyl. All three sulfone-based iridium complexes are green emitters with high quantum yields of 64 and 74% in solution and excited state lifetimes an order of magnitude longer than those of the remaining complexes in this series.

Complexes with fluoro-, *tert*-butylthio- and dodecylthio-substituted cyclometallating ligands are yellow emitters with maxima between 557 and 577 nm. They exhibit lower PLQYs than the sulfone complexes ranging from 15 to 36% and emission profiles are broad and unstructured. Compared to $[Ir(ppy)_2(bpy)]^+$, emission maxima of the thioether complexes are slightly blue-shifted, attributed to the weakly electron accepting character of the thioether groups. Alkyl substituents have a small influence on the emission bands, leading to a 9 nm red-shift on going from *tert*-butyl to dodecyl.

As powder samples, all complexes in this series are yellow emitters with λ_{em}^{max} between 532 and 558 nm and broad emission bands. Solid state quantum yields are substantially lower, with the highest value found for fluoro complex $[Ir(\mathbf{1})_2(bpy)][PF_6]$ (23%). Electrochemical data obtained from CH_3CN solutions of the complexes support the trends observed from photoluminescence measurements.

Complexes with methylsulfonyl and *tert*-butylsulfonyl substituents on the cyclometallating ligands were tested in light emitting electrochemical cells. Both complexes exhibited yellow-green electroluminescence in device configuration. Unfortunately, they showed relatively low maximum luminance levels, together with low efficiencies and short device lifetimes (<69 min). In conclusion, the introduction of a bulky substituent does not

have a beneficial effect in this case; superior device performance is observed for complex $[Ir(\mathbf{3})_2(bpy)][PF_6]$ with methylsulfone-containing cyclometallating ligands.

The results from this series of complexes support the possibility of using sulfone groups in the search of fluorine-free blue emitting iridium complexes. However, all complexes are substituted in 5-position of the cyclometallating ligands (*meta* to the Ir-C bond). Investigating the influence of the substitution position of the sulfonyl moiety (in 3- and 4-position) on the photophysical and electrochemical properties would be interesting. The investigation of regioisomerism in iridium complexes and its consequences on structural, photophysical, electrochemical and device properties will be reported in the following chapter.

8. Experimental

The following experimental procedures have been written by the author of this thesis and have been published in Dalton Transactions.[95]

8.1. General

2-(4-Fluorophenyl)pyridine (H**1**) was synthesized according to a literature protocol and ^{1}H NMR spectroscopic data matched those reported.[96] $[Ir(cod)Cl]_2$[111] and $[Ir(\mathbf{1})_2Cl]_2$[112] were prepared as reported.

8.2. 2-(4-(Methylthio)phenyl)pyridine (H2)

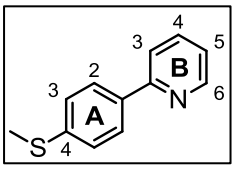

2-(4-(Methylthio)phenyl)pyridine (H**2**) has been synthesized previously,[97] but the following procedure gives a higher yield. 2-(4-Fluorophenyl)pyridine (H**1**) (617 mg, 3.56 mmol, 1.0 eq.) and an excess of NaSMe (1.06 g, 14.3 mmol, 4.0 eq.) were added to NMP (18 mL) in a microwave vial. The violet reaction mixture was heated at 80 °C for 1 h in a microwave reactor to give a dark brown suspension. This was poured into a mixture of H_2O and brine (3:1, 100 mL). The resulting yellow precipitate was separated by filtration, dissolved in CH_2Cl_2 and dried over Na_2SO_4. The solvent was removed under reduced pressure to yield 2-(4-(methylthio)phenyl)pyridine (H**2**) as a yellow solid (665 mg, 3.30 mmol, 92.7%). M.p.

59.5 °C. ^{1}H NMR (500 MHz, $CDCl_3$) δ/ppm 8.67 (ddd, J = 4.9, 1.9, 1.0 Hz, 1H, H^{B6}), 7.93 (m, 2H, H^{A2}), 7.76–7.67 (overlapping m, 2H, H^{B3+B4}), 7.34 (m, 2H, H^{A3}), 7.21 (ddd, J = 7.3, 4.8, 1.4 Hz, 1H, H^{B5}), 2.53 (s, 3H, H^{Me}). $^{13}C\{^{1}H\}$ NMR (126 MHz, $CDCl_3$) δ/ppm 157.0 (C^{B2}), 149.8 (C^{B6}), 139.9 (C^{A4}), 136.9 (C^{B4}), 136.2 (C^{A1}), 127.3 (C^{A2}), 126.5 (C^{A3}), 122.1 (C^{B5}), 120.2 (C^{B3}), 15.7 (C^{Me}). IR (solid, $\tilde{\nu}$/cm^{-1}) 3086 (w), 3046 (w), 3002 (w), 2981 (w), 2919 (w), 1982 (w), 1910 (w), 1767 (w), 1661 (w), 1605 (w), 1583 (s), 1569 (s), 1552 (m), 1498 (w), 1458 (s), 1431 (s), 1399 (m), 1322 (w), 1296 (w), 1256 (w), 1227 (w), 1190 (m), 1154 (w), 1121 (w), 1098 (m), 1089 (m), 1057 (w), 1008 (m), 988 (m), 969 (w), 958 (m), 884 (w), 830 (m), 772 (s), 738 (s), 725 (m), 708 (m), 675 (w), 636 (w), 616 (w), 569 (w), 544 (w), 484 (m), 461 (m). ESI-MS *m/z* 202.0 $[M+H]^+$ (calc. 202.1). Found C 71.43, H 5.57, N 6.75; $C_{12}H_{11}NS$ requires C 71.60, H 5.51, N 6.96%.

8.3. 2-(4-(Methylsulfonyl)phenyl)pyridine (H3)

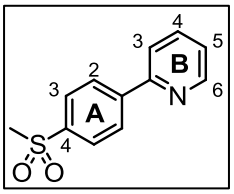

2-(4-(Methylthio)phenyl)pyridine (H**2**) (1.00 g, 4.97 mmol, 1.0 eq.) and sodium tungstate dihydrate (819 mg, 2.48 mmol, 0.50 eq.) were dissolved in MeOH (35 mL). H_2O_2 (30%, 1.20 mL, 1.36 g, 12.0 mmol, 2.4 eq.) was added and the mixture was stirred overnight at room temperature. The suspension was poured into a mixture of H_2O and brine (3:1, 200 mL) and extracted with CH_2Cl_2 (3 × 100 mL). The combined organic layers were dried over Na_2SO_4 and the solvent was removed under reduced pressure to yield 2-(4-(methylsulfonyl)phenyl)pyridine (H**3**) as a white powder (1.14 g, 4.89 mmol, 98.4%). M.p. 134.5 °C. ^{1}H NMR (500 MHz, $CDCl_3$) δ/ppm 8.75 (ddd, J = 4.7, 1.8, 1.0 Hz, 1H, H^{B6}), 8.21 (m, 2H, H^{A2}), 8.10–7.99 (m, 2H, H^{A3}), 7.87–7.75 (m, 2H, H^{B3+B4}), 7.34 (ddd, J = 7.0, 4.8, 1.6 Hz, 1H, H^{B5}), 3.09 (s, 3H, H^{Me}). $^{13}C\{^{1}H\}$ NMR (126 MHz, $CDCl_3$) δ/ppm 155.4 (C^{B2}), 150.2 (C^{B6}), 144.7 (C^{A1}), 140.7 (C^{A4}), 137.3 (C^{B4}), 128.0 (C^{A3}), 127.9 (C^{A2}), 123.5 (C^{B5}), 121.3 (C^{B3}), 44.7 (C^{Me}). IR (solid, $\tilde{\nu}$/cm^{-1}) 3000 (w), 2921 (w), 1586 (m), 1563 (w), 1465 (m), 1435 (m), 1392 (w), 1314 (w), 1292 (s), 1185 (w), 1146 (s), 1087 (m), 1030 (w), 1013 (w), 988 (w), 964 (m), 848 (m), 789 (m), 776 (s), 750 (s), 677 (m), 636 (w), 616 (m), 562 (m), 548 (s), 514 (s). ESI-MS *m/z* 234.0 $[M+H]^+$ (calc. 234.1). Found C 62.03, H 4.95, N 6.29; $C_{12}H_{11}NO_2S$ requires C 61.78, H 4.75, N 6.00%.

8.4. 2-(4-(*tert*-Butylthio)phenyl)pyridine (H4)

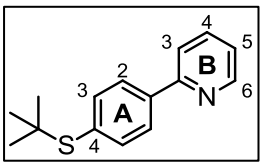

NaH (60% suspension in mineral oil, 235 mg, 5.88 mmol, 2.0 eq.) was suspended in DMF (8 mL) under N_2. 2-Methyl-2-propanethiol (0.660 mL, 528 mg, 5.80 mmol, 2.0 eq.) was added, leading to gas evolution and white foam. After the reaction mixture had been stirred for 10 min at room temperature, 2-(4-fluorophenyl)pyridine (H**1**) (501 mg, 2.89 mmol, 1.0 eq.) was added dissolved in DMF (2 mL). The mixture was heated at 120 °C for 24 h. The yellow-orange solution was allowed to cool to room temperature and was then poured into a mixture of H_2O and brine (3:1, 50 mL). The resulting suspension was stirred for 5 min. The precipitate was separated by filtration, washed with H_2O and dried under vacuum. 2-(4-(*tert*-Butylthio)phenyl)pyridine (H**4**) was isolated as a pale brown solid (704 mg, 2.89 mmol, quant.). M.p. 90.7 °C. ^{1}H NMR (500 MHz, $CDCl_3$) δ/ppm 8.70 (ddd, J = 4.8, 1.9, 1.1 Hz, 1H, H^{B6}), 7.95 (m, 2H, H^{A2}), 7.82–7.70 (overlapping m, 2H, H^{B3+B4}), 7.64 (m, 2H, H^{A3}), 7.26 (m, 1H, H^{B5}), 1.32 (s, 9H, $H^{t\mathrm{Bu}}$). ^{13}C{^{1}H} NMR (126 MHz, $CDCl_3$) δ/ppm 157.0 (C^{B2}), 149.9 (C^{B6}), 139.8 (C^{A1}), 137.9 (C^{A3}), 137.0 (C^{B4}), 133.9 (C^{A4}), 127.0 (C^{A2}), 122.5 (C^{B5}), 120.8 (C^{B3}), 46.4 ($C^{C\mathrm{tBu}}$), 31.2 ($C^{t\mathrm{Bu}}$). IR (solid, $\tilde{\nu}$/cm^{-1}) 1462 (m), 1429 (m), 1391 (w), 1366 (m), 1305 (w), 1289 (w), 1259 (w), 1168 (m), 1152 (m), 1098 (m), 1059 (w), 1031 (w), 1014 (m), 989 (m), 934 (w), 899 (w), 844 (s), 780 (s), 748 (s), 725 (m), 682 (w), 633 (w), 618 (w), 579 (w), 560 (m), 520 (m), 491 (m). ESI-MS *m/z* 244.0 $[M+H]^+$ (calc. 244.1). Found C 74.04, H 7.01, N 5.64; $C_{15}H_{17}NS$ requires C 74.03, H 7.04, N 5.76%.

8.5. 2-(4-(*tert*-Butylsulfonyl)phenyl)pyridine (H5)

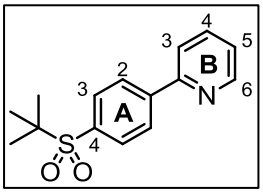

2-(4-(*tert*-Butylthio)phenyl)pyridine (H**4**) (501 mg, 2.06 mmol, 1.0 eq.) and sodium tungstate dihydrate (352 mg, 1.07 mmol, 0.52 eq.) were dissolved in MeOH (13 mL). H_2O_2 (30%, 0.500 mL, 568 mg, 5.01 mmol, 2.4 eq.) was added and the suspension was stirred at room temperature for 20 h. CH_2Cl_2 (100 mL) was then added and the white precipitate was separated by filtration. The filtrate was washed with H_2O (50 mL), the aqueous layer extracted with CH_2Cl_2 (100 mL) and the combined organic layers dried over Na_2SO_4. The solvent was removed under reduced pressure and the residue was purified by column chromatography (silica, CH_2Cl_2–1% MeOH). 2-(4-(*tert*-Butylsulfonyl)phenyl)pyridine (H**5**) was isolated as a white powder (473 mg, 1.72 mmol, 83.5%). M.p. 174.4 °C. ^{1}H NMR (500 MHz, $CDCl_3$) δ/ppm 8.75 (ddd, J = 4.7, 1.8, 1.1 Hz, 1H, H^{B6}), 8.17 (m, 2H, H^{A2}), 7.98

(m, 2H, H^{A3}), 7.88–7.75 (overlapping m, 2H, H^{B3+B4}), 7.33 (ddd, *J* = 6.7, 4.8, 1.7 Hz, 1H, H^{B5}), 1.37 (s, 9H, H^{tBu}). $^{13}C\{^1H\}$ NMR (126 MHz, $CDCl_3$) *δ*/ppm 155.7 (C^{B2}), 150.2 (C^{B6}), 144.5 (C^{A1}), 137.3 (C^{B4}), 135.5 (C^{A4}), 131.1 (C^{A3}), 127.3 (C^{A2}), 123.5 (C^{B5}), 121.3 (C^{B3}), 60.1 (C^{CtBu}), 23.8 (C^{tBu}). IR (solid, $\tilde{\nu}$/cm^{-1}) 2970 (w), 1586 (m), 1561 (w), 1463 (m), 1436 (w), 1395 (w), 1314 (w), 1287 (s), 1192 (w), 1159 (w), 1131 (s), 1113 (m), 1079 (s), 1011 (m), 990 (w), 853 (m), 801 (w), 778 (s), 752 (w), 741 (w), 722 (m), 694 (s), 646 (s), 616 (m), 579 (s), 555 (m), 517 (m), 505 (m). ESI-MS *m/z* 276.0 $[M+H]^+$ (calc. 276.1). Found C 65.41, H 6.31, N 5.14; $C_{15}H_{17}NO_2S$ requires C 65.43, H 6.22, N 5.09%.

8.6. 2-(4-(Dodecylthio)phenyl)pyridine (H6)

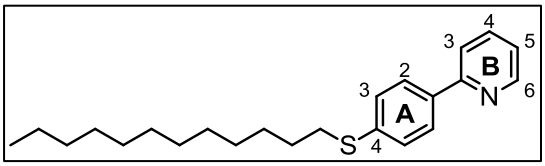

NaH (60% suspension in mineral oil, 187 mg, 4.67 mmol, 2.0 eq.) was suspended in DMF (6 mL) under N_2. 1-Dodecanethiol (1.14 mL, 956 mg, 4.63 mmol, 2.0 eq.) and then DMF (4 mL) were added and the mixture was stirred for 10 min. 2-(4-Fluorophenyl)pyridine (H**1**) (400 mg, 2.31 mmol, 1.0 eq.) was added dissolved in DMF (2 mL) and the mixture was heated at 120 °C for 4 h. The yellow mixture was allowed to cool to room temperature and was then poured into a mixture of H_2O and brine (3:1, 50 mL). The resulting suspension was stirred for 5 min and the precipitate was removed by filtration, washed with H_2O, dried under vacuum and purified by column chromatography (silica, *n*-hexane/EtOAc 6:1 changing to 2:1). 2-(4-(Dodecylthio)phenyl)pyridine (H**6**) was isolated as a white solid (542 mg, 1.52 mmol, 65.8%). M.p. 65.3 °C. ^1H NMR (500 MHz, $CDCl_3$) *δ*/ppm 8.67 (ddd, *J* = 4.8, 1.8, 1.0 Hz, 1H, H^{B6}), 7.91 (m, 2H, H^{A2}), 7.78–7.63 (overlapping m, 2H, H^{B3+B4}), 7.39 (m, 2H, H^{A3}), 7.21 (ddd, *J* = 7.2, 4.8, 1.4 Hz, 1H, H^{B5}), 2.97 (m, 2H, $H^{SC\underline{H}2}$), 1.68 (m, 2H, $H^{SCH2C\underline{H}2}$), 1.43 (m, 2H, $H^{SCH2CH2C\underline{H}2}$), 1.35–1.12 (overlapping m, 16H, H^{CH2}), 0.88 (t, *J* = 6.9 Hz, 3H, H^{CH3}). $^{13}C\{^1H\}$ NMR (126 MHz, $CDCl_3$) *δ*/ppm 157.0 (C^{B2}), 149.8 (C^{B6}), 138.7 (C^{A4}), 136.9 (C^{B4}), 136.7 (C^{A1}), 128.6 (C^{A3}), 127.3 (C^{A2}), 122.1 (C^{B5}), 120.3 (C^{B3}), 33.3 ($C^{S\underline{C}H2}$), 32.1 (C^{CH2}), 29.8 (C^{CH2}), 29.8 (C^{CH2}), 29.7 (C^{CH2}), 29.7 (C^{CH2}), 29.5 (C^{CH2}), 29.3 (C^{CH2}), 29.2 ($C^{SCH2\underline{C}H2}$), 29.0 ($C^{SCH2CH2\underline{C}H2}$), 22.8 ($C^{CH2}$), 14.3 ($C^{CH3}$). IR (solid, $\tilde{\nu}$/cm^{-1}) 3059 (w), 3003 (w), 2954 (m), 2917 (s), 2872 (m), 2850 (s), 1585 (s), 1571 (m), 1554 (w), 1496 (w), 1463 (s), 1432 (s), 1398 (w), 1379 (m), 1297 (m), 1259 (w), 1242 (w), 1191 (w), 1153 (w), 1122 (w), 1100 (m), 1056 (w), 1009 (m), 988 (w), 834 (m), 768 (s), 734 (m), 720 (m), 708 (m), 636 (w), 616 (w), 548

(w), 513 (w), 488 (w), 462 (m). MALDI-TOF MS (no matrix) *m/z* 355.7 $[M]^+$ (calc. 355.2). Found C 77.75, H 9.76, N 4.05; $C_{23}H_{33}NS$ requires C 77.69, H 9.35, N 3.94%.

8.7. 2-(4-(Dodecylsulfonyl)phenyl)pyridine (H7)

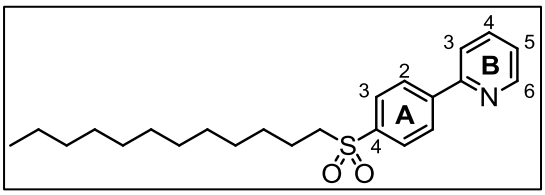

2-(4-(Dodecylthio)phenyl)pyridine (H**6**) (212 mg, 0.597 mmol, 1.0 eq.) and sodium tungstate dihydrate (98.4 mg, 0.298 mmol, 0.50 eq.) were suspended in MeOH (15 mL). H_2O_2 (35%, 0.120 mL, 136 mg, 1.40 mmol, 2.3 eq.) was added and the mixture was stirred at room temperature overnight. H_2O (50 mL) was added and the suspension was stirred for 15 min, after which time the precipitate was separated by filtration, washed with H_2O and dried under vacuum. 2-(4-(Dodecylsulfonyl)phenyl)pyridine (H**7**) was isolated as a white solid (207 mg, 0.534 mmol, 89.4%). M.p. 84.4 °C. ^{1}H NMR (500 MHz, $CDCl_3$) δ/ppm 8.74 (ddd, J = 5.0, 1.3 Hz, 1H, H^{B6}), 8.19 (m, 2H, H^{A2}), 8.00 (m, 2H, H^{A3}), 7.81 (m, 2H, H^{B3+B4}), 7.33 (ddd, J = 6.7, 4.7, 1.6 Hz, 1H, H^{B5}), 3.11 (m, 2H, $H^{SO2C\underline{H}2}$), 1.71 (m, 2H, $H^{SO2CH2C\underline{H}2}$), 1.35 (m, 2H, $H^{SO2CH2CH2C\underline{H}2}$), 1.31–1.18 (overlapping m, 16H, H^{CH2}), 0.87 (t, J = 7.0 Hz, 3H, H^{CH3}). $^{13}C\{^1H\}$ NMR (126 MHz, $CDCl_3$) δ/ppm 155.5 (C^{B2}), 150.2 (C^{B6}), 144.6 (C^{A1}), 139.3 (C^{A4}), 137.2 (C^{B4}), 128.7 (C^{A3}), 127.8 (C^{A2}), 123.5 (C^{B5}), 121.3 (C^{B3}), 56.6 ($C^{SO2C\underline{H}2}$), 32.0 (C^{CH2}), 29.72 (C^{CH2}), 29.69 (C^{CH2}), 29.6 (C^{CH2}), 29.5 (C^{CH2}), 29.4 (C^{CH2}), 29.2 (C^{CH2}), 28.4 ($C^{SO2CH2CH2C\underline{H}2}$), 22.9 ($C^{SO2CH2C\underline{H}2}$), 22.8 ($C^{CH2}$), 14.3 ($C^{CH3}$). IR (solid, $\tilde{\nu}$/cm^{-1}) 2915 (m), 2848 (m), 1586 (w), 1562 (w), 1468 (m), 1436 (w), 1399 (w), 1301 (m), 1285 (m), 1271 (m), 1144 (s), 1099 (w), 1086 (m), 1027 (w), 1009 (w), 991 (w), 853 (w), 776 (s), 758 (m), 739 (m), 722 (w), 691 (s), 635 (w), 621 (m), 606 (s), 557 (m), 528 (s), 496 (m). ESI-MS *m/z* 388.2 $[M+H]^+$ (calc. 388.2). Found C 71.30, H 8.79, N 3.77; $C_{23}H_{33}NO_2S$ requires C 71.27, H 8.58, N 3.61%.

8.8. $[Ir(3)_2Cl]_2$

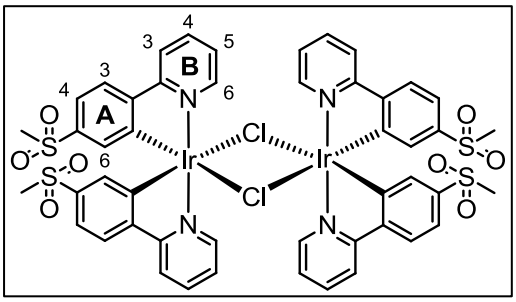

$[Ir(cod)Cl]_2$ (285 mg, 0.424 mmol, 1.0 eq.) and 2-(4-(methylsulfonyl)phenyl)pyridine (H**3**) (395 mg, 1.69 mmol, 4.0 eq.) were suspended in degassed 2-ethoxyethanol (10 mL) and the mixture was purged with argon. The suspension was heated at reflux

overnight and was then allowed to cool to room temperature. The yellow precipitate was separated by filtration, washed with H_2O and EtOH and dried under vacuum. $[Ir(\mathbf{3})_2Cl]_2$ was isolated as a yellow powder (516 mg, 0.373 mmol, 88.0%). ^{1}H NMR (500 MHz, $CDCl_3$) δ/ppm 9.21 (ddd, J = 5.8, 1.6, 0.7 Hz, 4H, H^{B6}), 8.06 (ddd, J = 8.4, 1.4, 0.7 Hz, 4H, H^{B3}), 7.95 (ddd, J = 8.1, 7.5, 1.6 Hz, 4H, H^{B4}), 7.68 (d, J = 8.2 Hz, 4H, H^{A3}), 7.36 (dd, J = 8.1, 1.9 Hz, 4H, H^{A4}), 7.01 (ddd, J = 7.3, 5.7, 1.4 Hz, 4H, H^{B5}), 6.36 (d, J = 1.9 Hz, 4H, H^{A6}), 2.75 (s, 12H, H^{Me}). ^{13}C{^{1}H} NMR (126 MHz, $CDCl_3$) δ/ppm 166.5 (C^{B2}), 151.8 (C^{B6}), 149.2 (C^{A2}), 144.8 ($C^{A1/A5}$), 139.8 ($C^{A1/A5}$), 138.0 (C^{B4}), 128.1 (C^{A6}), 124.4 (C^{B5}), 124.3 (C^{A3}), 121.0 (C^{A4}), 120.6 (C^{B3}), 44.3 (C^{Me}). LC-ESI-MS m/z 657.1 $[Ir(\mathbf{3})_2]^+$ (calc. 657.1), 698.2 $[Ir(\mathbf{3})_2(CH_3CN)]^+$ (calc. 698.1).

8.9. $[Ir(\mathbf{4})_2Cl]_2$

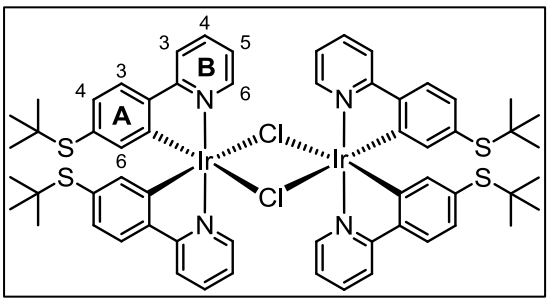

2-(4-(*tert*-Butylthio)phenyl)pyridine (H**4**) (401 mg, 1.65 mmol, 4.0 eq.) was dissolved in 2-ethoxyethanol (18 mL) in a microwave vial and the solution purged with N_2. $[Ir(cod)Cl]_2$ (280 mg, 0.417 mmol, 1.0 eq.) was added and the mixture heated at 110 °C for 1.5 h in a microwave reactor. The yellow precipitate was separated by filtration, washed with H_2O and EtOH and dried under vacuum to yield $[Ir(\mathbf{4})_2Cl]_2$ as a yellow solid (383 mg, 0.269 mmol, 64.5%). ^{1}H NMR (500 MHz, $CDCl_3$) δ/ppm 9.29 (d, J = 5.5 Hz, 4H, H^{B6}), 7.89 (d, J = 8.0 Hz, 4H, H^{B3}), 7.76 (*pseudo*-td, J = 7.8, 1.6 Hz, 4H, H^{B4}), 7.42 (d, J = 8.0 Hz, 4H, H^{A3}), 6.92 (dd, J = 7.9, 1.7 Hz, 4H, H^{A4}), 6.78 (ddd, J = 7.3, 5.7, 1.5 Hz, 4H, H^{B5}), 5.96 (d, J = 1.6 Hz, 4H, H^{A6}), 0.98 (s, 36H, H^{tBu}). LC-ESI-MS m/z 677.2 $[Ir(\mathbf{4})_2]^+$ (calc. 677.2), 718.3 $[Ir(\mathbf{4})_2(CH_3CN)]^+$ (calc. 718.2).

8.10. $[Ir(\mathbf{5})_2Cl]_2$

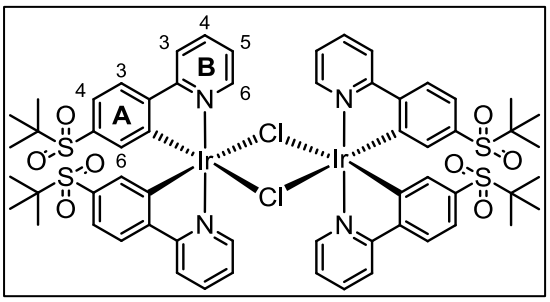

2-(4-(*tert*-Butylsulfonyl)phenyl)pyridine (H**5**) (151 mg, 0.548 mmol, 2.0 eq.) was suspended in 2-ethoxyethanol (3 mL) and H_2O (1 mL) under N_2 atmosphere. $IrCl_3 \cdot xH_2O$ (ca. 82% $IrCl_3$, 99.2 mg, 0.272 mmol, 1.0 eq.) was added and the

suspension was heated at reflux for 21 h. The mixture was allowed to cool to room temperature and then H_2O was added. The precipitate was removed by filtration and was washed with H_2O to give $[Ir(\mathbf{5})_2Cl]_2$ as a yellow powder (101 mg, 65.0 µmol, 47.8%). ^{1}H NMR (500 MHz, $CDCl_3$) δ/ppm 9.30 (ddd, J = 5.8, 1.5, 0.6 Hz, 4H, H^{B6}), 8.03 (ddd, J = 8.3, 1.3, 0.6 Hz, 4H, H^{B3}), 7.93 (td, J = 7.8, 1.5 Hz, 4H, H^{B4}), 7.64 (d, J = 8.2 Hz, 4H, H^{A3}), 7.30 (dd, J = 8.1, 1.7 Hz, 4H, H^{A4}), 6.98 (ddd, J = 7.3, 5.7, 1.5 Hz, 4H, H^{B5}), 6.21 (d, J = 1.8 Hz, 4H, H^{A6}), 1.00 (s, 36H, $H^{t\mathrm{Bu}}$). ^{13}C{^{1}H} NMR (126 MHz, $CDCl_3$) δ/ppm 166.7 (C^{B2}), 151.8 (C^{B6}), 148.9 (C^{A2}), 143.8 ($C^{A1/A5}$), 137.9 (C^{B4}), 134.4 ($C^{A5/A1}$), 131.6 (C^{A6}), 124.13 (C^{B5}), 124.07 (C^{A4}), 123.5 (C^{A3}), 120.5 (C^{B3}), 59.7 ($C^{C\mathrm{tBu}}$), 23.5 ($C^{t\mathrm{Bu}}$). LC-ESI-MS *m/z* 741.2 $[Ir(\mathbf{5})_2]^+$ (calc. 741.1), 782.1 $[Ir(\mathbf{5})_2(CH_3CN)]^+$ (calc. 782.2), 823.1 $[Ir(\mathbf{5})_2(CH_3CN)_2]^+$ (calc. 823.2).

8.11. $[Ir(\mathbf{7})_2Cl]_2$

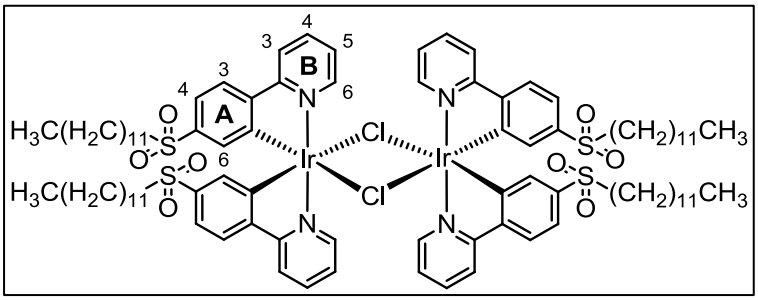

$IrCl_3{\cdot}xH_2O$ (ca. 82% $IrCl_3$, 93.5 mg, 0.257 mmol, 1.0 eq.) was added to a suspension of 2-(4-(dodecylsulfonyl)phenyl)-pyridine (H**7**) (200 mg, 0.516 mmol, 2.0 eq.) in 2-ethoxyethanol (3 mL) and H_2O (1 mL) under N_2 atmosphere. The mixture was heated at reflux for 22 h. After cooling to room temperature, the mixture was poured into H_2O (50 mL) and stirred at room temperature for a few minutes. The resulting suspension was poured into brine (40 mL) and stirred again at room temperature. The precipitate was removed by filtration, washed with H_2O, EtOH and Et_2O and dried under vacuum. $[Ir(\mathbf{7})_2Cl]_2$ was isolated as a yellow powder (216 mg, 0.108 mmol, 84.0%). ^{1}H NMR (500 MHz, $CDCl_3$) δ/ppm 9.23 (ddd, J = 5.7, 1.5, 0.6 Hz, 4H, H^{B6}), 8.04 (*pseudo*-dt, J = 8.4, 1.0 Hz, 4H, H^{B3}), 7.94 (*pseudo*-td, J = 7.8, 1.6 Hz, 4H, H^{B4}), 7.66 (d, J = 8.2 Hz, 4H, H^{A3}), 7.31 (dd, J = 8.1, 1.8 Hz, 4H, H^{A4}), 6.99 (ddd, J = 7.3, 5.7, 1.5 Hz, 4H, H^{B5}), 6.30 (d, J = 1.8 Hz, 4H, H^{A6}), 2.74 (m, 8H, $H^{SO2C\underline{H}2}$), 1.43 (m, 8H, $H^{SO2CH2C\underline{H}2}$), 1.33–1.05 (overlapping m, 72H, H^{CH2}), 0.88 (t, J = 7.0 Hz, 12H, H^{Me}). ^{13}C{^{1}H} NMR (126 MHz, $CDCl_3$) δ/ppm 166.6 (C^{B2}), 151.8 (C^{B6}), 149.0 (C^{A2}), 144.7 ($C^{A1/A5}$), 138.6 ($C^{A5/A1}$), 137.9 (C^{B4}), 128.9 (C^{A6}), 124.3 (C^{B5}), 124.2 (C^{A3}), 121.6 (C^{A4}), 120.5 (C^{B3}), 56.2 ($C^{SO2\underline{C}H2}$), 32.1 (C^{CH2}), 29.73 (C^{CH2}), 29.72 (C^{CH2}), 29.6 (C^{CH2}), 29.5 (C^{CH2}), 29.4 (C^{CH2}), 29.2 (C^{CH2}), 28.3 (C^{CH2}), 22.8 (C^{CH2}), 22.5 ($C^{SO2CH2\underline{C}H2}$), 14.3 ($C^{Me}$).

MALDI-TOF MS (no matrix) *m/z* 965.9 $[Ir(\mathbf{7})_2]^+$ (calc. 965.4).

8.12. $[Ir(1)_2(bpy)][PF_6]$

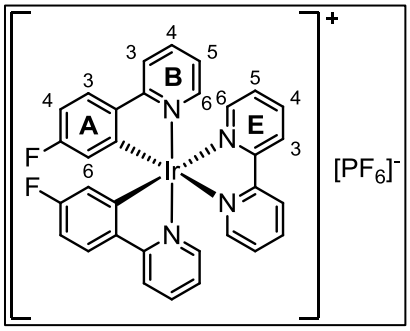

$[Ir(\mathbf{1})_2Cl]_2$ (350 mg, 0.306 mmol, 1.0 eq.) and bpy (150 mg, 0.960 mmol, 3.1 eq.) were suspended in MeOH (45 mL). The mixture was heated at reflux overnight and then allowed to cool to room temperature. After filtration, an excess of solid NH_4PF_6 was added to the filtrate and the mixture was stirred for 1 h at room temperature. The yellow precipitate was separated by filtration, washed with H_2O and redissolved in CH_2Cl_2. The solution was dried over Na_2SO_4 and the solvent removed under reduced pressure. The yellow residue was purified by column chromatography (silica, CH_2Cl_2 changing to CH_2Cl_2–2% MeOH). $[Ir(\mathbf{1})_2(bpy)][PF_6]$ was isolated as a yellow solid (405 mg, 0.483 mmol, 78.9%). ^{1}H NMR (500 MHz, CD_3CN) δ/ppm 8.53 (*pseudo*-dt, J = 8.3, 1.0 Hz, 2H, H^{E3}), 8.14 (*pseudo*-td, J = 8.0, 1.6 Hz, 2H, H^{E4}), 8.06–7.95 (overlapping m, 4H, H^{B3+E6}), 7.90–7.79 (overlapping m, 4H, H^{A3+B4}), 7.57 (ddd, J = 5.8, 1.5, 0.8 Hz, 2H, H^{B6}), 7.51 (ddd, J = 7.7, 5.5, 1.2 Hz, 2H, H^{E5}), 7.04 (ddd, J = 7.3, 5.8, 1.4 Hz, 2H, H^{B5}), 6.81 (m, 2H, H^{A4}), 5.89 (dd, J_{HF} = 9.6 Hz, J_{HH} = 2.6 Hz, 2H, H^{A6}). $^{13}C\{^1H\}$ NMR (126 MHz, CD_3CN) δ/ppm 167.1 (C^{B2}), 164.6 (d, J_{CF} = 253 Hz, C^{A5}), 156.6 (C^{E2}), 154.3 (d, J_{CF} = 5.8 Hz, C^{A1}), 151.8 (C^{E6}), 150.1 (C^{B6}), 141.4 (d, J_{CF} = 2.1 Hz, C^{A2}), 140.5 (C^{E4}), 139.8 (C^{B4}), 129.4 (C^{E5}), 128.1 (d_{CF}, J = 9.4 Hz, C^{A3}), 125.7 (C^{E3}), 124.5 (C^{B5}), 121.0 (C^{B3}), 118.3 (d_{CF}, J = 17.7 Hz, C^{A6}), 110.5 (d, J = 23.3 Hz, C^{A4}). IR (solid, $\tilde{\nu}$/cm^{-1}) 1594 (m), 1568 (m), 1555 (m), 1482 (w), 1447 (m), 1434 (m), 1314 (w), 1262 (w), 1245 (w), 1187 (m), 1163 (w), 1032 (w), 833 (s), 766 (s), 733 (m), 675 (w), 576 (m), 556 (s). UV/Vis (CH_3CN, 1.1×10^{-5} mol dm^{-3}) λ/nm (ε/dm^3 mol^{-1} cm^{-1}) 251 (62 000), 264 (60 000), 295 sh (33 000), 310 sh (2000), 395 sh (4300). Emission (CH_3CN, 1.1×10^{-5} mol dm^{-3}, λ_{exc} = 269 nm) λ_{em}^{max} = 557 nm. ESI-MS *m/z* 693.2 $[M–PF_6]^+$ (calc. 693.1). Found C 45.95, H 2.84, N 6.74; $C_{32}H_{22}F_8IrN_4P$ requires C 45.88, H 2.65, N 6.69%.

8.13. [Ir(3)$_2$(bpy)][PF$_6$]

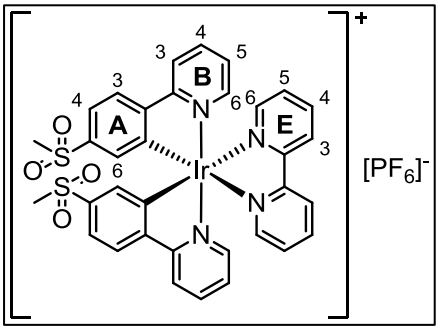

[Ir(**3**)$_2$Cl]$_2$ (109 mg, 57.4 µmol, 1.0 eq.) and bpy (26.9 mg, 0.172 mmol, 3.0 eq.) were suspended in MeOH (10 mL) and the mixture was heated at 120 °C in a microwave reactor for 1 h (15 bar). After cooling, an excess of solid NH_4PF_6 was added to the yellow solution and the resulting suspension was stirred for 15 min at room temperature. The yellow precipitate that formed was separated by filtration, washed with MeOH and redissolved in CH_2Cl_2. The solvent was removed under reduced pressure and the product was purified by column chromatography (silica, CH_2Cl_2 changing to CH_2Cl_2–4% MeOH). The major fraction was collected and solvent removed under reduced pressure. The residue was suspended in CH_2Cl_2 and the mixture sonicated and then filtered. [Ir(**3**)$_2$(bpy)][PF$_6$] was isolated as a yellow solid (92.3 mg, 96.4 µmol, 84.0%). ^{1}H NMR (500 MHz, CD_3CN) δ/ppm 8.54 (*pseudo*-dt, J = 8.3, 1.1 Hz, 2H, H^{E3}), 8.23 (*pseudo*-dt, J = 8.2, 1.1 Hz, 2H, H^{B3}), 8.15 (*pseudo*-td, J = 8.0, 1.6 Hz, 2H, H^{E4}), 8.02 (d, J = 8.3 Hz, 2H, H^{A3}), 7.98 (ddd, J = 8.0, 7.7, 1.5 Hz, 2H, H^{B4}), 7.95 (ddd, J = 5.4, 1.6, 0.8 Hz, 2H, H^{E6}), 7.72 (ddd, J = 5.8, 1.5, 0.7 Hz, 2H, H^{B6}), 7.58 (dd, J = 8.3, 1.9 Hz, 2H, H^{A4}), 7.51 (ddd, J = 7.7, 5.5, 1.2 Hz, 2H, H^{E5}), 7.21 (ddd, J = 7.4, 5.8, 1.4 Hz, 2H, H^{B5}), 6.70 (d, J = 1.9 Hz, 2H, H^{A6}), 2.89 (s, 6H, H^{Me}). ^{13}C{^{1}H} NMR (126 MHz, CD_3CN) δ/ppm 166.2 (C^{B2}), 156.6 (C^{E2}), 152.0 (C^{E6}), 151.2 (C^{A1}), 150.9 (C^{B6}), 150.2 (C^{A2}), 142.3 (C^{A5}), 140.7 (C^{E4}), 140.3 (C^{B4}), 129.6 (C^{A6+E5}), 126.31 (C^{A3}), 126.29 (C^{B5}), 125.8 (C^{E3}), 122.60 (C^{A4}), 122.58 (C^{B3}), 44.3 (C^{Me}). IR (solid, $\tilde{\nu}$/cm^{-1}) 2927 (w), 1608 (w), 1575 (w), 1475 (m), 1447 (w), 1430 (w), 1375 (w), 1294 (m), 1267 (w), 1144 (s), 1091 (m), 1062 (m), 1030 (w), 957 (m), 892 (w), 838 (s), 808 (m), 782 (m), 753 (s), 733 (m), 699 (m), 666 (w), 651 (w), 600 (w), 592 (w), 557 (s), 546 (s), 524 (m), 487 (s). UV/Vis (CH_3CN, 1.0 × 10^{-5} mol dm^{-3}) λ/nm (ε/dm^3 mol^{-1} cm^{-1}) 256 (58 000), 300 sh (30 000), 350 sh (7500), 390 (4900), 425 sh (3200). Emission (CH_3CN, 1.0 × 10^{-5} mol dm^{-3}, λ_{exc} = 262 nm) λ_{em}^{max} = 493, 525 nm. ESI-MS *m/z* 813.1 [M–PF$_6$]$^+$ (calc. 813.1). Found C 41.74, H 3.33, N 5.90; $C_{34}H_{28}F_6IrN_4O_4PS_2 \cdot H_2O$ requires C 41.84, H 3.10, N 5.74%.

8.14. $[Ir(4)_2(bpy)][PF_6]$

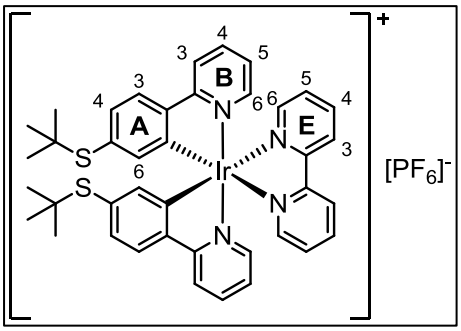

$[Ir(\mathbf{4})_2Cl]_2$ (144 mg, 0.101 mmol, 1.0 eq.) and bpy (66.0 mg, 0.423 mmol, 4.2 eq.) were suspended in MeOH (15 mL) and the mixture was heated at reflux for 16 h. The orange solution was allowed to cool to room temperature. An excess of solid NH_4PF_6 was added followed by enough H_2O to precipitate the product, and the resulting suspension was stirred for 10 min. The yellow precipitate was separated by filtration, washed with H_2O and MeOH and then redissolved in CH_2Cl_2. The solution was dried over Na_2SO_4 and the solvent was removed under reduced pressure. The residue was purified twice by column chromatography (silica, CH_2Cl_2 changing to CH_2Cl_2–1% MeOH; alumina, CH_2Cl_2 changing to CH_2Cl_2–5% MeOH). The residue was dissolved in MeOH and an excess of solid NH_4PF_6 followed by H_2O were added. The resulting suspension was stirred for 5 min, and the yellow precipitate was collected by filtration and redissolved in CH_2Cl_2. The solution was dried over Na_2SO_4 and the solvent was removed under reduced pressure. $[Ir(\mathbf{4})_2(bpy)][PF_6]$ was isolated as a yellow solid (139 mg, 0.142 mmol, 70.3%). ^{1}H NMR (500 MHz, CD_3CN) δ/ppm 8.54 (*pseudo*-dt, J = 8.2, 1.0 Hz, 2H, H^{E3}), 8.15 (*pseudo*-td, J = 7.9, 1.6 Hz, 2H, H^{E4}), 8.10–8.04 (overlapping m, 4H, H^{B3+E6}), 7.86 (ddd, J = 8.2, 7.6, 1.5 Hz, 2H, H^{B4}), 7.72 (d, J = 8.0 Hz, 2H, H^{A3}), 7.61 (*pseudo*-dt, J = 5.8, 1.2 Hz, 2H, H^{B6}), 7.51 (ddd, J = 7.5, 5.3, 1.2 Hz, 2H, H^{E5}), 7.13 (dd, J = 8.0, 1.7 Hz, 2H, H^{A4}), 7.05 (ddd, J = 7.4, 5.8, 1.4 Hz, 2H, H^{B5}), 6.30 (d, J = 1.7 Hz, 2H, H^{A6}), 1.00 (s, 18H, $H^{t\mathrm{Bu}}$). $^{13}C\{^1H\}$ NMR (126 MHz, CD_3CN) δ/ppm 167.7 (C^{B2}), 156.7 (C^{E2}), 151.8 (C^{E6}), 150.9 (C^{A5}), 150.3 (C^{B6}), 145.2 (C^{B6}), 140.4 (C^{A2}), 140.3 (C^{E4}), 139.7 (C^{A6}), 136.0 (C^{B4}), 131.6 (C^{A1}), 129.4 (C^{A4}), 125.7 (C^{E3}), 125.5 (C^{A3}), 124.8 (C^{B5}), 121.3 (C^{B3}), 46.8 ($C^{Ct\mathrm{Bu}}$), 31.1 ($C^{t\mathrm{Bu}}$). IR (solid, $\tilde{\nu}$/cm^{-1}) 2970 (w), 1607 (m), 1569 (m), 1472 (m), 1447 (m), 1425 (m), 1366 (m), 1313 (w), 1258 (w), 1162 (m), 1099 (w), 1062 (w), 875 (w), 834 (s), 778 (s), 765 (s), 733 (m), 650 (w), 600 (w), 557 (s). UV/Vis (CH_3CN, 1.0×10^{-5} mol dm^{-3}) λ/nm (ε/dm^3 mol^{-1} cm^{-1}) 261 (57 000), 305 sh (35 000), 415 sh (4800). Emission (CH_3CN, 1.0×10^{-5} mol dm^{-3}, λ_{exc} = 260 nm) λ_{em}^{max} = 568 nm. ESI-MS m/z 833.5 $[M–PF_6]^+$ (calc. 833.2). Found C 48.96, H 4.35, N 5.70; $C_{40}H_{40}F_6IrN_4PS_2$ requires C 49.12, H 4.12, N 5.73%.

8.15. $[Ir(5)_2(bpy)][PF_6]$

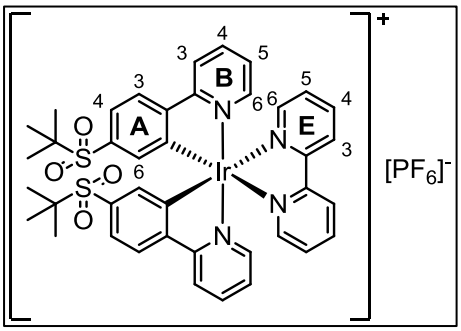

$[Ir(\mathbf{5})_2Cl]_2$ (101 mg, 65.0 µmol, 1.0 eq.) and bpy (44.3 mg, 0.284 mmol, 4.4 eq.) were suspended in MeOH (10 mL) and the mixture was heated at reflux for 14 h. The solution was left to cool to room temperature, and an excess of solid NH_4PF_6 was then added followed by enough H_2O to precipitate the product. The resulting suspension was stirred for 30 min. The yellow precipitate was separated by filtration, washed with H_2O and redissolved in CH_2Cl_2. After removal of the solvent under reduced pressure, the residue was purified by column chromatography (silica, CH_2Cl_2 changing to CH_2Cl_2–2% MeOH). $[Ir(\mathbf{5})_2(bpy)][PF_6]$ was isolated as a yellow solid (119 mg, 0.114 mmol, 87.7%). ^{1}H NMR (500 MHz, CD_3CN) δ/ppm 8.58 (dd, J = 8.2, 1.1 Hz, 2H, H^{E3}), 8.22 (d, J = 8.0 Hz, 2H, H^{B3}), 8.17 (*pseudo*-td, J = 8.0, 1.5 Hz, 2H, H^{E4}), 8.09 (d, J = 4.9 Hz, 2H, H^{E6}), 8.02–7.93 (overlapping m, 4H, H^{A3+B4}), 7.71 (*pseudo*-dt, J = 5.6, 1.1 Hz, 2H, H^{B6}), 7.51 (ddd, J = 6.9, 5.5, 1.2 Hz, 2H, H^{E5}), 7.45 (dd, J = 8.2, 1.8 Hz, 2H, H^{A4}), 7.20 (ddd, J = 7.4, 5.8, 1.4 Hz, 2H, H^{B5}), 6.50 (d, J = 1.8 Hz, 2H, H^{A6}), 0.93 (s, 18H, $H^{t\mathrm{Bu}}$). $^{13}C\{^1H\}$ NMR (126 MHz, CD_3CN) δ/ppm 166.2 (C^{B2}), 156.6 (C^{E2}), 152.3 (C^{E6}), 150.9 (C^{B6}), 150.6 ($C^{A1/A5}$), 150.1 (C^{A2}), 140.8 (C^{E4}), 140.4 (C^{B4}), 135.9 ($C^{A5/A1}$), 133.2 (C^{A6}), 129.6 (C^{E5}), 126.3 (C^{B5}), 125.9 (C^{E3}), 125.5 (C^{A4}), 125.4 (C^{A3}), 122.5 (C^{B3}), 60.3 ($C^{C\mathrm{tBu}}$), 23.5 ($C^{t\mathrm{Bu}}$). IR (solid, $\tilde{\nu}$/cm^{-1}) 2979 (w), 1607 (w), 1575 (w), 1475 (m), 1448 (w), 1430 (w), 1373 (w), 1285 (m), 1193 (w), 1129 (s), 1082 (m), 836 (s), 806 (m), 781 (m), 764 (m), 730 (w), 710 (m), 672 (m), 658 (m), 648 (m), 585 (m), 569 (m), 556 (s), 492 (m). UV/Vis (CH_3CN, 0.99 × 10^{-5} mol dm^{-3}) λ/nm (ε/dm^3 mol^{-1} cm^{-1}) 257 (59 000), 295 sh (35 000), 391 (4700), 420 sh (3400). Emission (CH_3CN, 0.99 × 10^{-5} mol dm^{-3}, λ_{exc} = 262 nm) λ_{em}^{max} = 493, 523 nm. ESI-MS *m/z* 897.2 $[M–PF_6]^+$ (calc. 897.2). Found C 45.51, H 4.05, N 5.56; $C_{40}H_{40}F_6IrN_4O_4PS_2 \cdot H_2O$ requires C 45.32, H 3.99, N 5.29%.

8.16. $[Ir(6)_2(bpy)][PF_6]$

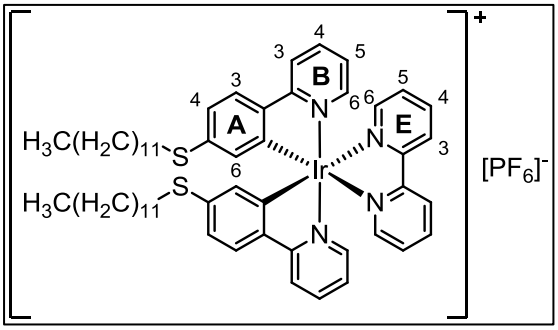

1-Dodecanethiol (60.0 µL, 50.4 mg, 0.249 mmol, 3.9 eq.) was added to a suspension of NaH (60% in mineral oil, 10.0 mg, 0.250 mmol, 3.9 eq.) in DMF (2 mL) under N_2 atmosphere. The mixture was stirred at room temperature for 10 min. $[Ir(\mathbf{1})_2(bpy)][PF_6]$ (53.0 mg, 63.3 mmol, 1.0 eq.) was added to the reaction mixture; this was heated at 120 °C for 1.5 h. The dark brown mixture was allowed to cool to room temperature and was then poured into a mixture of H_2O and brine (3:1, 20 mL). The resulting suspension was stirred for 30 min at room temperature. The brown-yellow precipitate was separated by filtration and was washed with H_2O. The solid was redissolved in CH_2Cl_2 and the solution dried over Na_2SO_4. Solvent was removed under reduced pressure and the product was purified by column chromatography (silica, CH_2Cl_2 changing to CH_2Cl_2–2% MeOH). $[Ir(\mathbf{6})_2(bpy)][PF_6]$ was isolated as an orange solid (56.1 mg, 46.7 µmol, 73.8%). ^{1}H NMR (500 MHz, CD_3CN) δ/ppm 8.54 (*pseudo*-dt, J = 8.3, 1.0 Hz, 2H, H^{E3}), 8.15 (*pseudo*-td, J = 7.9, 1.6 Hz, 2H, H^{E4}), 8.06 (ddd, J = 5.4, 1.5, 0.7 Hz, 2H, H^{E6}), 8.00 (*pseudo*-dt, J = 8.4, 1.1 Hz, 2H, H^{B3}), 7.83 (ddd, J = 8.2, 7.4, 1.5 Hz, 2H, H^{B4}), 7.68 (d, J = 8.3 Hz, 2H, H^{A3}), 7.58 (*pseudo*-dt, J = 5.9, 1.1 Hz, 2H, H^{B6}), 7.53 (ddd, J = 7.7, 5.4, 1.2 Hz, 2H, H^{E5}), 7.00 (ddd, J = 7.3, 5.8, 1.4 Hz, 2H, H^{B5}), 6.94 (dd, J = 8.2, 1.9 Hz, 2H, H^{A4}), 6.09 (d, J = 1.9 Hz, 2H, H^{A6}), 2.63 (m, 4H, H^{SCH2}), 1.40 (m, 4H, $H^{SCH2CH2}$), 1.35–1.16 (overlapping m, 36H, H^{CH2}), 0.89 (t, J = 7.0 Hz, 6H, H^{CH3}). $^{13}C\{^1H\}$ NMR (126 MHz, CD_3CN) δ/ppm 168.0 (C^{B2}), 156.7 (C^{E2}), 151.8 (C^{A1+E6}), 150.1 (C^{B6}), 141.6 (C^{A2}), 141.5 (C^{A5}), 140.3 (C^{E4}), 139.4 (C^{B4}), 129.4 (C^{E5}), 128.7 (C^{A6}), 126.1 (C^{A3}), 125.6 (C^{E3}), 123.9 (C^{B5}), 122.0 (C^{A4}), 120.5 (C^{B3}), 32.6 (C^{CH2}), 32.0 (C^{SCH2}), 30.3 (C^{CH2}), 30.3 (C^{CH2}), 30.2 (C^{CH2}), 30.1 (C^{CH2}), 29.9 (C^{CH2}), 29.7 ($C^{SCH2CH2}$), 29.4 (C^{CH2}), 23.4 (C^{CH2}), 14.4 (S^{CH3}). IR (solid, $\tilde{\nu}$/cm^{-1}) 2922 (m), 2852 (m), 1606 (m), 1567 (m), 1537 (w), 1472 (m), 1446 (m), 1423 (m), 1373 (w), 1315 (w), 1261 (w), 1244 (w), 1164 (w), 1095 (m), 1062 (w), 1030 (w), 876 (w), 835 (s), 791 (m), 769 (s), 732 (m), 650 (w), 639 (w), 556 (s), 520 (w). UV/Vis (CH_3CN, 0.99 × 10^{-5} mol dm^{-3}) λ/nm (ε/dm^3 mol^{-1} cm^{-1}) 251 (41 000), 310 (36 000), 400 sh (8200). Emission (CH_3CN, 0.99 × 10^{-5} mol dm^{-3}, λ_{exc} = 252 nm) λ_{em}^{max} = 583 nm. ESI-MS *m/z* 1058.1 $[M–PF_6]^+$ (calc. 1057.5). Found C 56.02, H 6.00, N 4.73; $C_{56}H_{72}F_6IrN_4PS_2$ requires C 55.93, H 6.04, N 4.66%.

8.17. [Ir(7)$_2$(bpy)][PF$_6$]

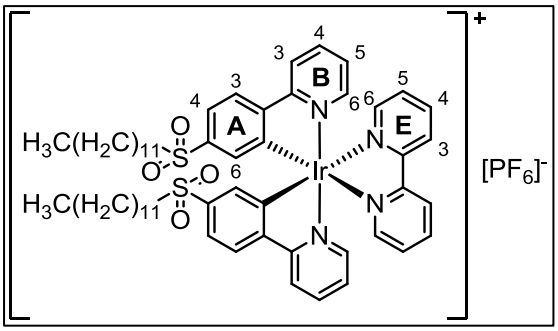

[Ir(**7**)$_2$Cl]$_2$ (214 mg, 0.107 mmol, 1.0 eq.) and bpy (50.1 mg, 0.321 mmol, 3.0 eq.) were suspended in MeOH (15 mL) and the mixture was heated at reflux for 2 d. After cooling to room temperature, the mixture was filtered. An excess of NH_4PF_6 followed by H_2O were added to the orange filtrate and the resulting suspension was stirred for 5 min. The precipitate was collected by filtration, washed with H_2O and redissolved in CH_2Cl_2. Solvent was removed under reduced pressure and the residue was purified twice by column chromatography (silica, CH_2Cl_2 changing to CH_2Cl_2–1% MeOH; silica, CH_2Cl_2–1% MeOH). [Ir(**7**)$_2$(bpy)][PF$_6$] was isolated as a yellow solid (81.1 mg, 64.0 µmol, 30.0%). ^{1}H NMR (500 MHz, CD_3CN) δ/ppm 8.56 (*pseudo*-dt, J = 8.4, 1.0 Hz, 2H, H^{E3}), 8.23 (*pseudo*-dt, J = 8.1, 0.9 Hz, 2H, H^{B3}), 8.17 (*pseudo*-td, J = 7.9, 1.5 Hz, 2H, H^{E4}), 8.04–7.96 (overlapping m, 6H, H$^{A3+B4+E6}$), 7.71 (ddd, J = 5.8, 1.5, 0.7 Hz, 2H, H^{B6}), 7.55–7.47 (m, 4H, H^{A4+E5}), 7.21 (ddd, J = 7.5, 5.8, 1.4 Hz, 2H, H^{B5}), 6.58 (d, J = 1.8 Hz, 2H, H^{A6}), 2.87 (m, 4H, H$^{SO2C\underline{H}2}$), 1.40–1.01 (overlapping m, 40H, H^{CH2}), 0.88 (t, J = 7.1 Hz, 6H, H^{CH3}). ^{13}C{^{1}H} NMR (126 MHz, CD_3CN) δ/ppm 166.2 (C^{B2}), 156.6 (C^{E2}), 152.1 (C^{E6}), 151.1 (C$^{A1/A5}$), 150.9 (C^{B6}), 150.1 (C^{A2}), 140.8 (C^{E4}), 140.4 (C^{B4}), 140.3 (C$^{A5/A1}$), 130.8 (C^{A6}), 129.6 (C^{E5}), 126.3 (C^{B5}), 126.2 (C^{A3}), 125.9 (C^{E3}), 123.2 (C^{A4}), 122.5 (C^{B3}), 56.3 (C$^{SO2\underline{C}H2}$), 32.6 (C^{CH2}), 30.33 (C^{CH2}), 30.32 (C^{CH2}), 30.2 (C^{CH2}), 30.1 (C^{CH2}), 30.0 (C^{CH2}), 29.7 (C^{CH2}), 28.6 (C^{CH2}), 23.8 (C^{CH2}), 23.4 (C^{CH2}), 14.4 (C^{CH3}). IR (solid, $\tilde{\nu}$/cm^{-1}) 2923 (m), 2853 (w), 1608 (w), 1576 (w), 1476 (m), 1448 (w), 1430 (w), 1375 (w), 1294 (m), 1140 (s), 1090 (m), 1063 (w), 836 (s), 762 (s), 728 (m), 667 (m), 652 (w), 606 (m), 582 (w), 556 (s), 500 (m). UV/Vis (CH_3CN, 1.0×10^{-5} mol dm^{-3}) λ/nm (ε/dm^3 mol^{-1} cm^{-1}) 256 (58 000), 310 sh (25 000), 350 sh (7900), 390 (5000), 420 sh (3700). Emission (CH_3CN, 1.0×10^{-5} mol dm^{-3}, λ_{exc} = 262 nm) λ_{em}^{max} = 493, 524 nm. ESI-MS *m/z* 1121.6 [*M*–PF$_6$]$^+$ (calc. 1121.5). Found C 53.38, H 5.57, N 4.72; $C_{56}H_{72}F_6IrN_4O_4PS_2$ requires C 53.11, H 5.73, N 4.42%.

8.18. Crystallography

2-(4-(Methylsulfonyl)phenyl)pyridine (H3). $C_{12}H_{11}NO_2S$, M = 233.29, colourless block, monoclinic, space group $C2/c$, a = 23.4437(15), b = 7.1763(5), c = 16.5008(11) Å, β = 129.026(3)°, U = 2156.6(2) Å^3, Z = 8, D_c = 1.437 Mg m^{-3}, μ(Mo-Kα) = 0.282 mm^{-1}, T =

123 K. Total 30251 reflections, 3021 unique, R_{int} = 0.0269. Refinement of 2681 reflections (146 parameters) with $I>2\sigma(I)$ converged at final $R1$ = 0.0323 ($R1$ all data = 0.0376), $wR2$ = 0.0913 ($wR2$ all data = 0.0962), gof = 1.057. CCDC 972690.

2-(4-(*tert*-Butylsulfonyl)phenyl)pyridine (H5). $C_{15}H_{17}NO_2S$, M = 275.37, colourless block, monoclinic, space group $C2/c$, a = 22.2664(12), b = 6.1121(4), c = 22.0876(11) Å, β = 110.398(2)°, U = 2817.5(3) Å^3, Z = 8, D_c = 1.298 Mg m^{-3}, μ(Mo-Kα) = 2.019 mm^{-1}, T = 296 K. Total 7450 reflections, 2523 unique, R_{int} = 0.0275. Refinement of 2228 reflections (175 parameters) with $I>2\sigma(I)$ converged at final $R1$ = 0.0378 ($R1$ all data = 0.0420), $wR2$ = 0.1024 ($wR2$ all data = 0.1068), gof = 1.080. CCDC 972692.

[Ir(3)$_2$Cl]$_2$·2CH$_2$Cl$_2$. $C_{50}H_{44}Cl_6Ir_2N_4O_8S_4$, M = 1554.31, yellow plate, orthorhombic, space group $Pbca$, a = 22.0732(12), b = 21.3598(11), c = 23.0604(12) Å, U = 10872.5(10) Å^3, Z = 8, D_c = 1.899 Mg m^{-3}, μ(Cu-Kα) = 13.963 mm^{-1}, T = 123 K. Total 59052 reflections, 9726 unique, R_{int} = 0.1107. Refinement of 6764 reflections (699 parameters) with $I>2\sigma(I)$ converged at final $R1$ = 0.0470 ($R1$ all data = 0.0820), $wR2$ = 0.1111 ($wR2$ all data = 0.1295), gof = 1.008. CCDC 972691.

Δ-[Ir(1)$_2$(bpy)][PF$_6$]. $C_{32}H_{22}F_2IrN_4P$, M = 837.73, yellow block, trigonal, space group $P3_121$, $a = b$ = 13.9523(9), c = 26.0654(17) Å, U = 4394.3(6) Å^3, Z = 6, D_c = 1.899 Mg m^{-3}, μ(Cu-Kα) = 10.083 mm^{-1}, T = 123 K. Total 67974 reflections, 5359 unique, R_{int} = 0.0341. Refinement of 5311 reflections (415 parameters) with $I>2\sigma(I)$ converged at final $R1$ = 0.0170 ($R1$ all data = 0.0172), $wR2$ = 0.0436 ($wR2$ all data = 0.0437), gof = 1.098, Flack parameter = 0.007(2). CCDC 972693.

***rac*-4{[Ir(1)$_2$(bpy)][PF$_6$]}·Et$_2$O·2CH$_2$Cl$_2$.** $C_{134}H_{102}Cl_4F_{32}Ir_4N_{16}OP_4$, M = 3594.88, yellow block, triclinic, space group $P\bar{1}$, a = 14.2353(6), b = 16.2890(7), c = 17.6451(7) Å, α = 66.1650(10), β = 81.642(2), γ = 67.3900(10)°, U = 3454.7(3) Å^3, Z = 1, D_c = 1.728 Mg m^{-3}, μ(Cu-Kα) = 9.298 mm^{-1}, T = 296 K. Total 23674 reflections, 11699 unique, R_{int} = 0.0287. Refinement of 10552 reflections (906 parameters) with $I>2\sigma(I)$ converged at final $R1$ = 0.0368 ($R1$ all data = 0.0399), $wR2$ = 0.1120 ($wR2$ all data = 0.1168), gof = 1.036. CCDC 972694.

CHAPTER II: GREEN EMITTERS – REGIOISOMERISM IN SULFONYL-FUNCTIONALIZED COMPLEXES

1. Introduction

The majority of iridium complexes used in OLEDs and LEECs contain substituents in 5-position of the cyclometallated phenyl ring (see Scheme 7 for numbering). Complexes with functional groups in 4-position are less well represented,[113,114] and even fewer examples are known with substitution in 3-position.[82] Furthermore, only a few reports exist in which a specific substituent was placed subsequently in each of the three positions and the influence of the substitution pattern was investigated. In the literature, series of regioisomeric iridium complexes that were examined include functionalization with diphenylamino,[115] fluoro,[116] methyl,[117] trifluoromethyl,[118,119] methylpyridinium,[120] bromo and fluorenyl[121] and benzylsulfonyl[90] groups. The largest influence on the emission colour was found to be exerted by a substituent in 4-position (*para* to the Ir–C bond). This finding was supported by DFT calculations.[117] Only in the study by Bronstein *et al.*[121] investigating bromo and fluorenyl substituents on the phenyl ring of the cyclometallating phenylisoquinoline ligands, differing results were obtained. They showed that the largest red-shift in the emission maximum is obtained by substitution in the 3-position (bromo) or 5-position (fluorenyl). In both cases, the functional group is placed *meta* to the Ir–C bond.

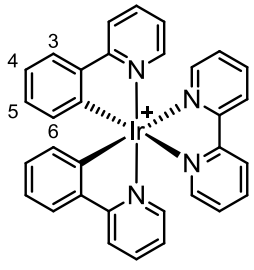

Scheme 7 Chemical structure of $[Ir(ppy)_2(bpy)]^+$ as a representative example including numbering of the phenyl ring of the cyclometallating ligand. 5- and 3-positions: *meta* with respect to Ir–C bond; 4-position: *para* to Ir–C bond.

In this chapter, the synthesis of a series of regioisomeric iridium complexes with methylsulfonyl groups in 3-, 4- and 5-position of the cyclometallating phenyl ring is described. Photophysical and electrochemical properties are compared with respect to the substitution pattern. Finally, the influence on device properties of light emitting electrochemical cells containing the prepared complexes is investigated.

2. Synthesis and NMR Spectroscopic Characterization

2.1. Ligand synthesis

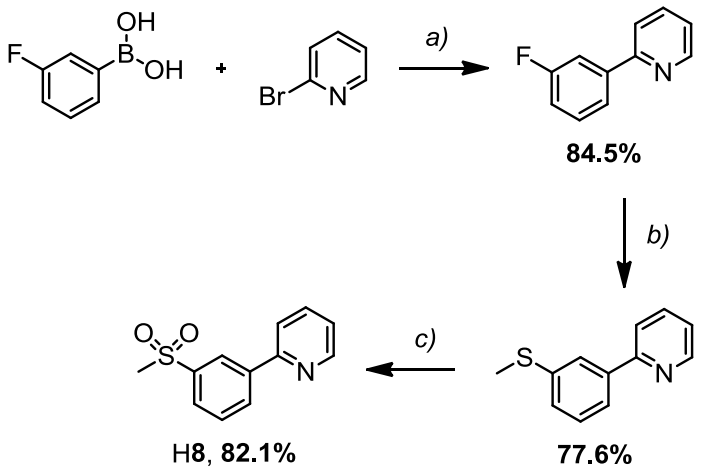

Scheme 8 Synthetic route to cyclometallating ligand H**8**. Reaction conditions: *a)* $PdCl_2$, K_2CO_3, EtOH/H_2O 1:1, reflux, overnight; *b)* NaSMe, NMP, MW, 120 °C, 1 h, N_2; *c)* $Na_2WO_4 \cdot 2H_2O$, H_2O_2, MeOH, room temperature, overnight.

2-(3-Methylsulfonylphenyl)pyridine (H**8**) was synthesized in a similar manner to ligand H**3**, described in Chapter I. The synthetic route is shown in Scheme 8. 2-(3-Fluorophenyl)pyridine is prepared *via* a Suzuki coupling reaction from 2-bromopyridine and 3-fluorophenylboronic acid, catalysed by $PdCl_2$. In the next step, the fluorine is replaced by a methylthiolate in a nucleophilic aromatic substitution reaction to yield 2-(3-methylthiophenyl)pyridine, which is subsequently oxidized with sodium tungstate dihydrate–hydrogen peroxide in methanolic solution to yield the desired ligand H**8** in 54% yield over three steps. 2-(3-

Methylsulfonylphenyl)pyridine (H**8**) was fully characterized by NMR and IR spectroscopies, LC-ESI mass spectrometry, melting point and elemental analysis.

The synthesis of the ligand 2-(2-methylsulfonylphenyl)pyridine (H**9**) was achieved using a different approach, according to a procedure described in the literature (Scheme 10).[122,123] The intermediate 2-(2-dibromoborylphenyl)pyridine was obtained in good yield *via* an electrophilic aromatic borylation reaction using 2-phenylpyridine and boron tribromide. The nitrogen atom of the pyridine ring acts as a directing group in this case. Ishida *et al.*[122] have proposed a probable mechanism for the borylation of 2-phenylpyridine, shown in Scheme 9. In the first step, coordination occurs from the Lewis basic pyridine nitrogen to the Lewis acidic boron atom of BBr_3. Next, a second BBr_3 molecule abstracts a bromide from intermediate **O**, leading to the formation of salt **P**. Subsequent electrophilic attack of the coordinated boron atom on the neighbouring phenyl ring and rearomatization by deprotonation with *N*,*N*-diisopropylethylamine leads to final product **R**.

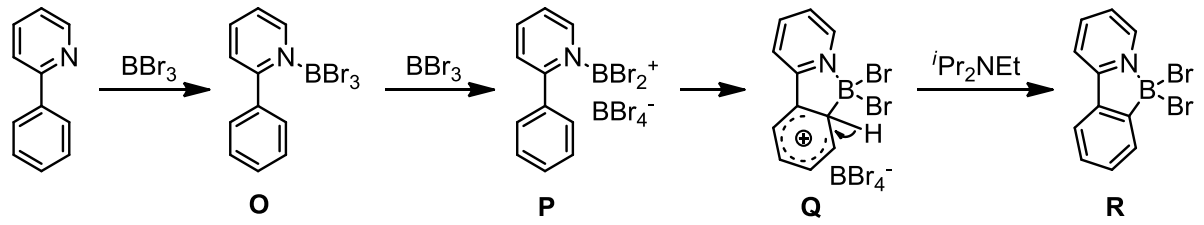

Scheme 9 Reaction mechanism for the borylation of 2-phenylpyridine, as proposed by Ishida *et al.*[122]

Treatment of the pyridine–dibromoborane intermediate with sodium methanesulfinate in a copper-catalysed aerobic oxidative coupling reaction yielded the desired ligand 2-(2-methylsulfonylphenyl)pyridine (H**9**).[123] Cu_2O/NH_3 was used as the catalyst in ethanolic solution at 45 °C under air to give H**9** in good yield (Scheme 10).

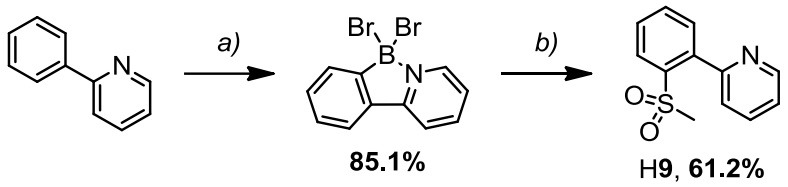

Scheme 10 Synthetic pathway to ligand H**9**. Reaction conditions: *a)* BBr_3, $^{i}Pr_2NEt$, CH_2Cl_2, room temperature, 24 h; *b)* $NaSO_2Me$, Cu_2O, aq. NH_3, 45 °C, overnight.

2.2. Synthesis of $[Ir(C\text{^}N)_2Cl]_2$ dimers

The synthetic pathway to chlorido-bridged dimers $[Ir(C\text{^}N)_2Cl]_2$ with C^N = **3**, **8** and **9** is shown in Scheme 11. $[Ir(\mathbf{3})_2Cl]_2$ (*cf.* Chapter I) and $[Ir(\mathbf{8})_2Cl]_2$ were prepared in excellent yields by reaction of $[Ir(cod)Cl]_2$ with the appropriate cyclometallating ligand (H**3** or H**8**) in 2-ethoxyethanol under reflux conditions. For $[Ir(\mathbf{9})_2Cl]_2$, different reaction conditions were tested: Starting from $IrCl_3{\cdot}xH_2O$, $[Ir(cod)Cl]_2$ and $Ir(tht)_3Cl_3$, both under reflux and in a microwave reactor. The most successful route proved to be a microwave-assisted complexation using $IrCl_3{\cdot}xH_2O$ in a mixture of 2-ethoxyethanol and H_2O (3:1). With this method, the desired iridium dimer was obtained in good yield. For both reactions with $Ir(tht)_3Cl_3$, only unreacted ligand was observed, as well as for the microwave reaction starting with $[Ir(cod)Cl]_2$. In the case of the reflux reactions with both $IrCl_3{\cdot}xH_2O$ and $[Ir(cod)Cl]_2$, the desired product was obtained containing undefined impurities.

Dimers $[Ir(C\text{^}N)_2Cl]_2$ with C^N = **8** and **9** were characterized by ^{1}H NMR and IR spectroscopies, LC-ESI mass spectrometry and, in the case of $[Ir(\mathbf{9})_2Cl]_2$, elemental analysis. The base peaks at *m*/*z* 657 in the LC-ESI mass spectra correspond to the $[Ir(C\text{^}N)_2]^+$ ions; further peaks at *m*/*z* 698 and 739 were observed for $[Ir(C\text{^}N)_2(CH_3CN)]^+$ and $[Ir(C\text{^}N)_2(CH_3CN)_2]^+$, respectively. The coordinating acetonitrile stems from the eluent of the LC column.

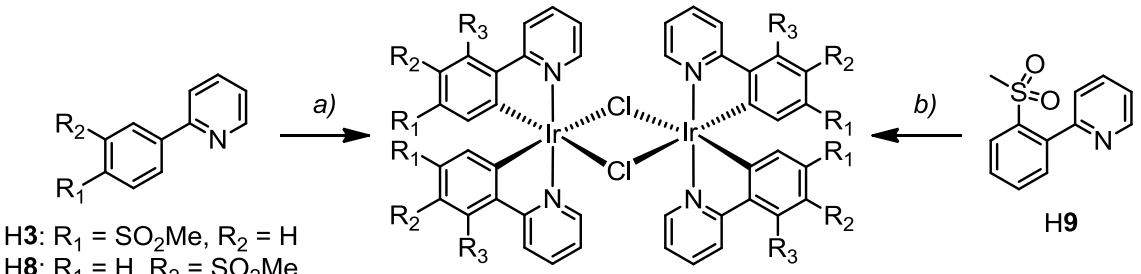

Scheme 11 Synthetic route to iridium dimers $[Ir(C\text{^}N)_2Cl]_2$ (C^N = **3**, **8**, **9**). Reaction conditions: *a)* $[Ir(cod)Cl]_2$, 2-ethoxyethanol, reflux, overnight, N_2; *b)* $IrCl_3 \cdot xH_2O$, 2-ethoxyethanol/H_2O 3:1, MW, 110 °C, 1.5 h, N_2.

2.3. Synthesis of $[Ir(C\text{^}N)_2(bpy)][PF_6]$ complexes

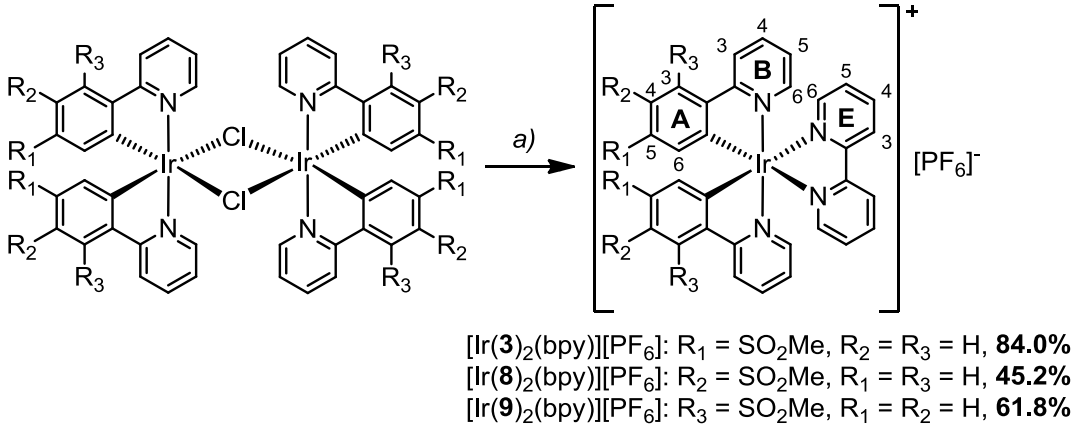

Scheme 12 Synthesis of iridium complexes $[Ir(C\text{^}N)_2(bpy)][PF_6]$ with C^N = **3**, **8** and **9**. Reaction conditions: *a)* 2,2'-bipyridine, MeOH, MW, 120 °C, 1 h; then NH_4PF_6.

Dimers were cleaved using the 2,2'-bipyridine ancillary ligand in MeOH under microwave conditions (Scheme 12). Subsequent anion exchange with an excess of solid NH_4PF_6 added to the chloride salts dissolved in a small amount of MeOH gave the desired complexes in 45 to 84% yield. The complexes were separated by filtration after ion metathesis; the low yield of

[Ir(**8**)$_2$(bpy)][PF$_6$] can be explained by the better solubility in MeOH of this complex with respect to [Ir(**3**)$_2$(bpy)][PF$_6$] and [Ir(**9**)$_2$(bpy)][PF$_6$].

Complexes [Ir(C^N)$_2$(bpy)][PF$_6$] with C^N = **3**, **8** and **9** were fully characterized using NMR and IR spectroscopies, ESI mass spectrometry and elemental analysis. The base peak in the ESI mass spectrum of each complex was assigned to the [Ir(C^N)$_2$(bpy)$^+$ ion; the characteristic iridium isotope pattern was observed for all three complexes. ^{1}H and ^{13}C NMR signals were assigned using 2D experiments (COSY, HMQC and HMBC). The ^{1}H NMR spectra including full assignment are shown in Fig. 20; for numbering see Scheme 12. By changing the substitution position from 5- to 4- and 3-position, the methyl group signal is shifted downfield from δ 2.89 to 3.04 to 3.25 ppm ($\Delta\delta$ = 0.36 ppm). The largest shift is observed for signal H^{B3} (on the C^N pyridyl ring), which moves from δ 8.23 and 8.26 ppm for [Ir(**3**)$_2$(bpy)][PF$_6$] and [Ir(**8**)$_2$(bpy)][PF$_6$], respectively, to δ 9.30 ppm for [Ir(**9**)$_2$(bpy)][PF$_6$], corresponding to a chemical shift difference $\Delta\delta$ of over 1 ppm. This significant shift can be explained by intramolecular interactions between the sulfone oxygen atoms and proton H^{B3} in [Ir(**9**)$_2$(bpy)][PF$_6$], supported by crystal structure data (*vide infra*). For phenyl proton H^{A6}, it is possible to see the distance influence of the sulfonyl group: H^{A6} resonates at highest frequency with the sulfone group *ortho* (5-position, δ 6.70 ppm), followed by *meta* (4-position, δ 6.54 ppm) and *para* (3-position, δ 6.47 ppm). Chemical shift differences of the remaining A ring protons (H^{A3}, H^{A4} and H^{A5}) are in the range $\Delta\delta$ 0.28 to 0.32 ppm. No or negligible shifts are observed for bipyridyl proton signals (E ring) and H^{B4}, H^{B5} and H^{B6}, with $\Delta\delta \leq 0.1$ ppm. All of these protons are remote from the strongly electron-withdrawing sulfone group and the substitution position therefore does not exert a large influence on the chemical shift.

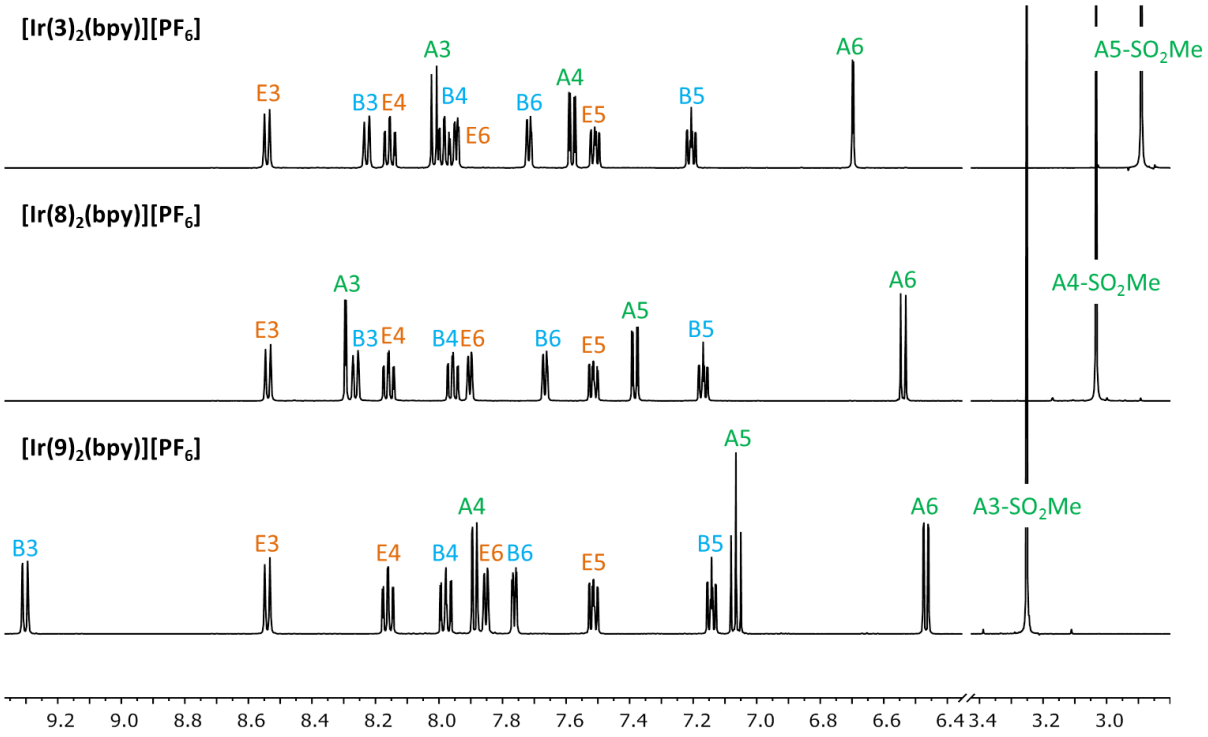

Fig. 20 500 MHz ^{1}H NMR spectra of complexes [Ir(C^N)$_2$(bpy)][PF$_6$] (C^N = **3**, **8**, **9**) in CD_3CN solution including assignments. For numbering, see Scheme 12. Scale: δ/ppm.

3. Crystal Structures

X-ray quality single crystals of 2{[Ir(**3**)$_2$(bpy)][PF$_6$]}·7CH_2Cl_2, 2{[Ir(**8**)$_2$(bpy)][PF$_6$]}·5.5H_2O and [Ir(**9**)$_2$(bpy)][PF$_6$] were grown by layering a CH_2Cl_2 solution of the complex with Et_2O, an CH_3CN solution of the complex with *tert*-butyl methyl ether (*t*-BME) and an CH_3CN solution of the complex with Et_2O, respectively. Structures of the [Ir(C^N)$_2$(bpy)]$^+$ cations are shown in Fig. 21 to Fig. 23; selected bond lengths and angles are given in the figure captions. 2{[Ir(**3**)$_2$(bpy)][PF$_6$]}·7CH_2Cl_2 crystallizes in the orthorhombic space group *Pbca*; 2{[Ir(**8**)$_2$(bpy)][PF$_6$]}·5.5H_2O and [Ir(**9**)$_2$(bpy)][PF$_6$] crystallize in the monoclinic space groups $P2_1/c$ and $C2/c$, respectively.

Solvent molecules are heavily disordered in 2{[Ir(**1**)$_2$(bpy)][PF$_6$]}·7CH_2Cl_2 and have been modelled over four sites with fractional occupancies. The asymmetric unit of 2{[Ir(**8**)$_2$(bpy)][PF$_6$]}·5.5H_2O contains two independent Λ-cations and two ordered [PF$_6$]$^-$ anions, one of which is half occupancy. Furthermore, the P atom of the third [PF$_6$]$^-$ anion lies on a special position and is shared equally between two unit cells. In [Ir(**9**)$_2$(bpy)][PF$_6$], half a

cation and half an anion are present in the asymmetric unit. The second half is generated by a C_2 axis through the central iridium atom, parallel to the *b* axis of the unit cell. All complexes crystallize in achiral space groups; both enantiomers are therefore present in the unit cell.

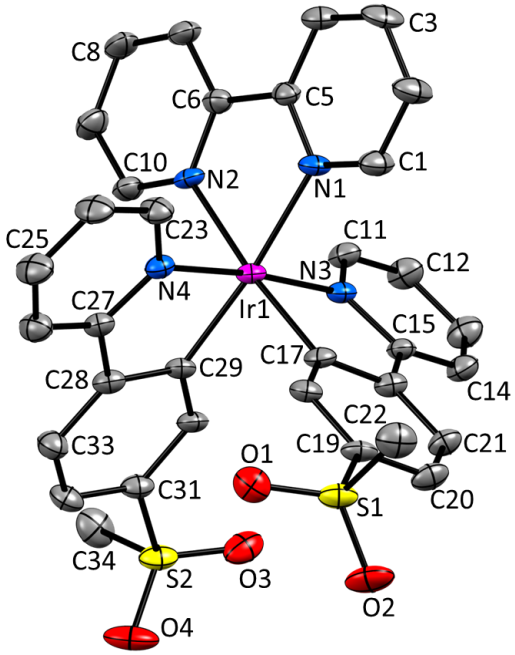

Fig. 21 Structure of the Λ-[Ir(**3**)$_2$(bpy)]$^+$ cation in 2{[Ir(**3**)$_2$(bpy)][PF_6]}·7CH_2Cl_2, H atoms and solvent molecules omitted and ellipsoids plotted at 40% probability level. Selected bond parameters: Ir1–N1 = 2.133(5), Ir1–N2 = 2.134(4), Ir1–N3 = 2.044(5), Ir1–N4 = 2.057(5), Ir1–C17 = 2.029(5), Ir1–C29 = 2.009(5), C34–S2 = 1.757(7), S1–O1 = 1.435(5), S1–O2 = 1.440(5), S2–O3 = 1.437(6), S2–O4 = 1.451(6), C22–S1 = 1.748(7) Å; N1–Ir1–N2 = 77.53(19), N3–Ir1–C17 = 80.70(19), N4–Ir1–C29 = 80.53(19), N3–Ir1–N4 = 174.41(18), N1–Ir1–C29 = 174.1(2), N2–Ir1–C17 = 174.4(2), O1–S1–O2 = 118.2(3), O3–S2–O4 = 118.2(4)°.

By moving the methylsulfonyl group from the 5- to 4- and 3-position, the twist between the two pyridyl ring planes in the bpy ancillary ligand becomes substantially larger. The bpy is nearly planar in 2{[Ir(**3**)$_2$(bpy)][PF_6]}·7CH_2Cl_2, with an angle of 3.0° between the planes. Moving to 2{[Ir(**8**)$_2$(bpy)][PF_6]}·5.5H_2O, the deviation from planarity becomes larger, as angles of 6.4 and 7.8° between the pyridyl ring planes are observed in the two independent cations. Due to the large steric hindrance introduced by substitution in the 3-position – as in

the case of [Ir(**9**)$_2$(bpy)][PF$_6$] – the two bpy pyridyl rings are significantly distorted from planarity, with an angle of 13.6° between the planes of the rings.

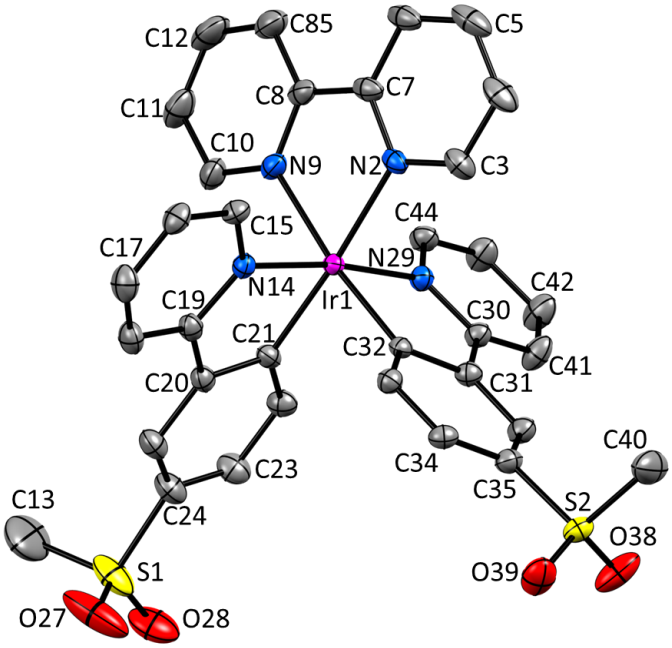

Fig. 22 Structure of one of the independent Λ-[Ir(**8**)$_2$(bpy)]$^+$ cations in the asymmetric unit in 2{[Ir(**8**)$_2$(bpy)][PF$_6$]}·5.5H$_2$O, H atoms and solvent molecules omitted and ellipsoids plotted at 40% probability level. Selected bond parameters: Ir1–N2 = 2.134(4), Ir1–N9 = 2.134(4), Ir1–N14 = 2.045(4), Ir1–N29 = 2.045(4), Ir1–C21 = 2.000(4), Ir1–C32 = 2.006(4), S1–C13 = 1.719(10), S1–O27 = 1.454(6), S1–O28 = 1.415(5), S2–O38 = 1.431(4), S2–O39 = 1.431(4), C40–S2 = 1.761(6) Å; N2–Ir1–N9 = 76.72(16), N14–Ir1–C21 = 80.67(16), N29–Ir1–C32 = 80.61(16), N14–Ir1–N29 = 172.70(14), N2–Ir1–C21 = 175.99(16), N9–Ir1–C32 = 173.13(16), O27–S1–O28 = 114.8(4), O38–S2–O39 = 117.5(3)°.

As described in the literature for series of aryl–aryl[105,124] and aryl–alkyl[105] sulfones, short intramolecular CH···OS contacts between the sulfonyl oxygen atoms and the aryl protons of the adjacent pyridyl ring were observed in ligands H**3** and H**5**[95] and dimer [Ir(**3**)$_2$Cl]$_2$[95] (Chapter I). Such interactions in the range 2.55–2.70 Å are also seen in [Ir(**3**)$_2$(bpy)]$^+$. These optimized contacts are due to twists of the sulfone groups with respect to the phenyl ring they are attached to, giving rise to torsion angles of 14.8 (O3–S2–C31–C30), –34.5 (O4–S2–C31–C32), 20.8 (O1–S1–C19–C18) and –30.2° (O2–S1–C19–C20). Similar observations are made for [Ir(**8**)$_2$(bpy)]$^+$, leading to intramolecular CH···OS contacts ranging from 2.50 to 2.80 Å. In

$[Ir(\mathbf{9})_2(bpy)]^+$, however, steric hindrance induces a different arrangement of the sulfone substituents, resulting in short contacts between the sulfonyl oxygen and the adjacent pyridyl ring of 2.49 Å (O1···HC4) and 2.77 Å (O2···HC4).

Furthermore, the steric hindrance introduced in $[Ir(\mathbf{9})_2(bpy)]^+$ causes a significant distortion of the phenylpyridine cyclometallating ligand, as observed by an angle of 22.2° between the phenyl and pyridyl ring planes. In both $[Ir(\mathbf{3})_2(bpy)]^+$ and $[Ir(\mathbf{8})_2(bpy)]^+$, no such severe deviation from planarity is seen and the corresponding angles between the ring planes lie in the range 2.0–6.2°.

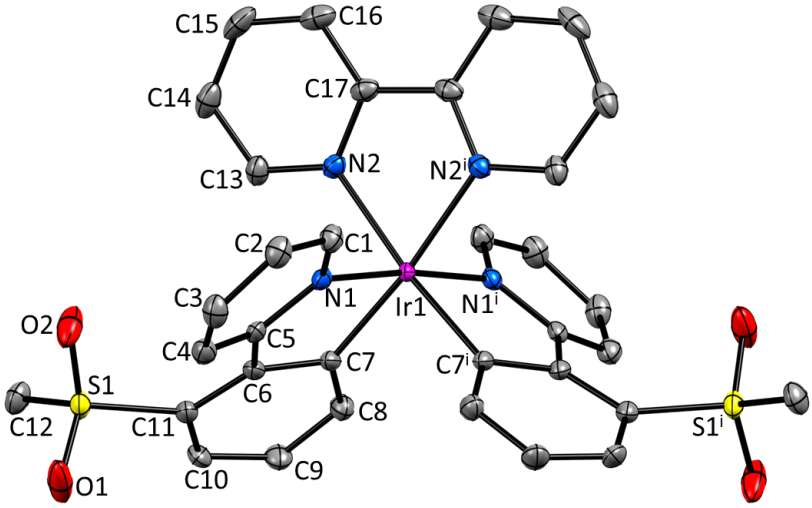

Fig. 23 Structure of the Λ-$[Ir(\mathbf{9})_2(bpy)]^+$ cation in $[Ir(\mathbf{9})_2(bpy)][PF_6]$, H atoms omitted for clarity and ellipsoids plotted at 40% probability level. Symmetry code: i = 1–x,y,½–z. Selected bond parameters: Ir1–N1 = 2.036(2), Ir1–N2 = 2.146(2), Ir1–C7 = 2.007(2), S1–O1 = 1.432(2), S1–O2 = 1.433(2), C12–S1 = 1.763(3) Å; N1–Ir1–C7 = 80.08(9), N2–Ir1–$N2^i$ = 76.83(11), N2–Ir1–$C7^i$ = 173.07(9), N1–Ir1–$N1^i$ = 173.67(11), O1–S1–O2 = 118.38(18)°.

4. Photophysical Properties

UV-Vis absorption spectra of compounds $[Ir(C\text{^}N)_2(bpy)][PF_6]$ with C^N = **3**, **8** and **9** in CH_3CN solution are given in Fig. 24. The spectra of the regioisomeric complexes are similar and show dominant absorption bands in the UV region (λ_{max} = 253–259 nm), ascribed to spin-allowed π*←π transitions based on the ligands. Between 350–450 nm, less intense absorption

bands correspond to spin-allowed ^{1}MLCT and ^{1}LLCT transitions. At even lower energy (<450 nm), very weak tails into the visible region are observable which arise from spin-forbidden direct population of the triplet excited states (^{3}MLCT, ^{3}LLCT and ^{3}LC).[21]

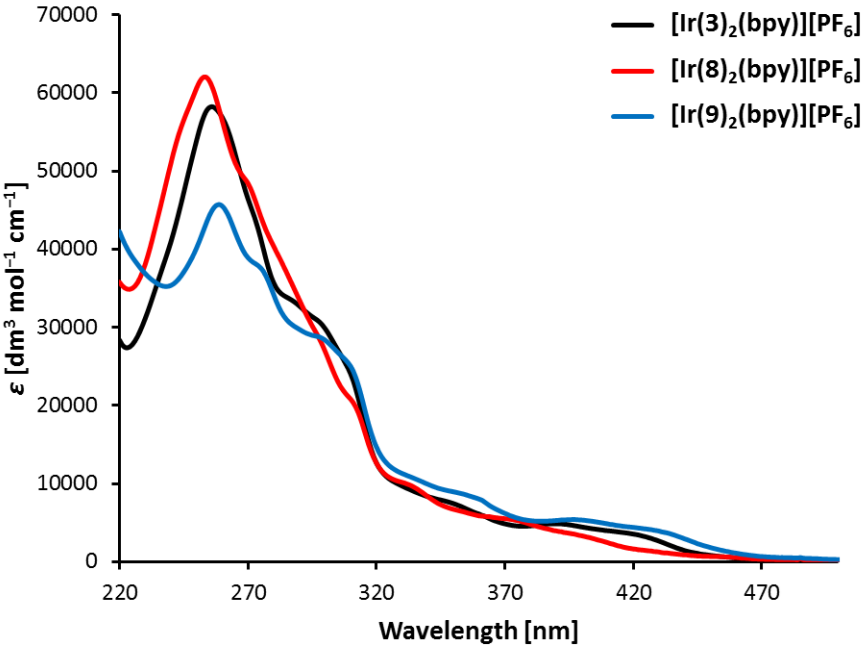

Fig. 24 UV-Vis absorption spectra of complexes [Ir(C^N)$_2$(bpy)][PF$_6$] with C^N = **3**, **8** and **9** in CH_3CN solution (1.0×10^{-5} M).

By excitation of CH_3CN solutions of complexes [Ir(C^N)$_2$(bpy)][PF$_6$] (C^N = **3**, **8**, **9**), the emission spectra shown in Fig. 25 were obtained. For all complexes, the emission maxima and profiles are independent of the excitation wavelength. All three complexes are green emitters in solution (*cf.* Fig. 26a); their emission maxima are blue-shifted by 68 to 92 nm with respect to unsubstituted parent complex [Ir(ppy)$_2$(bpy)]$^+$ (585 nm in CH_3CN).[103] The emission maximum blue-shift follows the trend 5-position > 3-position > 4-position. Comparison is difficult due to the different shapes of the emission bands, especially considering the broad and unstructured emission profile of [Ir(**8**)$_2$(bpy)][PF$_6$] in comparison to the vibrationally structured emission bands of [Ir(**3**)$_2$(bpy)][PF$_6$] and [Ir(**9**)$_2$(bpy)][PF$_6$]. From the spectra it can be seen that the emissions of [Ir(**8**)$_2$(bpy)][PF$_6$] and [Ir(**9**)$_2$(bpy)][PF$_6$] are in fact very similar, with the emission maximum of [Ir(**8**)$_2$(bpy)][PF$_6$] (517 nm) approximately halfway between

the two emission maxima of [Ir(**9**)$_2$(bpy)][PF$_6$] (506, 527 nm). [Ir(**3**)$_2$(bpy)][PF$_6$] (493, 525 nm) exhibits definitely blue-shifted photoluminescence maxima compared to the other two complexes; however, the emission band of [Ir(**8**)$_2$(bpy)][PF$_6$] extends furthest into the shorter wavelength region of the spectrum.

As mentioned above, both [Ir(**3**)$_2$(bpy)][PF$_6$] and [Ir(**9**)$_2$(bpy)][PF$_6$] exhibit vibrational structure in their photoluminescence bands. The emission of [Ir(**8**)$_2$(bpy)][PF$_6$] on the other hand is broad and unstructured. In general, a more structured emission profile indicates a larger ligand-centred (^{3}LC) character of the emissive triplet state. Broad and unstructured emission bands – as observed for complex [Ir(**8**)$_2$(bpy)][PF$_6$] – suggest a more pronounced charge transfer character (^{3}MLCT and ^{3}LLCT).[21] The trend in radiative decay rate constants (k_r = PLQY/τ) further supports this assumption (Table 4): the higher k_r, the larger the charge transfer character of the emissive triplet state.[21] [Ir(**8**)$_2$(bpy)][PF$_6$] has a radiative decay rate constant of 7.2×10^5 s^{-1} which is more than twice as high as those of the other two complexes (2.6 and 3.2×10^5 s^{-1}); the ^{3}LC contribution is therefore the lowest in the compound where the methylsulfonyl substituent is placed *para* to the cyclometallated Ir–C bond.

In most of the series of regioisomeric iridium complexes reported in the literature, the largest influence on the emission maximum has been observed by the introduction of a substituent in 4-position of the cyclometallating ligand. This means that the strongest emission maximum blue-shift has been achieved by the introduction of an electron-withdrawing moiety[90,113,116,118,120] and the largest red-shift by an electron-donating group[115,117] *para* to the Ir–C bond. A different trend has been described by Bronstein *et al.*[121] for their bromo- and fluorenyl-substituted regioisomers. In both of their series, a substituent in 5-position (*meta* to the Ir–C bond) of the cyclometallating phenyl ring exerted the largest influence on the emission maximum. Their observation therefore fits well with the trend we have seen in our sulfonyl-substituted isomeric complexes. Regarding the nature of the emissive triplet state, our sulfone series can be compared to a series of sulfur pentafluoride-functionalized iridium complexes.[113] In both cases, moving the substituent from the 5- to 4-position (from *meta* to *para* with respect to the Ir–C bond) increases the charge transfer and decreases the ligand-centred character of the emissive state. This is indicated by a broadening and loss of structure of the emission band as well as a shorter excited state lifetime. Due to

these different contributions of CT and ^{3}LC states to the emissive triplet state, comparison within the series of methylsulfonyl iridium complexes is difficult.

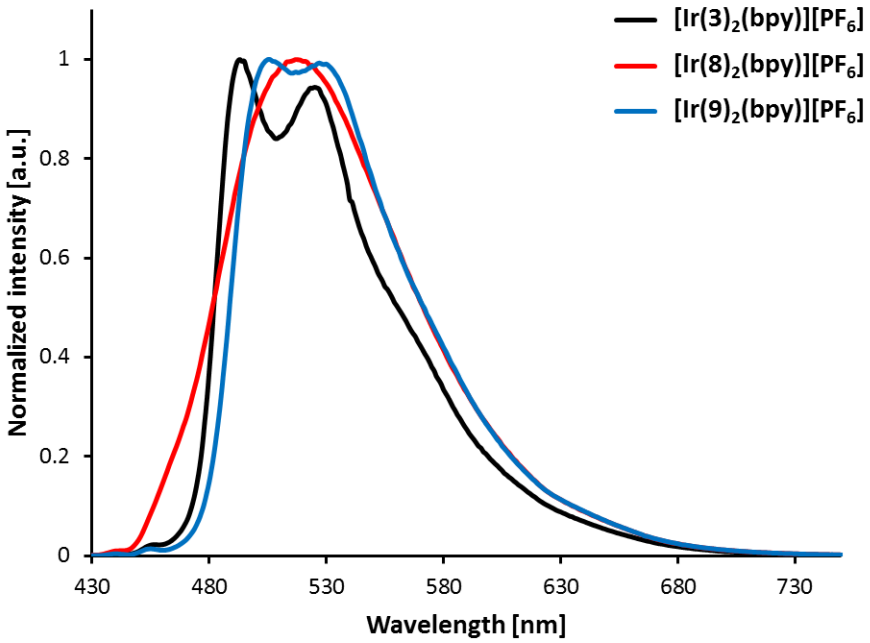

Fig. 25 Photoluminescence spectra in CH_3CN solution (1.0×10^{-5} M) of complexes $[Ir(C\text{^}N)_2(bpy)][PF_6]$ (C^N = **3**, **8**, **9**). λ_{exc} = 400 nm.

Table 4 Photophysical properties of complexes $[Ir(C\text{^}N)_2(bpy)][PF_6]$ with C^N = **3**, **8**, **9** in CH_3CN solution. PLQYs measured in de-aerated solution, τ in de-aerated solution under Ar atmosphere. k_r = PLQY/τ; k_{nr} = (1–PLQY)/τ.

Compound	λ_{exc} **[nm]**	λ_{em}^{max} **[nm]**	**PLQY [%]**	τ **[µs]** (χ)[a]	k_r **[10^5 s^{-1}]**	k_{nr} **[10^5 s^{-1}]**
$[Ir(\mathbf{3})_2(bpy)][PF_6]$	262	493, 525	74	2.33 (1.3)	3.2	1.1
$[Ir(\mathbf{8})_2(bpy)][PF_6]$	271	517	92	1.28 (1.1)	7.2	0.63
$[Ir(\mathbf{9})_2(bpy)][PF_6]$	261	506, 527	77	2.97 (1.2)	2.6	0.77

[a] λ_{exc} = 280 nm.

High photoluminescence quantum yields between 74 and 92% were obtained for de-aerated CH_3CN solutions of complexes $[Ir(C\text{^}N)_2(bpy)][PF_6]$ with C^N = **3**, **8** and **9** (Table 4). $[Ir(\mathbf{8})_2(bpy)][PF_6]$, containing the methylsulfone substituent in 4-position of the cyclometallating ligand, exhibits a considerably higher quantum yield (92%) than the other

two complexes (74 and 77%). The same trend has been observed in the bromo- and fluorenyl-functionalized isomeric complexes reported by Bronstein *et al.*[121] In their series, substitution *para* to the Ir–C bond also resulted in the largest solution PLQY.

Excited state lifetimes are in the order of a few microseconds for $[Ir(C^N)_2(bpy)][PF_6]$ (C^N = **3**, **8**, **9**) in de-aerated CH_3CN solution under argon atmosphere (Table 4). The τ values range from 1.28 µs for $[Ir(\mathbf{8})_2(bpy)][PF_6]$ to 2.97 µs for $[Ir(\mathbf{9})_2(bpy)][PF_6]$. When solutions are not de-aerated, PLQYs are significantly lower (4.5 to 7.0%) and lifetimes significantly shorter (0.14 to 0.31 µs), suggesting strong excited state quenching effects due to oxygen present in the system.

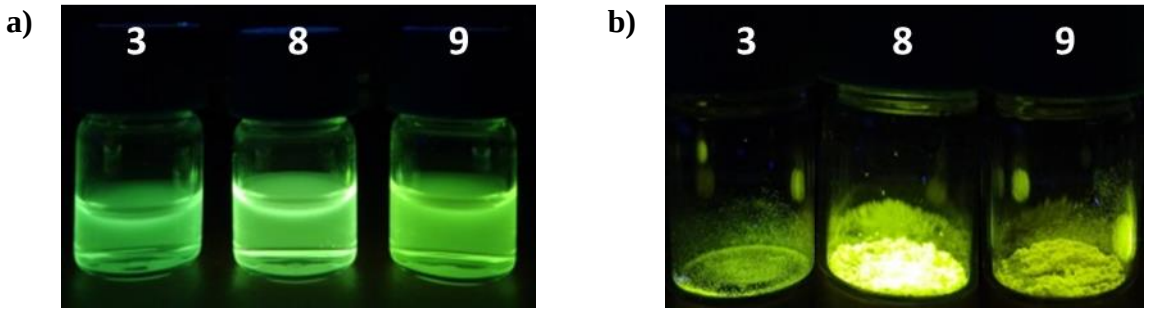

Fig. 26 Photographs of complexes $[Ir(C^N)_2(bpy)][PF_6]$ with C^N = **3**, **8** and **9** under 366 nm light excitation in a) CH_3CN solution and b) the solid state (powder).

Solid state emission spectra of powder samples of compounds $[Ir(C^N)_2(bpy)][PF_6]$ with C^N = **3**, **8** and **9** are depicted in Fig. 27. All three complexes are yellow emitters (*cf.* Fig. 26b) and the emission maxima lie in the range 535 to 542 nm. $[Ir(\mathbf{3})_2(bpy)][PF_6]$ shows the largest emission maximum red-shift on going from solution to powder (42 nm), whereas $[Ir(\mathbf{8})_2(bpy)][PF_6]$ has the smallest (25 nm). The vibrational structure observed in solution spectra of $[Ir(\mathbf{3})_2(bpy)][PF_6]$ and $[Ir(\mathbf{9})_2(bpy)][PF_6]$ is almost completely lost in the solid state.

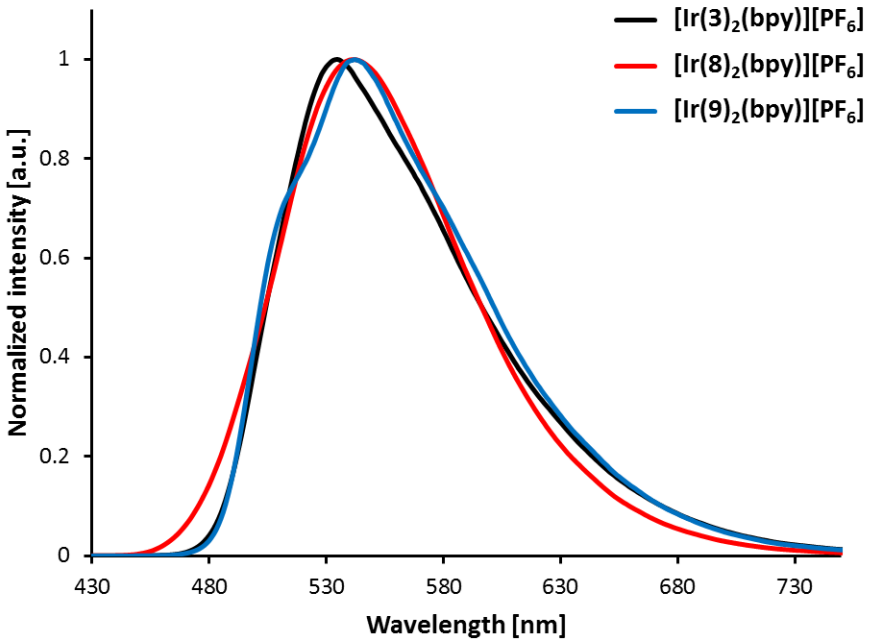

Fig. 27 Solid state emission spectra of powder samples of $[Ir(C\hat{}N)_2(bpy)][PF_6]$ with C^N = **3**, **8**, **9**. λ_{exc} = 340 nm.

Table 5 Solid state photophysical properties of powder samples of $[Ir(C\hat{}N)_2(bpy)][PF_6]$ (C^N = **3**, **8** and **9**). Biexponential fits were used for solid-state lifetime measurements, using the equation $\tau_{ave} = \Sigma A_i\tau_i/\Sigma A_i$ (A_i is the pre-exponential factor for the lifetime).

Compound	λ_{em}^{max} **[nm]**[a]	**PLQY [%]**[b]	τ_{ave} **[µs]** **(χ)**[c]	τ_1 **[µs]** **(A_1)**[c]	τ_2 **[µs]** **(A_2)**[c]
$[Ir(\mathbf{3})_2(bpy)][PF_6]$	535	6.6	0.475 (1.0)	0.299 (7035)	1.01 (691)
$[Ir(\mathbf{8})_2(bpy)][PF_6]$	542	27	1.19 (1.1)	0.456 (2233)	1.58 (1201)
$[Ir(\mathbf{9})_2(bpy)][PF_6]$	542	6.1	0.663 (1.0)	0.306 (4221)	1.41 (439)

[a] λ_{exc} = 340 nm. [b] For λ_{exc}, see Table 4. [c] λ_{exc} = 280 nm.

Photophysical properties of powder samples of complexes $[Ir(C\hat{}N)_2(bpy)][PF_6]$ (C^N = **3**, **8**, **9**) are summarized in Table 5. Quantum yields are much lower in the solid state and range from 6.1 and 6.6% for $[Ir(\mathbf{9})_2(bpy)][PF_6]$ and $[Ir(\mathbf{3})_2(bpy)][PF_6]$, respectively, to 27% for $[Ir(\mathbf{8})_2(bpy)][PF_6]$. As in solution, $[Ir(\mathbf{8})_2(bpy)][PF_6]$ (substituent *para* to Ir–C bond) again exhibits the highest quantum yield. Biexponential fits were used for the determination of excited state lifetimes of powder samples; τ values are shorter than for solution samples.

Strong photoluminescence quenching in the solid state due to intermolecular interactions is indicated by the loss of vibrational structure, lower quantum yields and shorter lifetimes.[78]

5. Electrochemical Properties

Electrochemical data of complexes $[Ir(C\hat{}N)_2(bpy)][PF_6]$ with C^N = **3**, **8** and **9** were obtained from cyclic voltammetry experiments in de-aerated CH_3CN solution and are summarized in Table 6. In Fig. 28, the cyclic voltammogram of $[Ir(\mathbf{8})_2(bpy)][PF_6]$ showing the oxidation and first reduction waves is depicted as a representative example. In complexes of the type $[Ir(C\hat{}N)_2(N\hat{}N)]^+$, the LUMO is located on the ancillary ligand. Since all three complexes contain a bpy ancillary ligand, the first reduction potentials should therefore be similar in $[Ir(C\hat{}N)_2(bpy)][PF_6]$ (C^N = **3**, **8** and **9**). The first reduction waves are reversible and values are in the range −1.67 to −1.72 V; the numbers are comparable to unsubstituted reference compound $[Ir(ppy)_2(bpy)][PF_6]$ (−1.77 V in DMF).[103] Up to four more reduction waves in the case of $[Ir(\mathbf{9})_2(bpy)][PF_6]$ are observed within the accessible solvent window.

Table 6 Cyclic voltammetric data of complexes $[Ir(C\hat{}N)_2(bpy)][PF_6]$ with C^N = **3**, **8**, **9** *vs.* Fc/Fc^+ in de-aerated CH_3CN solution. Measured with glassy carbon working, Pt counter and Ag pseudo-reference electrode and 0.1 M $TBAPF_6$ supporting electrolyte at a scan rate of 0.1 V s^{-1}. qr = quasi-reversible, ir = irreversible.

Compound	$E_{1/2}^{ox}$ **[V]**	$E_{1/2}^{red}$ **[V]**	$\Delta E_{1/2}$ **[V]**
$[Ir(\mathbf{3})_2(bpy)][PF_6]$	+1.18	–1.72, –2.16, –2.61^{ir}	2.90
$[Ir(\mathbf{8})_2(bpy)][PF_6]$	+1.29	–1.67, –2.27^{qr}, –2.52^{qr}	2.96
$[Ir(\mathbf{9})_2(bpy)][PF_6]$	+1.20^{qr}	–1.69, –2.06^{ir}, –2.16^{ir}, –2.34^{ir}, –2.52^{ir}	2.89

One quasi-reversible or reversible oxidation wave is seen for complexes $[Ir(C\hat{}N)_2(bpy)][PF_6]$ with C^N = **3**, **8** and **9** in CH_3CN solution. The oxidation is iridium-based with a considerable influence of the cyclometallating ligand. This is due to the location of the HOMO on the iridium centre and the phenyl rings of the C^N ligands. For the sulfone-substituted complexes, the oxidation potentials are in the range +1.18 to +1.29 V and are significantly shifted to higher potentials with respect to $[Ir(ppy)_2(bpy)]^+$ (+0.84 V in DMF).[103] The

observed stabilization of the HOMO and thus larger oxidation potential is attributed to the strongly electron-withdrawing character of the sulfone substituent, removing electron density from the central iridium atom. The position of the methylsulfonyl group also plays a role in the degree of stabilization of the HOMO. Substitution *para* to the Ir–C bond leads to the highest oxidation potential (+1.29 V), whereas $E^{ox}_{1/2}$ of the two complexes with sulfone substituents in *meta* position to the Ir–C bond are very similar (+1.18 and +1.20 V). As a consequence, compound [Ir(**8**)$_2$(bpy)][PF$_6$] has a slightly larger electrochemical HOMO-LUMO gap than [Ir(**3**)$_2$(bpy)][PF$_6$] and [Ir(**9**)$_2$(bpy)][PF$_6$] (2.96 V *vs.* 2.90 and 2.89 V).

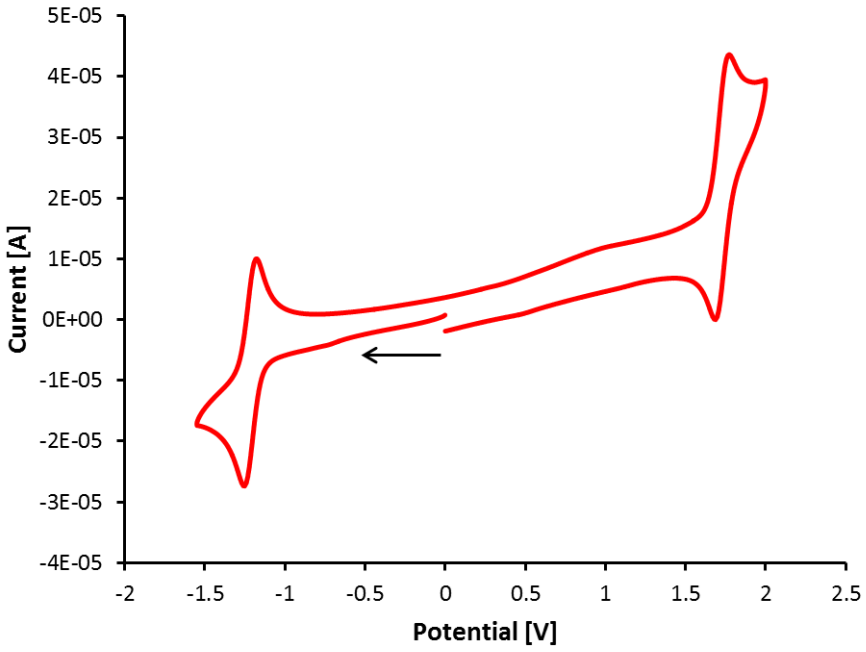

Fig. 28 Cyclic voltammogram of [Ir(**8**)$_2$(bpy)][PF$_6$] in de-aerated CH_3CN solution, showing the oxidation and the first reduction wave. The arrow indicates the initial scanning direction.

6. Electroluminescence and Device Data

Light-emitting electrochemical cells were assembled and measured by Dr. Henk Bolink and co-workers at the University of Valencia. Electroluminescence spectra were obtained for light emitting electrochemical cells containing complexes [Ir(C^N)$_2$(bpy)][PF$_6$] with C^N = **3**, **8** and **9** and are given in Fig. 29. The device configuration used was

ITO/PEDOT:PSS/[Ir(C^N)$_2$(bpy)][PF$_6$]:[Bmim][PF$_6$] 4:1/Al and LEECs were measured using block-wave pulsed current with a frequency of 1 kHz, 50% duty cycles and an average current density of 100 A m^{-2}.[21,80,82] Electroluminescence maxima and device data are summarized in Table 7.

All three regioisomeric methylsulfone complexes emit yellow-green electroluminescence with maxima in the range 549 to 560 nm. Electroluminescence maxima are therefore slightly red-shifted by 7–18 nm compared to solid state photoluminescence maxima of powder samples.

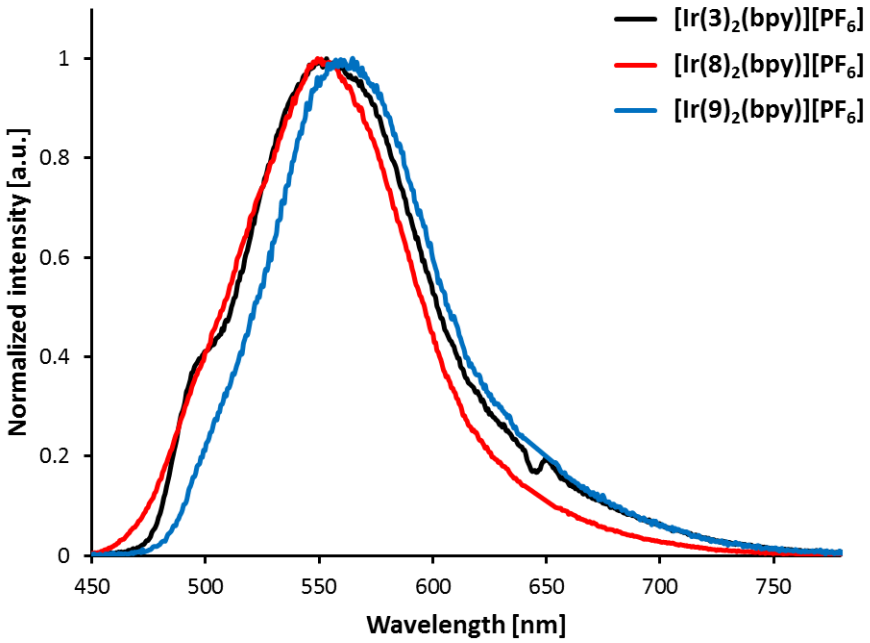

Fig. 29 Electroluminescence spectra of complexes [Ir(C^N)$_2$(bpy)][PF$_6$] with C^N = **3**, **8** and **9** in device configuration: ITO/PEDOT:PSS/[Ir(C^N)$_2$(bpy)][PF$_6$]:[Bmim][PF$_6$] 4:1/Al.

Maximum luminance levels (Lum_{max}), power conversion efficiencies (PCE) and external quantum efficiencies (EQE) gained from measurements of LEECs containing [Ir(C^N)$_2$(bpy)][PF$_6$] with C^N = **3** and **9** are similar to each other (*cf.* Table 7, *e.g.* Lum_{max} = 182 and 206 cd m^{-2}). For [Ir(**8**)$_2$(bpy)][PF$_6$], on the other hand, the values are roughly four to five times higher; the maximum luminance reaches 940 cd m^{-2} and maximum PCE and EQE

values are 4.4 lm W^{-1} and 2.6%, respectively. The significantly enhanced efficiency of a LEEC containing [Ir(**8**)$_2$(bpy)][PF_6], with respect to devices based on the other two regioisomers, may be rationalized by the significantly higher quantum yields of [Ir(**8**)$_2$(bpy)][PF_6] both in solution and powder. While maximum luminance levels and efficiency parameters of [Ir(C^N)$_2$(bpy)][PF_6] with C^N = **3** and **9** are poor, the values obtained from LEECs with [Ir(**8**)$_2$(bpy)][PF_6] are comparable to efficient green light emitting devices reported in the literature.[82,93,107,125]

Table 7 Performance parameters of LEECs containing complexes [Ir(C^N)$_2$(bpy)][PF_6] with C^N = **3**, **8** and **9**; measured under pulsed current conditions at an average current density of 100 A m^{-2} (block wave, 1 kHz frequency, 50% duty cycle).[21,80,82]

Compound	t_{on} **[min]**	Lum_{max} **[cd m^{-2}]**	$t_{1/2}$ **[min]**	**PCE [lm W^{-1}]**	**EQE [%]**	λ_{EL}^{max} **[nm]**
[Ir(**3**)$_2$(bpy)][PF_6]	19	182	69	0.9	0.5	495 sh, 553
[Ir(**8**)$_2$(bpy)][PF_6]	7	940	51	4.4	2.6	549
[Ir(**9**)$_2$(bpy)][PF_6]	4	206	38	0.9	0.6	560

Fig. 30 shows the performance of the different LEECs in terms of luminance and average voltage *vs.* time. One can see that turn-on times are reduced by moving the methylsulfone substituent from 5- to 4- and 3-position, resulting in a decrease from 19 minutes to seven and four minutes. In relation to the device lifetimes these values are still relatively high. The longest lifetime defined as $t_{1/2}$ is observed for [Ir(**3**)$_2$(bpy)][PF_6] (5-SO_2Me, 69 min), followed by [Ir(**8**)$_2$(bpy)][PF_6] (4-SO_2Me, 51 min) and [Ir(**9**)$_2$(bpy)][PF_6] (3-SO_2Me, 38 min). Device stability is therefore limited for LEECs containing our series of regioisomeric methylsulfonyl-substituted iridium complexes; values obtained for both t_{on} and $t_{1/2}$ are however within the range of comparable green emitters used in light emitting electrochemical cells. Lifetimes reported in the literature lie between a few minutes[80,93,107,108] and less than a hundred hours[80,82,93,107–110,125] and turn-on times range from <5 s[80,82,93,107] to several hours.[80,93,108,109,125]

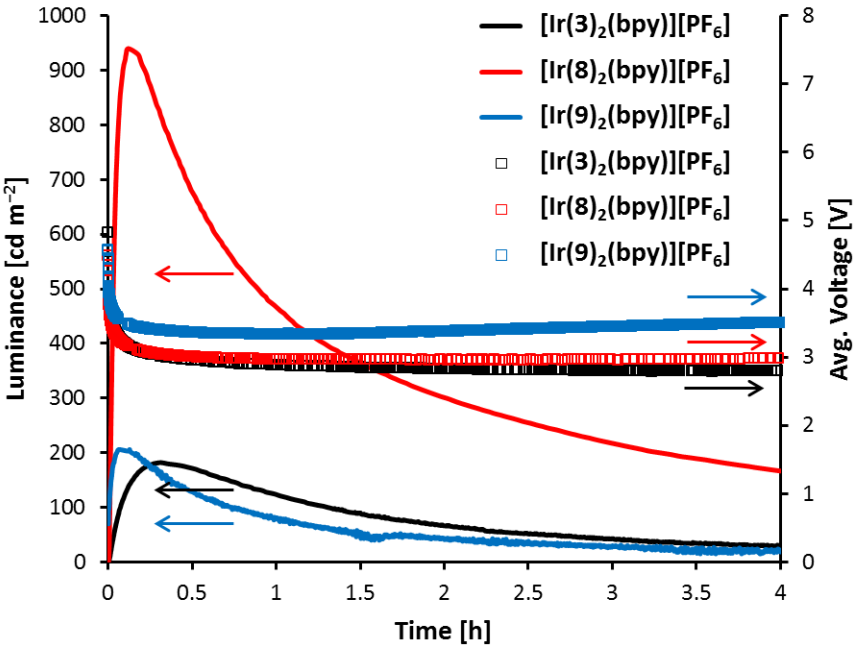

Fig. 30 Luminance (solid lines) and average voltage curves (open squares) *vs.* time for $[Ir(C\text{^}N)_2(bpy)][PF_6]$ (C^N = **3**, **8**, **9**), measured under block-wave pulsed current conditions with a frequency of 1 kHz, 50% duty cycles and an average current density of 100 A m^{-2}.[21,80,82] Device composition: ITO/PEDOT:PSS/$[Ir(C\text{^}N)_2(bpy)][PF_6]$:[Bmim][$PF_6$] 4:1/Al.

7. Conclusions

A series of regioisomeric iridium complexes containing methylsulfonyl-functionalized cyclometallating ligands was prepared in order to study the effect of the substituent's position on the photophysical, electrochemical and device properties. Single crystal data were obtained for all three complexes, showing the expected core structures and the influence of steric hindrance induced by the SO_2Me group in the 3-position of the cyclometallating ligand, leading to ligand distortions.

All complexes are green emitters in solution and yellow emitters as powder samples. Vibrationally structured emission bands in CH_3CN solution were observed for complexes with sulfone groups in the 3- and 5-position of the phenyl ring (*meta* to the Ir–C bond). The two complexes showed similar quantum yields and lifetimes. An enhanced PLQY of 92%, shorter excited state lifetime and a broad, unstructured emission profile were obtained for the 4-substituted compound (substituent *para* to Ir–C bond). The lack of a vibrational emission

profile suggests a more pronounced charge transfer character of the emissive triplet state compared to the other two complexes. In the solid state (powder), emission maxima are red-shifted, vibrational structure is lost and quantum yields and lifetimes are decreased, indicating excited state quenching due to intermolecular interactions. $[Ir(\mathbf{8})_2(bpy)][PF_6]$ (4-SO_2Me) again has the highest quantum yield of 27%. Electrochemical data parallel the photoluminescence trends and show that a methylsulfone substituent in *para* position to the Ir–C bond has the largest influence on the oxidation potential.

Yellow-green electroluminescence with maxima ranging from 549 to 560 nm is observed for LEECs with all complexes. Maximum luminance levels, power conversion efficiencies and EQEs are similar for complexes with the sulfone substituent *meta* to the Ir–C bond. For the complex containing the methylsulfonyl group in 4-position (*para* to the Ir–C bond), significantly higher luminance (940 cd m^{-2}) and efficiencies (PCE = 4.4 lm W^{-1} and EQE = 2.6%) are obtained. The increased efficiency correlates with the higher solid state quantum yield. Lifetimes are unfortunately rather short and comparable for all devices, ranging from 38 to 69 min.

In order to achieve the desired blue emission, it is necessary to replace the 2,2'-bipyridine by an electron-richer ancillary ligand which is capable of destabilizing the LUMO, leading to a larger HOMO-LUMO gap. As cyclometallating ligands, the methylsulfonyl-functionalized phenylpyridines substituted in the 4- and 5-positions of the phenyl ring should be chosen, as they gave the most promising results concerning largest emission maximum blue-shift and highest quantum yield. In principle, it should then be possible to obtain fluorine-free blue emitting iridium complexes. Attempts to reach this goal are discussed in the next chapter of this thesis.

8. Experimental

The following experimental procedures have been written by the author of this thesis and parts have been published in RSC Advances.[126]

8.1. General

The synthesis of [Ir(**3**)$_2$(bpy)][PF_6] was described in Chapter I.[127] [Ir(cod)Cl]$_2$[128] and 2-(2-methylsulfonylphenyl)pyridine (H**9**)[122,123] were synthesized according to literature procedures. 3-Fluorophenylboronic acid was obtained from Fluorochem and purity was determined by ^{1}H NMR spectroscopy to ca. 67%.

8.2. 2-(3-Fluorophenyl)pyridine

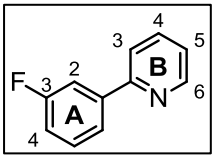

3-Fluorophenylboronic acid (67%, 1.67 g, 8.00 mmol, 1.5 eq.), 2-bromopyridine (0.500 mL, 5.22 mmol, 1.0 eq.), $PdCl_2$ (25.2 mg, 0.142 mmol, 0.027 eq.) and K_2CO_3 (1.54 g, 11.1 mmol, 2.1 eq.) were suspended in EtOH and H_2O (1:1, 40 mL). The mixture was heated at reflux overnight, then poured into brine (150 mL) and extracted with *t*-BME (3 × 150 mL). The combined organic layers were dried over Na_2SO_4 and the solvent was removed under reduced pressure. The residue was purified by column chromatography (silica, toluene–ethyl acetate 5:1) to yield 2-(3-fluorophenyl)pyridine as a colourless oil (764 mg, 4.41 mmol, 84.5%). ^{1}H NMR (500 MHz, $CDCl_3$) δ/ppm 8.66 (*pseudo*-dt, J = 4.9, 1.3 Hz, 1H, H^{B6}), 7.77–7.70 (overlapping m, 2H, H^{A2+A6}), 7.69–7.62 (overlapping m, 2H, H^{B3+B4}), 7.41–7.35 (m, 1H, H^{A5}), 7.18 (m, 1H, H^{B5}), 7.07 (*pseudo*-td, J = 8.4, 2.3 Hz, 1H, H^{A4}). $^{13}C\{^1H\}$ NMR (126 MHz, $CDCl_3$) δ/ppm 163.3 (d, J_{CF} = 245.3 Hz, C^{A3}), 155.9 (d, J_{CF} = 2.7 Hz, C^{B2}), 149.7 (C^{B6}), 141.7 (d, J_{CF} = 7.6 Hz, C^{A1}), 136.8 (C^{B4}), 130.2 (d, J_{CF} = 8.2 Hz, C^{A5}), 122.6 (C^{B5}), 122.4 (d, J_{CF} = 2.8 Hz, C^{A6}), 120.5 (C^{B3}), 115.7 (d, J_{CF} = 21.3 Hz, C^{A4}), 113.8 (d, J_{CF} = 22.8 Hz, C^{A2}). LC-ESI-MS *m/z* 174.0 $[M+H]^+$ (calc. 174.1). Found C 75.95, H 4.87, N 8.25; $C_{11}H_8FN$ requires C 76.29, H 4.66, N 8.09%. Spectroscopic data matched those reported in the literature.[129,130]

8.3. 2-(3-Methylthiophenyl)pyridine

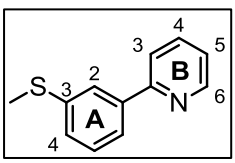

A microwave vial was charged with 2-(3-fluorophenyl)pyridine (916 mg, 5.29 mmol, 1.0 eq.) and *N*-methyl-2-pyrrolidone (18 mL) and purged with N_2. Sodium thiomethoxide (1.51 g, 21.5 mmol, 4.1 eq.) was added and the

dark pink mixture was heated at 120 °C for 1 h in a microwave reactor. The resulting pale brown mixture was poured into H_2O (150 mL) and brine (50 mL) and extracted with CH_2Cl_2 (4 × 100 mL). The combined organic layers were washed with H_2O (4 × 100 mL), dried over Na_2SO_4 and the solvent was removed under reduced pressure. The residue was purified by column chromatography (silica, toluene changing to toluene–ethyl acetate 1:1) to yield 2-(3-methylthiophenyl)pyridine as a colourless liquid (826 mg, 4.10 mmol, 77.6%). ^{1}H NMR (500 MHz, $CDCl_3$) δ/ppm 8.70 (ddd, J = 4.8, 1.8, 1.0 Hz, 1H, H^{B6}), 7.92 (*pseudo*-t, J = 1.9 Hz, 1H, H^{A2}), 7.79–7.69 (overlapping m, 3H, $H^{A6+B3+B4}$), 7.39 (*pseudo*-t, J = 7.8 Hz, 1H, H^{A5}), 7.31 (ddd, J = 7.8, 1.9, 1.1 Hz, 1H, H^{A4}), 7.26–7.23 (m, 1H, H^{B5}), 2.56 (s, 3H, H^{Me}). ^{13}C{^{1}H} NMR (126 MHz, $CDCl_3$) δ/ppm 157.1 (C^{B2}), 149.8 (C^{B6}), 140.2 (C^{A1}), 139.3 (C^{A3}), 136.9 (C^{B4}), 129.3 (C^{A5}), 127.2 (C^{A4}), 125.2 (C^{A2}), 123.8 (C^{A6}), 122.5 (C^{B5}), 120.8 (C^{B3}), 16.0 (C^{Me}). IR (solid, $\tilde{\nu}$/cm^{-1}) 3051 (w), 3006 (w), 2986 (w), 2920 (w), 2857 (w), 1722 (w), 1584 (s), 1560 (s), 1457 (s), 1431 (s), 1400 (m), 1279 (m), 1261 (m), 1153 (m), 1096 (m), 1083 (m), 1066 (m), 1041 (m), 990 (m), 966 (m), 902 (w), 882 (m), 800 (m), 764 (s), 742 (s), 687 (s), 640 (m), 635 (m), 614 (m), 585 (m), 505 (w). LC-ESI-MS m/z 202.0 $[M+H]^+$ (calc. 202.1). Found C 71.15, H 5.88, N 6.78; $C_{12}H_{11}NS$ requires C 71.60, H 5.51, N 6.96%.

8.4. 2-(3-Methylsulfonylphenyl)pyridine (H8)

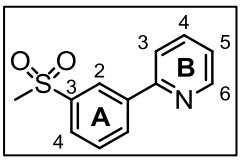

2-(3-Methylthiophenyl)pyridine (826 mg, 4.10 mmol, 1.0 eq.) and sodium tungstate dihydrate (677 mg, 2.05 mmol, 0.50 eq.) were suspended in MeOH (25 mL). H_2O_2 (30%, 1.00 mL, 10.0 mmol, 2.4 eq.) was added and the suspension stirred at room temperature overnight. The mixture was poured into a mixture of H_2O (150 mL) and saturated aqueous Na_2CO_3 solution (50 mL) and extracted with CH_2Cl_2 (3 × 100 mL). The combined organic layers were dried over Na_2SO_4 and the solvent was removed under reduced pressure. The residue was purified by column chromatography (silica, CH_2Cl_2–1% MeOH changing to CH_2Cl_2–2% MeOH) to yield 2-(3-methylsulfonylphenyl)pyridine (H**8**) as a white solid (786 mg, 3.37 mmol, 82.1%). M.p. 94.3 °C. ^{1}H NMR (500 MHz, $CDCl_3$) δ/ppm 8.74–8.68 (m, 1H, H^{B6}), 8.57 (*pseudo*-t, J = 1.9 Hz, 1H, H^{A2}), 8.30 (m, 1H, H^{A4}), 7.98 (*pseudo*-ddt, J = 7.7, 2.0, 1.0 Hz, 1H, H^{A6}), 7.84–7.75 (overlapping m, 2H, H^{B3+B4}), 7.68 (*pseudo*-td, J = 7.8, 0.9 Hz, 1H, H^{A5}), 7.30 (dddd, J = 7.1, 4.9, 2.3, 0.8 Hz, 1H, H^{B5}), 3.11 (s, 3H, H^{Me}). ^{13}C{^{1}H} NMR (126 MHz, $CDCl_3$) δ/ppm 155.2 (C^{B2}), 150.1 (C^{B6}), 141.3 (C^{A3}), 141.0 (C^{A1}), 137.2 (C^{B4}), 132.1 (C^{A4}), 130.0 (C^{A5}), 127.6 (C^{A6}), 125.9 (C^{A2}), 123.3 (C^{B5}), 120.8 (C^{B3}), 44.6 (C^{Me}). IR (solid, $\tilde{\nu}$/cm^{-1}) 3080 (w),

2997 (w), 2916 (w), 1586 (m), 1565 (w), 1458 (m), 1444 (m), 1408 (w), 1323 (m), 1297 (s), 1280 (m), 1145 (s), 1093 (m), 1066 (m), 992 (w), 975 (m), 916 (w), 886 (w), 818 (m), 780 (m), 754 (s), 680 (m), 638 (w), 614 (m), 593 (m), 539 (s), 511 (s), 486 (m). LC-ESI-MS *m/z* 234.0 $[M+H]^+$ (calc. 234.1). Found C 61.53, H 4.98, N 6.22; $C_{12}H_{11}NO_2S$ requires C 61.78, H 4.75, N 6.00%.

8.5. $[Ir(8)_2Cl]_2$

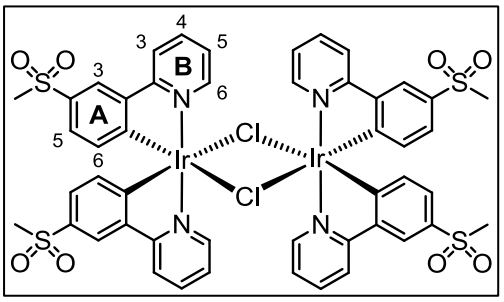

2-(3-Methylsulfonylphenyl)pyridine (H**8**) (105 mg, 0.450 mmol, 3.9 eq.) was dissolved in 2-ethoxyethanol (3 mL). The solution was purged with N_2, then $[Ir(cod)Cl]_2$ (77.2 mg, 0.115 mmol, 1.0 eq.) was added. The mixture was heated at reflux overnight. After letting the mixture cool to room temperature, the precipitate was filtered off, washed with 2-ethoxyethanol, H_2O and EtOH and dried under vacuum to yield $[Ir(\mathbf{8})_2Cl]_2$ as a yellow powder (131 mg, 94.6 µmol, 84.0%) which was used for subsequent reactions without further purification. ^{1}H NMR (500 MHz, $CDCl_3$) δ/ppm 9.19 (ddd, J = 5.7, 1.5, 0.7 Hz, 4H, H^{B6}), 8.11 (ddd, J = 8.5, 1.4, 0.7 Hz, 4H, H^{B3}), 8.05 (d, J = 2.0 Hz, 4H, H^{A3}), 7.96 (ddd, J = 8.1, 7.6, 1.5 Hz, 4H, H^{B4}), 7.09 (dd, J = 8.3, 2.0 Hz, 4H, H^{A5}), 6.98 (ddd, J = 7.3, 5.5, 1.4 Hz, 4H, H^{B5}), 6.05 (d, J = 8.3 Hz, 4H, H^{A6}), 2.91 (s, 12H, H^{Me}). IR (solid, $\tilde{\nu}$/cm^{-1}) 2922 (w), 1609 (m), 1577 (m), 1480 (m), 1423 (m), 1401 (w), 1298 (s), 1224 (w), 1146 (s), 1096 (m), 1068 (m), 1054 (m), 1032 (m), 959 (s), 887 (w), 827 (m), 784 (m), 761 (s), 728 (m), 703 (m), 639 (w), 593 (s), 558 (s), 522 (s), 486 (m), 463 (m). LC-ESI-MS *m/z* 657.1 $[Ir(C\text{^}N)_2]^+$ (calc. 657.1), 698.1 $[Ir(C\text{^}N)_2(CH_3CN)]^+$ (calc. 698.1), 739.1 $[Ir(C\text{^}N)_2(CH_3CN)_2]^+$ (calc. 739.1).

8.6. $[Ir(9)_2Cl]_2$

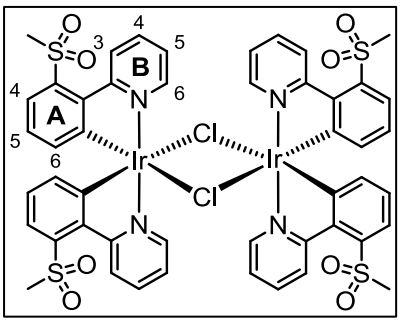

2-(2-Methylsulfonylphenyl)pyridine (H**9**) (354 mg, 1.52 mmol, 1.8 eq.) was suspended in a mixture of 2-ethoxyethanol and H_2O (3:1, 4 mL) in a microwave vial and purged with N_2. $IrCl_3 \cdot xH_2O$ (ca. 82%, 307 mg, 0.842 mmol, 1.0 eq.) was added and the mixture was heated at 110 °C for 1.5 h in a microwave reactor (2 bar). The resulting precipitate was filtered off, washed with H_2O and EtOH, redissolved in CH_2Cl_2 and the solvent was removed under reduced pressure. The orange precipitate which had formed in the filtrate was filtered off, washed with EtOH, redissolved with CH_2Cl_2 and the solvent removed. Both residues were combined to yield the product as a brownish-orange solid (424 mg, 0.306 mmol, 80.5%). ^{1}H NMR (500 MHz, $CDCl_3$) δ/ppm 9.33 (*pseudo*-dt, J = 8.5, 1.1 Hz, 4H, H^{B3}), 9.14 (ddd, J = 5.8, 1.8, 0.8 Hz, 4H, H^{B6}), 7.92 (ddd, J = 8.5, 7.4, 1.7 Hz, 4H, H^{B4}), 7.62 (dd, J = 7.7, 1.1 Hz, 4H, H^{A4}), 6.90 (ddd, J = 7.3, 5.7, 1.4 Hz, 4H, H^{B5}), 6.69 (*pseudo*-t, J = 7.8 Hz, 4H, H^{A5}), 5.88 (dd, J = 7.9, 1.1 Hz, 4H, H^{A5}), 3.22 (s, 12H, H^{Me}). IR (solid, $\tilde{\nu}$/cm^{-1}) 2928 (w), 1604 (w), 1561 (w), 1474 (m), 1422 (w), 1395 (w), 1290 (m), 1274 (m), 1256 (m), 1154 (m), 1129 (s), 1067 (m), 961 (m), 786 (m), 755 (m), 736 (m), 722 (m), 709 (m), 646 (w), 586 (w), 573 (w), 551 (w), 537 (s), 527 (s), 488 (s), 465 (m). LC-ESI-MS *m/z* 657.1 $[Ir(C\text{^}N)_2]^+$ (calc. 657.1), 698.1 $[Ir(C\text{^}N)_2(CH_3CN)]^+$ (calc. 698.1), 739.0 $[Ir(C\text{^}N)_2(CH_3CN)_2]^+$ (calc. 739.1). Found C 40.62, H 3.28, N 4.08; $C_{48}H_{40}Cl_2Ir_2N_4O_8S_4 \cdot 2H_2O$ requires C 40.59, H 3.12, N 3.94%.

8.7. General procedure for the synthesis of iridium(III) complexes

The iridium dimer and ancillary ligand were suspended in MeOH (15 mL) in a microwave vial and heated at 120 °C for 1 h in a microwave reactor. The resulting yellow solution was filtered through cotton and concentrated under reduced pressure. The residue was dissolved in little MeOH, an excess of solid NH_4PF_6 was added and the resulting suspension was stirred for 5 min at room temperature. The yellow precipitate was filtered off and redissolved in CH_2Cl_2. The solvent was removed under reduced pressure and the crude product was purified by column chromatography (silica). Further purification was done by dissolving the residue in little CH_2Cl_2, precipitating with Et_2O and leaving in the refrigerator overnight. The resulting precipitation was filtered off, washed with MeOH and Et_2O and dried under vacuum.

8.8. $[Ir(8)_2(bpy)][PF_6]$

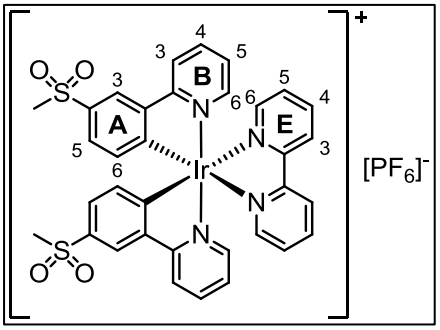

$[Ir(\mathbf{8})_2Cl]_2$ (101 mg, 73.0 µmol, 1.0 eq.) and bpy (36.4 mg, 0.233 mmol, 3.2 eq.). Purification by column chromatography (silica, CH_2Cl_2 changing to CH_2Cl_2–4% MeOH). $[Ir(\mathbf{8})_2(bpy)][PF_6]$ was isolated as a pale yellow solid (63.2 mg, 0.146 mmol, 45.2%). ^{1}H NMR (500 MHz, CD_3CN) δ/ppm 8.53 (*pseudo*-dt, J = 8.3, 1.0 Hz, 2H, H^{E3}), 8.30 (d, J = 2.0 Hz, 2H, H^{A3}), 8.26 (*pseudo*-dt, J = 8.2, 1.0 Hz, 2H, H^{B3}), 8.16 (*pseudo*-td, J = 8.0, 1.6 Hz, 2H, H^{E4}), 7.96 (*pseudo*-td, J = 7.9, 1.5 Hz, 2H, H^{B4}), 7.90 (ddd, J = 5.3, 1.5, 0.9 Hz, 2H, H^{E6}), 7.66 (*pseudo*-dt, J = 5.7, 1.2 Hz, 2H, H^{B6}), 7.52 (ddd, J = 7.7, 5.5, 1.2 Hz, 2H, H^{E5}), 7.39 (dd, J = 8.0, 2.0 Hz, 2H, H^{A5}), 7.17 (ddd, J = 7.4, 5.8, 1.4 Hz, 2H, H^{B5}), 6.54 (d, J = 8.0 Hz, 2H, H^{A6}), 3.04 (s, 6H, $H^{A4\text{-}SO2Me}$). $^{13}C\{^1H\}$ NMR (126 MHz, CD_3CN) δ/ppm 166.3 (C^{B2}), 159.7 (C^{A1}), 156.5 (C^{E2}), 151.8 (C^{E6}), 150.6 (C^{B6}), 146.3 (C^{A2}), 140.8 (C^{E4}), 140.3 (C^{B4}), 136.7 (C^{A4}), 133.4 (C^{A6}), 129.6 (C^{E5}), 129.0 (C^{A5}), 125.9 (C^{B5}), 125.8 (C^{E3}), 124.1 (C^{A3}), 122.0 (C^{B3}), 44.6 ($C^{A4\text{-}SO2Me}$). IR (solid, $\tilde{\nu}$/cm^{-1}) 3041 (w), 1609 (w), 1579 (w), 1480 (w), 1448 (w), 1426 (w), 1401 (w), 1300 (m), 1246 (w), 1225 (w), 1146 (s), 1096 (w), 1067 (w), 1056 (w), 1032 (m), 960 (m), 840 (s), 784 (m), 760 (s), 734 (m), 703 (w), 640 (w), 594 (m), 557 (s), 524 (m), 485 (m). UV/Vis (CH_3CN, 1.0 × 10^{-5} mol dm^{-3}) λ/nm (ε/dm^3 mol^{-1} cm^{-1}) 253 (62 000), 271 sh (48 000), 313 sh (19 000), 337 sh (9100), 406 sh (2800). Emission (CH_3CN, 1.0 × 10^{-5} mol dm^{-3}, λ_{exc} = 271 nm): λ_{em}^{max} = 517 nm. ESI-MS *m/z* 813.4 $[M–PF_6]^+$ (calc. 813.1). Found C 41.62, H 3.10, N 6.03; $C_{34}H_{28}F_6IrN_4O_4PS_2 \cdot H_2O$ requires C 41.84, H 3.10, N 5.74%.

8.9. $[Ir(9)_2(bpy)][PF_6]$

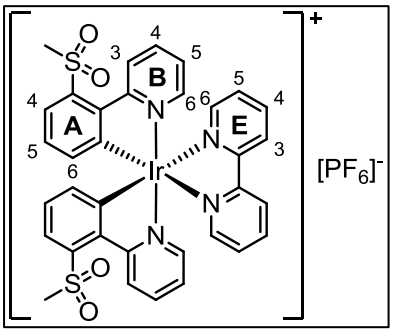

$[Ir(\mathbf{9})_2Cl]_2$ (114 mg, 82.3 µmol, 1.0 eq.) and bpy (28.5 mg, 0.182 mmol, 2.2 eq.). Purification by column chromatography (silica, CH_2Cl_2 changing to CH_2Cl_2–2% MeOH). $[Ir(\mathbf{9})_2(bpy)][PF_6]$ was isolated as a dark yellow solid (97.5 mg, 0.102 mmol, 61.8%). ^{1}H NMR (500 MHz, CD_3CN) δ/ppm 9.30 (ddd, J = 8.6, 1.3, 0.8 Hz, 2H, H^{B3}), 8.54 (*pseudo*-dt, J = 8.3, 1.1 Hz, 2H, H^{E3}), 8.16 (ddd, J = 7.7, 1.5 Hz, 2H, H^{E4}), 7.98 (ddd, J = 8.7, 7.5, 1.7 Hz, 2H, H^{B4}), 7.89 (dd, J = 7.8, 1.2 Hz, 2H, H^{A4}), 7.85 (ddd, J = 5.5, 1.6, 0.7 Hz, 2H, H^{E6}), 7.76 (ddd, J = 5.8, 1.7, 0.7 Hz, 2H, H^{B6}), 7.51 (ddd, J = 7.7, 5.5, 1.2 Hz, 2H, H^{E5}), 7.14

(ddd, J = 7.3, 5.8, 1.3 Hz, 2H, H^{B5}), 7.07 (*pseudo*-t, J = 7.7 Hz, 2H, H^{A5}), 6.47 (dd, J = 7.7, 1.2 Hz, 2H, H^{A6}), 3.25 (s, 6H, $H^{A3\text{-}SO2Me}$). $^{13}C\{^{1}H\}$ NMR (126 MHz, CD_3CN) δ/ppm 164.6 (C^{B2}), 156.5 (C^{E2}), 155.6 (C^{A1}), 151.5 (C^{E6}), 151.2 (C^{B6}), 141.1 (C^{A2}), 140.8 (C^{E4}), 140.6 (C^{A3}), 139.9 (C^{B4}), 137.7 (C^{A6}), 130.4 (C^{A5}), 129.6 (C^{E5}), 127.7 (C^{B3}), 126.0 (C^{B5}), 125.9 (C^{E3}), 125.5 (C^{A4}), 43.5 ($C^{A3\text{-}SO2Me}$). IR (solid, $\tilde{\nu}$/cm^{-1}) 3124 (w), 3039 (w), 2933 (w), 1609 (w), 1563 (w), 1477 (m), 1449 (w), 1411 (w), 1396 (w), 1308 (m), 1278 (m), 1243 (w), 1200 (w), 1170 (w), 1155 (m), 1131 (m), 1113 (m), 1070 (w), 1045 (w), 1031 (w), 1001 (w), 962 (m), 904 (w), 876 (w), 835 (s), 803 (m), 792 (m), 760 (s), 752 (s), 735 (m), 724 (m), 716 (m), 667 (w), 647 (w), 581 (w), 556 (s), 525 (s), 482 (s). UV/Vis (CH_3CN, 1.0 × 10^{-5} mol dm^{-3}) λ/nm (ε/dm^3 mol^{-1} cm^{-1}) 259 (46 000), 300 sh (28 000), 310 sh (25 000), 360 sh (8000), 397 (5400), 437 sh (3300). Emission (CH_3CN, 1.0 × 10^{-5} mol dm^{-3}, λ_{exc} = 400 nm): λ_{em}^{max} = 506, 527 nm. ESI-MS *m/z* 813.4 $[M–PF_6]^+$ (calc. 813.1). Found C 42.49, H 3.24, N 6.08; $C_{34}H_{28}F_6IrN_4O_4PS_2$ requires C 42.63, H 2.95, N 5.85%.

8.10. Crystallography

2{[Ir(1)$_2$(bpy)][PF$_6$]}·7CH$_2$Cl$_2$. $C_{75}H_{70}Cl_{14}F_{12}Ir_2N_8O_8P_2S_4$, M = 2510.39, needle, orthorhombic, space group *Pbca*, a = 18.1495(15), b = 22.5027(19), c = 23.189(2) Å, U = 9470.7(8) Å^3, Z = 4, D_c = 1.761 Mg m^{-3}, μ(Mo-Kα) = 3.403 mm^{-1}, T = 123 K. Total 72763 reflections, 14677 unique, R_{int} = 0.045. Refinement of 14611 reflections (661 parameters) with I >2σ (I) converged at final R1 = 0.0524 (R1 all data = 0.0871), wR2 = 0.1260 (wR2 all data = 0.1539), gof = 1.0026. CCDC 1421913.

2{[Ir(8)$_2$(bpy)][PF$_6$]}·5.5H$_2$O. $C_{68}H_{67}F_{12}Ir_2N_8O_{13.50}P_2S_4$, M = 2014.95, yellow block, monoclinic, space group $P2_1/c$, a = 20.6753(13), b = 20.9141(13), c = 18.3265(12) Å, β = 104.473(2)^o, U = 7673.0(5) Å^3, Z = 4, D_c = 1.744 Mg m^{-3}, μ(Cu-Kα) = 8.865 mm^{-1}, T = 123 K. Total 105992 reflections, 13988 unique, R_{int} = 0.041. Refinement of 13925 reflections (959 parameters) with I >2σ (I) converged at final R1 = 0.0422 (R1 all data = 0.0458), wR2 = 0.1120 (wR2 all data = 0.1143), gof = 0.9557. CCDC 1421914.

[Ir(9)$_2$(bpy)][PF$_6$]. $C_{34}H_{28}F_6IrN_4O_4PS_2$, M = 957.93, yellow needle, monoclinic, space group $C2/c$, a = 15.6899(16), b = 28.163(3), c = 8.4211(9) Å, β = 115.797(3)^o, U = 3350.3(4) Å^3, Z = 4, D_c = 1.899 Mg m^{-3}, μ(Cu-Kα) = 10.052 mm^{-1}, T = 123 K. Total 18964 reflections, 3003 unique, R_{int} = 0.029. Refinement of 3003 reflections (236 parameters) with I>2σ (I)

converged at final *R*1 = 0.0222 (*R*1 all data = 0.0223), *wR*2 = 0.0486 (*wR*2 all data = 0.0486), gof = 1.0000. CCDC 1421915.

CHAPTER III: GREEN & BLUE EMITTERS – PYRAZOLYLPYRIDINE ANCILLARY LIGANDS

1. Introduction

The development of efficient and stable blue emitters remains desirable in the field of light-emitting electrochemical cells. Up to date, most of the blue emitting iridium complexes used in LEECs comprise fluoro-substituted cyclometallating ligands, for example fluorine-functionalized phenylpyridines,[82,131] phenylpyrazoles[80,132,133] or phenyltriazoles.[134] The electron-withdrawing nature of fluorine leads to a stabilization of the HOMO, resulting in a larger HOMO-LUMO energy gap. Until now, not many alternative functional groups have been investigated, although fluorine substituents have been shown to lower device stability in both OLEDs[81] and LEECs[82] (*cf.* Chapter I). One of the main goals in the field of light emitting electrochemical cells is therefore the design of fluorine-free blue emitting iridium complexes. Mostly, this has been achieved by replacing the standard 2,2'-bipyridine by more electron-rich ancillary ligands. Examples include 4,4'-dimethylamino-2,2'-bipyridine,[134,135] strong-field ancillary ligands (*e.g.* PPh_3, CN^-, CO, CH_3CN),[136] triazolylpyridines,[131,137] imidazolylpyridines[138] and carbene-based ancillary ligands.[139,140] Another strategy which has been less often pursued is the use of electron-deficient cyclometallating ligands. Emission blue-shifts were achieved with phenylpyrazoles,[141] phenyltetrazoles,[142] methoxy-substituted 2,3'-bipyridines[107] or sulfone-substituted phenylpyrazoles[93] and phenylpyridines.[95]

Another ancillary ligand group which has been shown to efficiently tune the emission colour to the blue region is based on pyrazolylpyridines.[78,132,143–148] These ancillary ligands have been combined with fluoro-substituted or unsubstituted phenylpyridine[78,143–146,148] and phenylpyrazole[132,147] cyclometallating ligands to yield green to blue emitting iridium complexes.

That the introduction of sulfone-functionalized phenylpyridine C^N ligands can efficiently shift the emission maximum to the green region was shown in Chapters I and II.[95] To further blue-shift the emission, it is necessary to replace the bpy ancillary ligand by a more electron-rich ligand. This should lead to a destabilization of the LUMO and therefore a larger

HOMO-LUMO energy gap. In this chapter, the synthesis, characterization and device performance of a series of four iridium complexes with cyclometallating ligands containing methylsulfonyl groups in 4- or 5-position and pyrazolylpyridine-based ancillary ligands (2-(1*H*-pyrazol-1-yl)pyridine (pzpy) and 2-(3,5-dimethyl-1*H*-pyrazol-1-yl)pyridine (dmpzpy)) are reported.

2. Synthesis and NMR Spectroscopic Characterization

2.1. Ligand synthesis

The synthesis of cyclometallating ligands H**3** and H**8** was described in detail in Chapters I and II. Ancillary ligands 2-(1*H*-pyrazol-1-yl)pyridine (pzpy) and 2-(3,5-dimethyl-1*H*-pyrazol-1-yl)pyridine (dmpzpy) were prepared according to a procedure described in the literature (Scheme 13). 2-Bromopyridine was reacted with 1*H*-pyrazole or 3,5-dimethyl-1*H*-pyrazole in an Ullmann-type coupling reaction using CuI as catalyst and L-proline as additive.[149] The desired ligands were obtained in moderate to good yields and ^{1}H NMR data matched those reported.[150,151]

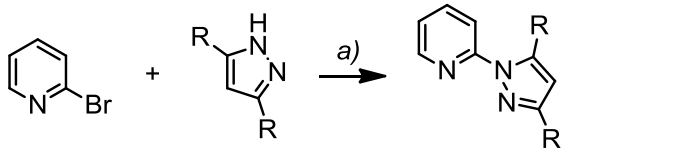

pzpy: R = H, **65.9%**
dmpzpy: R = Me, **39.6%**

Scheme 13 Synthetic route to ancillary ligands 2-(1*H*-pyrazol-1-yl)pyridine (pzpy) and 2-(3,5-dimethyl-1*H*-pyrazol-1-yl)pyridine (dmpzpy). Reaction conditions: *a)* CuI, L-proline, K_2CO_3, DMSO, 130 °C, 2–3 d, N_2.

2.2. Synthesis of $[Ir(C^N)_2Cl]_2$ dimers

The synthetic routes followed to obtain chlorido-bridged iridium dimers $[Ir(\mathbf{3})_2Cl]_2$ and $[Ir(\mathbf{8})_2Cl]_2$ were reported in Chapters I and II.

2.3. Synthesis of $[Ir(C^N)_2(N^N)][PF_6]$ complexes

The synthetic strategy leading to complexes $[Ir(C^N)_2(N^N)][PF_6]$ with C^N = **3**, **8** and N^N = pzpy, dmpzpy is shown in Scheme 14. Under microwave conditions, dimers $[Ir(\mathbf{3})_2Cl]_2$ and $[Ir(\mathbf{8})_2Cl]_2$ are treated with the appropriate ancillary ligand (pzpy or dmpzpy) in MeOH. Anion exchange is performed by addition of solid NH_4PF_6 to a methanolic solution of the chloride complexes, leading to precipitation of the $[PF_6]^-$ salts. Filtration and subsequent purification gave the desired compounds in yields ranging from 41 to 99%.

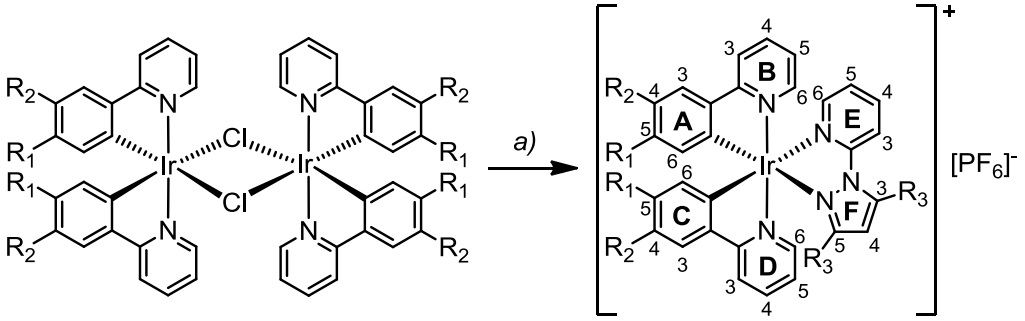

$[Ir(\mathbf{3})_2(pzpy)][PF_6]$: $R_1 = SO_2Me$, $R_2 = R_3 = H$, **99.0%**
$[Ir(\mathbf{3})_2(dmpzpy)][PF_6]$: $R_1 = SO_2Me$, $R_2 = H$, $R_3 = Me$, **80.0%**
$[Ir(\mathbf{8})_2(pzpy)][PF_6]$: $R_2 = SO_2Me$, $R_1 = R_3 = H$, **40.9%**
$[Ir(\mathbf{8})_2(dmpzpy)][PF_6]$: $R_2 = SO_2Me$, $R_1 = H$, $R_3 = Me$, **77.7%**

Scheme 14 Synthesis of $[Ir(C^N)_2(N^N)][PF_6]$ with C^N = **3** or **8** and N^N = pzpy or dmpzpy. Reaction conditions: *a)* pzpy or dmpzpy, MeOH, MW, 120 °C, 1 h; then NH_4PF_6.

Complexes $[Ir(C^N)_2(N^N)][PF_6]$ (C^N = **3** and **8**, N^N = pzpy and dmpzpy) were fully characterized using NMR and IR spectroscopies, ESI mass spectrometry and elemental analysis. In the ESI mass spectra, the base peaks correspond to the $[Ir(C^N)_2(N^N)]^+$ cations for all complexes, exhibiting the characteristic iridium isotope pattern. ^1H and ^{13}C signals

were assigned with the help of 2D experiments (COSY, NOESY, HMQC and HMBC). Due to the asymmetric ancillary ligand, the cyclometallating ligands are inequivalent and give rise to two sets of NMR signals; NOESY cross peaks are observed between protons H^{E6} and H^{A6}, as well as between protons H^{F5}/$H^{F5\text{-}Me}$ and H^{B6} and/or H^{C6}, making distinction between the two C^N ligands possible (see Scheme 14 for numbering).

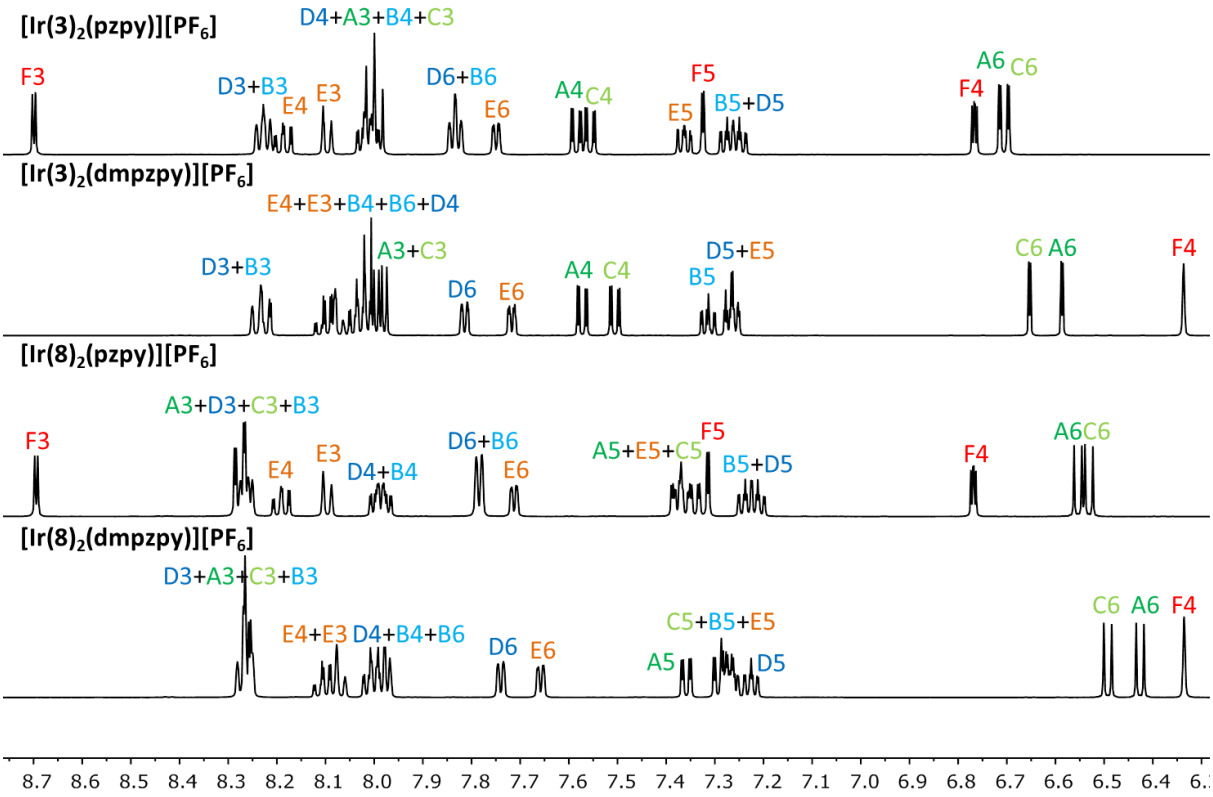

Fig. 31 Aromatic region of 500 MHz ^{1}H NMR spectra of complexes [Ir(C^N)$_2$(N^N)][PF$_6$] with C^N = **3**, **8** and N^N = pzpy, dmpzpy in CD_3CN including assignment. See Scheme 14 for numbering scheme. Scale: δ/ppm.

In Fig. 31, the aromatic regions of ^{1}H NMR spectra of [Ir(C^N)$_2$(N^N)][PF$_6$] with C^N = **3** or **8**, N^N = pzpy or dmpzpy are shown. Comparison of chemical shifts is made difficult by the many overlapping signals observed for all complexes. Pyrazole protons (F ring) resonate at the same frequency for the pzpy and dmpzpy complexes, regardless of the cyclometallating ligands. E ring protons on the pyridine moiety of the ancillary ligands are slightly affected by both the pyrazole moiety (methyl-substituted or unsubstituted) and the coordinated C^N

ligands. Methyl substitution on the ancillary ligand has an observable effect on protons H^{A6} and H^{B6}, moving the signal upfield ($\Delta\delta$ = 0.12 ppm) or downfield ($\Delta\delta$ = ca. 0.2 ppm, overlapping signals make exact determination difficult), respectively. Of the aromatic protons, H^{A6}, H^{C6} and H^{F4} appear at lowest frequency. Signals for H^{F4} are significantly shifted upfield by $\Delta\delta$ = 0.43 ppm in complexes [Ir(C^N)$_2$(dmpzpy)][PF$_6$] (δ = 6.34 ppm) with respect to [Ir(C^N)$_2$(pzpy)][PF$_6$] (δ = 6.77 ppm). The same effect, though less pronounced, is seen for H^{A6} ($\Delta\delta$ = 0.12 ppm) and H^{C6} ($\Delta\delta$ = 0.04–0.05 ppm).

3. Crystal Structure

Single crystals of [Ir(**8**)$_2$(dmpzpy)][PF$_6$]·CH$_3$CN were grown from an CH$_3$CN solution layered with Et$_2$O. The structure of the cation is shown in Fig. 32; important bond lengths and angles are reported in the figure caption. The compound crystallizes in the monoclinic space group *C*2/*c* and both Δ- and Λ-enantiomers are therefore present in the unit cell; the asymmetric unit contains the Λ-enantiomer. Both the $[PF_6]^-$ anion and the CH$_3$CN solvent molecule are ordered.

The methylsulfonyl groups are twisted with respect to the phenyl ring they are attached to with torsion angles of 27.4 (O1–S1–C18–C17), −22.4 (O2–S1–C18–C19), 15.0 (O3–S2–C30–C31) and −35.1° (O4–S2–C30–C29). These orientations lead to short intramolecular CH···OS contacts with distances of O1···HC17 = 2.61, O2···HC19 = 2.59, O3···HC31 = 2.61 and O4···HC29 = 2.68 Å. This is comparable to intramolecular interactions observed in series of alkyl–aryl[105] and aryl–aryl sulfones[105,124] reported in the literature and our sulfone-substituted ligands H**3** and H**5**,[95] dimer [Ir(**3**)$_2$Cl]$_2$[95] and complexes [Ir(C^N)$_2$(bpy)][PF$_6$] with C^N = **3** and **8** (*cf.* Chapters I and II).

The cyclometallating ligand containing N5 and C33 is nearly planar; the angle between the two ring planes amounts to 2.9°. The case is different for the dmpzpy ancillary ligand and the cyclometallating ligand containing N4 and C21: a considerable deviation from planarity is observed. Angles of 12.7 (C^N ligand) and 15.9° (N^N ligand) are the result of this distortion.

A preliminary structure was obtained for [Ir(**3**)$_2$(dmpzpy)][PF$_6$] from crystals grown by layering an CH_3CN solution of the complex with Et_2O. The expected structure containing the octahedral iridium centre and the three chelating ligands was confirmed.

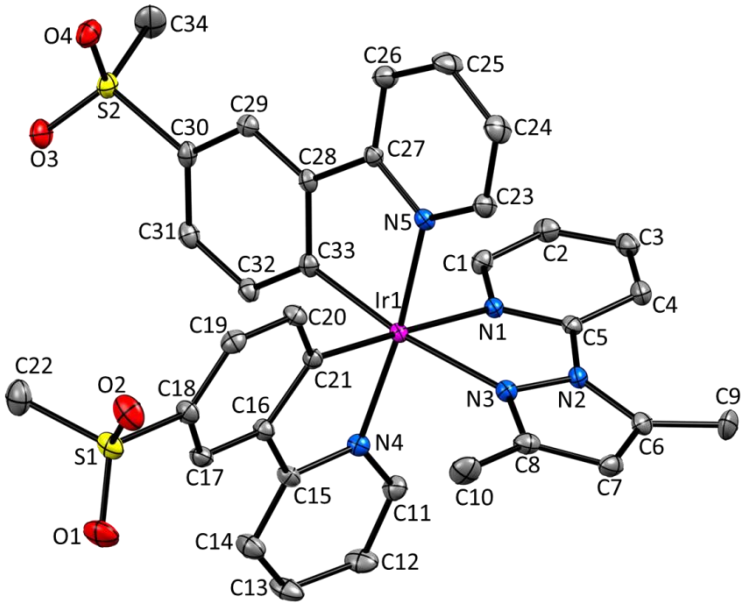

Fig. 32 Structure of the Λ-[Ir(**8**)$_2$(dmpzpy)]$^+$ cation in [Ir(**8**)$_2$(dmpzpy)][PF$_6$]·CH_3CN with ellipsoids plotted at 40% probability level and H atoms omitted. Selected bond parameters: Ir1–N1 = 2.144(2), Ir1–N3 = 2.126(2), Ir1–N4 = 2.050(2), Ir1–N5 = 2.044(2), Ir1–C21 = 1.998(2), Ir1–C33 = 2.012(3), N2–N3 = 1.385(3), S1–O1 = 1.435(2), S1–O2 = 1.441(2), S1–C22 = 1.769(3), S2–O3 = 1.442(2), S2–O4 = 1.437(2), S2–C34 = 1.763(3) Å; N1–Ir1–N3 = 75.53(8), N4–Ir1–C21 = 80.34(9), N5–Ir1–C33 = 80.67(9), N1–Ir1–C21 = 178.07(9), N3–Ir1–C33 = 171.26(9), N4–Ir1–N5 = 172.73(8), O1–S1–O2 = 119.32(14), O3–S2–O4 = 118.32(12)°.

4. Photophysical Properties

The UV-Vis absorption spectra in CH_3CN solution are similar for complexes [Ir(C^N)$_2$(N^N)][PF$_6$] with C^N = **3** or **8** and N^N = pzpy or dmpzpy (Fig. 33). Strong absorption maxima occur in the UV region (λ_{max} = 253–255 nm) correlating with spin-allowed ligand-centred π*←π transitions. Weaker bands are observed at higher wavelengths up to 450 nm, corresponding to spin-allowed charge transfer transitions of the type ^{1}MLCT and ^{1}LLCT.[21] Small differences are seen for the lower energy absorptions of complexes

[Ir(**3**)$_2$(N^N)][PF$_6$] compared to [Ir(**8**)$_2$(N^N)][PF$_6$]; the absorption tails of [Ir(**3**)$_2$(N^N)][PF$_6$] extend further into the visible region, comprising broad and weak maxima around 390 and 420 nm.

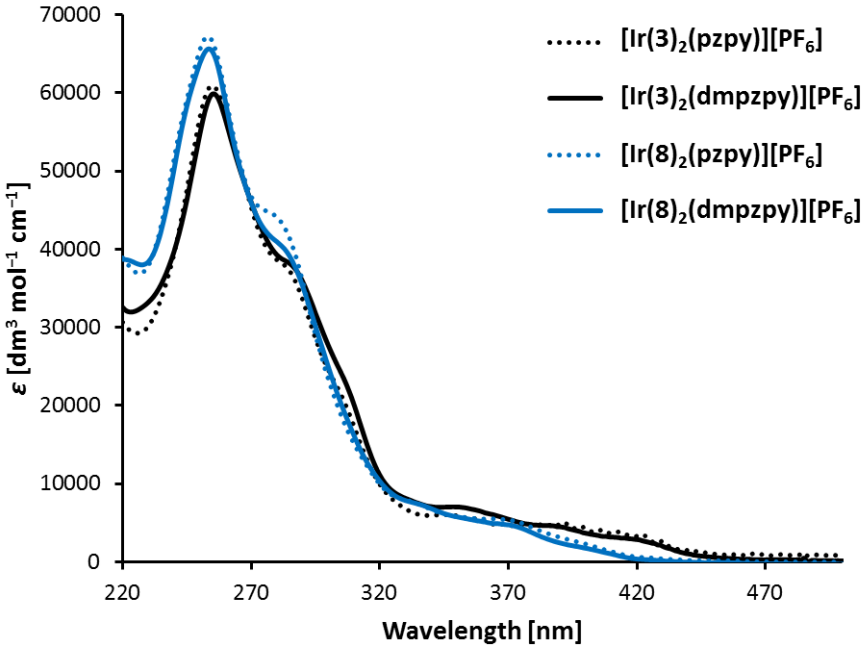

Fig. 33 UV-Vis absorption spectra in CH_3CN solution of [Ir(C^N)$_2$(N^N)][PF$_6$] with C^N = **3** or **8** and N^N = pzpy or dmpzpy (1.0×10^{-5} M).

Photoluminescence spectra were measured in CH_3CN solution at room temperature (Fig. 34) and at 77 K (Fig. 36); photophysical properties are reported in Table 8. Low temperature emission spectra were obtained by Dr. Henk Bolink and co-workers at the University of Valencia. The emission profiles are independent of the excitation wavelength. Vibrationally structured emission bands are observed for all complexes, with emission maxima at 491 and 523 nm for [Ir(**3**)$_2$(N^N)][PF$_6$] and 463 and 493 nm for [Ir(**8**)$_2$(N^N)][PF$_6$] (N^N = pzpy and dmpzpy). Complexes [Ir(**3**)$_2$(N^N)][PF$_6$] containing the methylsulfonyl substituent in the 5-position are therefore green emitters, while the emission of complexes [Ir(**8**)$_2$(N^N)][PF$_6$] (sulfone group in 4-position) is blue-shifted by approximately 30 nm, resulting in blue emission (*cf.* Fig. 35a). The structured emission profiles indicate a strong ligand-centred (^{3}LC) contribution to the emissive triplet state.[21]

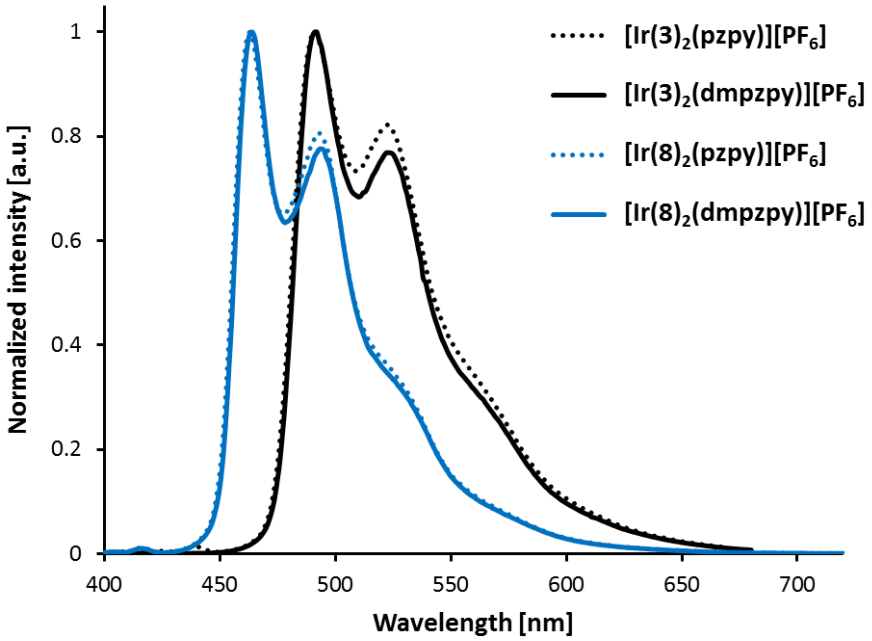

Fig. 34 Room temperature solution photoluminescence spectra of $[Ir(C\text{^}N)_2(N\text{^}N)][PF_6]$ complexes (C^N = **3** and **8**, N^N = pzpy and dmpzpy) in CH_3CN (1.0×10^{-5} M). λ_{exc} = 388 nm for $[Ir(\mathbf{3})_2(pzpy)][PF_6]$, 350 nm for $[Ir(\mathbf{3})_2(dmpzpy)][PF_6]$ and 370 nm for $[Ir(\mathbf{8})_2(N\text{^}N)][PF_6]$.

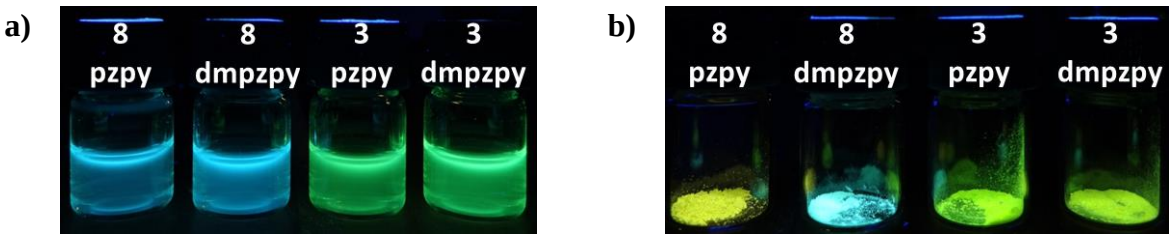

Fig. 35 Photographs of complexes $[Ir(C\text{^}N)_2(N\text{^}N)][PF_6]$ (C^N = **3** and **8**, N^N = pzpy and dmpzpy) under 366 nm light excitation: a) CH_3CN solution and b) powder samples. From left to right: $[Ir(\mathbf{8})_2(pzpy)][PF_6]$, $[Ir(\mathbf{8})_2(dmpzpy)][PF_6]$, $[Ir(\mathbf{3})_2(pzpy)][PF_6]$ and $[Ir(\mathbf{3})_2(dmpzpy)][PF_6]$.

Replacing the bpy ancillary ligand by electron-rich pzpy in $[Ir(ppy)_2(N\text{^}N)][PF_6]$ leads to a considerable blue-shift in the emission maximum of 110 nm (from 585 nm[103] to 475 nm[78] in CH_3CN solution). In contrast, going from $[Ir(\mathbf{3})_2(bpy)][PF_6]$ to $[Ir(\mathbf{3})_2(N\text{^}N)][PF_6]$ with N^N = pzpy and dmpzpy does not change the emission maxima (493, 525 nm[95] *vs.* 491, 523 nm). This further supports the assumption that in both cases, emission occurs from a triplet state with large ligand-centred character involving the cyclometallating ligands, which is

independent of the ancillary ligand. The situation is different for [Ir(**8**)$_2$(N^N)][PF$_6$] complexes when N^N is changed from bpy to pzpy or dmpzpy; the result is a 54 nm blue-shift of the emission maximum from 517 nm to 463 nm. This is probably due to a different composition of the emissive state from a higher charge transfer contribution to a more pronounced ligand-centred character: [Ir(**8**)$_2$(bpy)][PF$_6$] exhibits a broad, unstructured emission profile, whereas complexes [Ir(**8**)$_2$(N^N)][PF$_6$] with N^N = pzpy and dmpzpy have vibrationally structured emission bands. Almost no rigidochromic shift is seen when cooling CH$_3$CN solutions of all complexes within this series to 77 K (Fig. 36, Table 8), backing the theory that emission arises mainly from ^{3}LC states.[78,152,153]

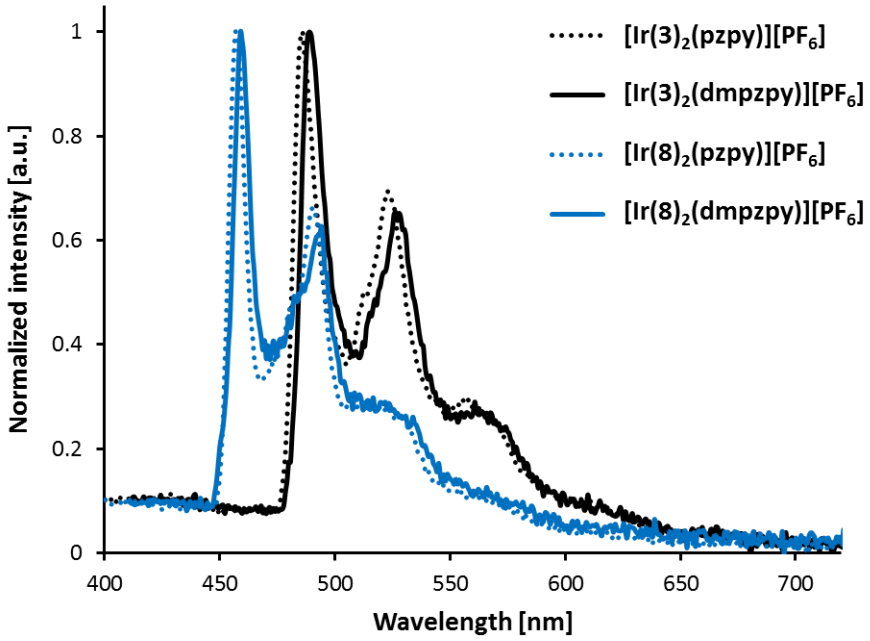

Fig. 36 Photoluminescence spectra at 77 K of compounds [Ir(C^N)$_2$(N^N)][PF$_6$] with C^N = **3** or **8** and N^N = pzpy or dmpzpy in CH$_3$CN. λ_{exc} = 320 nm.

Photoluminescence quantum yields obtained for de-aerated CH$_3$CN solutions of the complexes are in the range 53–77%. These values are comparable to the PLQY of [Ir(**3**)$_2$(bpy)][PF$_6$] (74%) and are lower than that of [Ir(**8**)$_2$(bpy)][PF$_6$] (92%). Strong emission quenching in solution has been reported for a series of alkylated pyrazolylpyridine-based iridium complexes upon methyl substitution in 5-position of the pyrazole ring.[148] Increased steric hindrance at the iridium metal centre was proposed by Shavaleev *et al*. as a possible

reason for this observation. The authors noted a three times higher non-radiative decay rate constant (k_{nr} = (1–PLQY)/τ) upon introduction of the 5-methyl group and attributed this to reversible dissociation of the sterically hindered Ir–N bond. This observation was made only in solution; powder samples of all their complexes showed visible emission. Within our series of pyrazolylpyridine complexes, no such significant decrease in the quantum yield is observed. PLQYs are only slightly lower for [Ir(C^N)$_2$(dmpzpy)][PF$_6$] with respect to unsubstituted [Ir(C^N)$_2$(pzpy)][PF$_6$]. Non-radiative decay rate constants (k_{nr}) are higher for complexes with dmpzpy than for those with pzpy, but not to such an extent as described by Shavaleev *et al.*[148] PLQYs drop significantly to <5.1% when solutions of [Ir(C^N)$_2$(N^N)][PF$_6$] (C^N = **3** and **8**, N^N = pzpy and dmpzpy) are not de-aerated.

Table 8 Photophysical properties of complexes [Ir(C^N)$_2$(N^N)][PF$_6$] (C^N = **3** and **8**, N^N = bpy, pzpy and dmpzpy) in CH$_3$CN solution at room temperature and at 77 K. PLQYs were measured in de-aerated solution, excited state lifetimes in de-aerated solution under Ar atmosphere. k_r = PLQY/τ, k_{nr} = (1–PLQY)/τ.

Compound	**Room temperature**					**77 K**
	λ_{em}^{max} **[nm]**[a]	**PLQY [%]**[a]	τ **[µs] (χ)**[b]	k_r **[10^5 s^{-1}]**	k_{nr} **[10^5 s^{-1}]**	λ_{em}^{max} **[nm]**[c]
[Ir(**3**)$_2$(bpy)][PF$_6$]	493, 525	74	2.33 (1.3)	3.2	1.1	---
[Ir(**3**)$_2$(pzpy)][PF$_6$]	491, 523	77	4.47 (1.1)	1.7	0.52	488, 526, 563
[Ir(**3**)$_2$(dmpzpy)][PF$_6$]	491, 523	66	5.12 (1.2)	1.3	0.66	489, 526, 564
[Ir(**8**)$_2$(bpy)][PF$_6$]	517	92	1.28 (1.1)	7.2	0.63	---
[Ir(**8**)$_2$(pzpy)][PF$_6$]	463, 493	72	2.30 (1.2)	3.1	1.2	459, 492, 521
[Ir(**8**)$_2$(dmpzpy)][PF$_6$]	463, 493	53	2.27 (1.1)	2.3	2.1	459, 494, 523

[a] λ_{exc} = 262 for [Ir(**3**)$_2$(bpy)][PF$_6$], 261 nm for [Ir(**3**)$_2$(N^N)][PF$_6$] (N^N = pzpy, dmpzpy), 271 nm for [Ir(**8**)$_2$(bpy)][PF$_6$] and 259 nm for [Ir(**8**)$_2$(N^N)][PF$_6$] (N^N = pzpy, dmpzpy). [b] λ_{exc} = 280 nm. [c] λ_{exc} = 320 nm.

Excited state lifetimes were measured in de-aerated CH$_3$CN solution under argon atmosphere and are in the microseconds region for complexes [Ir(C^N)$_2$(N^N)][PF$_6$] with C^N = **3** or **8** and N^N = pzpy or dmpzpy (Table 8). τ is slightly higher for [Ir(**3**)$_2$(N^N)][PF$_6$] (4.5 and 5.1 µs) with respect to [Ir(**8**)$_2$(N^N)][PF$_6$] (2.3 µs). Calculated radiative decay rate constants (k_r = PLQY/τ) are in the range 1.3 to 3.1 × 10^5 s^{-1}. These numbers are comparable to k_r values of [Ir(**3**)$_2$(bpy)][PF$_6$] (3.2 × 10^5 s^{-1}) and [Ir(ppy)$_2$(pzpy)][PF$_6$][78] (1.5 × 10^5 s^{-1}) and are significantly lower than k_r of [Ir(**8**)$_2$(bpy)][PF$_6$] (7.2 × 10^5 s^{-1}). A lower k_r correlates to a

higher ^{3}LC contribution to the emissive triplet state;[21] the obtained values are therefore in accordance with dominant ligand-centred character of the emission within the series reported in this chapter. Excited state lifetimes are considerably reduced when solutions are not de-aerated (τ = 0.22–0.42 µs); this together with a decrease in PLQY indicates strong oxygen quenching of the emissive state.

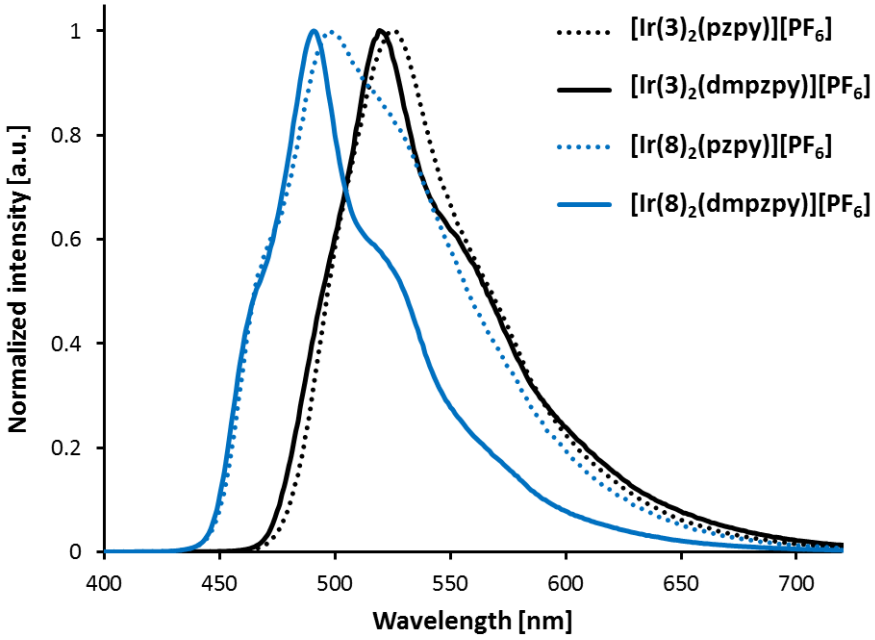

Fig. 37 Solid state photoluminescence spectra of powder samples of $[Ir(C\hat{}N)_2(N\hat{}N)][PF_6]$ (C^N = **3** and **8**, N^N = pzpy and dmpzpy). λ_{exc} = 280 nm.

The solid-state photophysical properties of $[Ir(C\hat{}N)_2(N\hat{}N)][PF_6]$ were studied for powder samples and in thin films of the composition complex:[Bmim][PF_6] 4:1. The thin films were spin-coated onto quartz substrates (Table 9) and evaluated by Dr. Henk Bolink and his team at the University of Valencia. Powder emission maxima (Fig. 37) are red-shifted by about 30 nm for all complexes with respect to solution maxima (Fig. 34). In fact, the position of the vibrational bands is not significantly different in powder and solution samples; the intensities differ considerably, however, leading to yellow emission from powder samples of $[Ir(\mathbf{3})_2(N\hat{}N)][PF_6]$ and $[Ir(\mathbf{8})_2(pzpy)][PF_6]$ (Fig. 35b). In contrast to $[Ir(\mathbf{8})_2(pzpy)][PF_6]$, methyl-functionalized complex $[Ir(\mathbf{8})_2(dmpzpy)][PF_6]$ exhibits less intense emission between

500 and 650 nm with respect to the emission maximum (Fig. 37, dotted blue line), resulting in sky-blue photoluminescence in powder (Fig. 35b). Photoluminescence quantum yields and excited state lifetimes are strongly reduced in powder samples compared to solution (PLQY ≤ 11%, $\tau_{ave} \leq 0.977$ µs); together with the red-shifted emission maxima and weaker vibrational structure, this suggests strong intermolecular interactions in the solid state.[78] Lifetimes were determined using biexponential fits for all complexes; detailed data are given in Table 9.

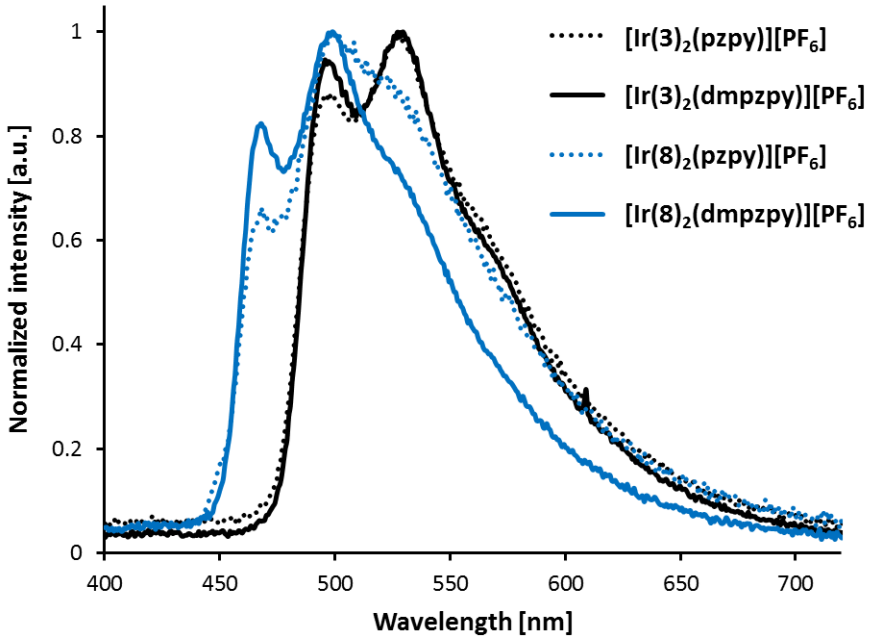

Fig. 38 Photoluminescence spectra of thin films of complexes $[Ir(C\hat{}N)_2(N\hat{}N)][PF_6]$ with C^N = **3** or **8** and N^N = pzpy or dmpzpy. Complex:$[Bmim][PF_6]$ 4:1 on quartz plate. λ_{exc} = 320 nm.

The emission profiles for the complexes in thin films are similar to those obtained in solution; again, the relative intensities of the vibrational bands differ from the solution intensities (Fig. 38). Photoluminescence quantum yields range from 6.9 to 16.9% and are slightly higher than for powder samples, but significantly lower than for solution samples. This observation is due to the lower dilution of complex molecules in thin film, leading to excited state quenching mechanisms as a result of intermolecular interactions.

Table 9 Solid state photoluminescence properties of complexes $[Ir(C\hat{}N)_2(N\hat{}N)][PF_6]$ with C^N = **3** or **8** and N^N = pzpy or dmpzpy as powder samples and in thin film (complex:[Bmim][PF_6] 4:1). Biexponential fits were used for powder excited state lifetimes, according to the equation $\tau_{ave}=\sum A_i\tau_i/\sum A_i$ (A_i = pre-exponential factor of the lifetime).

Compound	Powder samples					Thin film	
	λ_{em}^{max} [nm][a]	PLQY [%][b]	τ_{ave} [µs] (χ)[a]	τ_1 [µs] (A_1)	τ_2 [µs] (A_2)	λ_{em}^{max} [nm][c]	PLQY [%][c]
$[Ir(\mathbf{3})_2(pzpy)][PF_6]$	524	7.5	0.977 (1.2)	0.815 (17639)	2.48 (624)	499, 529, 564	13.2
$[Ir(\mathbf{3})_2(dmpzpy)][PF_6]$	519	5.9	0.537 (1.3)	0.398 (27831)	1.00 (3295)	496, 529, 564	16.9
$[Ir(\mathbf{8})_2(pzpy)][PF_6]$	498	4.6	0.659 (1.2)	0.346 (8587)	1.35 (997)	470, 500, 527	6.9
$[Ir(\mathbf{8})_2(dmpzpy)][PF_6]$	491	11	0.623 (1.2)	0.510 (25612)	1.33 (1558)	468, 499, 526	13.0

[a] λ_{exc} = 280 nm. [b] λ_{exc} = 261 nm for $[Ir(\mathbf{3})_2(N\hat{}N)][PF_6]$ and 259 nm for $[Ir(\mathbf{8})_2(N\hat{}N)][PF_6]$. [c] λ_{exc} = 320 nm.

5. Electrochemical Properties

Electrochemical data gained from cyclic voltammetry measurements of complexes $[Ir(C\hat{}N)_2(N\hat{}N)][PF_6]$ (C^N = **3** and **8**, N^N = pzpy and dmpzpy) in de-aerated CH_3CN solution are summarized in Table 10. The CV curves showing the oxidation and first reduction waves of $[Ir(\mathbf{3})_2(pzpy)][PF_6]$ and $[Ir(\mathbf{8})_2(pzpy)][PF_6]$ are given in Fig. 39. In $[Ir(C\hat{}N)_2(N\hat{}N)]^+$ type complexes, the HOMO is generally located on the iridium metal centre and the phenyl rings of the cyclometallating ligands; oxidation is therefore iridium-based with a strong influence of the C^N ligands. This assumption is reflected by the values obtained for the oxidation potentials, which are very similar when the cyclometallating ligands are the same; this is the case for $[Ir(\mathbf{3})_2(N\hat{}N)][PF_6]$ with N^N = pzpy, dmpzpy and bpy ($E_{1/2}^{ox}$ = +1.19, +1.20 and +1.18 V *vs.* Fc/Fc^+, respectively), as well as $[Ir(\mathbf{8})_2(N\hat{}N)][PF_6]$ with N^N = pzpy, dmpzpy and bpy ($E_{1/2}^{ox}$ = +1.26, +1.27 and +1.29 V). Reversible oxidation waves are observed for all complexes.

Table 10 Electrochemical data *vs.* Fc/Fc^+ for complexes $[Ir(C\hat{}N)_2(N\hat{}N)][PF_6]$ (C^N = **3** and **8**, N^N = bpy, pzpy and dmpzpy) obtained from cyclic voltammetry experiments in de-aerated CH_3CN solution. Measured with glassy carbon working, Pt counter and Ag pseudo-reference electrode, 0.1 M $TBAPF_6$ supporting electrolyte and a scan rate of 0.1 V s^{-1}. qr = quasi-reversible, ir = irreversible.

Compound	$E_{1/2}^{ox}$ **[V]**	$E_{1/2}^{red}$ **[V]**	$\Delta E_{1/2}$ **[V]**
$[Ir(\mathbf{3})_2(bpy)][PF_6]$	+1.18	–1.72, –2.16, –2.61^{ir}	2.90
$[Ir(\mathbf{3})_2(pzpy)][PF_6]$	+1.19	–2.02, –2.26^{ir}, –2.68^{ir}	3.21
$[Ir(\mathbf{3})_2(dmpzpy)][PF_6]$	+1.20	–2.00, –2.27^{ir}, –2.42^{ir}, –2.63^{ir}	3.20
$[Ir(\mathbf{8})_2(bpy)][PF_6]$	+1.29	–1.67, –2.27^{qr}, –2.52^{qr}	2.96
$[Ir(\mathbf{8})_2(pzpy)][PF_6]$	+1.26	–2.11^{ir}, –2.37^{ir}, –2.62^{ir}	3.37
$[Ir(\mathbf{8})_2(dmpzpy)][PF_6]$	+1.27	–2.14^{ir}, –2.37^{qr}, –2.68^{ir}	3.41

Three to four reduction waves are detected within the accessible solvent window. The first reductions are reversible for complexes $[Ir(\mathbf{3})_2(N\hat{}N)][PF_6]$ and irreversible for $[Ir(\mathbf{8})_2(N\hat{}N)][PF_6]$ (N^N = pzpy, dmpzpy). With respect to $[Ir(C\hat{}N)_2(bpy)][PF_6]$ (C^N = **3** and **8**), the reduction potentials of pyrazolylpyridine-based complexes are shifted to lower potential (from ca. −1.7 V to −2.0/−2.1 V). The LUMO is based almost exclusively on the ancillary ligand in $[Ir(C\hat{}N)_2(N\hat{}N)]^+$ complexes; replacing 2,2'-bipyridine by more electron-rich pyrazolylpyridine ligands therefore leads to a destabilization of the LUMO. Electrochemical HOMO-LUMO energy gaps are increased on going from $[Ir(\mathbf{3})_2(N\hat{}N)][PF_6]$ ($\Delta E_{1/2}$ = ca. 3.2 V) to $[Ir(\mathbf{8})_2(N\hat{}N)][PF_6]$ ($\Delta E_{1/2}$ = ca. 3.4 V) with N^N = pzpy and dmpzpy, in accordance with the observed blue-shift in the emission maxima.

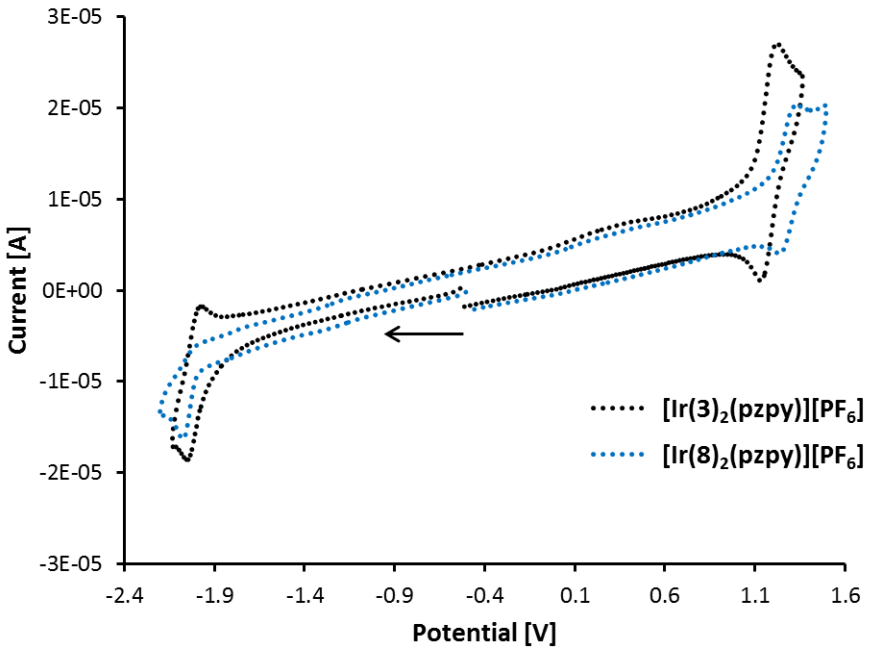

Fig. 39 Cyclic voltammetry curves of complexes $[Ir(C^N)_2(pzpy)][PF_6]$ (C^N = **3** and **8**) with respect to Fc/Fc^+, showing the first oxidation and reduction waves. Measured in de-aerated CH_3CN solution with glassy carbon working, Pt counter and Ag pseudo-reference electrodes, 0.1 M $TBAPF_6$ supporting electrolyte and a scan rate of 0.1 V s^{-1}. The arrow indicates the initial scanning direction.

6. Calculations

In order to better understand the electrochemical and photophysical properties of complexes $[Ir(C^N)_2(N^N)][PF_6]$ with C^N = **3** and **8**, N^N = pzpy and dmpzpy, combined DFT/TD-DFT calculations were carried out at the B3LYP/(6-31G**+LANL2DZ) level in the presence of CH_3CN as the solvent.[126] The calculations were performed by Prof. Enrique Ortí and co-workers at the University of Valencia. $[Ir(ppy)_2(pzpy)]^+$ is included as a reference complex.[154] The calculated frontier orbitals (HOMO, LUMO and LUMO+1) for all complexes including the reference compound are shown in Fig. 40, together with calculated energy values.

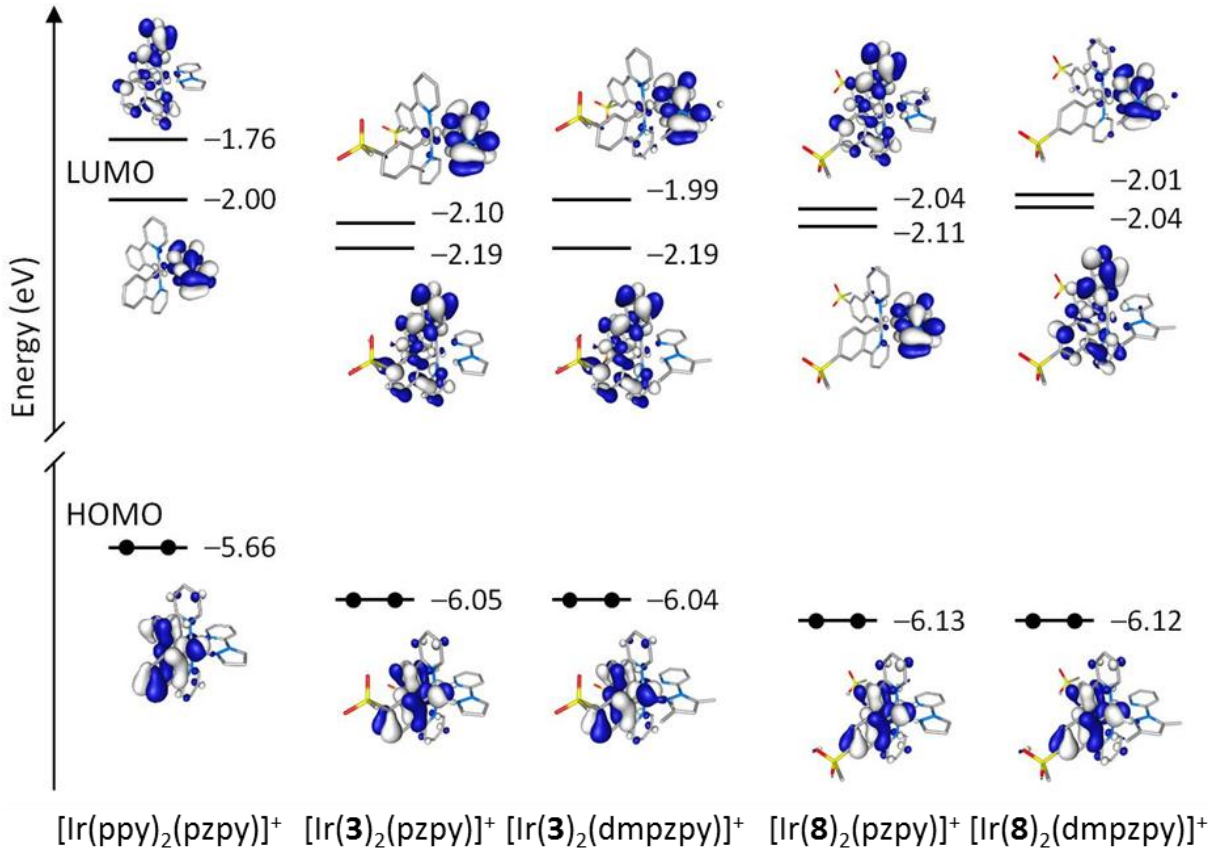

Fig. 40 Schematic representation showing the electron density contours (±0.03 au) and calculated energy values for the HOMO, LUMO and LUMO+1 of $[Ir(ppy)_2(pzpy)]^+$ and complexes $[Ir(C\text{^}N)_2(N\text{^}N)]^+$ with C^N = **3** and **8**, N^N = pzpy and dmpzpy. Hydrogen atoms omitted for clarity.

Introducing sulfone groups on the C^N ligands leads to a stabilization of the molecular orbitals localized on those ligands. A larger stabilization of the HOMO is observed when the sulfone substituent is placed in 4-position (*para* to the Ir–C bond) with respect to substitution in 5-position (*meta* to the Ir–C bond). A different observation is made for the LUMO or LUMO+1; a sulfone group in 5-position results in a larger stabilization in that case. For complexes $[Ir(ppy)_2(pzpy)]^+$ and $[Ir(\mathbf{8})_2(pzpy)]^+$, the LUMO is based on the ancillary ligand and the LUMO+1 is located on the cyclometallating ligands and the metal centre. For the remaining compounds, the orbitals are switched around and the LUMO is located on the C^N ligands and the iridium metal. Placing methyl substituents on the ancillary ligand leads to a destabilization of the molecular orbital of 0.1 eV compared to the unsubstituted analogues. The trends observed for the calculated HOMO and LUMO energies correlate well with the experimental oxidation and reduction potentials gained from electrochemical measurements

(Table 10). Calculated HOMO-LUMO energy gaps are in the order $[Ir(ppy)_2(pzpy)]^+$ (3.66 eV) < $[Ir(\mathbf{3})_2(pzpy)]^+$ (3.86 eV) ≈ $[Ir(\mathbf{3})_2(dmpzpy)]^+$ (3.85 eV) < $[Ir(\mathbf{8})_2(pzpy)]^+$ (4.02 eV) < $[Ir(\mathbf{8})_2(dmpzpy)]^+$ (4.08 eV). This trend is in accordance with the increase in the electrochemical energy gap determined experimentally (3.07 V[78] < 3.21 V ≈ 3.20 V < 3.37 V < 3.41 V, Table 10). The blue-shift in the emission maxima on going from $[Ir(ppy)_2(pzpy)]^+$ to $[Ir(\mathbf{8})_2(N\text{^}N)]^+$ (N^N = pzpy and dmpzpy) corresponds well to the calculated widening of the HOMO-LUMO gap. For complexes $[Ir(\mathbf{3})_2(N\text{^}N)]^+$ (N^N = pzpy, dmpzpy), a red-shift in the emission maximum is observed with respect to $[Ir(ppy)_2(pzpy)]^+$ which apparently contradicts the trend in the calculated energy values for the HOMO-LUMO gaps.

In order to shed light on the aforementioned contradiction between experimental values and theoretical calculations, the geometry of the lowest-energy excited triplet state (T_1) was optimized and emission energies calculated. In Fig. 41a, the adiabatic energy differences between S_0 and T_1 (ΔE) and the emission energies (E_{em}) are reported. Fig. 41b shows the calculated unpaired-electron spin density contours for the lowest-energy T_1 states of complexes $[Ir(C\text{^}N)_2(N\text{^}N)]^+$. For all complexes, T_1 is a ligand-centred state (^{3}LC) mainly located on one of the cyclometallating ligands with a small contribution of the iridium centre (^{3}MLCT). This result is in accordance with the experimental emission spectra obtained in CH_3CN solution, showing structured emission bands. The trends in the calculated emission energies correlate well with the observed red-shifts in the emission maxima of $[Ir(\mathbf{3})_2(N\text{^}N)]^+$ (491, 523 nm) with respect to $[Ir(ppy)_2(pzpy)]^+$ (475, 503 nm[78]) and the blue-shifts of $[Ir(\mathbf{8})_2(N\text{^}N)]^+$ (463, 493 nm). Time-dependent DFT calculations confirm the ligand-centred (^{3}LC) nature of the emissive triplet state. The first and second excited states are ligand-centred states that arise from excitation to molecular orbitals located on the cyclometallating ligands. Calculations show that the first ^{3}MLCT state lies higher in energy by 0.2 eV for $[Ir(ppy)_2(pzpy)]^+$ to 0.6 eV for $[Ir(\mathbf{3})_2(dmpzpy)]^+$.

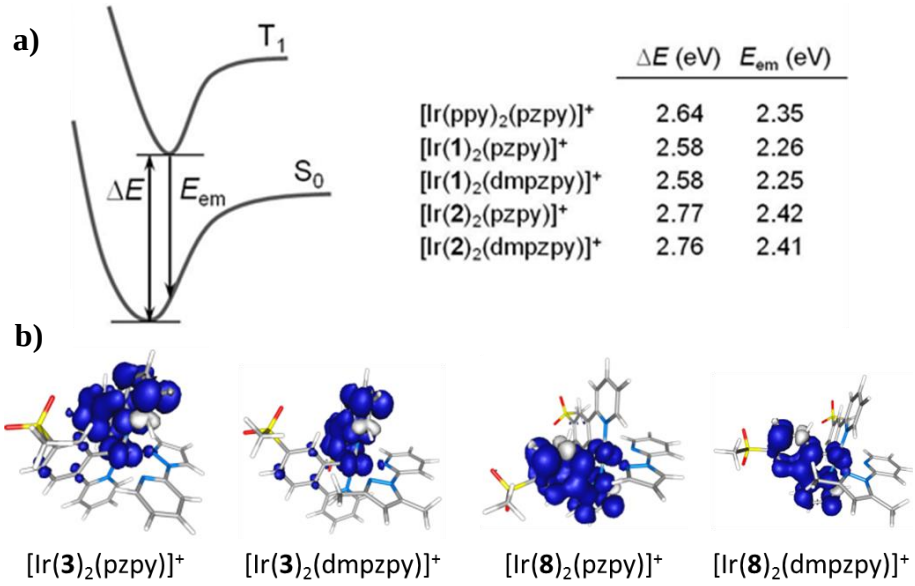

	ΔE (eV)	E_{em} (eV)
$[Ir(ppy)_2(pzpy)]^+$	2.64	2.35
$[Ir(\mathbf{1})_2(pzpy)]^+$	2.58	2.26
$[Ir(\mathbf{1})_2(dmpzpy)]^+$	2.58	2.25
$[Ir(\mathbf{2})_2(pzpy)]^+$	2.77	2.42
$[Ir(\mathbf{2})_2(dmpzpy)]^+$	2.76	2.41

Fig. 41 a) Schematic diagram showing the adiabatic energy difference between S_0 and T_1 states (ΔE) and emission energy from the T_1 state (E_{em}), together with calculated values for $[Ir(ppy)_2(pzpy)]^+$ and $[Ir(C\text{^}N)_2(N\text{^}N)]^+$ (C^N = 3, 8 and N^N = pzpy, dmpzpy). b) Unpaired-electron spin density contours (0.002 au) calculated for the fully relaxed T_1 states.

7. Electroluminescence and Device Data

Light emitting electrochemical cells were prepared with complexes $[Ir(C\text{^}N)_2(N\text{^}N)][PF_6]$ with C^N = **3** or **8** and N^N = pzpy or dmpzpy using the device configuration ITO/PEDOT:PSS/$[Ir(C\text{^}N)_2(N\text{^}N)][PF_6]$:$[Bmim][PF_6]$ 4:1/Al. The devices were assembled and measured by Dr. Henk Bolink and co-workers at the University of Valencia. The LEECs were evaluated using block-wave pulsed current driving conditions with a frequency of 1 kHz, 50% duty cycles and an average current density of 100 A m^{-2}.[21,53,93,126] The electroluminescence spectra obtained in that way are shown in Fig. 42. Structured electroluminescence spectra are observed for all complexes, indicating that electroluminescence also arises mainly from a ^{3}LC emissive state. While the positions of the electroluminescence bands are similar to the solution photoluminescence bands, the relative intensities vary significantly (compare Fig. 34 with Fig. 42 and Table 8 with Table 11). As a result, all complexes exhibit green electroluminescence.

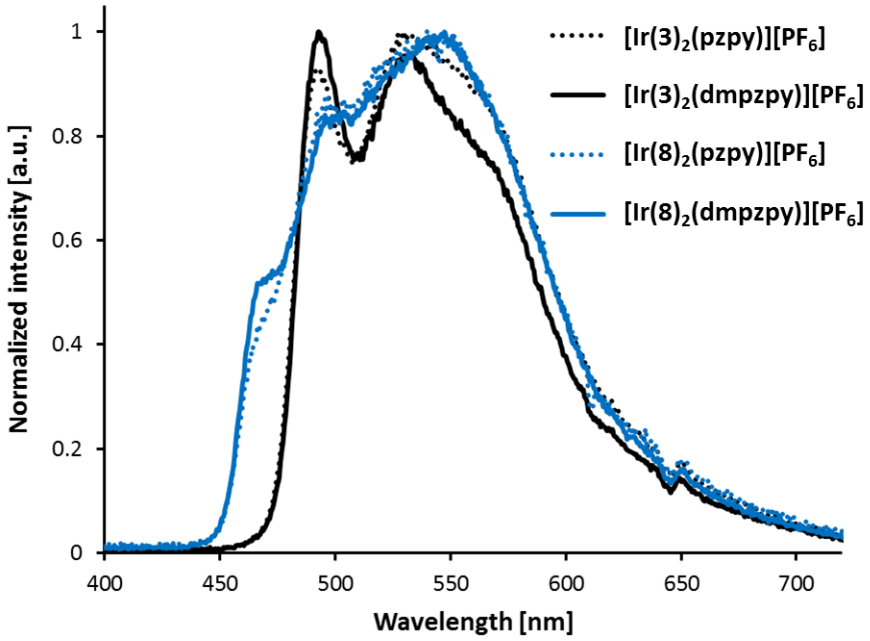

Fig. 42 Electroluminescence spectra of $[Ir(C^N)_2(N^N)][PF_6]$ (C^N = **3** and **8**, N^N = pzpy and dmpzpy) in LEEC devices.

Table 11 Device parameters for LEECs containing complexes $[Ir(C^N)_2(N^N)][PF_6]$ (C^N = **3** or **8,** N^N = pzpy or dmpzpy). Composition: ITO/PEDOT:PSS/$[Ir(C^N)_2(N^N)][PF_6]$:[Bmim][PF_6] 4:1/Al. Measured by applying a block-wave pulsed current of 100 A m^{-2} at a frequency of 1 kHz and duty cycles of 50%.[21,53,93,126]

Compound	t_{on} **[s]**	Lum_{max} **[cd m^{-2}]**	$t_{1/2}$ **[min]**	**PCE [lm W^{-1}]**	**EQE [%]**	λ_{EL}^{max} **[nm]**
$[Ir(\mathbf{3})_2(pzpy)][PF_6]$	35	141	3.7	0.5	0.4	492, 530, 568
$[Ir(\mathbf{3})_2(dmpzpy)][PF_6]$	78	125	6.2	0.6	0.4	492, 533, 568
$[Ir(\mathbf{8})_2(pzpy)][PF_6]$	42	49	3.5	0.2	0.2	466, 496, 547
$[Ir(\mathbf{8})_2(dmpzpy)][PF_6]$	30	129	2.4	0.5	0.4	466, 496, 547

LEEC performance parameters are reported in Table 11; luminance and average voltage curves of complexes $[Ir(C^N)_2(N^N)][PF_6]$ with C^N = **3**, **8** and N^N = pzpy, dmpzpy are plotted *vs.* time in Fig. 43a–d. Fast turn-on times (t_{on}, time to reach maximum luminance) in the range 30–78 s are observed together with short lifetimes ($t_{1/2}$, defined as the time needed to drop to half of the maximum luminance) on the order of a few minutes. Although device stability is poor, the $t_{1/2}$ values are not exceptionally low when compared to other blue and

green light emitting electrochemical cells reported in the literature, where lifetimes range from a few seconds to several hours.[80,107,131,140–142,145]

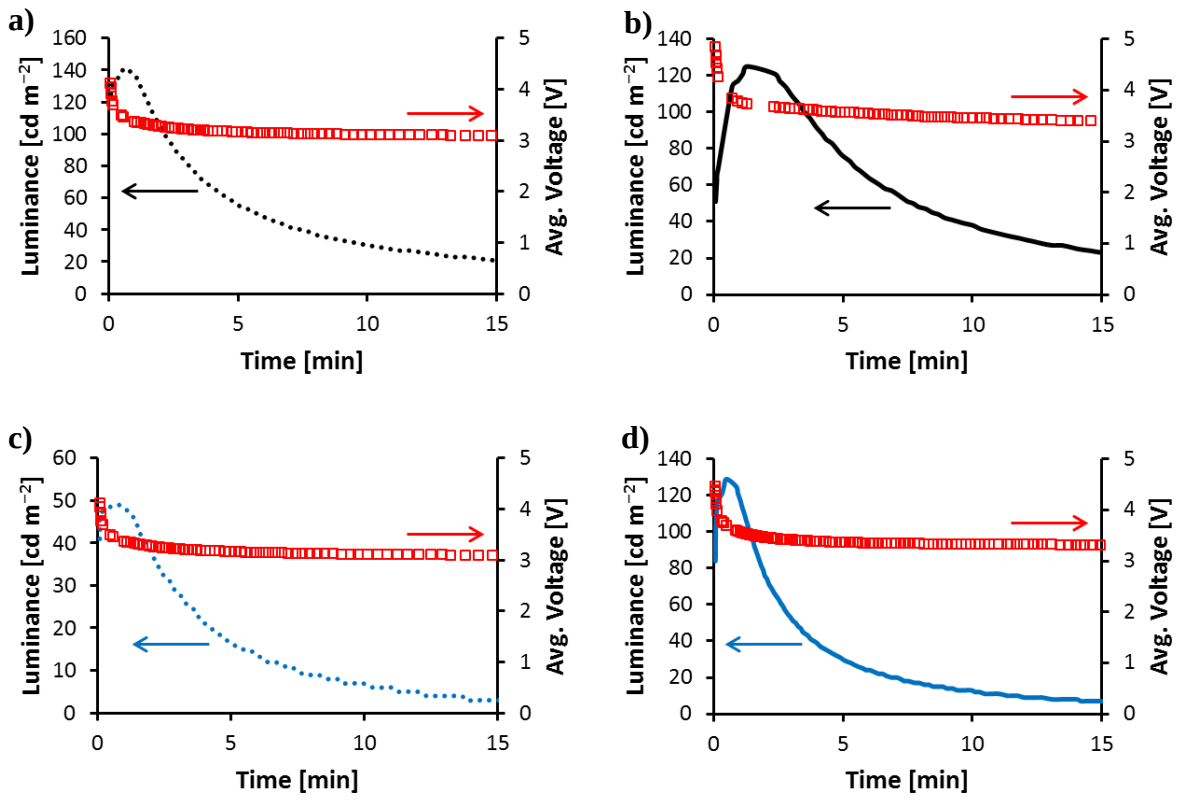

Fig. 43 Luminance and average voltage *vs.* time for LEECs containing complexes $[Ir(C\hat{}N)_2(N\hat{}N)][PF_6]$ with C^N = **3** or **8** and N^N = pzpy or dmpzpy, measured under a constant pulsed current (1 kHz, 50% duty cycle and block-wave) of 100 A m^{-2} (average current density).[21,53,93,126] Device configuration: ITO/PEDOT:PSS/$[Ir(C\hat{}N)_2(N\hat{}N)][PF_6]$:$[Bmim][PF_6]$ 4:1/Al. a) $[Ir(\mathbf{3})_2(pzpy)][PF_6]$, b) $[Ir(\mathbf{3})_2(dmpzpy)][PF_6]$, c) $[Ir(\mathbf{8})_2(pzpy)][PF_6]$ and d) $[Ir(\mathbf{8})_2(dmpzpy)][PF_6]$.

Low efficiencies were obtained for devices with $[Ir(C\hat{}N)_2(N\hat{}N)][PF_6]$ (C^N = **3** or **8,** N^N = pzpy or dmpzpy): power conversion efficiencies range from 0.2 to 0.6 lm W^{-1} and external quantum efficiencies lie between 0.2 and 0.4%. The trends in efficiency values are in line with the data obtained from PLQY measurements of thin films of the complexes mixed with ionic liquid; the lowest quantum yield and EQE values (6.9 and 0.2%, respectively) were obtained for $[Ir(\mathbf{8})_2(pzpy)][PF_6]$, while the other complexes showed higher PLQYs (13.0 to 16.9%), resulting in slightly higher EQEs (0.4%). Complex $[Ir(\mathbf{8})_2(pzpy)][PF_6]$ also exhibits

the lowest maximum luminance level of 49 cd m^{-2}; Lum_{max} of compounds [Ir(**3**)$_2$(N^N)][PF_6] and [Ir(**8**)$_2$(dmpzpy)][PF_6] are significantly higher and range from 125 to 141 cd m^{-2}. Maximum luminance values lie within the range observed for comparable blue and green iridium emitters used in light emitting electrochemical cells.[78,80,131,137,140–142]

8. Conclusions

A series of iridium complexes with phenylpyridine-based cyclometallating ligands containing sulfone substituents in 4- or 5-position of the phenyl ring and pyrazolylpyridine ancillary ligands was synthesized and characterized. The complexes were designed to induce a blue-shifted emission as a consequence of the electron-deficient C^N and electron-rich N^N ligands. The combination of these effects should lead to an enlarged HOMO-LUMO energy gap.

The complexes are green or blue emitters in CH_3CN solution; the emission colour depends on the substitution position of the methylsulfonyl moiety. Structured emission profiles are observed for all complexes, indicating a pronounced ^{3}LC character of the emissive triplet state, which was confirmed by DFT and TD-DFT calculations. In the solid state (powder samples and thin films containing ionic liquid), the position of the emission bands is similar to solution samples; however, the relative intensities of the vibrational bands are different. This leads to yellow-green emission in the solid state. High photoluminescence quantum yields ranging from 53 to 77% are obtained in de-aerated solution, together with excited state lifetimes in the microseconds region. Both PLQYs and lifetime values are significantly reduced when solutions are not de-aerated; this suggests strong quenching of the excited state due to oxygen present in the system.

All complexes were tested in LEEC devices and showed green electroluminescence; turn-on times are short, ranging from 30 to 78 s. Unfortunately, poor performance was observed for the maximum luminance, efficiency and lifetime of the devices. The highest Lum_{max} is observed for [Ir(**3**)$_2$(pzpy)][PF_6] (141 cd m^{-2}), EQEs range from 0.2 to 0.4% and device lifetimes are in the order of a few minutes. Although the complexes in this series do

not show promising LEEC performance, the results obtained are comparable to other blue and green light-emitting electrochemical cells reported in the literature.

With the design strategy of combining sulfone-functionalized C^N and electron-rich N^N ligands, it was possible to achieve blue emission in solution with complexes that contain the electron-withdrawing sulfone group in *para* position to the Ir–C bond. This proves that sulfones are an alternative to the excessively used fluorine substituents in order to tune the emission colour to the blue. However, the electroluminescence maxima are red-shifted for all complexes in this series, leading to green light emitting electrochemical cells. Furthermore, device stability is not enhanced compared to complexes with fluoro-functionalized cyclometallating ligands. This leads to the conclusion that sulfone groups are either unstable when operated in LEECs (similar to fluorine substituents) or that instability is an inherent feature of iridium complexes with a large HOMO-LUMO energy gap.

9. Experimental

The following experimental procedures have been written by the author of this thesis and have been published in RSC Advances.[126]

9.1. General

2-(1*H*-pyrazol-1-yl)pyridine (pzpy) and 2-(3,5-dimethyl-1*H*-pyrazol-1-yl)pyridine (dmpzpy) were synthesized following a procedure described in the literature.[149] ^{1}H NMR spectroscopic data matched those reported.[150,151]

9.2. General procedure for the synthesis of iridium(III) complexes

Iridium dimer and ancillary ligand were suspended in MeOH (15 mL) in a microwave vial and heated at 120 °C for 1 h in a microwave reactor. The resulting yellow solution was filtered through cotton and concentrated under reduced pressure. The residue was dissolved in little MeOH, an excess of solid NH_4PF_6 was added and the resulting suspension was stirred for 5 min at room temperature. The yellow precipitate was filtered off and redissolved in CH_2Cl_2/CH_3CN. The solvent was removed under reduced pressure, the crude product was purified by column chromatography (silica) and solvent removed under reduced pressure. The

residue was dissolved in little CH_2Cl_2 or CH_3CN, precipitated with Et_2O and left in the refrigerator overnight. The resulting precipitation was filtered off, washed with MeOH and Et_2O and dried under vacuum.

9.3. [Ir(3)$_2$(pzpy)][PF$_6$]

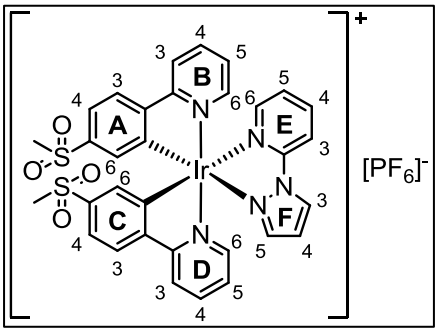

[Ir(**3**)$_2$Cl]$_2$ (125 mg, 90.3 µmol, 1.0 eq.) and pzpy (27.0 mg, 0.186 mmol, 2.1 eq.). Purification by column chromatography (silica, CH_2Cl_2 changing to CH_2Cl_2–5% MeOH) and precipitation from an CH_3CN solution. [Ir(**3**)$_2$(pzpy)][PF$_6$] was isolated as a yellow solid (169 mg, 0.179 mmol, 99.0%). ^{1}H NMR (500 MHz, CD_3CN) δ/ppm 8.70 (d, J = 3.1 Hz, 1H, H^{F3}), 8.25–8.21 (overlapping m, 2H, H^{B3+D3}), 8.19 (ddd, J = 8.5, 7.6, 1.6 Hz, 1H, H^{E4}), 8.10 (*pseudo*-dt, J = 8.5, 1.0 Hz, 1H, H^{E3}), 8.05–7.97 (overlapping m, 4H, $H^{A3+B4+C3+D4}$), 7.85–7.82 (overlapping m, 2H, H^{B6+D6}), 7.75 (ddd, J = 5.5, 1.7, 0.7 Hz, 1H, H^{E6}), 7.58 (dd, J = 8.2, 1.9 Hz, 1H, H^{A4}), 7.56 (dd, J = 8.2, 1.9 Hz, 1H, H^{C4}), 7.36 (ddd, J = 7.6, 5.6, 1.1 Hz, 1H, H^{E5}), 7.32 (d, J = 2.1 Hz, 1H, H^{F5}), 7.30–7.22 (overlapping m, 2H, H^{B5+D5}), 6.77 (dd, J = 3.1, 2.1 Hz, 1H, H^{F4}), 6.71 (d, J = 1.9 Hz, 1H, H^{A6}), 6.70 (d, J = 1.9 Hz, 1H, H^{C6}), 2.89 (s, 3H, $H^{A5\text{-}SO2Me}$), 2.88 (s, 3H, $H^{C5\text{-}SO2Me}$). ^{13}C{^{1}H} NMR (126 MHz, CD_3CN) δ/ppm 166.2 (C^{D2}), 166.1 (C^{B2}), 151.2 (C^{D6}), 150.9 (C^{B6}), 150.5 (C^{A2}), 150.40 ($C^{C2/E6}$), 150.39 ($C^{C2/E6}$), 150.2 (C^{E2}), 149.9 (C^{A1}), 146.8 (C^{C1}), 145.0 (C^{F5}), 142.8 (C^{E4}), 142.2 (C^{A5}), 141.9 (C^{C5}), 140.5 (C^{B4}), 140.4 (C^{D4}), 133.3 (C^{F3}), 129.8 (C^{C6}), 129.7 (C^{A6}), 126.34 ($C^{A3/B5}$), 126.32 ($C^{A3/B5}$), 126.21 (C^{E5}), 126.17 (C^{D5}), 126.0 (C^{C3}), 122.7 (C^{A4}), 122.54 (C^{C4}), 122.51 ($C^{B3/D3}$), 122.48 ($C^{B3/D3}$), 114.5 (C^{E3}), 112.3 (C^{F4}), 44.25 ($C^{A5\text{-}SO2Me/C5\text{-}SO2Me}$), 44.24 ($C^{A5\text{-}SO2Me/C5\text{-}SO2Me}$). IR (solid, $\tilde{\nu}$/cm^{-1}) 3121 (w), 1724 (w), 1611 (m), 1575 (w), 1524 (w), 1488 (m), 1477 (m), 1450 (w), 1430 (w), 1409 (w), 1375 (w), 1355 (w), 1309 (m), 1292 (m), 1143 (s), 1092 (m), 1063 (m), 1047 (w), 959 (m), 915 (w), 878 (w), 833 (s), 806 (m), 780 (m), 753 (s), 726 (m), 718 (m), 701 (m), 667 (m), 652 (m), 599 (m), 557 (s), 546 (s), 526 (m), 488 (m), 481 (m). UV/Vis (CH_3CN, 1.0 × 10^{-5} mol dm^{-3}) λ/nm (ε/dm^3 mol^{-1} cm^{-1}) 255 (61 000), 280 sh (39 000), 420 sh (3000). Emission (CH_3CN, 1.0 × 10^{-5} mol dm^{-3}, λ_{exc} = 261 nm) λ_{em}^{max} = 491, 523 nm. ESI-MS *m/z* 802.4 [M−PF$_6$]$^+$ (calc. 802.1). Found C 40.24, H 3.28, N 7.51; $C_{32}H_{27}F_6IrN_5O_4PS_2 \cdot 0.5H_2O$ requires C 40.21, H 2.95, N 7.33%.

9.4. [Ir(3)$_2$(dmpzpy)][PF$_6$]

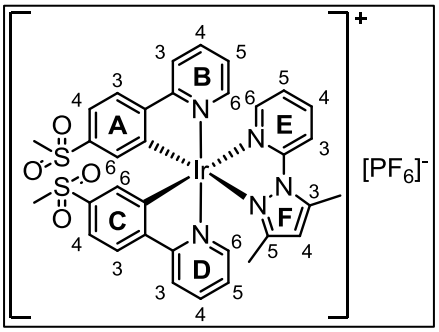

[Ir(**3**)$_2$Cl]$_2$ (118 mg, 85.2 mmol, 1.0 eq.) and dmpzpy (49.4 mg, 0.285 mmol, 3.3 eq.). Purification by column chromatography (silica, CH_2Cl_2 changing to CH_2Cl_2–2% MeOH) and precipitation from an CH_3CN solution. [Ir(**3**)$_2$(dmpzpy)][PF$_6$] was isolated as a yellow solid (133 mg, 0.136 mmol, 80.0%). ^{1}H NMR (500 MHz, CD_3CN) δ/ppm 8.26–8.20 (overlapping m, 2H, H^{B3+D3}), 8.10 (ddd, J = 8.7, 7.0, 1.7 Hz, 1H, H^{E4}), 8.07 (ddd, J = 8.7, 1.5, 0.9 Hz, 1H, H^{E3}), 8.06–8.00 (overlapping m, 3H, $H^{B4+B6+D4}$), 7.99 (d, J = 8.3 Hz, 1H, H^{A3}), 7.98 (d, J = 8.3 Hz, 1H, H^{C3}), 7.81 (ddd, J = 5.8, 1.6, 0.7 Hz, 1H, H^{D6}), 7.72 (ddd, J = 5.6, 1.7, 0.9 Hz, 1H, H^{E6}), 7.57 (dd, J = 8.2, 1.9 Hz, 1H, H^{A4}), 7.51 (dd, J = 8.2, 1.9 Hz, 1H, H^{C4}), 7.35–7.28 (m, 1H, H^{B5}), 7.29–7.25 (overlapping m, 2H, H^{D5+E5}), 6.65 (d, J = 1.9 Hz, 1H, H^{C6}), 6.59 (d, J = 1.9 Hz, 1H, H^{A6}), 6.34 (s, 1H, H^{F4}), 2.87 (s, 3H, $H^{A5\text{-}SO2Me}$), 2.84 (s, 3H, $H^{C5\text{-}SO2Me}$), 2.83 (d, J = 0.8 Hz, 3H, $H^{F3\text{-}Me}$), 1.58 (s, 3H, $H^{F5\text{-}Me}$). ^{13}C{^{1}H} NMR (126 MHz, CD_3CN) δ/ppm 166.3 (C^{D2}), 165.9 (C^{B2}), 156.5 (C^{F5}), 151.4 (C^{B6}), 151.3 (C^{E2}), 151.0 (C^{D6}), 150.6 (C^{E6}), 150.3 (C^{A2}), 150.15 (C^{C2}), 150.12 (C^{A1}), 149.4 (C^{C1}), 147.0 (C^{F3}), 142.4 (C^{E4}), 142.3 (C^{A5}), 141.9 (C^{C5}), 140.4 (C^{B4}), 140.3 (C^{D4}), 129.9 (C^{C6}), 129.1 (C^{A6}), 126.5 (C^{B5}), 126.4 (C^{A3}), 126.3 (C^{C3}), 126.1 (C^{D5}), 125.1 (C^{E5}), 122.8 (C^{A4}), 122.6 ($C^{B3/D3}$), 122.5 ($C^{B3/D3}$), 122.1 (C^{C4}), 115.3 (C^{E3}), 114.2 (C^{F4}), 44.24 ($C^{A5\text{-}SO2Me/C5\text{-}SO2Me}$), 44.23 ($C^{A5\text{-}SO2Me/C5\text{-}SO2Me}$), 15.6 ($C^{F3\text{-}Me}$), 13.9 ($C^{F5\text{-}Me}$). IR (solid, $\tilde{\nu}$/cm^{-1}) 2924 (w), 1610 (m), 1578 (w), 1564 (w), 1475 (m), 1453 (m), 1431 (w), 1414 (w), 1392 (w), 1373 (m), 1320 (m), 1295 (m), 1268 (m), 1148 (s), 1094 (m), 1062 (w), 1038 (w), 994 (w), 957 (m), 874 (w), 836 (s), 805 (m), 782 (m), 756 (s), 749 (s), 701 (m), 666 (m), 652 (m), 593 (m), 557 (m), 547 (s), 523 (m), 481 (m). UV/Vis (CH_3CN, 1.0 × 10^{-5} mol dm^{-3}) λ/nm (ε/dm^3 mol^{-1} cm^{-1}) 255 (60 000), 285 sh (38 000), 420 sh (2900). Emission (CH_3CN, 1.0 × 10^{-5} mol dm^{-3}, λ_{exc} = 261 nm) λ_{em}^{max} = 491, 523 nm. ESI-MS m/z 830.5 [M−PF$_6$]$^+$ (calc. 830.1). Found C 42.25, H 3.51, N 7.47; $C_{34}H_{31}F_6IrN_5O_4PS_2$ requires C 41.89, H 3.20, N 7.18%.

9.5. [Ir(8)$_2$(pzpy)][PF$_6$]

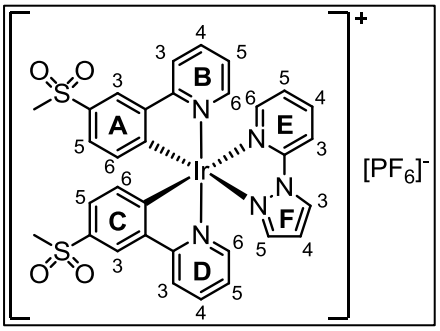

[Ir(**8**)$_2$Cl]$_2$ (142 mg, 0.103 mmol, 1.0 eq.) and pzpy (31.0 mg, 0.214 mmol, 2.1 eq.). Purification by column chromatography (silica, CH_2Cl_2 changing to CH_2Cl_2–10% MeOH) and precipitation from a CH_2Cl_2 solution. [Ir(**8**)$_2$(pzpy)][PF$_6$] was isolated as a pale yellow solid (79.5 mg, 84.0 µmol, 40.9%). ^{1}H NMR (500 MHz, CD_3CN) δ/ppm 8.69 (d, J = 3.1 Hz, 1H, H^{F3}), 8.29 (d, J = 2.0 Hz, 1H, H^{A3}), 8.30–8.23 (overlapping m, 3H, H$^{B3+C3+D3}$), 8.19 (ddd, J = 8.9, 7.5, 1.6 Hz, 1H, H^{E4}), 8.10 (dd, J = 8.5, 1.0 Hz, 1H, H^{E3}), 8.03–7.94 (overlapping m, 2H, H^{B4+D4}), 7.81–7.76 (overlapping m, 2H, H^{B6+D6}), 7.71 (ddd, J = 5.6, 1.7, 0.7 Hz, 1H, H^{E6}), 7.41–7.31 (overlapping m, 3H, H$^{A5+C5+E5}$), 7.31 (d, J = 2.1 Hz, 1H, H^{F5}), 7.27–7.18 (overlapping m, 2H, H^{B5+D5}), 6.77 (dd, J = 3.1, 2.1 Hz, 1H, H^{F4}), 6.55 (d, J = 8.0 Hz, 1H, H^{A6}), 6.53 (d, J = 8.1 Hz, 1H, H^{C6}), 3.03 (s, 3H, H$^{A4\text{-}SO2Me}$), 3.02 (s, 3H, H$^{C4\text{-}SO2Me}$). ^{13}C{^{1}H} NMR (126 MHz, CD_3CN) δ/ppm 166.3 (C^{B2}), 166.2 (C^{D2}), 158.3 (C^{A1}), 155.5 (C^{C1}), 150.9 (C^{D6}), 150.6 (C^{B6}), 150.2 (C^{E6}), 150.1 (C^{E2}), 146.6 (C^{A2}), 146.5 (C^{C2}), 144.8 (C^{F5}), 142.9 (C^{E4}), 140.5 (C^{B4}), 140.4 (C^{D4}), 136.8 (C^{A4}), 136.7 (C^{C4}), 133.6 (C^{C6}), 133.5 (C^{A6}), 133.3 (C^{F3}), 128.9 (C^{A5}), 128.5 (C^{C5}), 126.3 (C^{E5}), 125.9 (C^{B5}), 125.8 (C^{D5}), 124.1 (C^{A3}), 123.7 (C^{C3}), 121.89 (C$^{B3/D3}$), 121.86 (C$^{B3/D3}$), 114.5 (C^{E3}), 112.3 (C^{F4}), 44.6 (C$^{A4\text{-}SO2Me+C4\text{-}SO2Me}$). IR (solid, $\tilde{\nu}$/cm^{-1}) 3646 (w), 3133 (w), 1612 (m), 1578 (w), 1524 (w), 1481 (m), 1451 (w), 1409 (w), 1355 (w), 1299 (m), 1224 (w), 1165 (w), 1145 (s), 1111 (w), 1096 (w), 1067 (w), 1056 (m), 1033 (m), 960 (m), 837 (s), 781 (s), 758 (s), 716 (w), 703 (w), 639 (w), 593 (m), 556 (s), 524 (s), 478 (m). UV/Vis (CH_3CN, 1.0 × 10^{-5} mol dm^{-3}) λ/nm (ε/dm^3 mol^{-1} cm^{-1}) 253 (67 000), 280 sh (44 000), 375 sh (5000). Emission (CH_3CN, 1.0 × 10^{-5} mol dm^{-3}, λ_{exc} = 259 nm) λ_{em}^{max} = 463, 493 nm. ESI-MS *m/z* 802.5 [M–PF$_6$]$^+$ (calc. 802.1). Found C 39.62, H 3.20, N 7.51; $C_{32}H_{27}F_6IrN_5O_4PS_2\cdot H_2O$ requires C 39.83, H 3.03, N 7.26%.

9.6. [Ir(8)$_2$(dmpzpy)][PF$_6$]

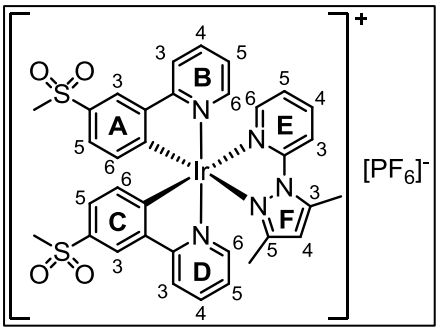

[Ir(**8**)$_2$Cl]$_2$ (143 mg, 0.103 mmol, 1.0 eq.) and dmpzpy (34.6 mg, 0.200 mmol, 1.9 eq.). Purification by column chromatography (silica, CH_2Cl_2 changing to CH_2Cl_2–10% MeOH) and precipitation from a CH_2Cl_2 solution. [Ir(**8**)$_2$(dmpzpy)][PF$_6$] was isolated as a pale yellow solid (151 mg, 0.155 mmol, 77.7%). ^{1}H NMR (500 MHz, CD_3CN) δ/ppm 8.30–8.22 (overlapping m, 4H, H$^{A3+B3+C3+D3}$), 8.11 (ddd, J = 8.8, 7.2, 1.7 Hz, 1H, H^{E4}), 8.07 (*pseudo*-dt, J = 8.8, 1.1 Hz, 1H, H^{E3}), 8.03–7.95 (overlapping m, 3H, H$^{B4+D4+B6}$), 7.74 (ddd, J = 5.8, 1.4, 0.7 Hz, 1H, H^{D6}), 7.66 (ddd, J = 5.5, 1.6, 0.8 Hz, 1H, H^{E6}), 7.36 (dd, J = 8.1, 2.0 Hz, 1H, H^{A5}), 7.32–7.24 (overlapping m, 3H, H$^{B5+C5+E5}$), 7.23 (ddd, J = 7.4, 5.8, 1.4 Hz, 1H, H^{D5}), 6.49 (d, J = 8.1 Hz, 1H, H^{C6}), 6.43 (d, J = 8.1 Hz, 1H, H^{A6}), 6.34 (s, 1H, H^{F4}), 3.03 (s, 3H, H$^{A4\text{-}SO2Me}$), 3.00 (s, 3H, H$^{C4\text{-}SO2Me}$), 2.83 (d, J = 0.8 Hz, 3H, H$^{F3\text{-}Me}$), 1.60 (s, 3H, H$^{F5\text{-}Me}$). ^{13}C{^{1}H} NMR (126 MHz, CD_3CN) δ/ppm 166.4 (C^{D2}), 166.0 (C^{B2}), 158.6 (C^{A1}), 158.1 (C^{C1}), 156.6 (C^{F5}), 151.2 (C^{E2}), 151.1 (C^{B6}), 150.7 (C^{D6}), 150.4 (C^{E6}), 147.0 (C^{F3}), 146.4 (C^{A2}), 146.3 (C^{C2}), 142.5 (C^{E4}), 140.4 (C^{B4}), 140.2 (C^{D4}), 136.9 (C^{A4}), 136.3 (C^{C4}), 133.6 (C^{C6}), 133.0 (C^{A6}), 129.1 (C^{A5}), 128.4 (C^{C5}), 126.0 (C^{B5}), 125.7 (C^{D5}), 125.1 (C^{E5}), 124.1 (C^{A3}), 123.9 (C^{C3}), 122.0 (C^{B3}), 121.9 (C^{D3}), 115.3 (C^{E3}), 114.2 (C^{F4}), 44.6 (C$^{A4\text{-}SO2Me/C4\text{-}SO2Me}$), 44.5 (C$^{A4\text{-}SO2Me/C4\text{-}SO2Me}$), 15.6 (C$^{F3\text{-}Me}$), 13.8 (C$^{F5\text{-}Me}$). IR (solid, $\tilde{\nu}$/cm^{-1}) 3086 (w), 2923 (w), 1609 (w), 1579 (w), 1538 (w), 1479 (m), 1451 (w), 1423 (w), 1396 (w), 1372 (w), 1323 (w), 1297 (s), 1285 (m), 1274 (w), 1227 (w), 1169 (w), 1144 (s), 1094 (m), 1077 (w), 1063 (w), 1055 (w), 1031 (w), 999 (w), 981 (w), 964 (m), 954 (m), 898 (w), 880 (w), 833 (s), 823 (s), 795 (m), 783 (m), 761 (s), 741 (m), 701 (m), 651 (w), 639 (w), 595 (m), 556 (s), 523 (m), 486 (m), 457 (w). UV/Vis (CH_3CN, 1.0 × 10^{-5} mol dm^{-3}) λ/nm (ε/dm^3 mol^{-1} cm^{-1}) 254 (66 000), 280 sh (41 000), 375 sh (4300). Emission (CH_3CN, 1.0 × 10^{-5} mol dm^{-3}, λ_{exc} = 259 nm) λ_{em}^{max} = 463, 493 nm. ESI-MS *m/z* 830.5 [M−PF$_6$]$^+$ (calc. 830.1). Found C 41.89, H 3.54, N 7.22; $C_{34}H_{31}F_6IrN_5O_4PS_2$ requires C 41.89, H 3.20, N 7.18%.

9.7. Crystallography

[Ir(8)$_2$(dmpzpy)][PF$_6$]·CH$_3$CN. $C_{36}H_{28}F_6IrN_6O_4PS_2$, M = 1009.97, yellow plate, monoclinic, space group $C2/c$, a = 25.335(3), b = 12.8383(13), c = 24.821(3) Å, β = 109.755(4)^o, U = 7598.2(8) Å^3, Z = 8, D_c = 1.766 Mg m^{-3}, μ(Cu-Kα) = 8.920 mm^{-1}, T = 123 K. Total 50748 reflections, 6985 unique, R_{int} = 0.049. Refinement of 6361 reflections (505 parameters) with $I>2\sigma$ (I) converged at final $R1$ = 0.0239 ($R1$ all data = 0.0251), $wR2$ = 0.0257 ($wR2$ all data = 0.0282), gof = 1.0886. CCDC 1055780.

CHAPTER IV: RED EMITTERS – BENZOTHIAZOLE-BASED ANCILLARY LIGANDS

1. Introduction

Despite the amount of research that has been conducted on light emitting electrochemical cells and Ir-iTMCs for LEECs in particular, there is still a lack of stable and efficient red emitters. Not only are they important for the production of red, but also of white light emitting electrochemical cells. From the first report of an iTMC-LEEC in 1996[40] until the introduction of cationic iridium complexes in 2004,[51] most light emitting electrochemical cells described in the literature were based on red and orange-red Ru(II)[41–48] and Os(II)[49,50] complexes. Later, more and more iridium-based red emitters started to appear alongside Ru(II) complexes with bipyridine and 2,2':6',2''-terpyridine (tpy) ligands.[69,155–160] In Scheme 15, structures of the cationic iridium complexes which have been successfully implemented in host-free red emitting LEECs are shown. Among those are complexes with 2,2'-biquinoline (**S**),[133] imidazole-based (**T**),[76,147] ester-substituted bpy (**U**),[161] bis(diphenylamino)-9,9'-spirobifluorene functionalized bpy (**V**),[162] substituted tpy (**W**)[163] and 1,3,4-oxadiazole-based (**X**)[164] ancillary ligands and complexes containing methoxy-substituted cyclometallating ligands (**Y**).[165] Complexes **Z-Cbz** and **Z-B(Mes)$_2$** combine more complicated cyclometallating ligands than the standard ppy- or ppz-based ligands with a carbazole-substituted bpy ancillary ligand.[166] Compound **AA** is a perylenediimide-iridium-complex dyad, exhibiting deep-red emission.[167,168] Furthermore, red emitters $[Ir(ppy)_2(biq)]^+$ (biq = 2,2'-biquinoline) and imidazole-based complex **T** have been used as dopants in host-guest red[147,169] and white light emitting electrochemical cells.[75–77]

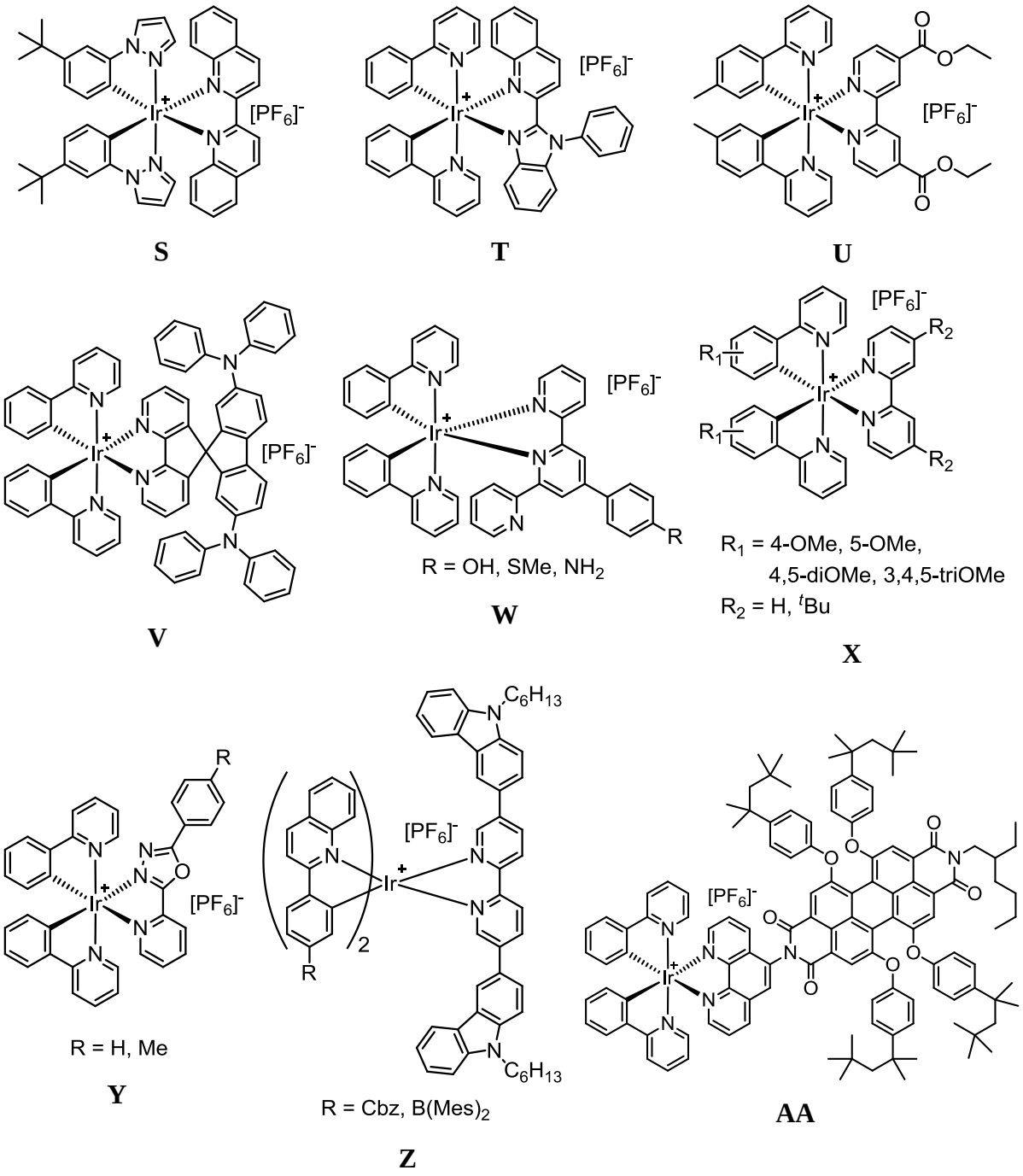

Scheme 15 Structures of red emitting iridium(III) complexes used in light emitting electrochemical cells.

Table 12 and Table 13 summarize photophysical properties in solution and solid state as well as LEEC parameters of selected complexes shown in Scheme 15. All complexes exhibit photoluminescence maxima in the orange to red region and electroluminescence maxima in the red region of the visible spectrum. Functioning LEECs have been prepared with all complexes reported in Table 12 and Table 13; device performance varies significantly, however. Turn-on times range from under one minute for complex **W** containing phenol-substituted tpy as the ancillary ligand to 27.8 h (1668 min) for complex **Z-B(Mes)$_2$** with a boron-substituted cyclometallating and a carbazole-functionalized bpy ligand. Compound **S**, containing a phenylpyrazole cyclometallating and biq ancillary ligand shows the highest maximum luminance of 7500 cd m^{-2} as well as the second-highest EQE value of 7.4%. The lowest luminance level (3 cd m^{-2}) and EQE (0.02%) of the selected complexes is observed from LEECs using bis(diphenylamino)-9,9'-spirobifluorene functionalized complex **V**. LEECs incorporating complex **Y** (1,3,4-oxadiazole-based ancillary ligand) exhibit the highest EQE value of 9.51% so far reported for red light emitting electrochemical cells. While high maximum luminance levels and EQE values have been reached for red LEECs with Ir-iTMCs, there remains room for improvement concerning the stability of these devices. For the complexes with reported device lifetimes, $t_{1/2}$ generally lies in the range of 0.5 to 10 h. Lifetimes are slightly higher for complexes **Z-Cbz** and **Z-B(Mes)$_2$**, but do not exceed 74 h to reach half of the maximum luminance. This poses a huge drawback regarding possible final application as artificial lighting or in displays.

In this chapter, the synthesis and properties of a series of iridium complexes containing benzothiazole-based ancillary ligands are presented. In the literature, the benzothiazole moiety has mainly been used in the cyclometallating part of iridium complexes,[170–172] for example as 2-phenylbenzo[*d*]thiazole (pbtz). Although coordination of other metal complexes by 2-(pyridin-2-yl)benzo[*d*]thiazole (btzpy) has been reported,[173,174] there is only one example of an iridium complex containing the related ligand 2-(pyridin-2-yl)-4,5-dihydrothiazole for use as a photosensitizing complex.[175]

Table 12 Photoluminescence and electroluminescence properties of selected iridium complexes used as emissive materials in red light emitting electrochemical cells.

Compound	λ_{em}^{max} [nm] and PLQY (solution)	λ_{em}^{max} [nm] and PLQY (film)	EL [nm]	CIE coord. (x, y)
S[133]	624, 0.68% (2-MeTHF)	622, --- (neat)	635	0.67, 0.32
T[76,147]	627, 646, 3% (CH_3CN)	631, --- (neat)	650	0.66, 0.33
U[161]	687, 2% (CH_3CN)	---, 18% (in PMMA)	630	0.71, 0.28
V[162]	595, 0.1% (EtOH, 77 K)	ca. 645, --- (neat)	ca. 655	---
W (R = OH)[163]	590, 5.8% (CH_2Cl_2)	593, 11.3% (+IL)	625	---
X (R_1 = 3,4,5-triOMe, R_2 = ^{t}Bu)[165]	685, 0.2% (CH_3CN)	ca. 625, 9.0% (+IL)	650	0.61, 0.38
Y (R = H)[164]	556, 24.3% (CH_2Cl_2)	627, 20% (neat)	616	0.59, 0.40
Y (R = Me)[164]	573, 58.2% (CH_2Cl_2)	625, 17.8% (neat)	624	0.50, 0.41
Z-Cbz[166]	559, 9% (CH_3CN)	603, 19% (in PMMA)	633, 659	0.65, 0.36
Z-B(Mes)$_2$[166]	583, 49% (CH_3CN)	597, 52% (in PMMA)	604, 629, 651	0.62, 0.38
AA[168]	619, 55% (CH_3CN)	---	644	0.65, 0.34

Table 13 Device performance of selected iridium complexes used as emissive materials in red light emitting electrochemical cells.

Compound	t_{on} [min]	$t_{1/2}$ [h]	Lum_{max} [cd m^{-2}]	Efficacy [cd A^{-1}]	PCE [lm W^{-1}]	EQE [%]
S[133]	70	---	7500	---	10	7.4
T[76,147]	432	---	70.3	1.6	---	2.6
U[161]	10	0.52	ca. 38	0.83	0.87	---
V[162]	---	ca. 1.3	3	0.013	0.017	0.02
W (R = OH)[163]	<1	ca. 0.5	60	---	---	0.4
X (R_1 = 3,4,5-triOMe, R_2 = ^{t}Bu)[165]	66	2	18	0.050	0.013	0.05
Y (R = H)[164]	35	8.2	154	6.29	---	9.51
Y (R = Me)[164]	72	9.8	217	13.05	---	2.74
Z-Cbz[166]	516	40.0	8.4	0.10	---	0.14
Z-B(Mes)$_2$[166]	1668	73.6	31.4	0.18	---	0.13
AA[168]	---	---	ca. 13	2.5	2.56	3.27

2. Synthesis and NMR Spectroscopic Characterization

2.1. Ligand synthesis

The chemical structures of all ligands used in this series are shown in Scheme 16, sorted by benzothiazole-based ancillary ligands (top row) and cyclometallating ligands (bottom row). To facilitate comparison, all ancillary ligands are combined with ppy as cyclometallating ligand and all cyclometallating ligands are combined with the simplest ancillary ligand (btzpy) in complexes. Ancillary ligands 2,2'-bibenzo[*d*]thiazole (bbtz)[176] and 2,6-bis(benzo[*d*]thiazol-2-yl)pyridine (btzpybtz)[177] were synthesized following reported literature procedures by a condensation reaction of 2-aminothiophenol with oxalic acid or 2,6-pyridinedicarboxaldehyde, respectively. 2-(pyridin-2-yl)benzo[*d*]thiazole (btzpy), 2-(4-(*tert*-butyl)pyridin-2-yl)benzo[*d*]thiazole (tpybtz) and 2-(pyridin-2-yl)benzo[*d*]oxazole (bozpy) were prepared by adaptation of a copper-catalysed coupling reaction described in the literature,[178] starting from the corresponding bromopyridines and benzothiazole or benzoxazole.

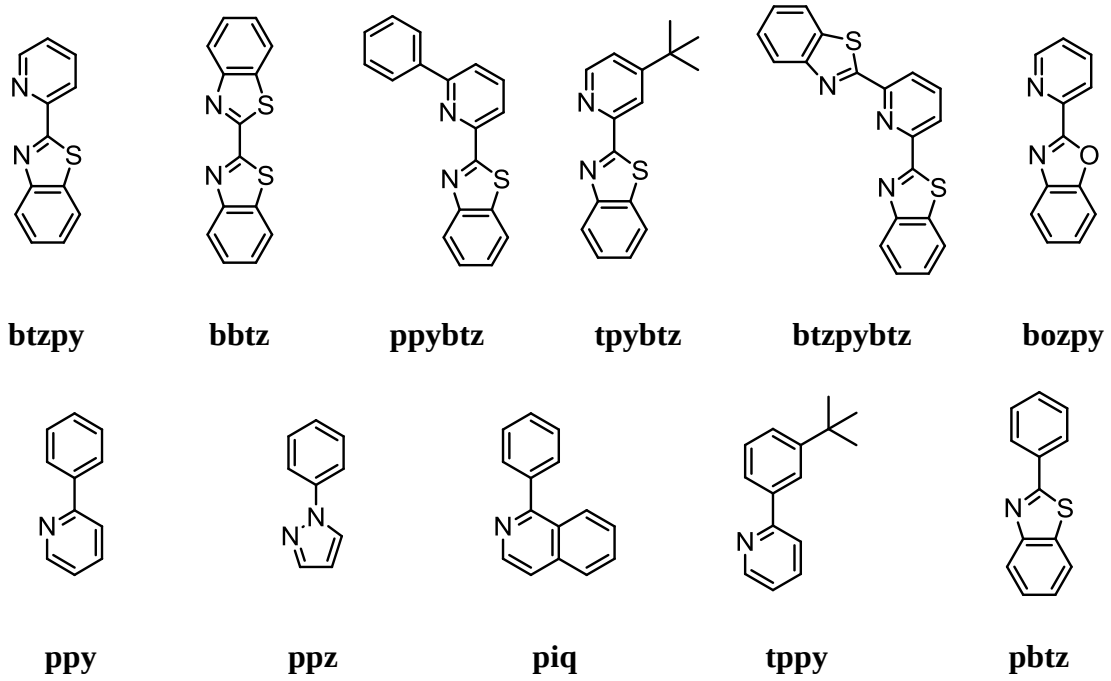

Scheme 16 Structures of ancillary (top row) and cyclometallating ligands (bottom row) used within this series of complexes.

The synthesis of 2-(6-phenylpyridin-2-yl)benzo[*d*]thiazole (ppybtz) has not yet been reported. Bromination of 2-phenylpyridine with *n*-BuLi/LiDMAE and CBr_4 gave 2-bromo-6-phenylpyridine,[179] which was then used in a Cu(I)-catalysed coupling reaction with benzothiazole[178] to yield the desired product in moderate yield (Scheme 17). Ligand ppybtz was characterized by 1D and 2D NMR spectroscopy and all ^{1}H and ^{13}C signals were assigned. In the LC-ESI mass spectrum, the base peak at *m/z* 289.0 corresponds to the protonated ligand $[M+H]^+$.

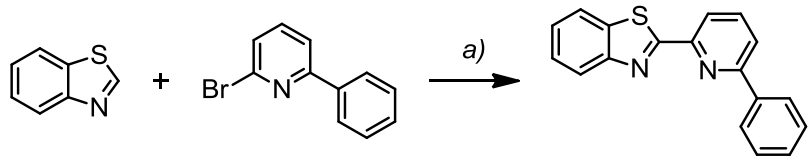

ppybtz
51.1%

Scheme 17 Synthesis of 2-(6-phenylpyridin-2-yl)benzo[*d*]thiazole (ppybtz). Reaction conditions: *a)* CuI, 1,10-phenanthroline monohydrate, K_3PO_4, DMF, 120 °C, overnight, N_2.

Cyclometallating ligands 1-phenyl-1*H*-pyrazole (ppz),[149] 1-phenylisoquinoline (piq)[180] and 2-phenylbenzo[*d*]thiazole (pbtz)[178] were prepared using literature procedures. The synthesis of 2-(3-(*tert*-butyl)phenyl)pyridine (tppy) has been reported before, but the following procedure gives a higher yield. 1-bromo-3-(*tert*-butyl)benzene was transformed into 2-(3-(*tert*-butyl)phenyl)-4,4,5,5-tetramethyl-1,3,2-dioxaborolane *via* a microwave-assisted Miyaura borylation using bis(pinacolato)diboron and KOAc, catalysed by $Pd(dppf)_2Cl_2 \cdot CH_2Cl_2$.[181] Suzuki coupling with 2-bromopyridine gave the desired ligand in excellent yield (91.3% over two steps, Scheme 18).

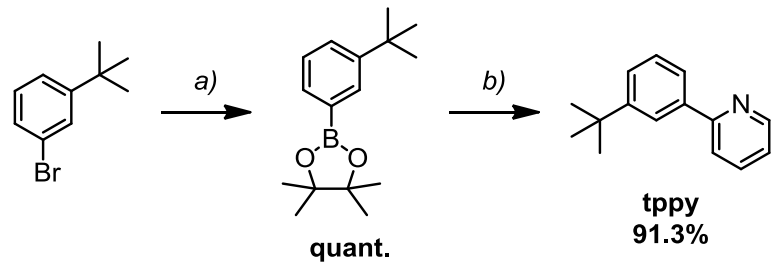

Scheme 18 Synthesis of 2-(3-(*tert*-butyl)phenyl)pyridine (tppy). Reaction conditions: *a)* bis(pinacolato)diboron, KOAc, $Pd(dppf)_2Cl_2 \cdot CH_2Cl_2$, THF, MW, 90 °C, 1 h, N_2; *b)* 2-bromopyridine, Na_2CO_3, $Pd(PPh_3)_2Cl_2$, THF/H_2O 1:1, MW, 100 °C, 30 min.

2.2. Synthesis of $[Ir(C\hat{}N)_2Cl]_2$ dimers

Iridium dimers $[Ir(ppy)_2Cl]_2$, $[Ir(ppz)_2Cl]_2$, $[Ir(piq)_2Cl]_2$, $[Ir(tppy)_2Cl]_2$ and $[Ir(pbtz)_2Cl]_2$ were synthesized according to the standard protocol.[100,101] The cyclometallating ligand and $IrCl_3 \cdot xH_2O$ were suspended in 2-ethoxyethanol and H_2O (3:1) and heated at reflux overnight. The precipitated dimers were collected, washed with EtOH and Et_2O and used for subsequent reactions without further purification. All of the dimers have been described before. For $[Ir(ppy)_2Cl]_2$[182] and $[Ir(piq)_2Cl]_2$,[183] ^{1}H NMR spectroscopic data matched those reported in the literature. For $[Ir(ppz)_2Cl]_2$, $[Ir(tppy)_2Cl]_2$ and $[Ir(pbtz)_2Cl]_2$, ^{1}H NMR spectroscopy supported the expected structures. No characterization was reported in the literature.

2.3. Synthesis of $[Ir(C\hat{}N)_2(N\hat{}N)][PF_6]$ complexes

Cationic iridium complexes of the type $[Ir(C\hat{}N)_2(N\hat{}N)]^+$ are typically synthesized by cleavage of the dimer with the desired N^N ligand in MeOH or CH_2Cl_2/MeOH.[93,103,104] Using this method, however, traces of chloride ions can be carried through to the final product, despite using an excess of NH_4PF_6 for ion metathesis. We have recently shown that these chloride impurities are detrimental to device performance.[94] Therefore, the complexes in this series were prepared *via* an intermediate solvento complex, formed by the reaction of the iridium dimer with $AgPF_6$ in MeOH (Scheme 19 and Scheme 20). During the reaction, AgCl precipitates and is removed by filtration through Celite®. The filtrate is concentrated and the

solvento intermediate is used immediately without purification or characterization for subsequent transformations. As shown in a series of stable orange emitters, the purity obtained by this synthetic route can lead to excellent LEEC performance, decreasing the risk of chloride ion impurities in the final complexes.[73] In Scheme 19, the synthetic strategy to the six complexes with ppy as cyclometallating ligand and different ancillary ligands is shown. Reaction of the $[Ir(ppy)_2(MeOH)_2][PF_6]$ intermediate with the corresponding benzothiazole-based N^N ligands in MeOH at room temperature gave the desired iridium complexes in moderate to good yields based on the iridium dimer starting material.

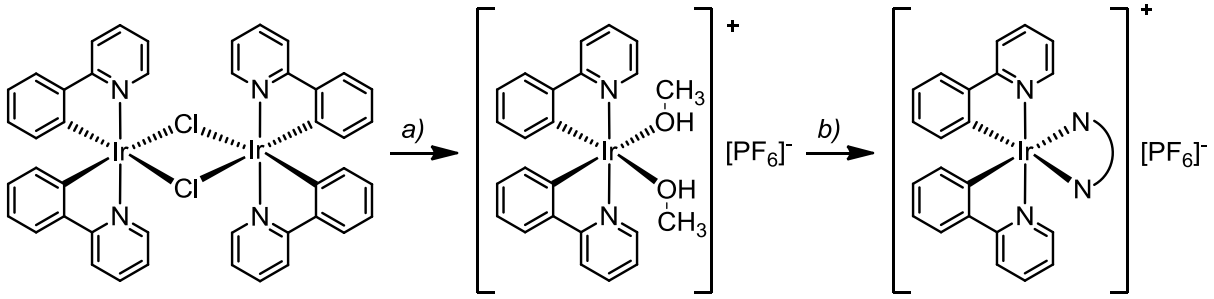

$[Ir(ppy)_2(btzpy)][PF_6]$ **80.6%**
$[Ir(ppy)_2(bbtz)][PF_6]$ **81.9%**
$[Ir(ppy)_2(ppybtz)][PF_6]$ **87.5%**
$[Ir(ppy)_2(tpybtz)][PF_6]$ **70.9%**
$[Ir(ppy)_2(btzpybtz)][PF_6]$ **49.0%**
$[Ir(ppy)_2(bozpy)][PF_6]$ **78.6%**

Scheme 19 Synthesis of $[Ir(ppy)_2(N^N)][PF_6]$ complexes with different ancillary ligands. Reaction conditions: *a)* $AgPF_6$, MeOH, room temperature, 2–3.5 h; *b)* N^N, MeOH, room temperature, overnight. Reported yields (over two steps) are calculated based on the dimer starting materials.

Similarly, four complexes with different cyclometallating ligands (ppz, piq, tppy and pbtz) and 2-(pyridin-2-yl)benzo[*d*]thiazole (btzpy) as ancillary ligand were synthesized. The corresponding iridium dimers were transformed to the solvento intermediates and subsequently reacted with btzpy, leading to the final products with yields ranging from 48.7 to 80.0% over two steps (Scheme 20). All complexes in this series were fully characterized by 1D and 2D NMR spectroscopy, IR spectroscopy, ESI-MS and elemental analysis.

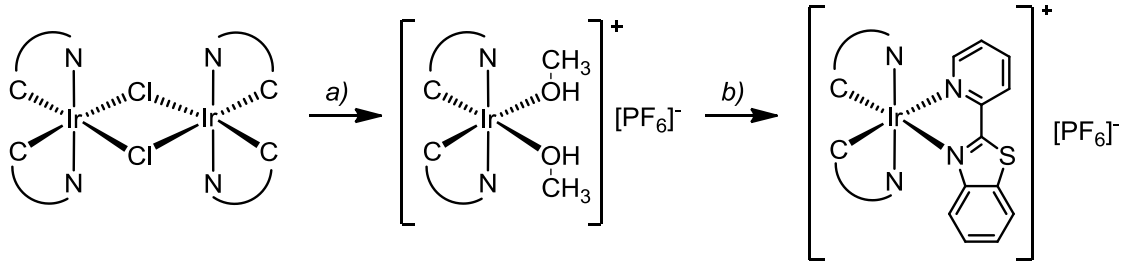

[Ir(ppz)$_2$(btzpy)][PF$_6$] 48.7%
[Ir(piq)$_2$(btzpy)][PF$_6$] 78.9%
[Ir(tppy)$_2$(btzpy)][PF$_6$] 80.0%
[Ir(pbtz)$_2$(btzpy)][PF$_6$] 57.8%

Scheme 20 Synthesis of [Ir(C^N)$_2$(btzpy)][PF$_6$] complexes with different cyclometallating ligands. Reaction conditions: *a)* AgPF$_6$, MeOH, room temperature, 2.5–4 h; *b)* btzpy, MeOH, room temperature, overnight. Reported yields (over two steps) are calculated based on the dimer starting materials.

2.3.1. Decomposition in acetonitrile solution

The complexes reported in Chapters I–III have been characterized and analysed in acetonitrile solutions. During NMR spectroscopic characterization of the red emitter series it was found that four of the complexes, namely [Ir(ppy)$_2$(bbtz)][PF$_6$], [Ir(ppy)$_2$(ppybtz)][PF$_6$], [Ir(ppy)$_2$(btzpybtz)][PF$_6$] and [Ir(piq)$_2$(btzpy)][PF$_6$], are not stable in acetonitrile solution. Rates of decomposition vary between the four complexes; [Ir(ppy)$_2$(btzpybtz)][PF$_6$] shows degradation within a few minutes, whereas [Ir(ppy)$_2$(bbtz)][PF$_6$] is stable over the course of three days in acetonitrile solution and shows only slight decomposition after 20 days. For the remaining six complexes, no change is observed in the ^{1}H NMR spectrum from immediately after preparation to 20 days in acetonitrile solution. A simple replacement of the ancillary ligand by solvent molecules is proposed as the decomposition process, shown in Scheme 21. This assumption is corroborated by the observation of free ppybtz ligand in the case of [Ir(ppy)$_2$(ppybtz)][PF$_6$] (see Fig. 44 for ^{1}H NMR spectra). Furthermore, the appearance of the same species in the NMR spectra of [Ir(ppy)$_2$(bbtz)][PF$_6$], [Ir(ppy)$_2$(ppybtz)][PF$_6$] and [Ir(ppy)$_2$(btzpybtz)][PF$_6$] strongly suggests [Ir(ppy)$_2$(CD$_3$CN)$_2$]$^+$ to be the other dissociation product. The ligand displacement is accompanied by a colour change from an orange-red to a pale yellow solution, which is easily observed for complexes [Ir(ppy)$_2$(btzpybtz)][PF$_6$] and

$[Ir(ppy)_2(ppybtz)][PF_6]$, where decomposition is complete within six hours or three days, respectively. A similar dissociation reaction has been observed for $[Ir(dFphtl)_2(btl)][PF_6]$ (dFphtl = 1-benzyl-4-(2,4-difluorophenyl)-1*H*-1,2,3-triazole, btl = 1,1'-benzyl-4,4'-bi-1*H*-1,2,3-triazole), in which ancillary ligand btl is replaced by acetonitrile molecules in solution.[184] In this case, however, high energy irradiation (290/300 nm) is necessary for decomposition to take place which is not required in our case.

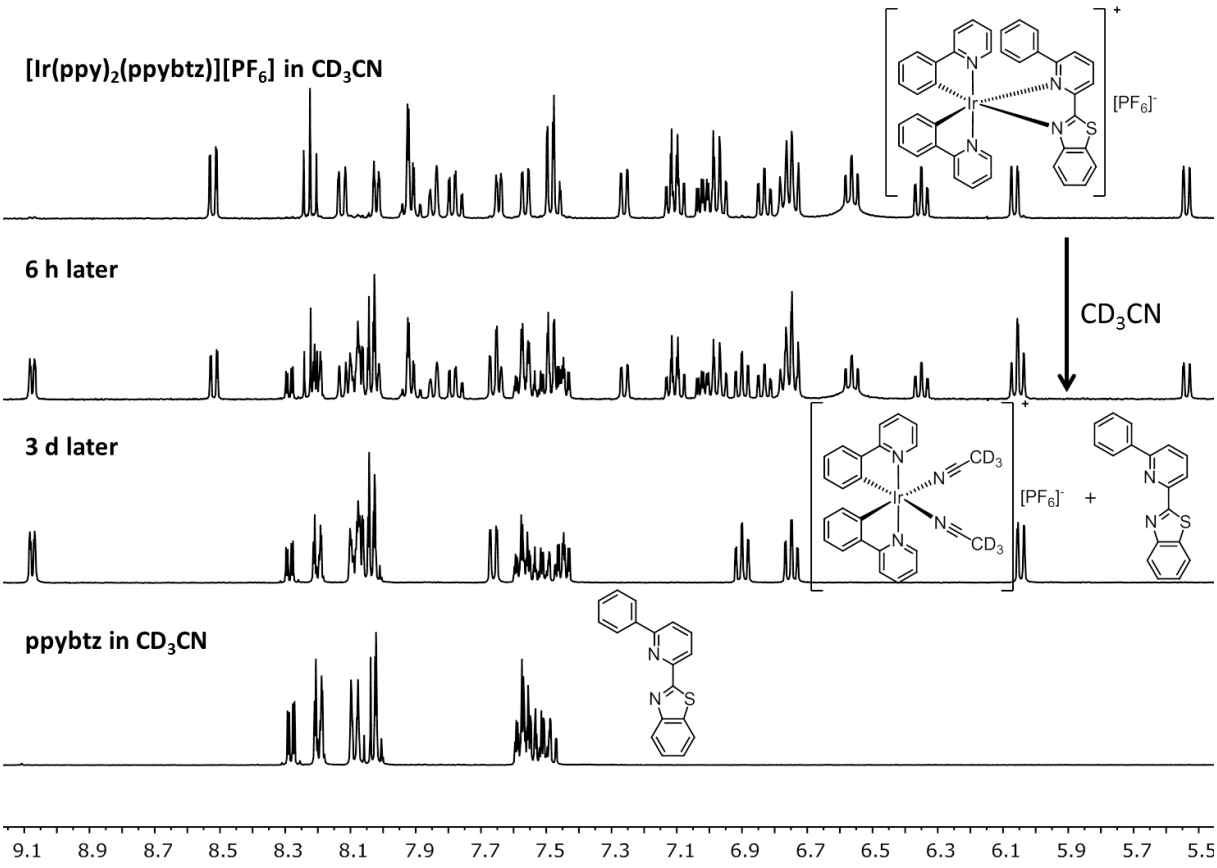

Fig. 44 400 MHz ^{1}H NMR spectra of $[Ir(ppy)_2(ppybtz)][PF_6]$ immediately after dissolving in CD_3CN, after 6 h and after 3 d, showing decomposition according to Scheme 21. The NMR spectrum of ligand ppybtz in CD_3CN (bottom spectrum) is shown to confirm the dissociation reaction occurring in CD_3CN solution. Scale: δ/ppm.

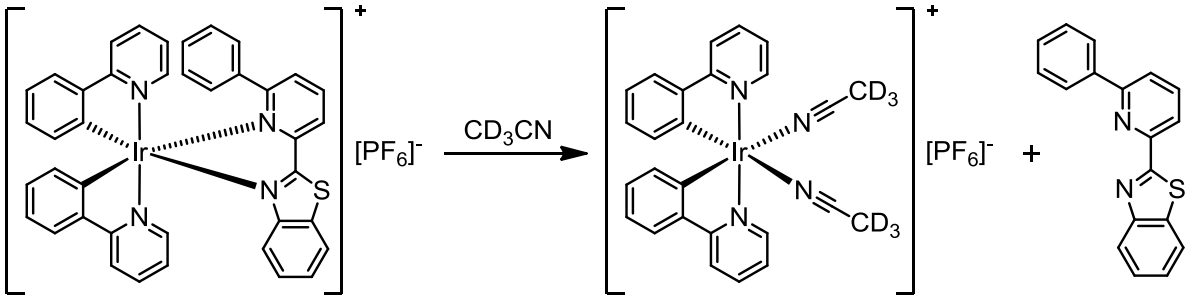

Scheme 21 Decomposition reaction of $[Ir(ppy)_2(ppybtz)][PF_6]$ in CD_3CN solution as a representative example.

2.3.2. Variable temperature NMR spectroscopy of $[Ir(ppy)_2(btzpybtz)][PF_6]$

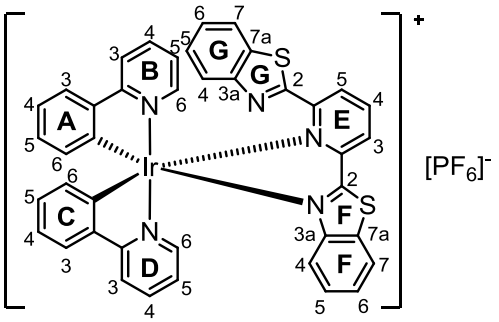

Scheme 22 Chemical structure of $[Ir(ppy)_2(btzpybtz)][PF_6]$ including numbering scheme used for NMR assignment.

The 600 MHz ^1H NMR spectra of $[Ir(ppy)_2(btzpybtz)][PF_6]$ measured at elevated temperatures (298–350 K) in $C_2D_2Cl_4$ solution are shown in Fig. 45. For comparison, the 500 MHz room temperature ^1H NMR spectrum in CD_2Cl_2 solution is added (top spectrum). The NMR experiments were performed by PD Dr. Daniel Häußinger and Yann Baumgartner at the University of Basel. At room temperature, significant broadening of the A ring proton signals as well as the signals for H^{B6} and H^{D6} is observed. These are the protons which are most affected by the proximity of the pendant benzothiazole moiety (G ring). Upon increasing the temperature, sharpening of the peaks occurs. Protons H^{A5}, H^{A6} and H^{B6} are shifted

downfield by $\Delta\delta$ = 0.08 to 0.10 ppm from 298 to 350 K, while protons H^{A3} and H^{A4} retain their chemical shift. At 350 K, proton H^{D6} still shows a broad signal and overlaps with the signal of H^{E3}.

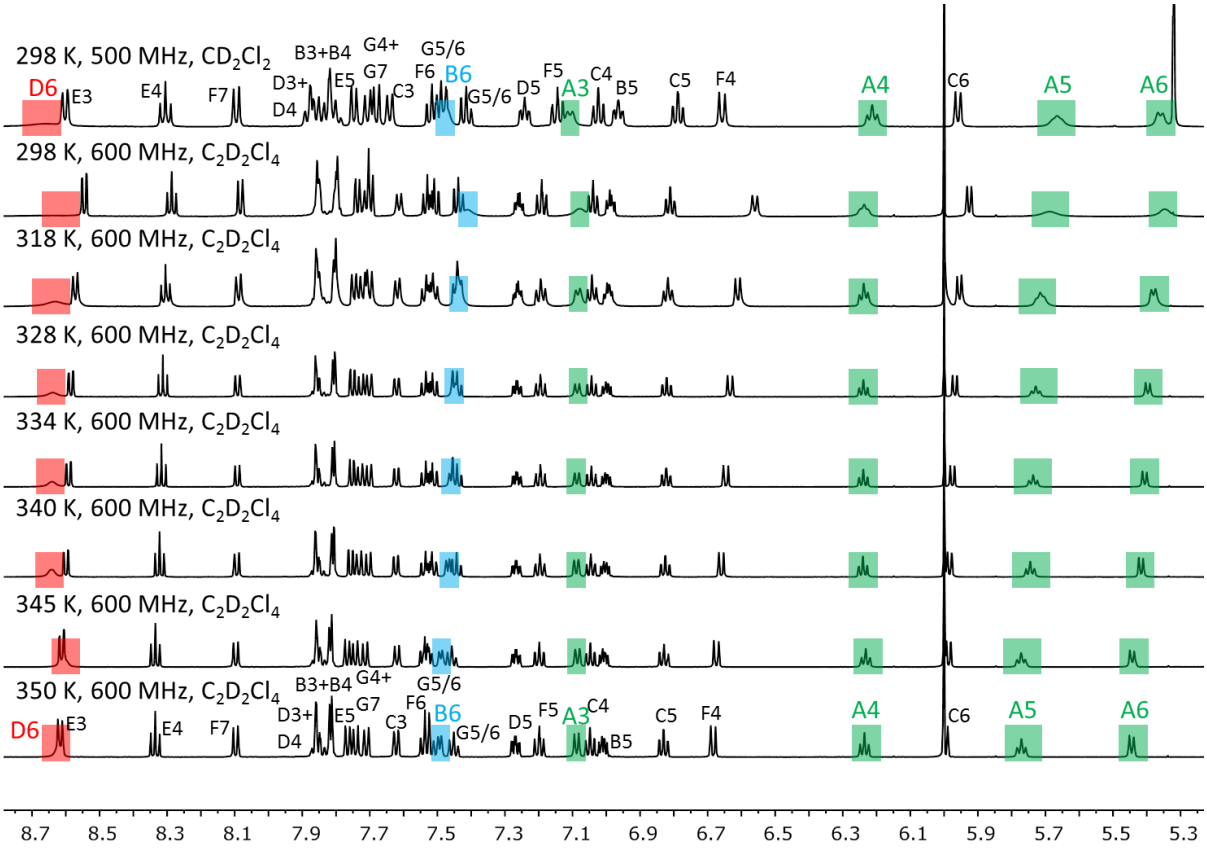

Fig. 45 Aromatic region of the NMR spectra of $[Ir(ppy)_2(btzpybtz)][PF_6]$ at different temperatures, from room temperature to 350 K (top to bottom), including complete assignment for the room temperature CD_2Cl_2 and high temperature $C_2D_2Cl_4$ spectra. Proton signals that sharpen significantly upon increasing temperature are shown in colour. See Scheme 22 for numbering. Scale: δ/ppm.

2D NMR experiments (COSY, ROESY, HMQC and HMBC) were conducted at 345 K to allow for full assignment at elevated temperature in $C_2D_2Cl_4$. In the ROESY spectrum (Fig. 46), EXSY peaks are observed in addition to COSY and NOESY cross peaks. Exchange takes place between the proton signals of rings A and C (phenyl rings of C^N ligands), B and D (pyridyl rings of C^N ligands) and F and G (coordinated and non-coordinated benzothiazole rings). EXSY cross peaks are also observed between protons H^{E3} and H^{E5} of the pyridyl ring

of the N^N ligand. These observations lead to the assumption that a dynamic process occurs in solution. Since only one set of signals is observed in the ^{1}H NMR spectrum, the two species which are transformed into each other must be equivalent in terms of NMR spectroscopy.

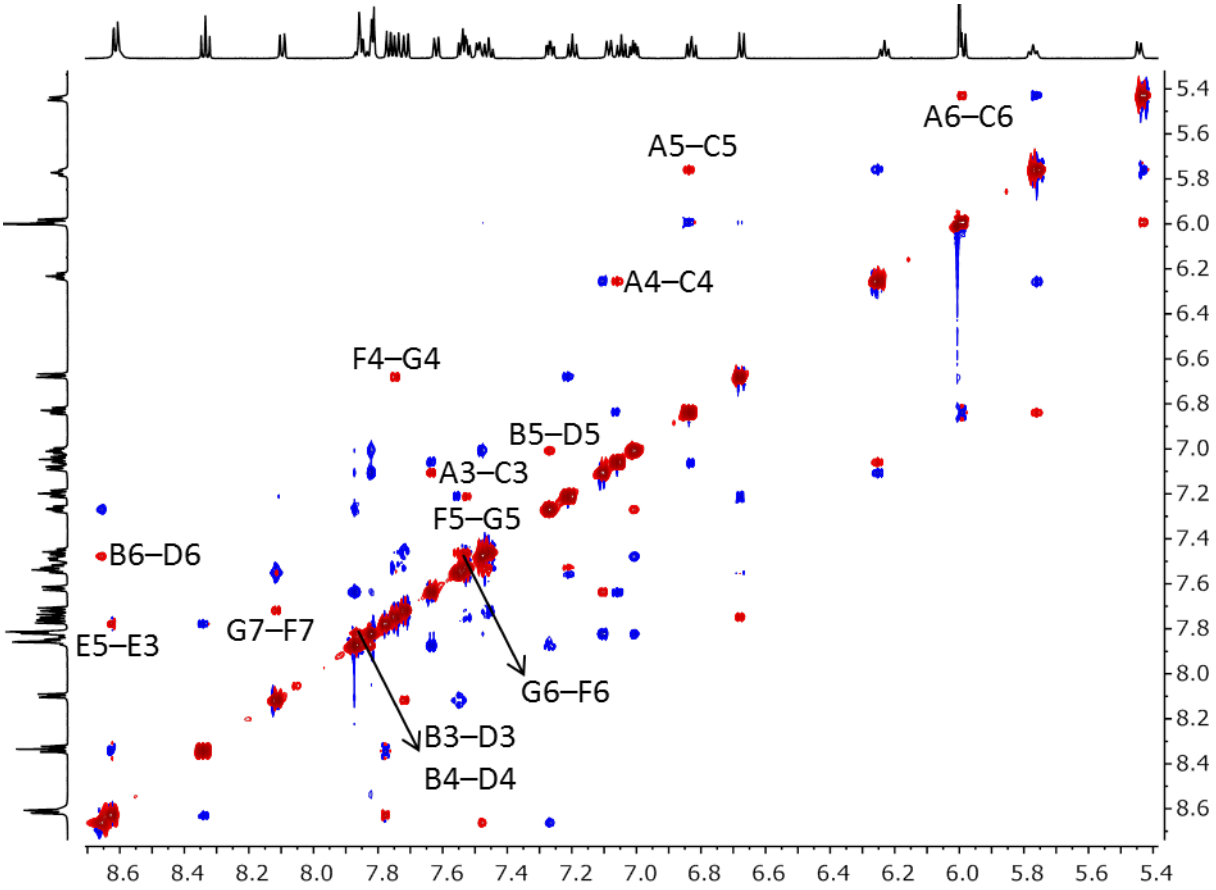

Fig. 46 600 MHz high temperature (345 K) ROESY spectrum of $[Ir(ppy)_2(btzpybtz)][PF_6]$ in $C_2D_2Cl_4$ solution. EXSY cross peaks are shown in red with labels. See Scheme 22 for the numbering scheme used for signal assignment. Scale: δ/ppm.

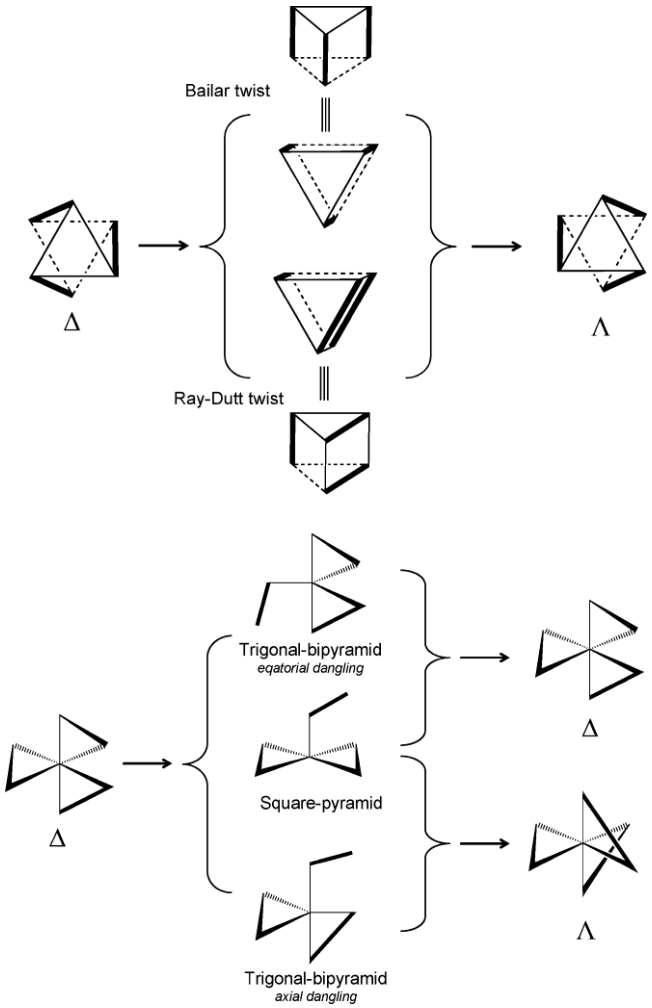

Fig. 47 Schematic representation of the different possible Δ- to Λ- isomerization mechanisms for an octahedral metal complex with three equivalent symmetric bidentate ligands. Reprinted with permission from *Inorg. Chem.*, 2010, **49**, 4194–4211. Copyright (2010) American Chemical Society.[185]

One possibility is an interconversion of the Δ- and Λ-enantiomers. This can occur in octahedral molecules *via* a non-bond breaking mechanism, for example the Bailar[186,187] or Rây-Dutt twist.[187] In both cases, the transition state is of trigonal prismatic geometry. Isomerization can also take place *via* the breaking of one coordination bond, leading to a trigonal-bipyramidal or a square-pyramidal transition state, and subsequently to a reformation of the bond.[185] All these mechanisms are summarized in Fig. 47 for an octahedral metal complex with three equivalent symmetrical bidentate ligands. Another process which could explain the observed exchange mechanisms is a switching of the coordination sites of the

ancillary ligand. While the pyridyl ring of btzpybtz stays coordinated to the iridium metal, the second coordination bond can arise from either of the two benzothiazolyl units.

3. Crystal Structures

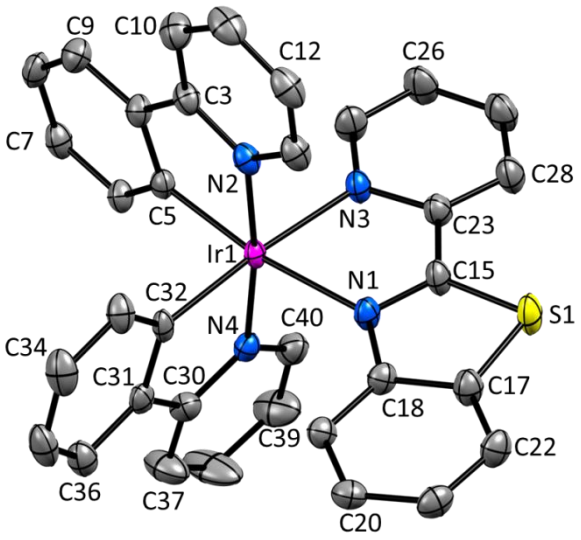

Fig. 48 Structure of the Λ-$[Ir(ppy)_2(btzpy)]^+$ cation in $[Ir(ppy)_2(btzpy)][PF_6]\cdot 1.5CH_2Cl_2$. H atoms omitted for clarity and ellipsoids plotted at 50% probability level. Selected bond parameters: Ir1–N1 = 2.172(2), Ir1–N2 = 2.050(2), Ir1–N3 = 2.143(2), Ir1–N4 = 2.041(2), Ir1–C5 = 2.007(3), Ir1–C32 = 2.014(3), S1–C15 = 1.731(3), S1–C17 = 1.742(3) Å; N1–Ir1–N3 = 76.15(9), N2–Ir1–C5 = 80.63(10), N4–Ir1–C32 = 80.65(10), N1–Ir1–C5 = 171.48(9), N2–Ir1–N4 = 172.68(9), N3–Ir1–C32 = 175.40(10), C15–S1–C17 = 88.97(14)°.

Single crystals of $[Ir(ppy)_2(btzpy)][PF_6]\cdot 1.5CH_2Cl_2$, $[Ir(ppy)_2(bbtz)][PF_6]$ and $[Ir(ppy)_2(bozpy)][PF_6]\cdot CH_2Cl_2$ were grown by layering CH_2Cl_2 solutions of the complexes with Et_2O. Structures of the complex cations are shown in Fig. 48 to Fig. 50 and important bond lengths and angles are given in the figure captions. $[Ir(ppy)_2(btzpy)][PF_6]\cdot 1.5CH_2Cl_2$ and $[Ir(ppy)_2(bozpy)][PF_6]\cdot CH_2Cl_2$ crystallize in the monoclinic space groups $P2_1/c$ and $P2_1/n$, respectively, whereas $[Ir(ppy)_2(bbtz)][PF_6]$ crystallizes in the orthorhombic space group *Fdd*2. CH_2Cl_2 solvent molecules are heavily disordered in $[Ir(ppy)_2(btzpy)][PF_6]\cdot 1.5CH_2Cl_2$ and have been removed using the SQUEEZE[188] method. In $[Ir(ppy)_2(bozpy)][PF_6]\cdot CH_2Cl_2$, the CH_2Cl_2 solvent molecule is ordered. The asymmetric unit

of $[Ir(ppy)_2(bbtz)][PF_6]$ contains half a cation and half an anion; in each case, the second half is generated by a C_2 rotation axis which is parallel to the *c* axis of the unit cell and runs through the iridium or the phosphorus centre, respectively.

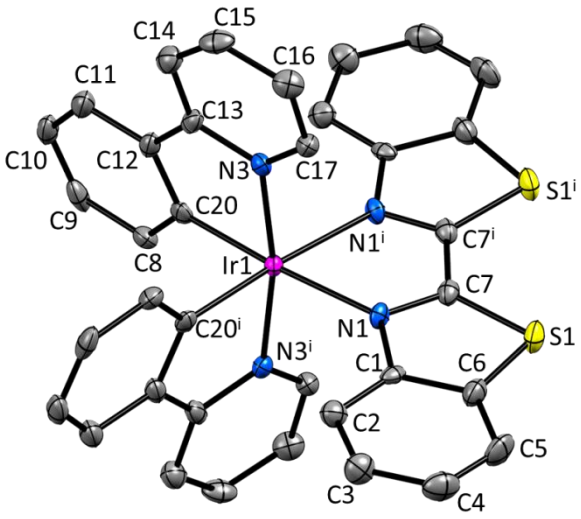

Fig. 49 Structure of the Λ-$[Ir(ppy)_2(bbtz)]^+$ cation in $[Ir(ppy)_2(bbtz)][PF_6]$, H atoms omitted and ellipsoids plotted at 50% probability level. Symmetry code: i = −x+½,−y+½,z+1. Selected bond parameters: Ir1–N1 = 2.176(3), Ir1–N3 = 2.048(2), Ir1–C20 = 2.004(3), S1–C6 = 1.730(4), S1–C7 = 1.718(3) Å; N1–Ir1–$N1^i$ = 75.58(14), N3–Ir1–C20 = 80.75(12), N1–Ir1–C20 = 175.83(13), N3–Ir1–$N3^i$ = 168.96(15), C6–S1–C7 = 88.77(16)°.

For $[Ir(ppy)_2(btzpy)][PF_6]\cdot 1.5CH_2Cl_2$ and $[Ir(ppy)_2(bozpy)][PF_6]\cdot CH_2Cl_2$, the phenylpyridine ligand of which the coordinating C atom is *trans* to the benzothiazole/benzoxazole unit is nearly planar (angles between the ring planes are 3.3 and 2.7°, respectively). The other ppy cyclometallating ligand (coordinating carbon *trans* to the pyridine ring of the ancillary ligand) shows deviation from planarity, with angles between the ring planes of 8.2 and 10.9°. Whereas the btzpy ancillary ligand in $[Ir(ppy)_2(btzpy)][PF_6]\cdot 1.5CH_2Cl_2$ is distorted from planarity (angle between ring planes = 8.2°), the bozpy ligand in $[Ir(ppy)_2(bozpy)][PF_6]\cdot CH_2Cl_2$ does not exhibit the same behaviour (angle between the ring planes = 2.2°). In $[Ir(ppy)_2(bbtz)][PF_6]$, both the ppy and the bbtz ligands are twisted so that the angles between the ring planes amount to 7.1 and 7.5°, respectively.

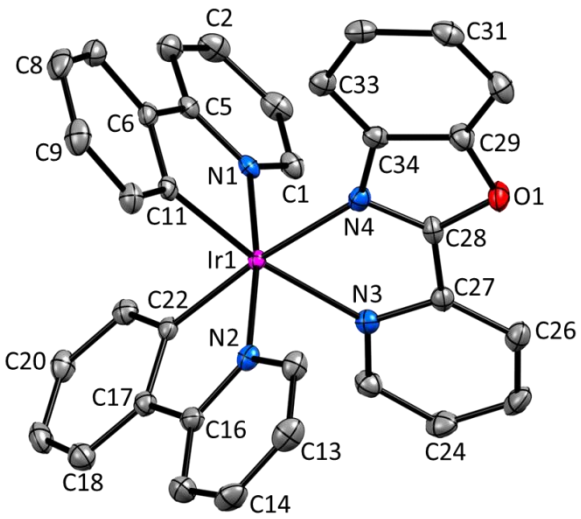

Fig. 50 Structure of the Δ-$[Ir(ppy)_2(bozpy)]^+$ cation in $[Ir(ppy)_2(bozpy)][PF_6]\cdot CH_2Cl_2$. H atoms omitted for clarity and ellipsoids plotted at 50% probability level. Selected bond parameters: Ir1–N1 = 2.044(2), Ir1–N2 = 2.055(2), Ir1–N3 = 2.173(2), Ir1–N4 = 2.140(2), Ir1–C11 = 2.009(3), Ir1–C22 = 2.008(3), O1–C28 = 1.355(4), O1–C29 = 1.394(4) Å; N1–Ir1–C11 = 80.60(11), N2–Ir1–C22 = 80.60(11), N3–Ir1–N4 = 76.33(9), N1–Ir1–N2 = 172.13(9), N3–Ir1–C11 = 170.59(10), N4–Ir1–C22 = 173.90(10), C28–O1–C29 = 103.9(2)°.

4. Photophysical Properties

UV-Vis absorption spectra in CH_2Cl_2 solution are shown in Fig. 51 for complexes with ppy as cyclometallating and different ancillary ligands and in Fig. 52 for complexes with different cyclometallating ligands and btzpy as ancillary ligand. All complexes show intense absorption bands in the UV with maxima in the range 254–324 nm, which are ascribed to spin-allowed π*←π transitions of the ligands. Lower energy bands between 350 and 450 nm correspond to spin-allowed ^{1}MLCT and ^{1}LLCT excitations, whereas the low intensity tails above 450 nm arise from spin-forbidden ^{3}MLCT, ^{3}LLCT and ^{3}LC transitions.[21]

The UV-Vis absorption spectra of all complexes in this series are similar, with only three compounds showing significantly different spectra; these are $[Ir(ppy)_2(bbtz)][PF_6]$, $[Ir(piq)_2(btzpy)][PF_6]$ and $[Ir(pbtz)_2(btzpy)][PF_6]$ and their absorption profiles will be discussed in more detail. $[Ir(ppy)_2(bbtz)][PF_6]$ (orange line, Fig. 51) exhibits more intense absorption bands at wavelengths higher than 360 nm compared to the other complexes, with considerably stronger absorption bands extending into the visible region (around 450 nm).

This feature is attributed to the 2,2'-bibenzo[*d*]thiazole (bbtz) ancillary ligand. In the literature, there is only one example of a metal complex coordinated by the bbtz ligand, a cationic ruthenium complex of the formula $[Ru(bpy)_2(bbtz)][PF_6]_2$.[174] Unfortunately, neither an absorption curve nor any extinction coefficients are reported; the authors describe however red-shifted MLCT maxima on going from $[Ru(bpy)_3]^{2+}$ to $[Ru(bpy)_2(btzpy)]^{2+}$ to $[Ru(bpy)_2(bbtz)]^{2+}$.

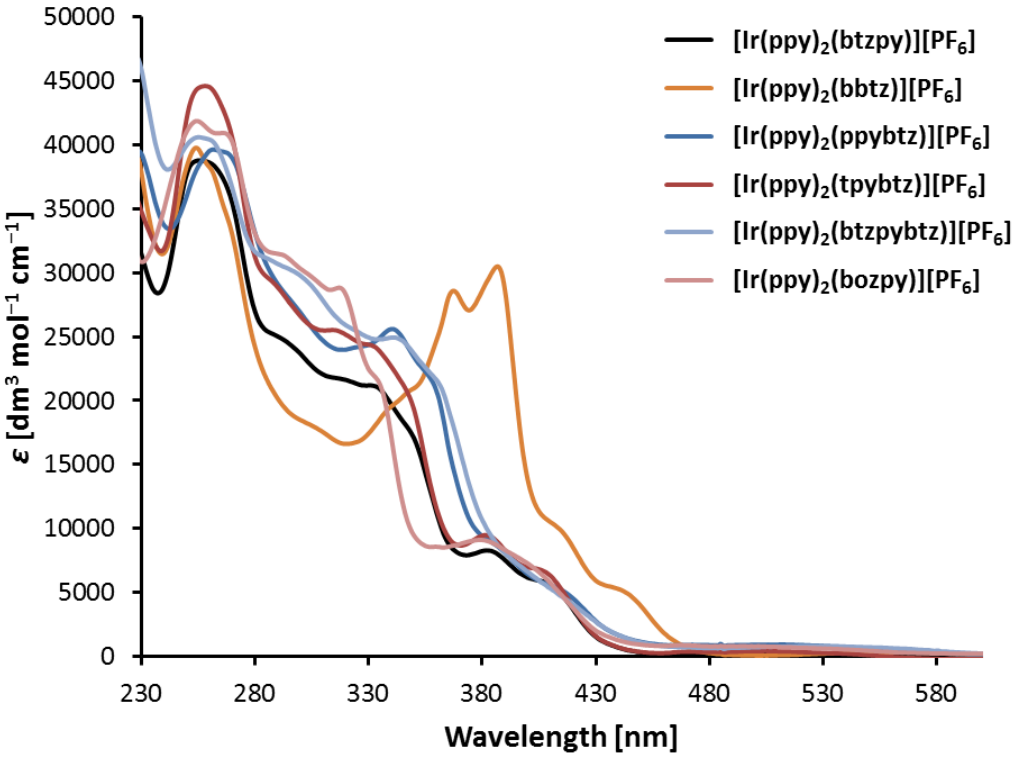

Fig. 51 UV-Vis absorption spectra in CH_2Cl_2 solution (1.0×10^{-5} mol dm^{-3}) of complexes with ppy cyclometallating and different ancillary ligands.

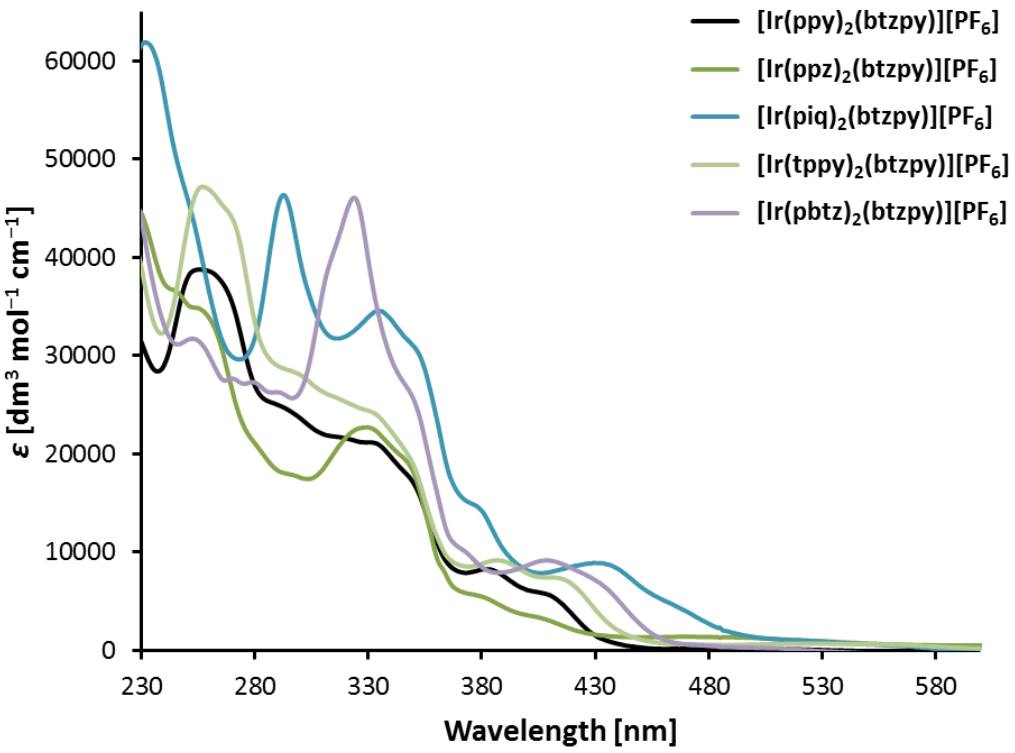

Fig. 52 UV-Vis absorption spectra in CH_2Cl_2 solution (1.0×10^{-5} mol dm^{-3}) of complexes with different cyclometallating ligands and btzpy ancillary ligand.

Characteristic peaks at 293 (ε = 46 000 dm^3 mol^{-1} cm^{-1}) and 433 nm (ε = 8900 dm^3 mol^{-1} cm^{-1}) are observed in the absorption spectrum of $[Ir(piq)_2(btzpy)][PF_6]$ (blue line, Fig. 52) which arise due to the presence of the 1-phenylisoquinoline (piq) cyclometallating ligand. Those maxima are also observed for $[Ir(piq)_2(bpy)][PF_6]$ at 290/291 and 439/440 nm (in CH_2Cl_2), as described in the literature.[189–191] Extinction coefficients are in the same range as those found for $[Ir(piq)_2(btzpy)][PF_6]$. The distinctive absorption band at 324 nm (ε = 46 000 dm^3 mol^{-1} cm^{-1}) of $[Ir(pbtz)_2(btzpy)][PF_6]$ (purple line, Fig. 52) is not present in $[Ir(ppy)_2(btzpy)][PF_6]$ and must therefore be a characteristic of the 2-phenylbenzo[*d*]thiazole (pbtz) cyclometallating ligand. Comparison with literature data of $[Ir(pbtz)_2(bpy)]^+$ shows the presence of an absorption band with two maxima in the same region (310–325 nm) in CH_2Cl_2,[192] CH_3CN,[192] MeOH[193] and THF[194] solutions. The corresponding absorption intensities reported in the literature are lower, indicating the contribution of a transition involving the btzpy ancillary ligand in $[Ir(pbtz)_2(btzpy)][PF_6]$ to the absorption band, thus leading to a higher extinction coefficient in this case.

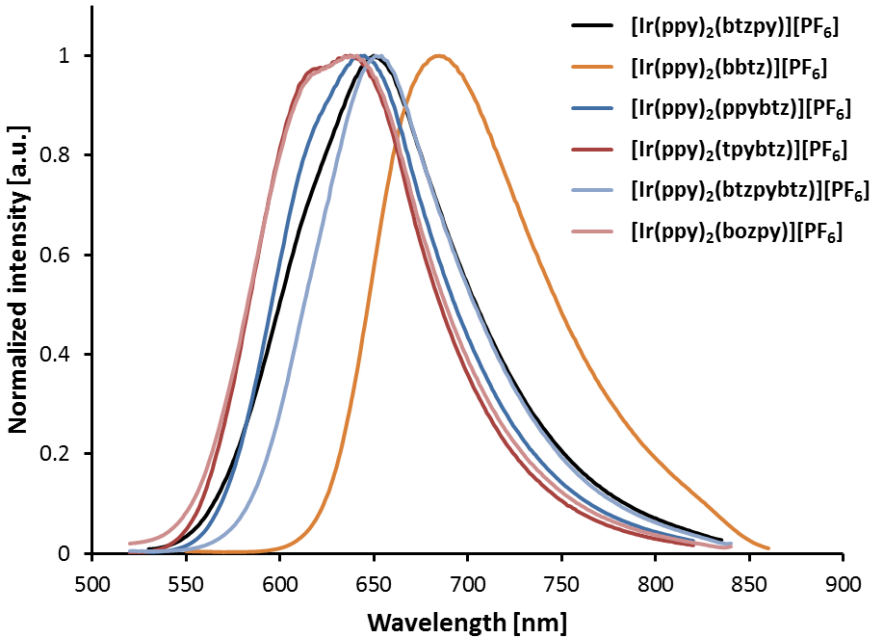

Fig. 53 Emission spectra in CH_2Cl_2 solution (1.0×10^{-5} mol dm^{-3}) of complexes with ppy cyclometallating and different ancillary ligands. λ_{exc} = 445 nm for $[Ir(ppy)_2(bbtz)][PF_6]$, λ_{exc} = 430 nm for the other compounds.

Excitation of CH_2Cl_2 solutions of the complexes in this series gives the emission spectra shown in Fig. 53 and Fig. 54 with solution photophysical data summarized in Table 14. Emission maxima lie in the orange to deep-red region, ranging from 600 to 686 nm. For all complexes, the shapes and positions of the emission bands are independent of the excitation wavelength.

Introduction of the btzpy ancillary ligand leads to a 49 nm red-shift of the emission maximum in CH_2Cl_2 when compared to the parent complex $[Ir(ppy)_2(bpy)][PF_6]$ (595 nm).[195] This red-shift can be explained by the electron-deficient nature of the benzothiazole moiety, leading to stabilization of the LUMO and as a consequence a smaller energy gap. Replacing the pyridine ring of btzpy by another benzothiazole unit leads to a further 42 nm bathochromic shift of the emission maximum in $[Ir(ppy)_2(bbtz)][PF_6]$ (orange line, Fig. 53). Substituting btzpy with a further benzothiazole group (btzpybtz ligand) does not have the same effect as bbtz; the pendant btz ring in $[Ir(ppy)_2(btzpybtz)][PF_6]$ red-shifts the emission maximum by only 8 nm (light blue line, Fig. 53). Coordination of the benzothiazole to the iridium centre is therefore crucial for a substantial bathochromic shift. With the exception of

$[Ir(ppy)_2(bbtz)][PF_6]$ (orange line, Fig. 53), $[Ir(ppz)_2(btzpy)][PF_6]$ (dark green line, Fig. 54) and $[Ir(pbtz)_2(btzpy)][PF_6]$ (purple line, Fig. 54), the emission maxima of all complexes in this series are found in a small 24 nm range between 636 and 660 nm, corresponding to red emission. Introduction of a pendant phenyl or benzothiazole ring (dark and light blue lines, Fig. 53) as well as substitution of ppy by piq (blue line, Fig. 54) exerts a negligible influence on the luminescence maximum. Whereas functionalization of ppy with a *tert*-butyl group red-shifts the emission by 16 nm (light green line, Fig. 54), a blue-shift of the emission band is observed upon *tert*-butyl substitution on the pyridyl ring of btzpy (dark red line, Fig. 53). The same effect is observed by changing the benzothiazole to a benzoxazole unit in the ancillary ligand (light red line, Fig. 53). As for $[Ir(ppz)_2(btzpy)][PF_6]$ and $[Ir(pbtz)_2(btzpy)][PF_6]$, both ppz (dark green) and pbtz (purple line, Fig. 54) cyclometallating ligands stabilize the HOMO, thus increasing the HOMO-LUMO gap. Both complexes are therefore orange emitters, with blue-shifted λ_{em}^{max} of 607 and 600 nm, respectively. This observation is in accordance with the reported hypsochromic shifts of $[Ir(ppz)_2(bpy)][PF_6]$[133] and $[Ir(pbtz)_2(bpy)][PF_6]$[192] with respect to the archetypal $[Ir(ppy)_2(bpy)][PF_6]$.

The majority of complexes in this series show broad, unstructured emission profiles, indicating a large charge transfer character of the emissive state. Some vibrational structure is observed in the emission bands of $[Ir(ppy)_2(tpybtz)][PF_6]$, $[Ir(ppy)_2(bozpy)][PF_6]$ (dark and light red lines, Fig. 53), $[Ir(ppz)_2(btzpy)][PF_6]$ and $[Ir(pbtz)_2(btzpy)][PF_6]$ (dark green and purple lines, Fig. 54), suggesting that the ^{3}LC contribution is more pronounced in the emissive state of these four complexes.

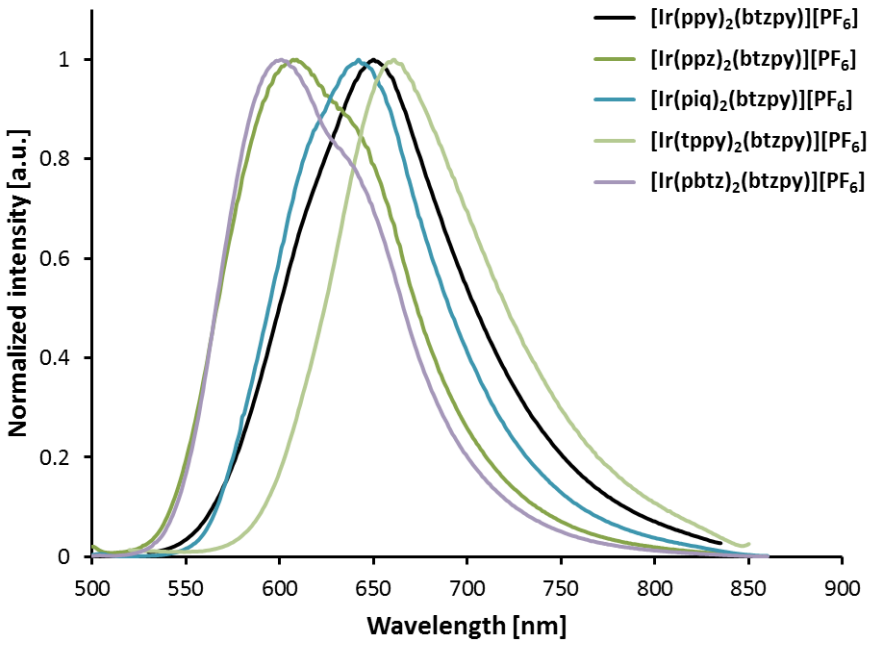

Fig. 54 Emission spectra in CH_2Cl_2 solution (1.0×10^{-5} mol dm^{-3}) of complexes with different cyclometallating ligands and btzpy ancillary ligand. λ_{exc} = 430 nm for $[Ir(ppy)_2(btzpy)][PF_6]$ and $[Ir(ppz)_2(btzpy)][PF_6]$; λ_{exc} = 435 nm for $[Ir(tppy)_2(btzpy)][PF_6]$; λ_{exc} = 437 nm for $[Ir(piq)_2(btzpy)][PF_6]$ and $[Ir(pbtz)_2(btzpy)][PF_6]$.

Photoluminescence quantum yields in solution are generally low (<10%) within this series of complexes (Table 14), but comparable to most of the red emitters reported in the literature (*vide supra*). A *tert*-butyl substituent on the ancillary ligand in $[Ir(ppy)_2(tpybtz)][PF_6]$ and the exchange of ppy by ppz in $[Ir(ppz)_2(btzpy)][PF_6]$ lead to slightly higher PLQYs of 14 and 16%, respectively. With a substantially higher quantum yield of 41%, $[Ir(pbtz)_2(btzpy)][PF_6]$ is an exception in this series. $[Ir(pbtz)_2(btzpy)][PF_6]$ exhibits also a significantly longer excited state lifetime (1.2 µs) than the remaining nine complexes, which show lifetimes in the range 55–459 ns. Lifetimes were determined using biexponential fits in the case of $[Ir(ppy)_2(btzpybtz)][PF_6]$, $[Ir(ppy)_2(bozpy)][PF_6]$ and $[Ir(piq)_2(btzpy)][PF_6]$; data are given in Table 14.

Table 14 Photophysical properties in CH_2Cl_2 solution.

Compound	λ_{exc} [nm]	λ_{em}^{max} [nm]	PLQY [%][a]	τ_{ave} [ns] (χ)[a,b]	τ_1 [ns] (A_1)	τ_2 [ns] (A_2)
[Ir(ppy)$_2$(bozpy)][PF$_6$]	270	636	5.9	166 (1.2)	143 (6297)	237 (1185)
[Ir(ppy)$_2$(btzpybtz)][PF$_6$]	265	652	4.1	169 (1.0)	139 (6306)	274 (917)
[Ir(ppy)$_2$(tpybtz)][PF$_6$]	270	636	14	329 (1.0)	---	---
[Ir(ppy)$_2$(ppybtz)][PF$_6$]	270	645	6.5	183 (1.1)	---	---
[Ir(ppy)$_2$(bbtz)][PF$_6$]	259	686	3.6	126 (1.2)	---	---
[Ir(ppy)$_2$(btzpy)][PF$_6$]	266	644	7.7	222 (1.1)	---	---
[Ir(ppz)$_2$(btzpy)][PF$_6$]	261	607	16	459 (1.1)	---	---
[Ir(piq)$_2$(btzpy)][PF$_6$]	293	642	8.7	380 (1.1)	251 (8009)	1349 (199)
[Ir(tppy)$_2$(btzpy)][PF$_6$]	268	660	1.9	55 (1.1)	---	---
[Ir(pbtz)$_2$(btzpy)][PF$_6$]	326	600	41	1200 (1.1)	---	---

[a] Measured in de-aerated solution. [b] λ_{exc} = 280 nm; 340 nm for [Ir(pbtz)$_2$(btzpy)][PF$_6$]. Biexponential fits were used for the excited state lifetime determination of three of the complexes, according to the equation $\tau_{ave} = \sum A_i \tau_i / \sum A_i$ (A_i = pre-exponential factor of the lifetime). Monoexponential fits were used for the remaining complexes (no τ_1 and τ_2 reported).

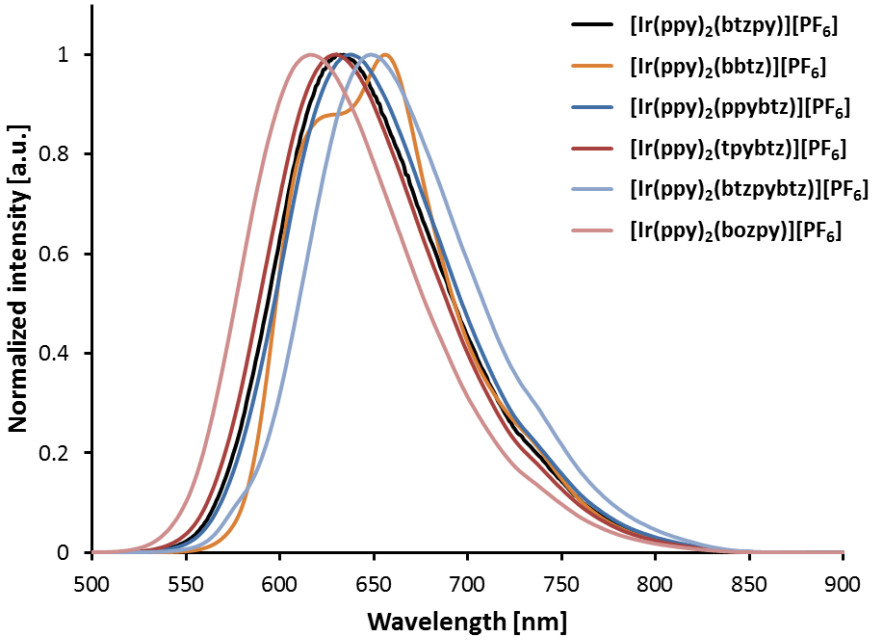

Fig. 55 Solid-state emission spectra of powder samples of complexes with ppy cyclometallating and different ancillary ligands. λ_{exc} = 280 nm.

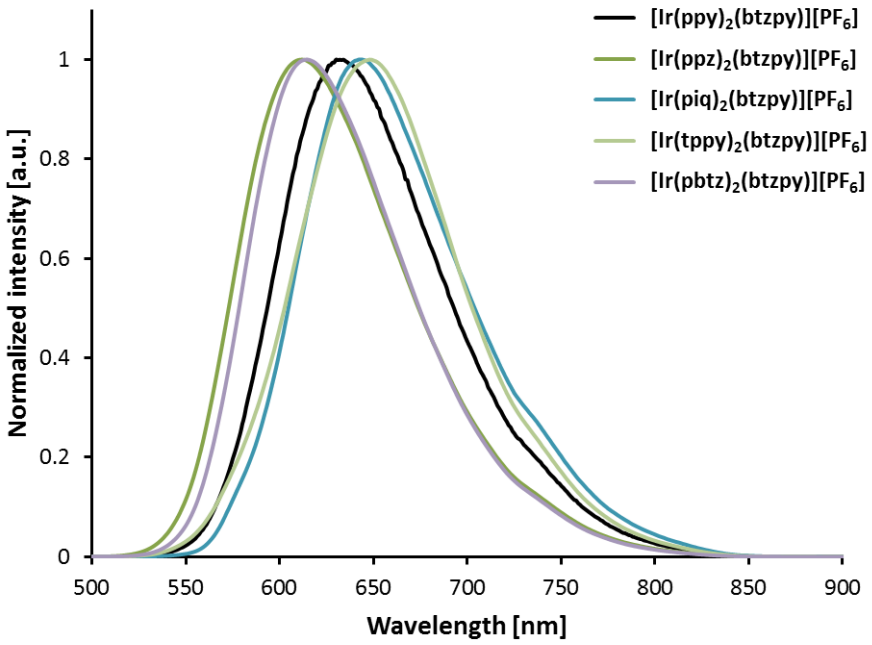

Fig. 56 Solid-state emission spectra of powder samples of complexes with different cyclometallating ligands and btzpy ancillary ligand. λ_{exc} = 280 nm.

Emission spectra of powder samples are depicted in Fig. 55 and Fig. 56; emission maxima, quantum yields and excited state lifetimes are summarized in Table 15. No shift of the emission maximum is observed for [Ir(piq)$_2$(btzpy)][PF$_6$] (blue line, Fig. 56) on going from CH_2Cl_2 solution to the solid state. [Ir(ppz)$_2$(btzpy)][PF$_6$] (dark green) and [Ir(pbtz)$_2$(btzpy)][PF$_6$] (purple line, Fig. 56) both show a slight red-shift of the emission maximum by 5 and 14 nm, respectively; all remaining complexes exhibit a blue-shift in the range 4–30 nm. The largest shift is seen for [Ir(ppy)$_2$(bbtz)][PF$_6$] (orange line, Fig. 55); this is also the only complex in this series which has a structured emission profile in the solid state. PLQYs vary from 2.3% for [Ir(piq)$_2$(btzpy)][PF$_6$] to 33% for [Ir(pbtz)$_2$(btzpy)][PF$_6$]. Solid state quantum yields are significantly higher with respect to solution quantum yields for [Ir(ppy)$_2$(bbtz)][PF$_6$] (17% in powder) and [Ir(tppy)$_2$(btzpy)][PF$_6$] (10%) and considerably lower for [Ir(ppz)$_2$(btzpy)][PF$_6$] (11%), [Ir(piq)$_2$(btzpy)][PF$_6$] (2.3%) and [Ir(pbtz)$_2$(btzpy)][PF$_6$] (33%). A decrease in quantum yields of solid samples compared to solution data is commonly observed in iridium complexes and suggests strong quenching of the excited state due to intermolecular interactions.[78] A significant increase from solution to solid state PLQY – as seen for [Ir(ppy)$_2$(bbtz)][PF$_6$] and [Ir(tppy)$_2$(btzpy)][PF$_6$] – occurs less

frequently in this type of complex and can be attributed to the phenomenon of Aggregation-Induced Emission (AIE),[196–199] also called Enhanced Phosphorescence Emission in the Solid State (EPESS).[200] Biexponential fits were used for solid state decay curves of all complexes. Average lifetimes lie in the range 142–730 ns, with $[Ir(pbtz)_2(btzpy)][PF_6]$ exhibiting not only the highest quantum yield, but also the longest τ_{ave}.

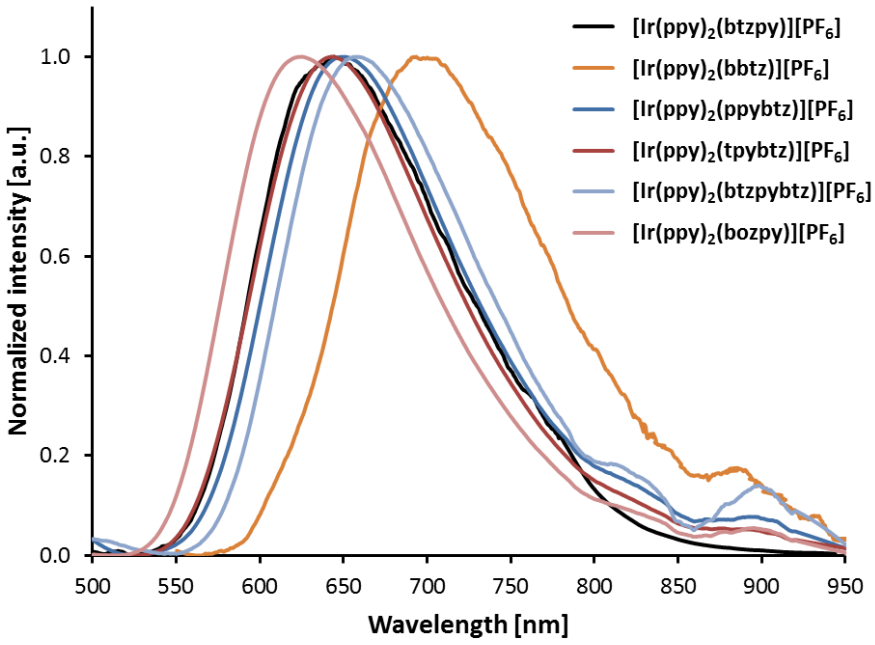

Fig. 57 Thin film photoluminescence spectra of complexes with ppy as cyclometallating ligand and different ancillary ligands. Composition: $[Ir(ppy)_2(N^\wedge N)][PF_6]$:$[Bmim][PF_6]$ 4:1. For thin film with $[Ir(ppy)_2(tpybtz)][PF_6]$, 2 wt-% PMMA was added. λ_{exc} = 320 nm.

Thin films of the complexes combined with $[Bmim][PF_6]$ as ionic liquid (4:1 ratio) were spin-coated onto quartz substrates and photophysical properties determined by Dr. Henk Bolink and co-workers at the University of Valencia. For $[Ir(ppy)_2(tpybtz)][PF_6]$, 2 wt-% poly(methyl methacrylate) (PMMA) was added to facilitate film formation. Photoluminescence spectra are depicted in Fig. 57 for $[Ir(ppy)_2(N^\wedge N)][PF_6]$ with different N^N ligands and Fig. 58 for $[Ir(C^\wedge N)_2(btzpy)][PF_6]$ with different C^N ligands. Emission maxima and quantum yields are reported in Table 15. Red-shifts in the emission maxima are observed for all complexes on going from powder samples to thin films. A pronounced red-shift of 37 nm is seen for

$[Ir(ppy)_2(bbtz)][PF_6]$ (orange line, Fig. 57), resulting in an emission maximum close to the near-infrared region (693 nm). All other complexes exhibit smaller bathochromic shifts in the range 9–18 nm. Interaction of the complexes with the ionic liquid in thin films apparently leads to a slight stabilization of the triplet emissive state and thus a smaller energy gap. In thin films, quantum yields of nearly all complexes stay the same or are slightly increased when compared to powder samples (Table 15). Only for $[Ir(ppy)_2(bbtz)][PF_6]$ (6.7%) and $[Ir(tppy)_2(btzpy)][PF_6]$ (5.1%), PLQYs are significantly lower in films than as powder samples (17 and 10%, respectively). This observation further supports the theory of an AIE process taking place, as the complexes are diluted with ionic liquid in the case of thin film samples.[196–200]

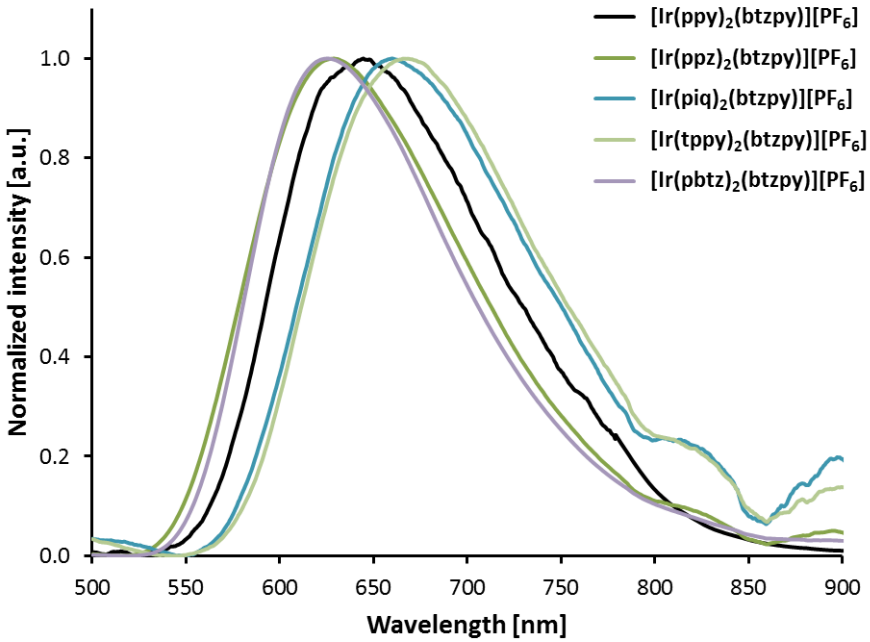

Fig. 58 Solid state emission spectra of thin films of complexes with different cyclometallating ligands and btzpy as ancillary ligand. Composition: $[Ir(C\text{^}N)_2(btzpy)][PF_6]$:[Bmim][$PF_6$] 4:1. λ_{exc} = 320 nm.

Table 15 Solid state photophysical properties of powder samples and in thin film (complex:[Bmim][PF_6] 4:1). Thin film of [$Ir(ppy)_2(tpybtz)$][PF_6] included 2 wt-% PMMA.

Compound	Powder samples					Thin film	
	λ_{em}^{max} [nm][a]	PLQY [%][b]	τ_{ave} [ns] (χ)[c]	τ_1 [ns] (A_1)	τ_2 [ns] (A_2)	λ_{em}^{max} [nm][d]	PLQY [%][d]
$[Ir(ppy)_2(bozpy)][PF_6]$	616	9.7	236 (1.0)	113 (2466)	253 (7659)	625	12
$[Ir(ppy)_2(btzpybtz)][PF_6]$	648	3.1	185 (1.0)	109 (4892)	229 (4022)	658	5.8
$[Ir(ppy)_2(tpybtz)][PF_6]$	630	16	305 (1.1)	224 (5183)	370 (3953)	642	18
$[Ir(ppy)_2(ppybtz)][PF_6]$	638	8.5	214 (1.0)	148 (5424)	266 (3743)	651	9.7
$[Ir(ppy)_2(bbtz)][PF_6]$	656	17	565 (1.1)	340 (2834)	613 (7404)	693	6.7
$[Ir(ppy)_2(btzpy)][PF_6]$	630	8.6	277 (1.0)	206 (6796)	397 (2094)	645	11
$[Ir(ppz)_2(btzpy)][PF_6]$	612	11	337 (1.2)	176 (3291)	379 (5783)	629	12
$[Ir(piq)_2(btzpy)][PF_6]$	642	2.3	142 (1.1)	111 (8362)	256 (1006)	659	3.3
$[Ir(tppy)_2(btzpy)][PF_6]$	648	10	328 (1.0)	175 (5547)	444 (2858)	666	5.1
$[Ir(pbtz)_2(btzpy)][PF_6]$	614	33	730 (1.1)	538 (3936)	808 (6488)	625	29

[a] λ_{exc} = 280 nm. [b] For λ_{exc}, see Table 14. [c] λ_{exc} = 280 nm; 340 nm for [$Ir(pbtz)_2(btzpy)$][PF_6]. Biexponential fits were used for the excited state lifetime determination of all complexes, according to the equation $\tau_{ave} = \sum A_i \tau_i / \sum A_i$ (A_i = pre-exponential factor of the lifetime). [d] λ_{exc} = 320 nm.

5. Electrochemical Properties

Electrochemical data gained from cyclic voltammetry measurements in CH_2Cl_2 with both glassy carbon and Pt working electrodes are summarized in Table 16. For complexes with different cyclometallating ligands [$Ir(C^N)_2(btzpy)$][PF_6] (C^N = ppy, ppz, piq, tppy, pbtz), the reduction potentials lie in a close range (−1.52 to −1.57 V), as shown in Fig. 59. This is in accordance with the localization of the LUMO on the ancillary ligand (btzpy in our case) in this type of iridium complexes. Since the HOMO is localized mainly on the iridium centre and the phenyl ring of the cyclometallating ligand, the oxidation potential is sensitive to variation of the C^N ligand. With respect to [$Ir(ppy)_2(btzpy)$][PF_6] ($E_{1/2}^{ox}$ = +0.93 V for glassy carbon and 0.94 V for Pt electrode), complex [$Ir(tppy)_2(btzpy)$][PF_6] is more readily oxidized. This observation is attributed to the electron-donating nature of the introduced *tert*-butyl

substituent. Replacing ppy by ppz or pbtz shifts the observed oxidation to higher potentials (by 0.09 to 0.18 V), due to a destabilization of the HOMO, leading to a larger HOMO-LUMO gap. Introducing the piq cyclometallating ligand has no influence on the oxidation potential. These observations correlate well with the photoluminescence maxima (*vide supra*), as a larger HOMO-LUMO gap leads to a blue-shift in the emission of $[Ir(ppz)_2(btzpy)][PF_6]$ and $[Ir(pbtz)_2(btzpy)][PF_6]$, whereas a red-shift can be assigned to a smaller energy gap of $[Ir(tppy)_2(btzpy)][PF_6]$.

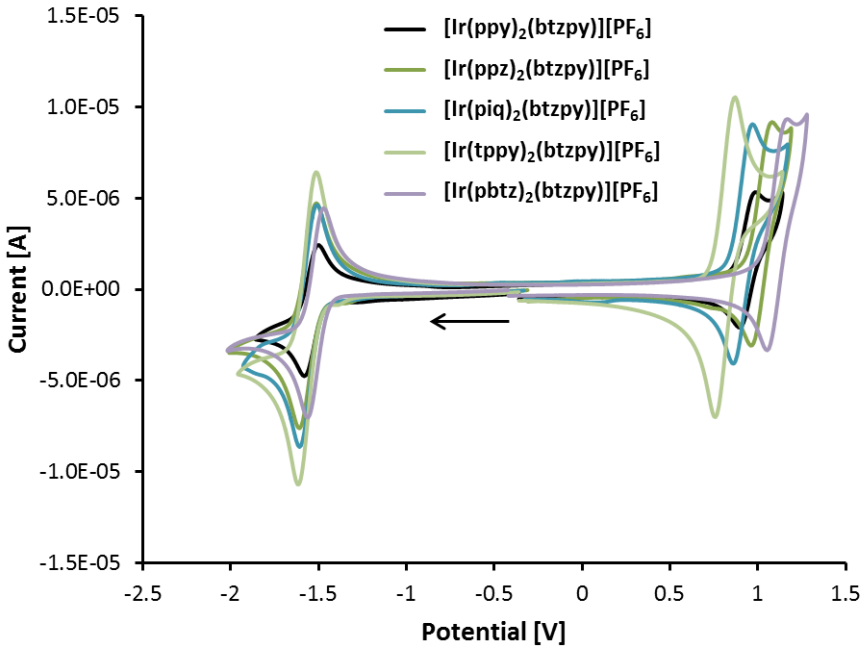

Fig. 59 Cyclic voltammograms of complexes with different cyclometallating ligands and btzpy ancillary ligand with respect to Fc/Fc^+, measured in CH_2Cl_2 solution; Pt working and counter electrodes, Ag pseudo-reference electrode, 0.1 M $TBAPF_6$ supporting electrolyte, scan rate = 0.1 V s^{-1}. The arrow indicates the initial scanning direction.

Table 16 Cyclic voltammetric data in de-aerated CH_2Cl_2 solutions with respect to Fc/Fc^+, using Pt counter and Ag pseudo-reference electrodes and 0.1 M $TBAPF_6$ supporting electrolyte. Measured at a scan rate of 0.1 V s^{-1}. For each complex, the first row values correspond to measurements with glassy carbon, the second row values to Pt working electrode. ir = irreversible, qr = quasi-reversible.

Compound	$E^{ox}_{1/2}$ [V] (E_{pa}–E_{pc} [mV])	$E^{red}_{1/2}$ [V] (E_{pc}–E_{pa} [mV])	$\Delta E_{1/2}$ [V]
$[Ir(ppy)_2(bozpy)][PF_6]$	+0.92 (132) +0.92 (114)	−1.61 (123) −1.61 (104)	2.53 2.53
$[Ir(ppy)_2(btzpybtz)][PF_6]$	$+0.99^{ir}$, $+1.17^{ir}$ $+0.99^{ir}$, $+1.17^{ir}$	−1.48 (113), -2.32^{ir} −1.47 (86), -2.30^{ir}	2.47 2.46
$[Ir(ppy)_2(tpybtz)][PF_6]$	+0.92 (125) +0.92 (95)	−1.60 (118) −1.59 (89)	2.52 2.51
$[Ir(ppy)_2(ppybtz)][PF_6]$	+0.84 (148) +0.86 (126)	−1.60 (105) −1.57 (95)	2.44 2.43
$[Ir(ppy)_2(bbtz)][PF_6]$	+1.01 (149) +1.01 (144)	−1.28 (125), −2.05 (160) −1.27 (123), −2.03 (140)	2.29 2.28
$[Ir(ppy)_2(btzpy)][PF_6]$	+0.93 (102) +0.94 (92)	−1.56 (85) −1.55 (83)	2.49 2.49
$[Ir(ppz)_2(btzpy)][PF_6]$	+1.02 (131) +1.02 (121)	−1.57 (124) −1.57 (103)	2.59 2.59
$[Ir(piq)_2(btzpy)][PF_6]$	+0.93 (127) +0.92 (109)	−1.56 (118) −1.56 (98)	2.49 2.48
$[Ir(tppy)_2(btzpy)][PF_6]$	+0.82 (133) +0.81 (113)	−1.57 (125) −1.56 (100)	2.39 2.37
$[Ir(pbtz)_2(btzpy)][PF_6]$	+1.11 (113) +1.11 (113)	−1.52 (104) −1.52 (91)	2.63 2.63

Reduction potentials are also similar for complexes $[Ir(ppy)_2(btzpy)][PF_6]$, $[Ir(ppy)_2(ppybtz)][PF_6]$, $[Ir(ppy)_2(tpybtz)][PF_6]$ and $[Ir(ppy)_2(bozpy)][PF_6]$ (−1.55 to −1.61 V), indicating that reduction takes place mainly on the benzothiazole unit of the ancillary ligand and replacing benzothiazole by benzoxazole does not significantly influence the reduction potential. Both $[Ir(ppy)_2(bbtz)][PF_6]$ and $[Ir(ppy)_2(btzpybtz)][PF_6]$ are more readily reduced than $[Ir(ppy)_2(btzpy)][PF_6]$, with $E^{red}_{1/2}$ shifted by 0.08 and 0.28 V, respectively. The introduction of a second benzothiazole moiety therefore has a pronounced stabilization effect on the LUMO, especially in bbtz, where the two benzothiazoles are directly linked. A second reduction peak is observed for both complexes, which is not seen for the remaining eight compounds within the accessible solvent window. Oxidation potentials are in a close range (+0.84 to +1.01 V), as expected for $[Ir(ppy)_2(N^N)][PF_6]$ complexes in which the HOMO is located on the iridium centre and the cyclometallating ligand. For $[Ir(ppy)_2(bbtz)][PF_6]$, oxidation is shifted to higher potential, which can be explained by the

extremely electron-deficient nature of the bbtz ligand, making oxidation of the iridium centre more difficult. The opposite trend is seen in $[Ir(ppy)_2(ppybtz)][PF_6]$, where the introduction of a phenyl group on the ancillary ligand facilitates oxidation. In $[Ir(ppy)_2(btzpybtz)][PF_6]$, two irreversible oxidation waves are observed, whereas all other complexes exhibit only one reversible to quasi-reversible oxidation.

6. Electroluminescence and Device Data

Light emitting electrochemical cells of all complexes in this series were prepared by Dr. Henk Bolink and his team at the University of Valencia. The device configuration used was ITO/PEDOT:PSS/$[Ir(C\hat{}N)_2(N\hat{}N)][PF_6]$:$[Bmim][PF_6]$ 4:1/Al. Block-wave pulsed current driving (frequency 1 kHz, 50% duty cycle, average current density 100 or 700 A m^{-2}) was applied to evaluate the LEEC performance.[21,163] Electroluminescence spectra obtained under these conditions are shown in Fig. 61 for complexes with different N^N ligands and Fig. 62 for complexes containing different C^N ligands. Electroluminescence maxima and LEEC performance parameters are summarized in Table 17. Photographs of the LEEC devices in operation are presented in Fig. 60, showing the orange to red electroluminescence colours.


$[Ir(ppy)_2(btzpy)][PF_6]$


$[Ir(ppy)_2(ppybtz)][PF_6]$


$[Ir(ppy)_2(tpybtz)][PF_6]$


$[Ir(ppy)_2(bozpy)][PF_6]$


$[Ir(ppz)_2(btzpy)][PF_6]$


$[Ir(piq)_2(btzpy)][PF_6]$


$[Ir(tppy)_2(btzpy)][PF_6]$


$[Ir(pbtz)_2(btzpy)][PF_6]$

Fig. 60 Photographs of LEEC devices in operation of selected iridium complexes, showing orange to red electroluminescence.

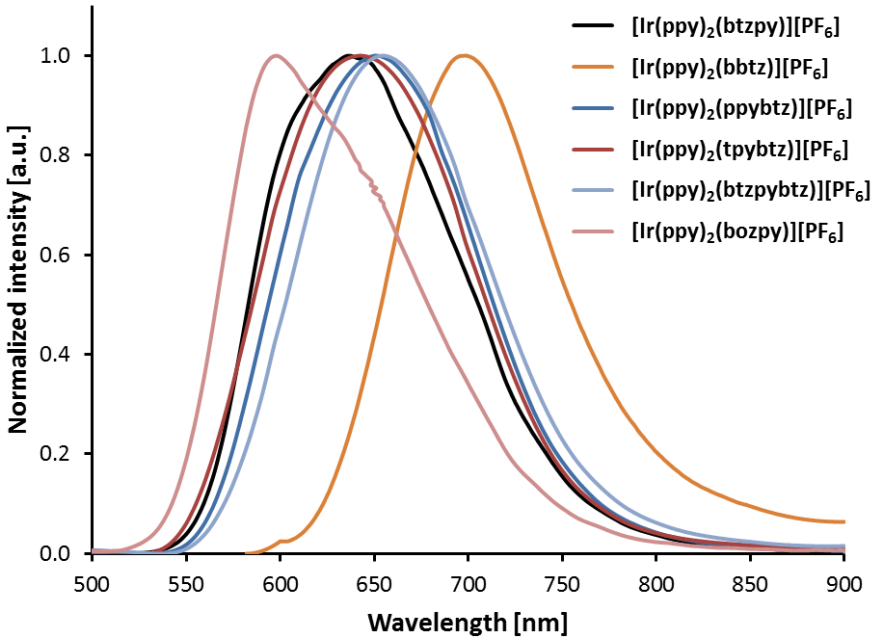

Fig. 61 Electroluminescence spectra of complexes with ppy cyclometallating ligands and different ancillary ligands.

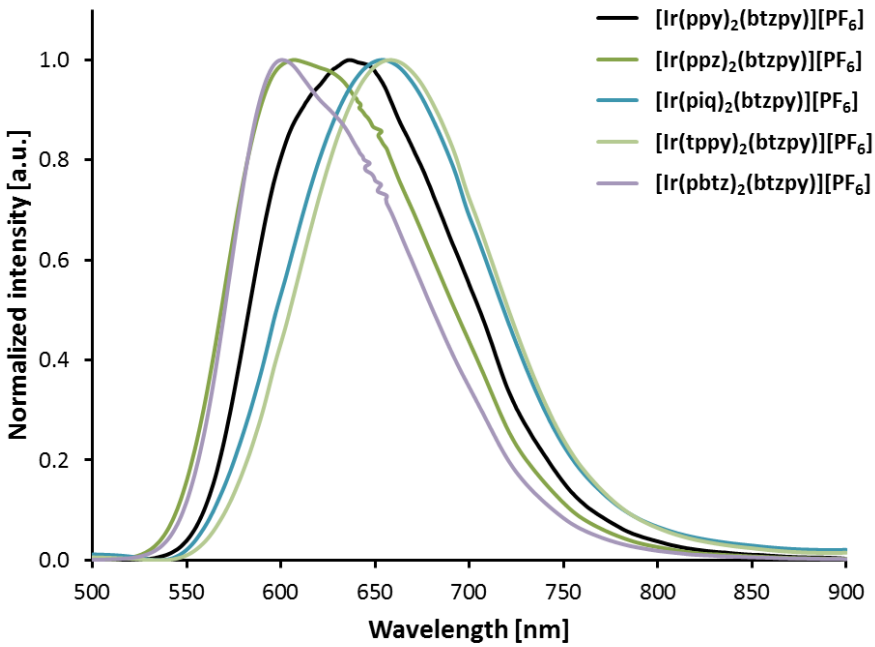

Fig. 62 Electroluminescence spectra of complexes with different cyclometallating ligands and btzpy ancillary ligand.

Luminescence maxima are retained or slightly blue-shifted (<9 nm) for most of the complexes with respect to photoluminescence maxima in thin film. A more pronounced blue-shift of over 20 nm is observed for complexes $[Ir(ppy)_2(bozpy)][PF_6]$, $[Ir(ppz)_2(btzpy)][PF_6]$ and $[Ir(pbtz)_2(btzpy)][PF_6]$. In contrast, a small red-shift to the near-infrared region occurs for $[Ir(ppy)_2(bbtz)][PF_6]$ on going from thin film photoluminescence (693 nm) to electroluminescence (699 nm).

Luminance curves are plotted against time in Fig. 63 for $[Ir(ppy)_2(C\text{^}N)][PF_6]$ with different N^N ligands and Fig. 64 for $[Ir(C\text{^}N)_2(btzpy)][PF_6]$ with different C^N ligands. Device parameters are given in Table 17. Due to problems with film formation, it was not possible to obtain working LEECs with complex $[Ir(ppy)_2(bbtz)][PF_6]$. Complexes with ppy as cyclometallating ligand and different ancillary ligands were measured at an average current density of 100 A m^{-2}. Under these conditions, the simplest complex $[Ir(ppy)_2(btzpy)][PF_6]$ reaches a maximum luminance of 78 cd m^{-2} and shows high stability. The recorded lifetime of >1000 h is much longer than the longest lifetime for a red LEEC reported in the literature (compound **Z-B(Mes)$_2$**, $t_{1/2}$ = 73.6 h, see Table 13).[166] However, the turn-on time is long (58 h) and the efficacy low (1.16 cd A^{-1}). By adding a pendant phenyl ring to the ancillary ligand and thus allowing for intramolecular π-stacking interactions (complex $[Ir(ppy)_2(ppybtz)][PF_6]$), an increase in the maximum luminance is observed (119 cd m^{-2}), together with an increase in efficacy (1.22 cd A^{-1}). Furthermore, the turn-on time is significantly reduced to 17 h, while the stability is enhanced ($t_{1/2}$ >4500 h). Introduction of a *tert*-butyl group on the benzothiazolyl-pyridine backbone further increases the lifetime to >6000 h, as observed for complex $[Ir(ppy)_2(tpybtz)][PF_6]$. Furthermore, both maximum luminance (200 cd m^{-2}) and efficacy (1.5 cd A^{-1}) are improved. The turn-on time becomes significantly longer (778 h), this is due to a very slow increase in luminance after reaching 140 cd m^{-2} (see Fig. 63). A luminance level of 100 cd m^{-2} on the other hand is obtained after only 9 h. A pendant benzothiazolyl unit on the ancillary ligand does not have the same beneficial effect on device performance as does a phenyl ring. While stability is reasonable for $[Ir(ppy)_2(btzpybtz)][PF_6]$, maximum luminance (9 cd m^{-2}) and efficacy (0.094 cd A^{-1}) are dramatically reduced. This is in accordance with the much lower PLQY in thin film. By replacing the benzothiazolyl-pyridine ancillary ligand by benzoxazolyl-pyridine, maximum luminance levels and efficacy are comparable: 97 cd m^{-2} and 0.97 cd A^{-1} for $[Ir(ppy)_2(bozpy)][PF_6]$ compared to 78 cd m^{-2} and 1.16 cd A^{-1} for $[Ir(ppy)_2(btzpy)][PF_6]$.

However, both turn-on time (0.84 h) and lifetime (9 h) decrease considerably for $[Ir(ppy)_2(bozpy)][PF_6]$. The high stability of LEECs containing the other complexes is therefore attributed to the benzothiazolyl moiety and is lost by changing the sulfur to oxygen.

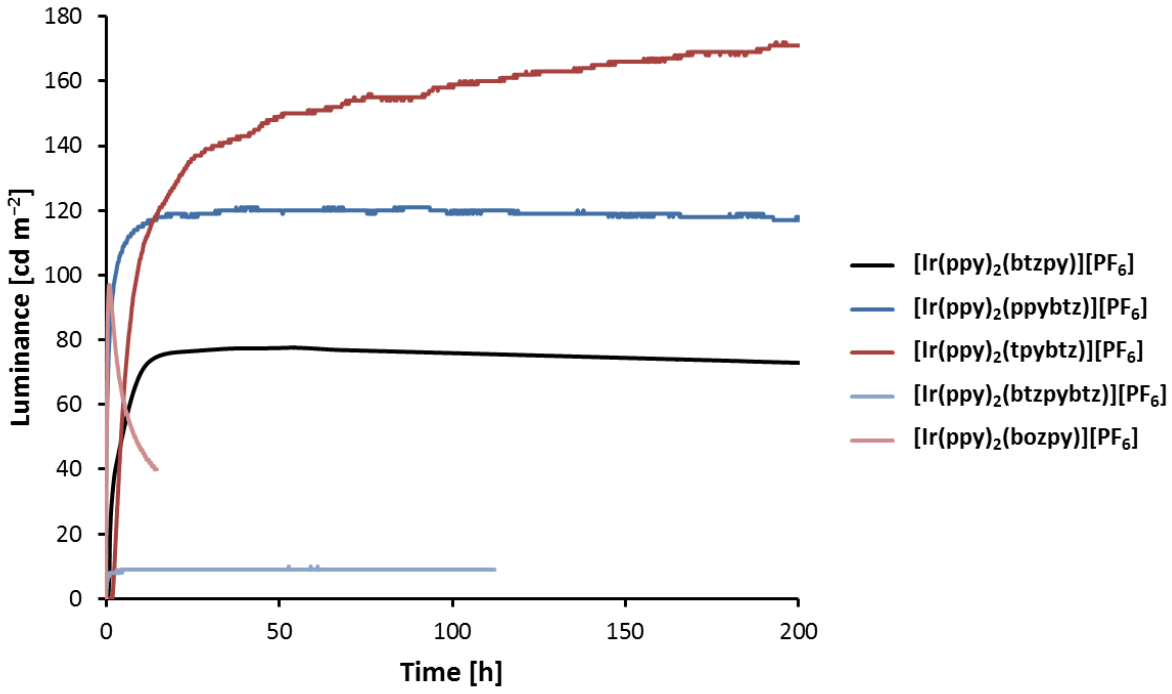

Fig. 63 Luminance *vs.* time curves of LEECs containing the complexes with ppy cyclometallating ligands and different ancillary ligands, measured under block-wave pulsed current conditions (50% duty cycle, frequency 1 kHz, average current density 100 A m^{-2}).[21,163] Device configuration: ITO/PEDOT:PSS/$[Ir(ppy)_2(N^N)][PF_6]$:[Bmim][PF_6] 4:1/Al. The active layer in the LEEC with $[Ir(ppy)_2(tpybtz)][PF_6]$ contained 2 wt-% PMMA.

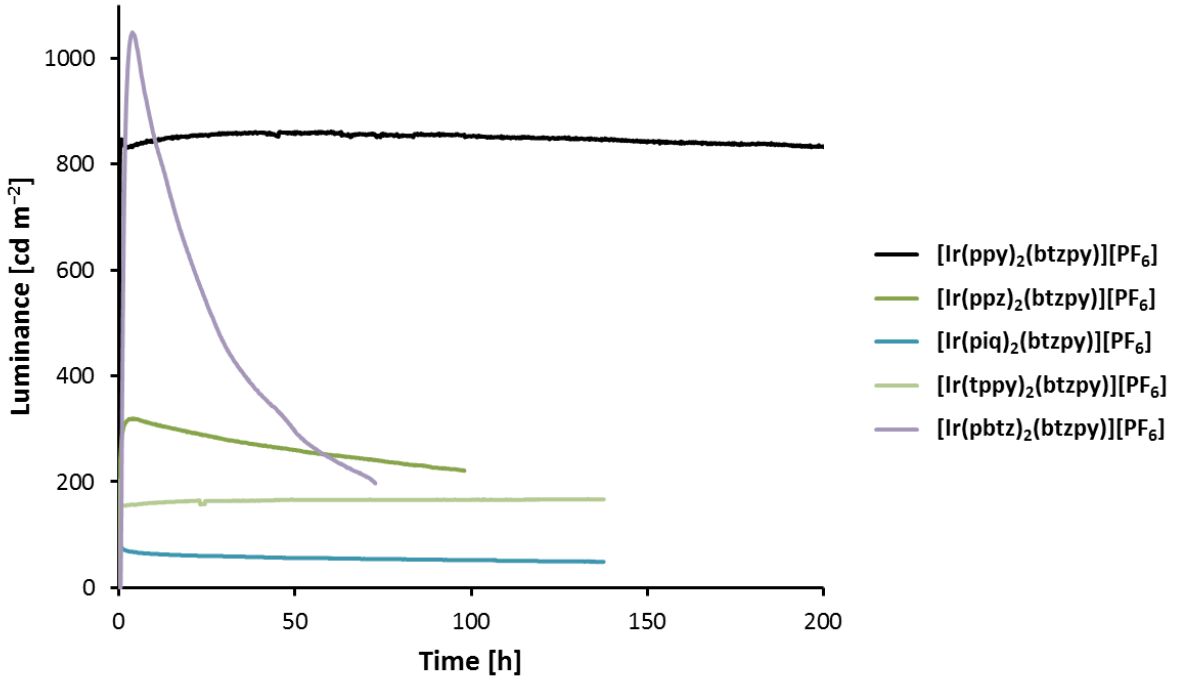

Fig. 64 Luminance plotted *vs.* time of devices containing complexes with different cyclometallating and btzpy ancillary ligand, measured applying block-wave pulsed current conditions (50% duty cycle, frequency 1 kHz, average current density 700 A m^{-2}).[21,163] LEEC configuration: ITO/PEDOT:PSS/[Ir(C^N)$_2$(btzpy)][PF$_6$]:[Bmim][PF$_6$] 4:1/Al.

Devices containing complexes [Ir(C^N)$_2$(btzpy)][PF$_6$] with different cyclometallating ligands were measured at an average current density of 700 A m^{-2}. These conditions lead to an enhancement of the maximum luminance (861 cd m^{-2}) and efficacy (1.23 cd A^{-1}) of [Ir(ppy)$_2$(btzpy)][PF$_6$] with respect to the measurement at 100 A m^{-2}. The turn-on time is reduced to 39 h, while the lifetime stays long (>1200 h). Replacing the ppy cyclometallating ligands by ppz or piq results in reduced maximum luminance levels (320 cd m^{-2} and 84 cd m^{-2}, respectively) and reduced efficacies (0.46 cd A^{-1} and 0.12 cd A^{-1}, respectively). For [Ir(ppz)$_2$(btzpy)][PF$_6$], this finding is surprising, since the quantum yield in thin film is comparable to that of [Ir(ppy)$_2$(btzpy)][PF$_6$] (both between 11 and 12%). Turn-on times are also significantly reduced for [Ir(ppz)$_2$(btzpy)][PF$_6$] (3.88 h) and [Ir(piq)$_2$(btzpy)][PF$_6$] (3.3 min) with respect to [Ir(ppy)$_2$(btzpy)][PF$_6$] (39 h). While lifetimes are considerably lower for [Ir(ppz)$_2$(btzpy)][PF$_6$] (>200 h) and [Ir(piq)$_2$(btzpy)][PF$_6$] (250 h) compared to [Ir(ppy)$_2$(btzpy)][PF$_6$], they are still much longer than those reported in the literature for red emitters (*cf.* Table 13). Complex [Ir(tppy)$_2$(btzpy)][PF$_6$] shows similar stability, however, the

maximum luminance amounts only to 164 cd m^{-2} and the efficacy to 0.23 cd A^{-1}. The highest maximum luminance level in this series is observed for $[Ir(pbtz)_2(btzpy)][PF_6]$ (1049 cd m^{-2}). With 1.49 cd A^{-1}, the efficacy is also higher than for $[Ir(ppy)_2(btzpy)][PF_6]$ (1.23 cd A^{-1}). The measured lifetime of a LEEC containing $[Ir(pbtz)_2(btzpy)][PF_6]$ is drastically decreased to 26 h. In general, substitution of the ppy cyclometallating ligand does not lead to a better overall device performance and the stability is greatly reduced for complexes $[Ir(C\hat{}N)_2(btzpy)][PF_6]$ with C^N = ppz, piq, tppy and pbtz.

Table 17 Performance parameters of LEECs with benzothiazole-based iridium complexes, obtained under pulsed current driving conditions (frequency 1 kHz, 50% duty cycle, block-wave).[21,163] Device configuration: ITO/PEDOT:PSS/$[Ir(C\hat{}N)_2(N\hat{}N)][PF_6]$: $[Bmim][PF_6]$ 4:1/Al. For $[Ir(ppy)_2(tpybtz)][PF_6]$, PMMA (2 wt-%) was added to the active layer.

Compound	t_{on} **[h]**	Lum_{max} **[cd m^{-2}]**	$t_{1/2}$ **[h]**	**PCE [lm W^{-1}]**	**efficacy [cd A^{-1}]**	λ_{EL}^{max} **[nm]**
$[Ir(ppy)_2(bozpy)][PF_6]$[a]	0.84	97	9	0.54	0.97	598
$[Ir(ppy)_2(btzpybtz)][PF_6]$[a]	3	9	>150	0.062	0.094	655
$[Ir(ppy)_2(tpybtz)][PF_6]$[a]	778	200	>6000	1.02	1.5	642
$[Ir(ppy)_2(ppybtz)][PF_6]$[a]	17.4	119	>4500	0.77	1.22	651
$[Ir(ppy)_2(bbtz)][PF_6]$[a]	---	---	---	---	---	699
$[Ir(ppy)_2(btzpy)][PF_6]$[a]	58	78	>1000	0.88	1.16	636
$[Ir(ppy)_2(btzpy)][PF_6]$[b]	38.7	861	>1200	0.54	1.23	636
$[Ir(ppz)_2(btzpy)][PF_6]$[b]	3.88	320	>200	0.21	0.46	607
$[Ir(piq)_2(btzpy)][PF_6]$[b]	0.055	84	250	0.057	0.12	654
$[Ir(tppy)_2(btzpy)][PF_6]$[b]	18.5	164	>150	0.14	0.23	658
$[Ir(pbtz)_2(btzpy)][PF_6]$[b]	3.8	1049	26	0.84	1.49	601

[a] Average current density = 100 A m^{-2}. [b] Average current density = 700 A m^{-2}.

7. Conclusions

A series of benzothiazolyl- and in one case benzoxazolyl-containing iridium complexes was prepared and investigated. Starting from simple benzothiazolyl-pyridine, ancillary ligands with different functionalizations, such as *tert*-butyl or pendant phenyl and benzothiazole groups, were synthesized. The benzothiazolyl-pyridine ancillary ligand was also combined with different cyclometallating ligands. The influence of these functionalizations and ligand combinations on photophysics, electrochemistry and device performance was determined.

Single crystal structures were obtained for complexes $[Ir(ppy)_2(btzpy)][PF_6]$, $[Ir(ppy)_2(bbtz)][PF_6]$ and $[Ir(ppy)_2(bozpy)][PF_6]$. The expected chemical structure and coordination through the N atom of the benzothiazole or benzoxazole units was confirmed.

Introduction of the btzpy ligand leads to a 49 nm red-shift in the emission maximum of $[Ir(ppy)_2(btzpy)][PF_6]$ in CH_2Cl_2 with respect to $[Ir(ppy)_2(bpy)][PF_6]$. All complexes in this series are dark orange to deep red emitters in solution (λ_{em}^{max} = 600–686 nm), as powder samples (λ_{em}^{max} = 612–656 nm) and in thin films (λ_{em}^{max} = 625–693 nm). The emission maximum depends strongly on the nature of the ancillary ligand as well as the cyclometallating ligand. Together with the mostly broad, featureless emission profiles, this suggests a large ^{3}MLCT and/or ^{3}LLCT character of the emissive triplet state. Electrochemical data follow the trends observed for photoluminescence maxima in solution.

Light emitting electrochemical cells were assembled with all complexes included in this series. Unfortunately, $[Ir(ppy)_2(bbtz)][PF_6]$ yielded no working devices. Electroluminescence maxima range from 598 to 699 nm and are slightly blue-shifted for most complexes with respect to photoluminescence maxima in thin films. Highly stable red LEECs were obtained from $[Ir(ppy)_2(btzpy)][PF_6]$ with lifetimes of over 1000 h, much longer than those reported so far for red light emitting electrochemical cells based on iridium complexes. By introducing a *tert*-butyl substituent or pendant phenyl ring on the ancillary ligand it was possible to further increase the lifetime as well as the maximum luminance level and the efficacy. The benzothiazole moiety seems to be crucial for device stability, since the lifetime is dramatically reduced for the benzoxazole-based complex. The same is true for the ppy cyclometallating ligand: for complexes containing different cyclometallating ligands, a decrease in device stability was observed.

Iridium complexes with benzothiazole-based ancillary ligands are a promising new class of materials for highly stable red light emitting electrochemical cells. Combining the beneficial effect on device performance of the *tert*-butyl group and the pendant phenyl ring could lead to devices with even higher efficiency and lifetimes.

8. Experimental

8.1. General

2-Bromo-6-phenylpyridine,[201] 2-(pyridin-2-yl)benzo[*d*]thiazole (btzpy),[178] 2,2'-bibenzo[*d*]thiazole (bbtz),[176,202] 2-bromo-4-(*tert*-butyl)pyridine,[203] 2,6-bis(benzo[*d*]thiazol-2-yl)pyridine (btzpybtz)[177] and 1-phenylisoquinoline (piq)[180] were synthesized according to literature procedures and their ^{1}H NMR spectroscopic data matched those reported. Adaptation of the reported synthesis of 2-(pyridin-2-yl)benzo[*d*]thiazole (btzpy)[178] gave 2-(4-(*tert*-butyl)pyridin-2-yl)benzo[*d*]thiazole (tpybtz),[204] 2-(pyridin-2-yl)benzo[*d*]oxazole (bozpy)[205] and 2-phenylbenzo[*d*]thiazole (pbtz)[206] and their ^{1}H NMR spectroscopic data were compared to those described in the literature. 1-Phenyl-1*H*-pyrazole (ppz) was synthesized adapting a literature procedure;[149] ^{1}H NMR spectroscopic data matched those reported.[207]

8.2. 2-(6-Phenylpyridin-2-yl)benzo[*d*]thiazole (ppybtz)

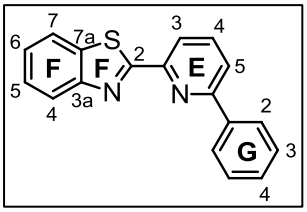

2-(6-Phenylpyridin-2-yl)benzo[*d*]thiazole (ppybtz) was synthesized by adaptation of a literature procedure.[178] Benzothiazole (110 µL, 135 mg, 0.971 mmol), 2-bromo-6-phenylpyridine (455 mg, 1.94 mmol), CuI (17.9 mg, 94.0 µmol), phenanthroline monohydrate (19.1 mg, 96.4 µmol), K_3PO_4 (412 mg, 1.94 mmol) and dry DMF (0.8 mL) were added to a microwave vial, purged with N_2, sealed and heated at 120 °C overnight. The mixture was let to cool to room temperature. H_2O (50 mL) and EtOAc (50 mL) were added to the mixture and the layers were separated. The aqueous layer was extracted with EtOAc (3 × 50 mL), the combined organic layers were washed with brine (100 mL), dried over Na_2SO_4 and the solvent was removed under reduced pressure. The crude product was purified by column chromatography (silica, cyclohexane/EtOAc 6:1), the solvent removed and the residue washed with *n*-pentane to yield 2-(6-phenylpyridin-2-yl)benzo[*d*]thiazole (ppybtz) as an off-white solid (143 mg, 0.496 mmol, 51.1%). M.p. 129.3 °C. ^{1}H NMR (500 MHz, $CDCl_3$) δ/ppm 8.31 (dd, J = 7.6, 1.0 Hz, 1H, H^{E3}), 8.20–8.15 (m, 2H, H^{G2}), 8.12 (*pseudo*-dt, J = 8.3, 0.9 Hz, 1H, H^{F4}), 7.97 (ddd, J = 8.0, 1.1, 0.6 Hz, 1H, H^{F7}), 7.92 (*pseudo*-t, J = 7.7 Hz, 1H, H^{E4}), 7.85 (dd, J = 7.9, 1.0 Hz, 1H, H^{E5}), 7.56–7.50 (overlapping m, 3H, H^{F5+G3}), 7.50–7.45 (m, 1H, H^{G4}), 7.43 (ddd, J = 8.2, 7.2, 1.2 Hz, 1H, H^{F6}). ^{13}C{^{1}H} NMR (126 MHz, $CDCl_3$) δ/ppm 170.4 (C^{F2}), 157.1 (C^{E6}), 154.5 (C^{F3a}), 151.2 (C^{E2}), 138.3 (C^{G1}), 138.0 (C^{E4}), 136.5 (C^{F7a}), 129.6 (C^{G4}), 129.0 (C^{G3}), 127.1 (C^{G2}), 126.3 (C^{F5}), 125.7 (C^{F6}), 123.7 (C^{F4}), 122.1 (C^{F7}),

121.8 (C^{E5}), 119.0 (C^{E3}). IR (solid, $\tilde{\nu}$/cm^{-1}) 2982 (w), 1589 (w), 1566 (m), 1509 (w), 1447 (s), 1435 (m), 1319 (m), 1270 (w), 1250 (w), 1237 (w), 1183 (w), 1155 (w), 1083 (m), 1028 (w), 988 (m), 946 (w), 922 (w), 870 (w), 811 (m), 786 (w), 757 (s), 732 (s), 691 (s), 667 (m), 623 (m), 587 (w), 574 (w), 531 (w), 486 (w), 432 (m). LC-ESI-MS *m/z* 289.0 $[M+H]^+$ (calc. 289.1). Found C 74.67, H 4.43, N 10.01; $C_{18}H_{12}N_2S$ requires C 74.97, H 4.19, N 9.71%.

8.3. 2-(3-(*tert*-Butyl)phenyl)-4,4,5,5-tetramethyl-1,3,2-dioxaborolane

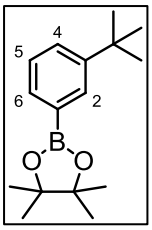

1-Bromo-3-*tert*-butylbenzene (0.24 mL, 300 mg, 1.38 mmol), bis(pinacolato)diboron (712 mg, 2.78 mmol), KOAc (406 mg, 4.14 mmol) and $Pd(dppf)_2Cl_2{\cdot}CH_2Cl_2$ (56.6 mg, 69.3 μmol) were suspended in THF (dry, 20 mL) in a microwave vial, purged with N_2 and the reaction mixture heated at 90 °C for 1 h in a microwave reactor (4 bar). The resulting mixture was filtered over celite, washed with EtOAc (100 mL) and the filtrate was concentrated under reduced pressure. The crude product was purified by column chromatography (silica, cyclohexane–5% EtOAc) to yield 2-(3-(*tert*-butyl)phenyl)-4,4,5,5-tetramethyl-1,3,2-dioxaborolane as a yellow oil which solidified upon standing (258 mg, 0.992 mmol, 71.9%). ^{1}H NMR (500 MHz, $CDCl_3$) δ/ppm 7.83 (ddd, J = 1.9, 1.2, 0.6 Hz, 1H, H^2), 7.64 (dt, J = 7.3, 1.2 Hz, 1H, H^6), 7.50 (ddd, J = 7.9, 2.3, 1.3 Hz, 1H, H^4), 7.31 (ddd, J = 7.9, 7.2, 0.6 Hz, 1H, H^5), 1.35 (s, 12H, $H^{BO2C2(C\underline{H}3)4}$), 1.35 (s, 9H, $H^{C(C\underline{H}3)3}$). ^{13}C{^{1}H} NMR (126 MHz, $CDCl_3$) δ/ppm 150.4 (C^3), 132.2 (C^6), 131.5 (C^2), 128.5 (C^4), 127.6 (C^5), 83.8 ($C^{BO2\underline{C}2(CH3)4}$), 34.8 ($C^{\underline{C}(CH3)3}$), 31.6 ($C^{C(\underline{C}H3)3}$), 25.0 ($C^{BO2C2(\underline{C}H3)4}$). The signal for C^1 was not resolved. ^{11}B NMR (160 MHz, $CDCl_3$) δ/ppm 31.25.

8.4. 2-(3-(*tert*-Butyl)phenyl)pyridine (tppy)

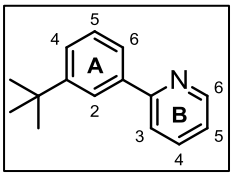

The synthesis of 2-(3-(*tert*-butyl)phenyl)pyridine (tppy) has been previously reported,[208] but the following procedure gives a higher yield. 2-(3-(*tert*-Butyl)phenyl)-4,4,5,5-tetramethyl-1,3,2-dioxaborolane (205 mg, 0.788 mmol), $PdCl_2(PPh_3)_2$ (23.1 mg, 32.9 μmol), 2-bromopyridine (63 μL, 104 mg, 0.658 mmol) and Na_2CO_3 (210 mg, 1.98 mmol) were suspended in THF (5 mL) and H_2O (5 mL) in a microwave vial. The mixture was heated at 100 °C for 30 min in a microwave reactor (7 bar), then poured into H_2O (100 mL) and extracted with CH_2Cl_2 (3 × 60 mL). The combined organic layers were dried over Na_2SO_4 and the solvent was removed under reduced pressure. The crude product was purified by column chromatography (silica, cyclohexane–5% EtOAc) to yield 2-(3-(*tert*-butyl)phenyl)pyridine

(tppy) as a colourless oil (127 mg, 0.601 mmol, 91.3%). ^{1}H NMR spectroscopic data matched those reported in the literature.[208]

8.5. General procedure for the synthesis of chlorido-bridged iridium(III) dimers

$[Ir(ppy)_2Cl]_2$, $[Ir(ppz)_2Cl]_2$, $[Ir(piq)_2Cl]_2$, $[Ir(tppy)_2Cl]_2$ and $[Ir(pbtz)_2Cl]_2$ were synthesized according to the standard method.[100,101] The cyclometallating ligand was suspended in a mixture of 2-ethoxyethanol and H_2O (3:1) and purged with N_2. $IrCl_3 \cdot xH_2O$ was added and the reaction mixture was heated at reflux overnight. After letting the mixture cool to room temperature, the precipitation was collected, washed with EtOH and Et_2O and dried. The dimers were characterized by ^{1}H NMR spectroscopy and used for subsequent reactions without further purification. ^{1}H NMR spectroscopic data of $[Ir(ppy)_2Cl]_2$ matched those reported in the literature.[182]

8.6. $[Ir(ppz)_2Cl]_2$

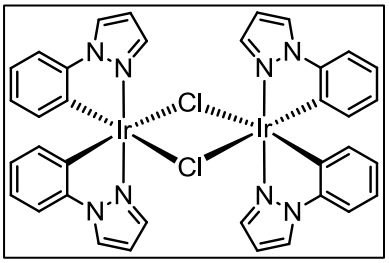

$IrCl_3 \cdot xH_2O$ (ca. 82% $IrCl_3$, 564 mg, 1.55 mmol) and 1-phenyl-1*H*-pyrazole (ppz) (447 mg, 3.10 mmol) in 28 mL solvent. $[Ir(ppz)_2Cl]_2$ was isolated as an off-white powder (733 mg, 775 µmol, 92.0%). ^{1}H NMR (400 MHz, acetone-d_6) δ/ppm 8.71 (dd, J = 2.9, 0.7 Hz, 4H), 7.81 (dd, J = 2.1, 0.7 Hz, 4H), 7.40 (dd, J = 7.9, 1.3 Hz, 4H), 6.87 (dd, J = 2.9, 2.2 Hz, 4H), 6.75 (ddd, J = 7.8, 7.3, 1.3 Hz, 4H), 6.48 (*pseudo*-td, J = 7.5, 1.3 Hz, 4H), 5.94 (dd, J = 7.6, 1.3 Hz, 4H).

8.7. $[Ir(piq)_2Cl]_2$

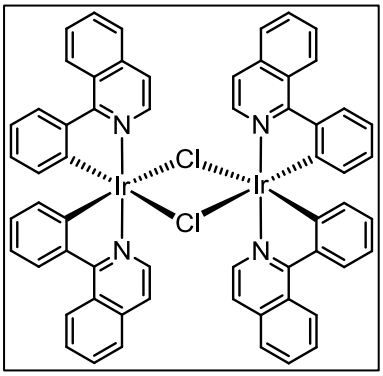

$IrCl_3 \cdot xH_2O$ (ca. 82% $IrCl_3$, 444 mg, 1.22 mmol) and 1-phenylisoquinoline (piq) (501 mg, 2.44 mmol) in 20 mL solvent. $[Ir(piq)_2Cl]_2$ was isolated as a dark red powder (532 mg, 610 µmol, 68.5%). ^{1}H NMR (400 MHz, $CDCl_3$) δ/ppm 9.05 (d, J = 6.4 Hz, 4H), 8.99–8.95 (m, 4H), 8.15–8.11 (m, 4H), 7.88–7.80 (overlapping m, 8H), 7.76 (ddd, J = 8.4, 6.4, 2.0 Hz, 4H), 6.81 (ddd, J = 8.2, 7.1, 1.3 Hz, 4H), 6.55 (dd, J = 6.5, 0.8 Hz, 4H), 6.50 (ddd, J = 8.3, 7.1, 1.3 Hz, 4H), 6.03 (dd, J = 7.9, 1.2 Hz, 4H). ^{1}H NMR spectroscopic data matched those reported in the literature.[183]

8.8. $[Ir(tppy)_2Cl]_2$

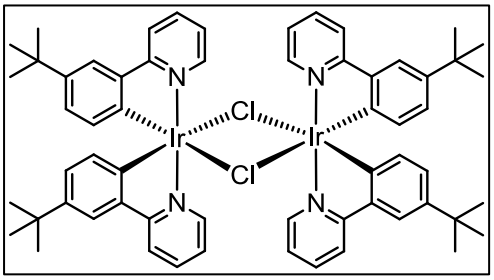

$IrCl_3 \cdot xH_2O$ (ca. 82% $IrCl_3$, 772 mg, 2.12 mmol) and 2-(3-(*tert*-butyl)phenyl)pyridine (tppy) (894 mg, 4.23 mmol) in 40 mL solvent. $[Ir(tppy)_2Cl]_2$ was isolated as a yellow powder (905 mg, 1.06 mmol, 65.9%). ^{1}H NMR (400 MHz, $CDCl_3$) δ/ppm 9.17 (ddd, J = 5.8, 1.7, 0.7 Hz, 4H), 7.89–7.84 (m, 4H), 7.71 (ddd, J = 8.1, 7.4, 1.6 Hz, 4H), 7.48 (d, J = 2.2 Hz, 4H), 6.73 (ddd, J = 7.3, 5.8, 1.4 Hz, 4H), 6.64 (dd, J = 8.2, 2.2 Hz, 4H), 5.93 (d, J = 8.2 Hz, 4H), 1.17 (s, 36H).

8.9. $[Ir(pbtz)_2Cl]_2$

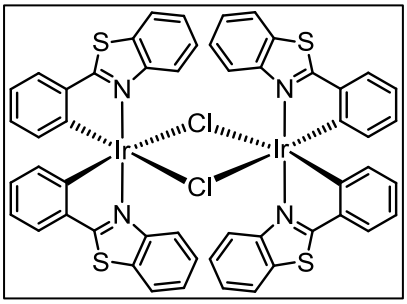

$IrCl_3 \cdot xH_2O$ (ca. 82% $IrCl_3$, 221 mg, 606 µmol) and 2-phenylbenzo[*d*]thiazole (pbtz) (256 mg, 1.21 mmol) in 10 mL solvent. $[Ir(pbtz)_2Cl]_2$ was isolated as an orange powder (323 mg, 249 µmol, 82.2%). ^{1}H NMR (400 MHz, $CDCl_3$) δ/ppm 8.76 (dd, J = 7.8, 1.7 Hz, 4H), 7.53 (dd, J = 7.6, 1.5 Hz, 4H), 7.43–7.39 (m, 4H), 7.10–7.01 (overlapping m, 8H), 6.75 (*pseudo*-td, J = 7.4, 1.2 Hz, 4H), 6.42 (*pseudo*-td, J = 7.6, 1.5 Hz, 4H), 5.99 (d, J = 7.7 Hz, 4H).

8.10. General procedure for the synthesis of iridium(III) complexes

The iridium dimer and $AgPF_6$ were suspended in MeOH (15–25 mL) and stirred at room temperature for 2–4 h. The mixture was filtered through Celite® and washed with MeOH. The filtrate was concentrated under reduced pressure to yield $[Ir(C\text{^}N)_2(MeOH)_2][PF_6]$ which was neither purified nor characterized. Ancillary ligand and MeOH (2–10 mL) were added immediately to the solvento intermediate and the mixture stirred at room temperature overnight. The resulting orange-red precipitate was filtered off, redissolved in CH_2Cl_2 and concentrated under reduced pressure. The crude product was purified by column chromatography (silica) and solvent removed. The residue was dissolved in little CH_2Cl_2 and precipitated with Et_2O and/or *n*-hexane. Where necessary, the complex was dissolved in little CH_2Cl_2, layered with toluene and *n*-hexane and kept in the refrigerator overnight. The resulting precipitation was filtered off and dried under vacuum. The reported yields (over two steps) were calculated based on the iridium dimer starting material.

8.11. $[Ir(ppy)_2(btzpy)][PF_6]$

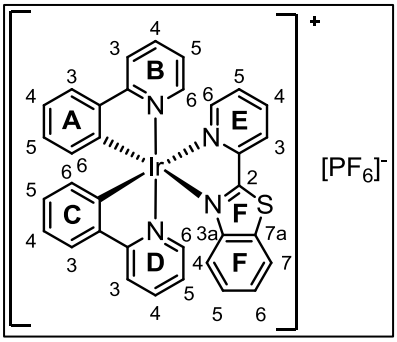

$[Ir(ppy)_2Cl]_2$ (100 mg, 93.3 μmol) and $AgPF_6$ (51.4 mg, 0.203 mmol) in MeOH (20 mL), 2 h 45 min at room temperature. Addition of 2-(pyridin-2-yl)benzo[*d*]thiazole (btzpy) (39.7 mg, 0.187 mmol) and MeOH (10 mL). Purification by column chromatography (silica, CH_2Cl_2 changing to CH_2Cl_2–1% MeOH) and precipitation with Et_2O. $[Ir(ppy)_2(btzpy)][PF_6]$ was isolated as an orange solid (129 mg, 0.151 mmol, 80.6%). ^{1}H NMR (500 MHz, CD_3CN) δ/ppm 8.48 (*pseudo*-dt, J = 8.0, 1.1 Hz, 1H, H^{E3}), 8.19–8.15 (overlapping m, 2H, H^{E4+F7}), 8.07 (*pseudo*-dt, J = 8.2, 1.2 Hz, 1H, H^{D3}), 8.01 (*pseudo*-dt, J = 8.2, 1.2 Hz, 1H, H^{B3}), 7.97 (ddd, J = 5.5, 1.6, 0.8 Hz, 1H, H^{E6}), 7.87–7.78 (overlapping m, 4H, $H^{A3+B4+C3+D4}$), 7.74 (ddd, J = 5.8, 1.5, 0.8 Hz, 1H, H^{D6}), 7.59 (ddd, J = 5.8, 1.5, 0.8 Hz, 1H, H^{B6}), 7.57–7.51 (overlapping m, 2H, H^{E5+F6}), 7.20 (ddd, J = 8.4, 7.2, 1.2 Hz, 1H, H^{F5}), 7.11 (*pseudo*-td, J = 7.6, 1.2 Hz, 1H, H^{A4}), 7.07 (ddd, J = 7.8, 7.4, 1.2 Hz, 1H, H^{C4}), 7.02 (ddd, J = 7.4, 5.8, 1.4 Hz, 1H, H^{B5}), 7.00–6.91 (overlapping m, 4H, $H^{A5+C5+D5+F4}$), 6.38 (dd, J = 7.5, 1.3 Hz, 1H, H^{A6}), 6.22 (dd, J = 7.6, 1.1 Hz, 1H, H^{C6}). $^{13}C\{^1H\}$ NMR (126 MHz, CD_3CN) δ/ppm 171.4 (C^{F2}), 168.4 (C^{B2}), 167.9 (C^{D2}), 152.6 (C^{E2}), 151.8 (C^{E6}), 151.5 (C^{F3a}), 151.4 (C^{D6}), 150.5 (C^{B6}), 148.5 (C^{A1}), 148.3 (C^{C1}), 145.5 (C^{A2}), 145.0 (C^{C2}), 140.8 (C^{E4}), 139.6 (C^{D4}), 139.5 (C^{B4}), 135.5 (C^{F7a}), 133.1 (C^{A6}), 131.9 (C^{C6}), 131.4 (C^{C5}), 131.1 (C^{A5}), 130.5 (C^{E5}), 129.2 (C^{F5}), 129.1 (C^{F6}), 127.5 (C^{E3}), 125.9 (C^{C3}), 125.8 (C^{A3}), 124.7 (C^{D5}), 124.5 ($C^{B5/F7}$), 124.5 ($C^{B5/F7}$), 123.9 (C^{C4}), 123.6 (C^{A4}), 123.0 (C^{F4}), 120.9 (C^{D3}), 120.5 (C^{B3}). IR (solid, $\tilde{\nu}$/cm^{-1}) 3045 (w), 1608 (m), 1584 (m), 1563 (w), 1479 (s), 1458 (w), 1440 (m), 1421 (m), 1323 (w), 1269 (m), 1229 (w), 1165 (m), 1065 (w), 1031 (m), 1008 (w), 835 (s), 794 (m), 757 (s), 739 (s), 730 (s), 713 (m), 670 (m), 631 (m), 556 (s), 477 (w). UV/Vis (CH_2Cl_2, 1.0 × 10^{-5} mol dm^{-3}) λ/nm (ε/dm^3 mol^{-1} cm^{-1}) 255 (39 000), 295 sh (24 000), 330 (21 000), 350 sh (17 000), 382 (8300), 410 sh (5600). Emission (CH_2Cl_2, 1.0 × 10^{-5} mol dm^{-3}, λ_{exc} = 266 nm) λ_{em}^{max} = 644 nm. ESI-MS *m/z* 713.4 $[M–PF_6]^+$ (calc. 713.1). Found C 47.16, H 2.97, N 6.76; $C_{34}H_{24}F_6IrN_4PS\cdot0.5H_2O$ requires C 47.11, H 2.91, N 6.46%.

8.12. $[Ir(ppy)_2(bbtz)][PF_6]$

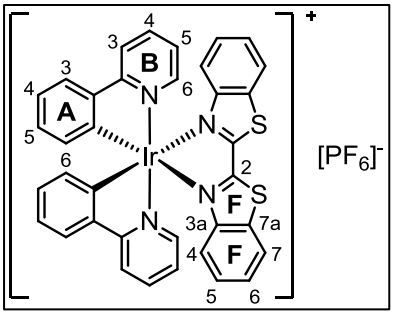

$[Ir(ppy)_2Cl]_2$ (59.9 mg, 55.9 μmol) and $AgPF_6$ (39.3 mg, 0.155 mmol) in MeOH (15 mL), 3 h at room temperature. Addition of 2,2'-bibenzo[*d*]thiazole (bbtz) (30.0 mg, 0.112 mmol) and MeOH (5 mL). Purification by column chromatography (silica, CH_2Cl_2 changing to CH_2Cl_2–2% MeOH) and precipitation with Et_2O. $[Ir(ppy)_2(bbtz)][PF_6]$ was isolated as an orange-red solid (83.7 mg, 92.0 μmol, 81.9%). ^{1}H NMR (500 MHz, CD_2Cl_2) δ/ppm 8.12 (*pseudo*-dt, J = 8.2, 0.7 Hz, 2H, H^{E7}), 7.95 (*pseudo*-dt, J = 8.1, 0.9 Hz, 2H, H^{B3}), 7.80–7.74 (overlapping m, 4H, H^{A3+B4}), 7.63–7.55 (overlapping m, 4H, H^{B6+E6}), 7.28 (ddd, J = 8.4, 7.1, 1.2 Hz, 2H, H^{E5}), 7.19 (*pseudo*-td, J = 7.6, 1.2 Hz, 2H, H^{A4}), 7.02 (*pseudo*-td, J = 7.5, 1.4 Hz, 2H, H^{A5}), 6.96 (ddd, J = 7.4, 5.8, 1.4 Hz, 2H, H^{B5}), 6.86 (*pseudo*-dt, J = 8.9, 0.8 Hz, 2H, H^{E4}), 6.34 (dd, J = 7.8, 1.1 Hz, 2H, H^{A6}). $^{13}C\{^1H\}$ NMR (126 MHz, CD_2Cl_2) δ/ppm 168.1 (C^{B2}), 163.3 (C^{E2}), 151.0 (C^{E3a}), 150.2 (C^{B6}), 144.9 (C^{A1}), 144.8 (C^{A2}), 139.0 (C^{B4}), 136.1 (C^{E7a}), 132.4 (C^{A6}), 131.2 (C^{A5}), 129.9 (C^{E5}), 129.7 (C^{E6}), 125.6 (C^{A3}), 124.2 (C^{B5}), 124.00 (C^{A4}), 123.97 (C^{E7}), 123.6 (C^{E4}), 120.5 (C^{B3}). IR (solid, $\tilde{\nu}$/cm^{-1}) 3093 (w), 1603 (m), 1587 (m), 1562 (w), 1477 (m), 1460 (m), 1441 (w), 1422 (m), 1409 (w), 1326 (m), 1297 (w), 1271 (w), 1257 (m), 1163 (m), 1134 (w), 1085 (w), 1073 (w), 1025 (m), 870 (m), 834 (s), 772 (s), 760 (s), 748 (s), 727 (m), 709 (m), 671 (m), 630 (w), 600 (w), 557 (s), 492 (w), 419 (m). UV/Vis (CH_2Cl_2, 1.0 × 10^{-5} mol dm^{-3}) λ/nm (ε/dm^3 mol^{-1} cm^{-1}) 254 (40 000), 338 sh (19 000), 367 (29 000), 387 (30 000), 415 sh (9800), 445 sh (4800). Emission (CH_2Cl_2, 1.0 × 10^{-5} mol dm^{-3}, λ_{exc} = 259 nm) λ_{em}^{max} = 686 nm. ESI-MS *m/z* 769.1 $[M–PF_6]^+$ (calc. 769.1). Found C 47.35, H 2.91, N 6.50; $C_{36}H_{24}F_6IrN_4PS_2$ requires C 47.31, H 2.65, N 6.13%.

8.13. $[Ir(ppy)_2(ppybtz)][PF_6]$

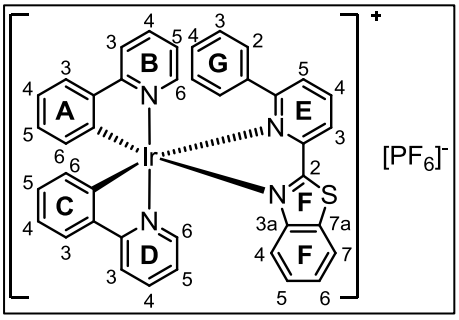

$[Ir(ppy)_2Cl]_2$ (100 mg, 93.3 μmol) and $AgPF_6$ (62.1 mg, 0.246 mmol) in MeOH (20 mL), 3 h 15 min at room temperature. Addition of 2-(6-phenylpyridin-2-yl)benzo[*d*]thiazole (ppybtz) (55.5 mg, 0.192 mmol) and MeOH (10 mL). Purification by column chromatography (silica, CH_2Cl_2 changing to CH_2Cl_2–1% MeOH) and precipitation with Et_2O. $[Ir(ppy)_2(ppybtz)][PF_6]$ was isolated as an orange solid (152 mg, 0.163 mmol, 87.5%). ^{1}H NMR (500 MHz, CD_2Cl_2) δ/ppm 8.48 (dd, J = 7.9, 1.3 Hz, 1H, H^{E3}), 8.25 (*pseudo*-t, J = 7.8 Hz, 1H, H^{E4}), 8.03 (ddd, J = 8.3, 1.1, 0.5 Hz, 1H, H^{F7}), 7.92 (*pseudo*-dt, J = 5.9, 1.1 Hz, 1H, H^{B6}), 7.90–7.82 (overlapping m, 2H, H^{B3+B4}), 7.77–7.70 (overlapping m, 2H, H^{D3+D4}), 7.53–7.45 (overlapping m, 3H, $H^{C3+E5+F6}$), 7.42 (*pseudo*-dt, J = 5.9, 1.1 Hz, 1H, H^{D6}), 7.21 (dd, J = 7.8, 1.3 Hz, 1H, H^{A3}), 7.16–7.07 (overlapping m, 2H, H^{D5+F5}), 7.04–6.98 (overlapping m, 3H, $H^{B5+C4+G4}$), 6.86 (*pseudo*-td, J = 7.5, 1.4 Hz, 1H, H^{C5}), 6.82–6.75 (overlapping m, 3H, H^{F4+G3}), 6.62 (*pseudo*-td, J = 7.6, 1.2 Hz, 1H, H^{A4}), 6.53 (br, 2H, H^{G2}), 6.41 (*pseudo*-td, J = 7.4, 1.3 Hz, 1H, H^{A5}), 6.10 (dd, J = 7.8, 1.1 Hz, 1H, H^{C6}), 5.59 (dd, J = 7.7, 1.1 Hz, 1H, H^{A6}). $^{13}C\{^1H\}$ NMR (126 MHz, CD_2Cl_2) δ/ppm 171.5 (C^{F2}), 169.1 (C^{B2}), 167.8 (C^{D2}), 167.0 (C^{E6}), 152.9 (C^{E2}), 151.6 (C^{F3a}), 150.4 (C^{B6}), 149.4 (C^{D6}), 148.3 (C^{A1}), 144.1 (2C, C^{C1+C2}), 143.4 (C^{A2}), 140.5 (C^{E4}), 138.8 (C^{D4}), 138.7 (C^{B4}), 137.6 (C^{G1}), 134.7 (C^{F7a}), 132.0 (C^{E5}), 131.7 (C^{C6}), 131.4 (C^{A6}), 130.7 (C^{C5}), 130.3 (C^{A5}), 129.8 (C^{G4}), 128.8 (C^{F5}), 128.6 (C^{F6}), 128.5 (C^{G3}), 127.8 (C^{G2}), 126.0 (C^{E3}), 125.4 (C^{A3}), 125.1 (C^{C3}), 124.0 (C^{D5}), 123.6 (C^{C4}), 123.4 (C^{F7}), 123.2 (C^{F4}), 123.1 (C^{B5}), 121.8 (C^{A4}), 120.7 (C^{B3}), 120.2 (C^{D3}). IR (solid, $\tilde{\nu}$/cm^{-1}) 3055 (w), 1608 (m), 1585 (m), 1563 (m), 1479 (m), 1459 (w), 1440 (m), 1424 (m), 1326 (w), 1270 (w), 1228 (w), 1180 (w), 1165 (w), 1064 (w), 1031 (w), 836 (s), 756 (s), 729 (s), 699 (m), 670 (m), 630 (m), 556 (s), 418 (m). UV/Vis (CH_2Cl_2, 1.0 × 10^{-5} mol dm^{-3}) λ/nm (ε/dm^3 mol^{-1} cm^{-1}) 261 (40 000), 271 sh (39 000), 340 (26 000), 355 sh (22 000), 420 sh (4500). Emission (CH_2Cl_2, 1.0 × 10^{-5} mol dm^{-3}, λ_{exc} = 270 nm) λ_{em}^{max} = 642 nm. ESI-MS *m/z* 789.1 $[M-PF_6]^+$ (calc. 789.2). Found C 51.03, H 3.33, N 6.32; $C_{40}H_{28}F_6IrN_4PS\cdot0.5H_2O$ requires C 50.95, H 3.10, N 5.94%.

8.14. $[Ir(ppy)_2(tpybtz)][PF_6]$

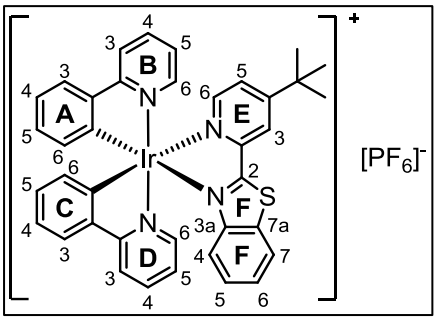

$[Ir(ppy)_2Cl]_2$ (100 mg, 93.3 μmol) and $AgPF_6$ (51.9 mg, 0.205 mmol) in MeOH (20 mL), 2 h at room temperature. Addition of 2-(4-(*tert*-butyl)pyridin-2-yl)benzo[*d*]thiazole (tpybtz) (50.1 mg, 0.187 mmol) and MeOH (10 mL). Purification by column chromatography (silica, CH_2Cl_2 changing to CH_2Cl_2–1% MeOH) and precipitation with Et_2O. $[Ir(ppy)_2(tpybtz)][PF_6]$ was isolated as an orange solid (121 mg, 0.133 mmol, 70.9%). ^{1}H NMR (500 MHz, CD_2Cl_2) δ/ppm 8.26 (dd, J = 2.0, 0.6 Hz, 1H, H^{E3}), 8.08 (*pseudo*-dt, J = 8.2, 0.9 Hz, 1H, H^{F7}), 7.98 (*pseudo*-dt, J = 8.3, 1.2 Hz, 1H, H^{B3}), 7.93 (*pseudo*-dt, J = 8.0, 0.9 Hz, 1H, H^{D3}), 7.87 (dd, J = 5.9, 0.6 Hz, 1H, H^{E6}), 7.80 (ddd, J = 8.3, 7.5, 1.5 Hz, 1H, H^{B4}), 7.78–7.73 (overlapping m, 3H, $H^{A3+C3+D4}$), 7.62 (ddd, J = 5.8, 1.5, 0.7 Hz, 1H, H^{B6}), 7.54 (ddd, J = 8.3, 7.2, 1.1 Hz, 1H, H^{F6}), 7.51–7.46 (overlapping m, 2H, H^{D6+E5}), 7.24 (ddd, J = 8.5, 7.2, 1.2 Hz, 1H, H^{F5}), 7.14 (*pseudo*-td, J = 7.6, 1.2 Hz, 1H, H^{C4}), 7.10 (*pseudo*-td, J = 7.6, 1.2 Hz, 1H, H^{A4}), 7.04–6.94 (overlapping m, 5H, $H^{A5+B5+C5+D5+F4}$), 6.40 (dd, J = 7.7, 1.2 Hz, 1H, H^{C6}), 6.25 (dd, J = 7.6, 1.2 Hz, 1H, H^{A6}), 1.43 (s, 9H, $H^{E4\text{-}t\text{Bu}}$). $^{13}C\{^1H\}$ NMR (126 MHz, CD_2Cl_2) δ/ppm 170.3 (C^{F2}), 168.5 (C^{D2}), 167.9 (C^{B2}), 165.6 (C^{E4}), 152.1 (C^{E2}), 151.2 (C^{F3a}), 151.0 (C^{E6}), 150.3 (C^{B6}), 149.2 (C^{D6}), 147.9 (C^{C1}), 147.7 (C^{A1}), 144.8 (C^{C2}), 144.2 (C^{A2}), 138.84 ($C^{B4/D4}$), 138.82 ($C^{B4/D4}$), 134.6 (C^{F7a}), 132.8 (C^{C6}), 131.6 (C^{A6}), 131.4 (C^{A5}), 131.1 (C^{C5}), 129.3 (C^{F5}), 129.0 (C^{F6}), 127.3 (C^{E5}), 125.51 ($C^{A3/C3}$), 125.50 ($C^{A3/C3}$), 124.1 (C^{B5}), 123.9 (C^{D5}), 123.71 (C^{E3}), 123.67 (C^{F7}), 123.66 (C^{A4}), 123.4 (C^{C4}), 123.3 (C^{F4}), 120.5 (C^{B3}), 120.3 (C^{D3}), 36.3 ($C^{E4\text{-}\underline{C}(CH3)3}$), 30.5 ($C^{E4\text{-}C(\underline{C}H3)3}$). IR (solid, $\tilde{\nu}$/cm^{-1}) 2963 (w), 1609 (m), 1584 (m), 1563 (w), 1479 (m), 1440 (w), 1423 (m), 1369 (w), 1326 (w), 1269 (w), 1247 (w), 1228 (w), 1165 (w), 1065 (w), 1033 (m), 834 (s), 794 (m), 757 (s), 730 (m), 709 (w), 670 (w), 631 (w), 556 (s), 462 (w), 418 (m). UV/Vis (CH_2Cl_2, 1.0 × 10^{-5} mol dm^{-3}) λ/nm (ε/dm^3 mol^{-1} cm^{-1}) 258 (45 000), 314 (26 000), 348 sh (20 000), 381 (9500), 410 sh (6300). Emission (CH_2Cl_2, 1.0 × 10^{-5} mol dm^{-3}, λ_{exc} = 270 nm) λ_{em}^{max} = 638 nm. ESI-MS *m/z* 769.2 $[M-PF_6]^+$ (calc. 769.2). Found C 49.41, H 3.72, N 6.39; $C_{38}H_{32}F_6IrN_4PS\cdot0.5H_2O$ requires C 49.45, H 3.60, N 6.07%.

8.15. $[Ir(ppy)_2(btzpybtz)][PF_6]$

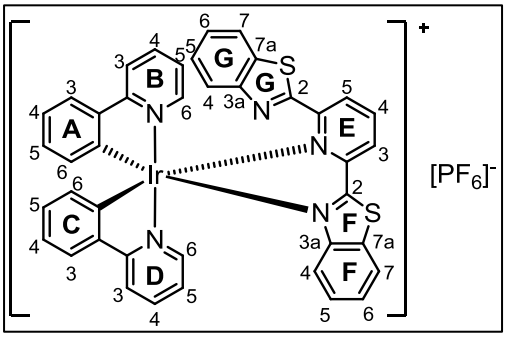

$[Ir(ppy)_2Cl]_2$ (150 mg, 0.140 mmol) and $AgPF_6$ (88.1 mg, 0.348 mmol) in MeOH (25 mL), 2 h at room temperature. Addition of 2,6-bis(benzo[*d*]thiazol-2-yl)pyridine (btzpybtz) (98.0 mg, 0.284 mmol) and MeOH (10 mL). Purification by column chromatography (silica, CH_2Cl_2 changing to CH_2Cl_2–1% MeOH), layering with toluene/*n*-hexane and subsequent precipitation with *n*-hexane from a CH_2Cl_2 solution. $[Ir(ppy)_2(btzpybtz)][PF_6]$ was isolated as a dark red solid (136 mg, 0.137 mmol, 49.0%). ^{1}H NMR (500 MHz, CD_2Cl_2) δ/ppm 8.66 (br, 1H, H^{D6}), 8.60 (dd, J = 7.9, 1.2 Hz, 1H, H^{E3}), 8.31 (*pseudo*-t, J = 7.8 Hz, 1H, H^{E4}), 8.10 (dd, J = 8.2, 1.0 Hz, 1H, H^{F7}), 7.91–7.77 (overlapping m, 4H, $H^{B3+B4+D3+D4}$), 7.75 (dd, J = 7.8, 1.1 Hz, 1H, H^{E5}), 7.71 (d, J = 8.1 Hz, 1H, $H^{G4/G7}$), 7.68 (dd, J = 8.2, 1.1 Hz, 1H, $H^{G4/G7}$), 7.64 (dd, J = 7.8, 1.4 Hz, 1H, H^{C3}), 7.55–7.45 (overlapping m, 3H, $H^{B6+F6+G5/G6}$), 7.41 (ddd, J = 8.3, 7.2, 1.2 Hz, 1H, $H^{G5/G6}$), 7.24 (ddd, J = 7.3, 5.8, 1.8 Hz, 1H, H^{D5}), 7.18–7.06 (overlapping m, 2H, H^{A3+F5}), 7.02 (*pseudo*-td, J = 7.5, 1.2 Hz, 1H, H^{C4}), 6.97 (*pseudo*-td, J = 6.3, 2.0 Hz, 1H, H^{B5}), 6.79 (*pseudo*-td, J = 7.5, 1.4 Hz, 1H, H^{C5}), 6.66 (d, J = 8.6 Hz, 1H, H^{F4}), 6.21 (*pseudo*-t, J = 7.5 Hz, 1H, H^{A4}), 5.96 (dd, J = 7.8, 1.1 Hz, 1H, H^{C6}), 5.67 (*pseudo*-t, J = 7.2 Hz, 1H, H^{A5}), 5.36 (d, J = 7.6 Hz, 1H, H^{A6}). $^{13}C\{^1H\}$ NMR (126 MHz, CD_2Cl_2) δ/ppm 170.6 (C^{F2}), 168.6 (C^{B2}), 167.3 (C^{D2}), 162.9 (C^{G2}), 157.4 (C^{E6}), 153.8 (C^{E2}), 153.1 ($C^{G3a/G7a}$), 151.7 (C^{F3a}), 148.9 (C^{B6}), 145.5 (C^{A1}), 144.3 (C^{C2}), 143.4 (C^{C1}), 142.9 (C^{A2}), 141.1 (C^{E4}), 138.90 (2C, $C^{B3/B4+D3/D4}$), 138.88 (2C, $C^{B3/B4+D3/D4}$), 137.3 ($C^{G3a/G7a}$), 134.9 (C^{F7a}), 132.7 (C^{A6}), 131.83 ($C^{C6/E5}$), 131.81 ($C^{C6/E5}$), 130.8 (C^{C5}), 129.1 (C^{F5}), 129.0 (C^{F6}), 128.9 (C^{A5}), 127.6 (C^{E3}), 127.1 ($C^{G5/G6}$), 126.8 ($C^{G5/G6}$), 125.2 (C^{C3}), 124.6 ($C^{G4/G7}$), 124.0 (C^{A3}), 123.62 ($C^{C4/F7}$), 123.60 ($C^{C4/F7}$), 123.43 ($C^{B5/F4}$), 123.38 ($C^{B5/F4}$), 123.3 (C^{D5}), 122.2 ($C^{G4/G7}$), 121.4 (C^{A4}), 120.3 ($C^{B3/B4}$), 119.8 ($C^{D3/D4}$). IR (solid, $\tilde{\nu}$/cm^{-1}) 3058 (w), 1608 (m), 1584 (m), 1564 (w), 1480 (m), 1459 (w), 1439 (w), 1423 (m), 1319 (w), 1270 (w), 1230 (w), 1180 (w), 1165 (w), 1119 (w), 1063 (w), 1031 (w), 983 (w), 835 (s), 756 (s), 728 (s), 669 (m), 630 (m), 556 (s), 420 (m). UV/Vis (CH_2Cl_2, 1.0 × 10^{-5} mol dm^{-3}) λ/nm (ε/dm^3 mol^{-1} cm^{-1}) 255 (41 000), 261 sh (40 000), 300 sh (30 000), 340 (25 000), 365 sh (19 000), 420 sh (4100). Emission (CH_2Cl_2, 1.0 × 10^{-5} mol dm^{-3}, λ_{exc} = 265 nm) λ_{em}^{max} = 652 nm. ESI-MS

m/z 846.0 $[M–PF_6]^+$ (calc. 846.1). HR ESI-MS *m/z* 846.1340 (calc. 846.1332). Satisfactory elemental analysis could not be obtained.

8.16. $[Ir(ppy)_2(bozpy)][PF_6]$

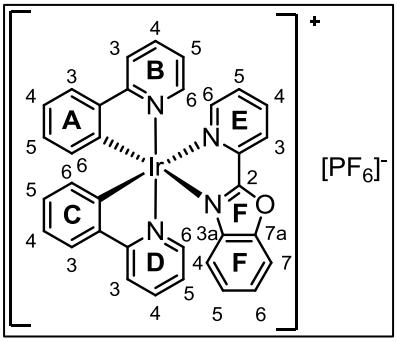

$[Ir(ppy)_2Cl]_2$ (149 mg, 0.139 mmol) and $AgPF_6$ (91.6 mg, 0.362 mmol) in MeOH (25 mL), 3.5 h at room temperature. Addition of 2-(pyridin-2-yl)benzo[*d*]oxazole (bozpy) (56.6 mg, 0.288 mmol) and MeOH (10 mL). Purification by column chromatography (silica, CH_2Cl_2 changing to CH_2Cl_2–1% MeOH) and precipitation with Et_2O. $[Ir(ppy)_2(bozpy)][PF_6]$ was isolated as an orange solid (184 mg, 0.219 mmol, 78.6%). ^{1}H NMR (500 MHz, CD_2Cl_2) δ/ppm 8.52 (*pseudo*-dt, J = 7.9, 1.0 Hz, 1H, H^{E3}), 8.25 (*pseudo*-td, J = 7.8, 1.5 Hz, 1H, H^{E4}), 8.05 (*pseudo*-dt, J = 5.4, 1.1 Hz, 1H, H^{E6}), 7.99 (*pseudo*-dt, J = 8.3, 1.1 Hz, 1H, H^{B3}), 7.93 (*pseudo*-dt, J = 8.3, 1.0 Hz, 1H, H^{D3}), 7.86–7.81 (overlapping m, 2H, H^{B4+F7}), 7.80–7.75 (overlapping m, 4H, $H^{A3+B6+C3+D4}$), 7.64 (ddd, J = 7.8, 5.4, 1.3 Hz, 1H, H^{E5}), 7.58 (ddd, J = 8.7, 7.5, 1.2 Hz, 1H, H^{F6}), 7.54 (*pseudo*-dt, J = 5.8, 1.1 Hz, 1H, H^{D6}), 7.26 (ddd, J = 8.4, 7.5, 1.0 Hz, 1H, H^{F5}), 7.16 (*pseudo*-td, J = 7.5, 1.2 Hz, 1H, H^{C4}), 7.12 (*pseudo*-td, J = 7.6, 1.2 Hz, 1H, H^{A4}), 7.05 (ddd, J = 7.4, 5.9, 1.4 Hz, 1H, H^{D5}), 7.02–6.96 (overlapping m, 3H, $H^{A5+B5+C5}$), 6.46 (dd, J = 7.7, 1.3 Hz, 1H, H^{C6}), 6.39 (*pseudo*-dt, J = 8.1, 0.9 Hz, 1H, H^{F4}), 6.37 (dd, J = 7.7, 1.2 Hz, 1H, H^{A6}). $^{13}C\{^1H\}$ NMR (126 MHz, CD_2Cl_2) δ/ppm 168.4 (C^{D2}), 168.1 (C^{B2}), 166.8 (C^{F2}), 152.3 (C^{E6}), 152.1 (C^{F7a}), 150.2 (C^{B6}), 149.5 (C^{D6}), 148.3 (C^{A1}), 145.0 (C^{C2}), 144.53 (C^{C1}), 144.46 (C^{A2}), 144.0 (C^{E2}), 140.6 (C^{E4}), 139.01 (C^{B4}), 138.98 (C^{D4}), 137.9 (C^{F3a}), 132.9 (C^{C6}), 132.1 (C^{A6}), 131.3 (C^{A5}), 131.0 (C^{E5}), 130.8 (C^{C5}), 129.6 (C^{F6}), 128.1 (C^{F5}), 126.8 (C^{E3}), 125.6 (C^{C3}), 125.2 (C^{A3}), 124.17 ($C^{B5/D5}$), 124.15 ($C^{5/D5}$), 123.7 (2C, C^{A4+C4}), 120.5 (C^{B3}), 120.2 (C^{D3}), 119.4 (C^{F4}), 113.2 (C^{F7}). IR (solid, $\tilde{\nu}$/cm^{-1}) 3054 (w), 1608 (m), 1584 (m), 1565 (w), 1542 (w), 1479 (m), 1439 (m), 1423 (m), 1393 (m), 1304 (w), 1269 (w), 1229 (w), 1164 (w), 1142 (w), 1108 (w), 1093 (w), 1065 (w), 1032 (w), 1019 (w), 836 (s), 792 (m), 755 (s), 698 (w), 670 (w), 646 (w), 631 (w), 556 (s), 494 (w), 434 (w), 418 (m). UV/Vis (CH_2Cl_2, 1.0 × 10^{-5} mol dm^{-3}) λ/nm (ε/dm^3 mol^{-1} cm^{-1}) 254 (42 000), 266 (41 000), 295 sh (31 000), 317 (29 000), 335 sh (21 000), 378 (9100), 410 sh (5700). Emission (CH_2Cl_2, 1.0 × 10^{-5} mol dm^{-3}, λ_{exc} = 270 nm) λ_{em}^{max} = 636 nm. ESI-MS *m/z* 697.1 $[M–PF_6]^+$ (calc. 697.2). Found C 48.19, H 3.26, N 6.89; $C_{34}H_{24}F_6IrN_4OP·0.5H_2O$ requires C 48.00, H 2.96, N 6.59%.

8.17. $[Ir(ppz)_2(btzpy)][PF_6]$

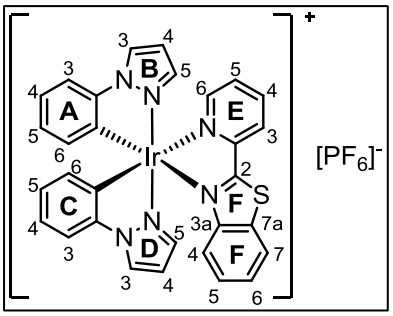

$[Ir(ppz)_2Cl]_2$ (101 mg, 98.2 μmol) and $AgPF_6$ (57.6 mg, 0.228 mmol) in MeOH (20 mL), 4 h at room temperature. Addition of 2-(pyridin-2-yl)benzo[*d*]thiazole (btzpy) (31.0 mg, 0.198 mmol) and MeOH (2 mL). Purification by column chromatography (silica, CH_2Cl_2 changing to CH_2Cl_2–1% MeOH) and precipitation with Et_2O. $[Ir(ppz)_2(btzpy)][PF_6]$ was isolated as an orange solid (79.8 mg, 95.0 μmol, 48.7%). ^{1}H NMR (500 MHz, CD_2Cl_2) δ/ppm 8.42 (*pseudo*-dt, J = 8.1, 1.0 Hz, 1H, H^{E3}), 8.24–8.15 (overlapping m, 3H, $H^{B3+E4+E6}$), 8.13 (d, J = 2.9 Hz, 1H, H^{D3}), 8.08 (dd, J = 8.2, 0.9 Hz, 1H, H^{F7}), 7.59–7.52 (overlapping m, 2H, H^{E5+F6}), 7.37 (dd, J = 8.1, 1.1 Hz, 2H, H^{A3+C3}), 7.28 (ddd, J = 8.5, 7.2, 1.2 Hz, 1H, H^{F5}), 7.18–7.10 (overlapping m, 3H, $H^{A4+C4+F4}$), 6.99–6.88 (overlapping m, 3H, $H^{A5+B5+C5}$), 6.87 (d, J = 2.2 Hz, 1H, H^{D5}), 6.55 (*pseudo*-t, J = 2.6 Hz, 2H, H^{B4+D4}), 6.38 (dd, J = 7.6, 1.3 Hz, 1H, H^{C6}), 6.28 (dd, J = 7.5, 1.3 Hz, 1H, H^{A6}). $^{13}C\{^1H\}$ NMR (126 MHz, CD_2Cl_2) δ/ppm 170.5 (C^{F2}), 152.8 (C^{E2}), 151.9 (C^{F3a}), 151.8 (C^{E6}), 143.6 (C^{C2}), 143.3 (C^{A2}), 140.6 (C^{E4}), 139.8 (C^{B5}), 138.8 (C^{D5}), 134.5 (C^{C6}), 134.3 (C^{F7a}), 133.4 (C^{A6}), 129.8 (C^{A1}), 129.5 (C^{E5}), 129.31 (C^{F5}), 129.28 (C^{C1}), 129.0 (C^{F6}), 127.9 (C^{B3}), 127.7 (C^{D3}), 127.6 (C^{A5}), 127.2 (C^{C5}), 126.5 (C^{E3}), 124.4 (C^{A4}), 124.2 (C^{C4}), 123.7 (C^{F7}), 123.2 (C^{F4}), 112.5 (C^{A3}), 112.4 (C^{C3}), 109.0 (C^{B4}), 108.8 (C^{D4}). IR (solid, $\tilde{\nu}$/cm^{-1}) 3147 (w), 1589 (w), 1482 (m), 1459 (w), 1446 (m), 1413 (m), 1338 (m), 1325 (m), 1277 (m), 1248 (w), 1163 (w), 1111 (w), 1075 (m), 1058 (m), 1032 (m), 1010 (w), 968 (w), 918 (w), 836 (s), 751 (s), 730 (m), 703 (m), 656 (m), 610 (m), 557 (s), 477 (m), 457 (m), 437 (m). UV/Vis (CH_2Cl_2, 1.0 × 10^{-5} mol dm^{-3}) λ/nm (ε/dm^3 mol^{-1} cm^{-1}) 255 (35 000), 330 (23 000), 350 sh (18 000), 380 sh (5500), 410 sh (3000). Emission (CH_2Cl_2, 1.0 × 10^{-5} mol dm^{-3}, λ_{exc} = 261 nm) λ_{em}^{max} = 607 nm. ESI-MS *m/z* 691.1 $[M–PF_6]^+$ (calc. 691.1). Found C 42.66, H 3.03, N 10.29; $C_{30}H_{22}F_6IrN_6PS{\cdot}0.5H_2O$ requires C 42.65, H 2.74, N 9.95%.

8.18. $[Ir(piq)_2(btzpy)][PF_6]$

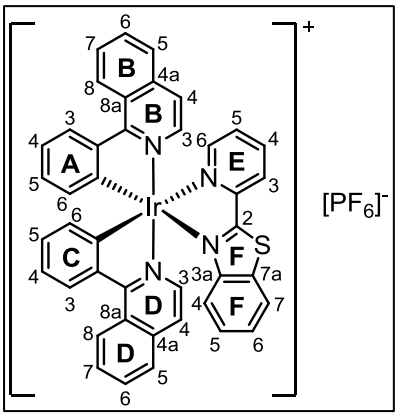

$[Ir(piq)_2Cl]_2$ (151 mg, 0.119 mmol) and $AgPF_6$ (77.4 mg, 0.306 mmol) in MeOH (25 mL), 3 h at room temperature. Addition of 2-(pyridin-2-yl)benzo[*d*]thiazole (btzpy) (50.8 mg, 0.239 mmol) and MeOH (10 mL). Purification by column chromatography (silica, CH_2Cl_2 changing to CH_2Cl_2–2% MeOH), layering with toluene/*n*-hexane and subsequent precipitation with *n*-hexane from a CH_2Cl_2 solution. $[Ir(piq)_2(btzpy)][PF_6]$ was isolated as a dark orange solid (180 mg, 0.188 mmol, 78.9%). ^{1}H NMR (500 MHz, CD_2Cl_2) δ/ppm 9.04–8.97 (overlapping m, 1H, H^{B8}), 8.94 (*pseudo*-dt, J = 7.1, 3.5 Hz, 1H, H^{D8}), 8.49 (d, J = 7.9 Hz, 1H, H^{E3}), 8.36 (*pseudo*-dt, J = 8.2, 1.5 Hz, 2H, H^{A3+C3}), 8.19 (*pseudo*-td, J = 7.9, 1.5 Hz, 1H, H^{E4}), 8.06 (dd, J = 8.3, 0.9 Hz, 1H, H^{F7}), 7.95–7.88 (overlapping m, 2H, H^{B5+D5}), 7.85–7.80 (overlapping m, 3H, $H^{B6+B7+E6}$), 7.80–7.75 (overlapping m, 2H, H^{D6+D7}), 7.54 (d, J = 6.4 Hz, 1H, H^{B3}), 7.52–7.47 (overlapping m, 2H, H^{E5+F6}), 7.37 (s, 2H, H^{D3+D4}), 7.32 (d, J = 6.4 Hz, 1H, H^{B4}), 7.25 (ddd, J = 8.2, 7.3, 1.3 Hz, 1H, H^{C4}), 7.22–7.16 (overlapping m, 2H, H^{A4+F5}), 7.00–6.90 (overlapping m, 2H, H^{A5+C5}), 6.68 (d, J = 8.4 Hz, 1H, H^{F4}), 6.43 (dd, J = 7.8, 1.2 Hz, 1H, H^{C6}), 6.27 (dd, J = 7.6, 1.2 Hz, 1H, H^{A6}). $^{13}C\{^1H\}$ NMR (126 MHz, CD_2Cl_2) δ/ppm 170.0 (C^{F2}), 169.6 (C^{D1}), 169.0 (C^{B1}), 152.1 (C^{E2}), 151.5 (C^{E6}), 151.1 (C^{F3a}), 150.9 (C^{C1}), 150.8 (C^{A1}), 146.7 (C^{C2}), 146.0 (C^{A2}), 141.8 (C^{B3}), 140.7 (C^{D3}), 140.5 (C^{E4}), 137.7 (C^{B4a}), 137.6 (C^{D4a}), 134.8 (C^{F7a}), 133.3 (C^{C6}), 132.54 (C^{B6}), 132.45 (C^{D6}), 132.2 (C^{A6}), 131.5 (C^{A5}), 131.42 ($C^{A3/C3}$), 131.39 ($C^{A3/C3}$), 131.0 (C^{C5}), 129.9 (C^{E5}), 129.6 (C^{B7}), 129.4 (C^{D7}), 129.2 (C^{F5}), 128.9 (C^{F6}), 128.1 (C^{B5}), 128.0 (C^{D5}), 127.4 (C^{D8}), 127.3 (C^{B8}), 126.99 (C^{B8a}), 126.95 (C^{E3}), 126.8 (C^{D8a}), 123.7 (C^{F7}), 123.4 (C^{A4}), 123.2 (C^{F4}), 123.1 (C^{C4}), 122.8 (C^{B4}), 122.5 (C^{D4}). IR (solid, $\tilde{\nu}$/cm^{-1}) 3046 (w), 1576 (m), 1541 (m), 1502 (w), 1485 (w), 1448 (m), 1434 (m), 1382 (m), 1352 (m), 1324 (m), 1298 (w), 1272 (m), 1159 (m), 1049 (w), 1030 (w), 1009 (w), 836 (s), 757 (s), 741 (s), 731 (s), 712 (m), 676 (m), 664 (m), 628 (m), 581 (m), 556 (s), 516 (m), 499 (m), 481 (w), 439 (m), 407 (m). UV/Vis (CH_2Cl_2, 1.0 × 10^{-5} mol dm^{-3}) λ/nm (ε/dm^3 mol^{-1} cm^{-1}) 293 (46 000), 335 (35 000), 350 sh (31 000), 380 sh (14 000), 433 (8900), 465 sh (4600). Emission (CH_2Cl_2, 1.0 × 10^{-5} mol dm^{-3}, λ_{exc} = 293 nm) λ_{em}^{max} = 642 nm. ESI-MS *m/z* 813.1 $[M–PF_6]^+$ (calc. 813.2). HRMS *m/z* 813.1665 (calc. 813.1658). Found C 50.71, H 3.52, N 5.82; $C_{42}H_{28}F_6IrN_4PS·2H_2O$ requires C 50.75, H 3.25, N 5.64%.

8.19. [Ir(tppy)$_2$(btzpy)][PF$_6$]

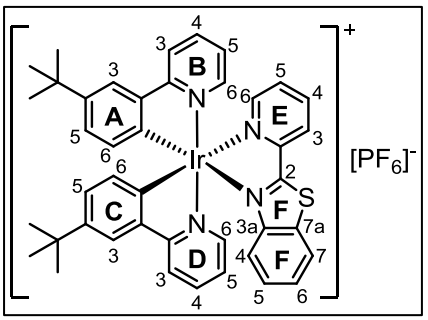

[Ir(tppy)$_2$Cl]$_2$ (151 mg, 0.116 mmol) and $AgPF_6$ (83.3 mg, 0.329 mmol) in MeOH (25 mL), 3.5 h at room temperature. Addition of 2-(pyridin-2-yl)benzo[*d*]thiazole (btzpy) (49.3 mg, 0.232 mmol) and MeOH (5 mL). Purification by column chromatography (silica, CH_2Cl_2 changing to CH_2Cl_2–2% MeOH) and precipitation with Et_2O/*n*-hexane. [Ir(tppy)$_2$(btzpy)][PF$_6$] was isolated as a red solid (180 mg, 0.186 mmol, 80.0%). ^{1}H NMR (500 MHz, CD_2Cl_2) δ/ppm 8.43 (*pseudo*-dt, J = 8.0, 1.1 Hz, 1H, H^{E3}), 8.19 (*pseudo*-td, J = 7.9, 1.5 Hz, 1H, H^{E4}), 8.06 (*pseudo*-dt, J = 8.4, 0.8 Hz, 1H, H^{F7}), 8.02–7.98 (overlapping m, 2H, H^{B3+E6}), 7.93 (*pseudo*-dt, J = 8.3, 1.0 Hz, 1H, H^{D3}), 7.83–7.71 (overlapping m, 4H, $H^{A3+B4+C3+D4}$), 7.61 (ddd, J = 5.8, 1.6, 0.8 Hz, 1H, H^{B6}), 7.57–7.49 (overlapping m, 2H, H^{E5+F6}), 7.47 (*pseudo*-dt, J = 5.8, 1.2 Hz, 1H, H^{D6}), 7.16 (ddd, J = 8.4, 7.1, 1.2 Hz, 1H, H^{F5}), 7.12 (dd, J = 8.0, 2.1 Hz, 1H, H^{C5}), 7.07 (dd, J = 8.0, 2.1 Hz, 1H, H^{A5}), 6.99 (ddd, J = 7.3, 5.8, 1.4 Hz, 1H, H^{D5}), 6.93 (ddd, J = 7.3, 5.8, 1.4 Hz, 1H, H^{B5}), 6.79 (dd, J = 8.5, 0.8 Hz, 1H, H^{F4}), 6.35 (d, J = 8.0 Hz, 1H, H^{C6}), 6.20 (d, J = 8.0 Hz, 1H, H^{A6}), 1.38 (s, 9H, $H^{C4\text{-}t\text{Bu}}$), 1.35 (s, 9H, $H^{A4\text{-}t\text{Bu}}$). ^{13}C{^{1}H} NMR (126 MHz, CD_2Cl_2) δ/ppm 170.0 (C^{F2}), 168.8 (C^{D2}), 168.2 (C^{B2}), 152.3 (C^{E2}), 151.5 (C^{E6}), 151.2 (C^{F3a}), 150.3 (C^{B6}), 149.2 (C^{D6}), 146.8 (C^{C4}), 146.6 (C^{A4}), 144.5 (C^{C2}), 143.8 (C^{C1}), 143.7 (C^{A2}), 143.6 (C^{A1}), 140.4 (C^{E4}), 138.7 ($C^{B4/D4}$), 138.6 ($C^{B4/D4}$), 134.9 (C^{F7a}), 132.6 (C^{C6}), 131.3 (C^{A6}), 129.9 (C^{E5}), 129.10 ($C^{A5/F5}$), 129.08 ($C^{A5/F5}$), 128.9 (C^{F6}), 128.6 (C^{C5}), 126.8 (C^{E3}), 123.9 (C^{B5}), 123.8 (C^{D5}), 123.6 (C^{F7}), 123.4 (C^{F4}), 122.4 (C^{A3}), 122.2 (C^{C3}), 120.4 (C^{B3}), 120.2 (C^{D3}), 34.84 ($C^{C4\text{-}\underline{C}(CH3)3}$), 34.80 ($C^{A4\text{-}\underline{C}(CH3)3}$), 31.8 ($C^{C4\text{-}C(\underline{C}H3)3}$), 31.7 ($C^{A4\text{-}C(\underline{C}H3)3}$). IR (solid, $\tilde{\nu}$/cm^{-1}) 2953 (w), 2865 (w), 1608 (w), 1561 (w), 1537 (w), 1479 (m), 1429 (m), 1362 (w), 1323 (w), 1297 (w), 1269 (w), 1254 (m), 1202 (w), 1161 (w), 1114 (w), 1070 (w), 1029 (w), 1007 (w), 876 (w), 834 (s), 780 (s), 754 (s), 729 (m), 709 (m), 644 (m), 623 (m), 556 (s), 477 (w), 436 (w), 416 (w). UV/Vis (CH_2Cl_2, 1.0 × 10^{-5} mol dm^{-3}) λ/nm (ε/dm^3 mol^{-1} cm^{-1}) 257 (47 000), 270 sh (44 000), 335 (24 000), 350 sh (19 000), 387 (9200), 412 (7400). Emission (CH_2Cl_2, 1.0 × 10^{-5} mol dm^{-3}, λ_{exc} = 268 nm) λ_{em}^{max} = 660 nm. ESI-MS *m/z* 825.2 [M–PF$_6$]$^+$ (calc. 825.3). Found C 51.84, H 4.34, N 6.03; $C_{42}H_{40}F_6IrN_4PS$ requires C 52.00, H 4.16, N 5.78%.

8.20. [Ir(pbtz)$_2$(btzpy)][PF$_6$]

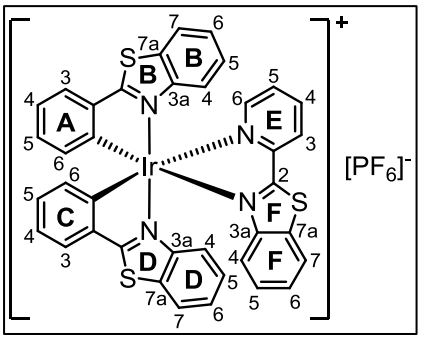

[Ir(pbtz)$_2$Cl]$_2$ (151 mg, 0.116 mmol) and AgPF$_6$ (73.8 mg, 0.292 mmol) in MeOH (25 mL), 2.5 h at room temperature. Addition of 2-(pyridin-2-yl)benzo[*d*]thiazole (btzpy) (49.1 mg, 0.134 mmol) and MeOH (10 mL). Purification by column chromatography (silica, CH_2Cl_2 changing to CH_2Cl_2–2% MeOH) and precipitation with Et_2O/*n*-hexane. [Ir(pbtz)$_2$(btzpy)][PF$_6$] was isolated as a bright orange solid (130 mg, 0.134 mmol, 57.8%). ^{1}H NMR (500 MHz, CD_2Cl_2) δ/ppm 8.40 (*pseudo*-dt, J = 8.1, 1.1 Hz, 1H, H^{E3}), 8.23 (*pseudo*-td, J = 7.8, 1.5 Hz, 1H, H^{E4}), 8.11 (*pseudo*-dt, J = 5.5, 1.0 Hz, 1H, H^{E6}), 8.08 (*pseudo*-dt, J = 8.4, 0.9 Hz, 1H, H^{F7}), 7.93–7.85 (overlapping m, 4H, $H^{A3+B7+C3+D7}$), 7.64–7.55 (overlapping m, 2H, H^{E5+F6}), 7.39–7.32 (overlapping m, 2H, H^{B6+D6}), 7.28 (ddd, J = 8.5, 7.3, 1.2 Hz, 1H, H^{F5}), 7.22–7.14 (overlapping m, 2H, H^{A4+C4}), 7.11 (ddd, J = 8.5, 7.3, 1.2 Hz, 1H, H^{D5}), 7.00–6.89 (overlapping m, 4H, $H^{A5+B5+C5+F4}$), 6.52 (dd, J = 7.8, 1.0 Hz, 1H, H^{C6}), 6.40–6.33 (overlapping m, 2H, H^{A6+B4}), 6.01 (d, J = 8.4 Hz, 1H, H^{D4}). ^{13}C{^{1}H} NMR (126 MHz, CD_2Cl_2) δ/ppm 182.3 (C^{D2}), 181.5 (C^{B2}), 170.3 (C^{F2}), 153.1 (C^{E2}), 151.8 (C^{E6}), 151.6 (C^{F3a}), 149.7 (C^{D3a}), 149.5 (C^{B3a}), 147.4 (C^{C1}), 147.3 (C^{A1}), 141.4 (C^{C2}), 141.0 (C^{E4}), 140.6 (C^{A2}), 134.4 (C^{F7a}), 134.3 (C^{C6}), 133.2 (C^{A6}), 132.9 (C^{A5}), 132.7 (C^{C5}), 132.08 ($C^{B7a/D7a}$), 132.05 ($C^{B7a/D7a}$), 130.1 (C^{E5}), 129.7 (C^{F5}), 129.2 (C^{F6}), 128.72 ($C^{B5/D5}$), 128.69 ($C^{B5/D5}$), 127.37 ($C^{A3/C3}$), 127.36 ($C^{A3/C3}$), 126.73 ($C^{B6/D6/E3}$), 126.69 ($C^{B6/D6/E3}$), 126.5 ($C^{B6/D6}$), 124.3 (C^{A4}), 124.2 (C^{D7}), 124.14 (C^{B7}), 124.08 (C^{C4}), 124.0 (C^{F7}), 123.1 (C^{F4}), 118.3 (C^{B4}), 117.7 (C^{D4}). IR (solid, $\tilde{\nu}$/cm^{-1}) 3059 (w), 1581 (w), 1552 (w), 1485 (w), 1470 (w), 1459 (w), 1448 (m), 1439 (m), 1408 (m), 1324 (w), 1299 (w), 1267 (m), 1162 (w), 1126 (w), 1078 (w), 1053 (w), 1028 (w), 997 (w), 836 (s), 754 (s), 741 (m), 725 (m), 712 (m), 685 (w), 657 (w), 646 (w), 583 (w), 557 (s), 509 (w), 480 (w), 449 (m). UV/Vis (CH_2Cl_2, 1.0 × 10^{-5} mol dm^{-3}) λ/nm (ε/dm^3 mol^{-1} cm^{-1}) 253 (32 000), 270 (28 000), 279 (27 000), 290 (26 000), 324 (46 000), 409 (9200), 435 sh (6300). Emission (CH_2Cl_2, 1.0 × 10^{-5} mol dm^{-3}, λ_{exc} = 326 nm) λ_{em}^{max} = 600 nm. ESI-MS *m/z* 825.0 [*M*–PF$_6$]$^+$ (calc. 825.1). Found C 46.88, H 2.79, N 6.16; $C_{38}H_{24}F_6IrN_4PS_3$ requires C 47.05, H 2.49, N 5.78%.

8.21. Crystallography

Solvent molecules were severely disordered in $[Ir(ppy)_2(btzpy)][PF_6]$ and the SQUEEZE[188] procedure was used; residual electron density corresponds to 1.5 CH_2Cl_2 per formula unit.

$[Ir(ppy)_2(btzpy)][PF_6]\cdot 1.5CH_2Cl_2$. $C_{35.50}H_{27}Cl_3F_6Ir_1N_4P_1S_1$, M = 985.24, yellow block, monoclinic, space group $P2_1/c$, a = 14.4951(15), b = 13.7676(14), c = 18.7348(19) Å, β = 106.359(3)°, U = 3587.4(6) Å^3, Z = 4, D_c = 1.82 Mg m^{-3}, μ(Cu-K$_\alpha$) = 10.8 mm^{-1}, T = 123 K. Total 33781 reflections, 6209 unique, R_{int} = 0.022. Refinement of 6169 reflections (424 parameters) with $I > 2\sigma(I)$ converged at final R_1 = 0.0243 (R_1 all data = 0.0244), wR_2 = 0.0546 (wR_2 all data = 0.0547), gof = 0.9999. CCDC 1062206.

$[Ir(ppy)_2(bbtz)][PF_6]$. $C_{34}H_{24}F_6Ir_1N_6P_1S_2$, M = 917.92, red block, orthorhombic, space group $Fdd2$, a = 12.2991(19), b = 13.340(2), c = 40.350(7) Å, U = 6620.3(18) Å^3, Z = 8, D_c = 1.842 Mg m^{-3}, μ(Cu-K$_\alpha$) = 10.068 mm^{-1}, T = 123 K. Total 10929 reflections, 2564 unique, R_{int} = 0.030. Refinement of 2553 reflections (228 parameters) with $I > 2\sigma(I)$ converged at final R_1 = 0.0170 (R_1 all data = 0.0171), wR_2 = 0.0405 (wR_2 all data = 0.0405), gof = 0.9244.

$[Ir(ppy)_2(bozpy)][PF_6]\cdot CH_2Cl_2$. $C_{35}H_{26}Cl_2F_6Ir_1N_4O_1P_1$, M = 926.70, red block, monoclinic, space group $P2_1/n$, a = 14.6181(15), b = 13.8956(14), c = 16.9244(17) Å, β = 107.448(2)°, U = 3279.6(6) Å^3, Z = 4, D_c = 1.877 Mg m^{-3}, μ(Cu-K$_\alpha$) = 10.478 mm^{-1}, T = 123 K. Total 19957 reflections, 5966 unique, R_{int} = 0.022. Refinement of 5956 reflections (451 parameters) with $I > 2\sigma(I)$ converged at final R_1 = 0.0256 (R_1 all data = 0.0257), wR_2 = 0.0556 (wR_2 all data = 0.0556), gof = 0.9994.

CHAPTER V: GLYCOSYLATED IRIDIUM COMPLEXES

1. Introduction

Carbohydrates play a vital role in living organisms. They form part of essential biomolecules, such as starch, adenosine triphosphate (ATP), ribonucleic acid (RNA) and deoxyribonucleic acid (DNA), and are important for recognition within cells.[209–212]

Few examples exist in which iridium complexes were functionalized with glycosyl moieties: these include application as sensors,[209] phosphorescent labels in cells,[210–212] water-soluble drugs[213] and catalysts,[213–215] as well as for analytical purposes.[216]

In this chapter, ongoing work in the field of iridium(III) complexes containing sugar moieties either on the ancillary or on the cyclometallating ligand is presented.

2. Synthesis and NMR Spectroscopic Characterization

2.1. Ligand synthesis

Bpy glycoside ligand **12** was synthesized according to a procedure reported in the literature.[217] In the first step, β-D-ribofuranose 1,2,3,5-tetraacetate (**10**) was reacted with 2-bromoethanol in the presence of Lewis acidic $SnCl_4$ to an anomeric mixture of bromo-substituted ribofuranose **11** in moderate yield.[217,218] Separation of the anomers was challenging and was achieved by repeated column chromatography, resulting in a relatively low yield of the pure β-anomer. 4,4'-Dihydroxy-2,2'-bipyridine was treated with glycoside donor **11** to give bpy ligand **12** in good yield (Scheme 23). ^{1}H NMR spectroscopic data of ligand **12** were compared with literature data.[217]

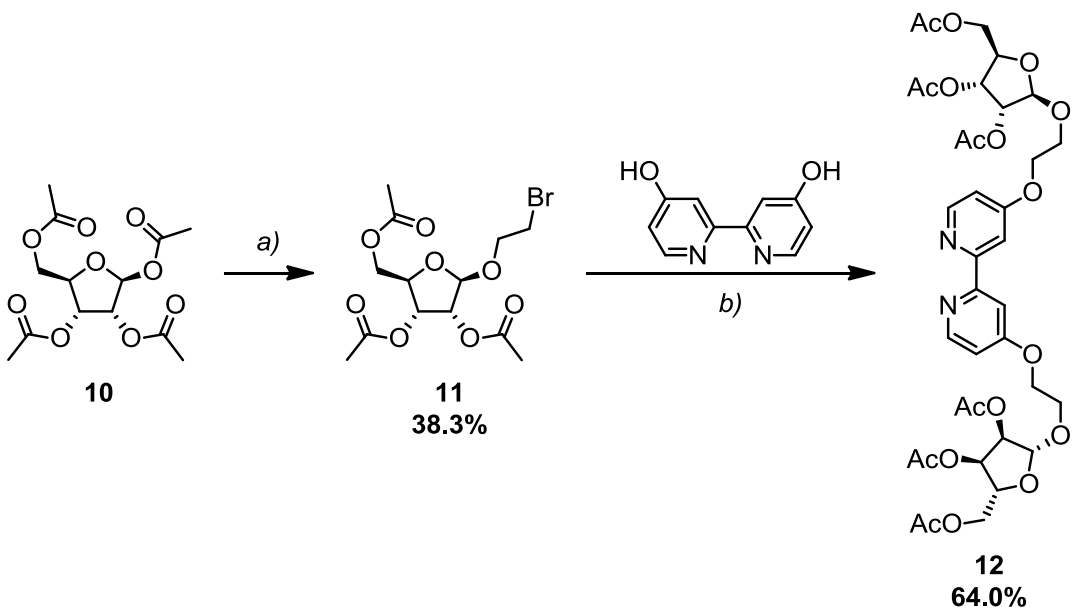

Scheme 23 Synthesis of glycosylated bpy ligand **12**. Reaction conditions: *a)* $SnCl_4$, 2-bromoethanol, CH_2Cl_2/CH_3CN, room temperature, 1 h 45 min, N_2; *b)* K_2CO_3, KI, DMF, 75 °C, overnight, N_2.

Glycosylated cyclometallating ligand **14** was prepared according to Scheme 24. 2-(4-Hydroxyphenyl)pyridine (**13**) was obtained in excellent yield by a literature known Suzuki coupling reaction of 4-hydroxyphenylboronic acid with 2-bromopyridine, catalysed by $Pd(OAc)_2$.[219] By adaptation of the reported literature procedure,[217] the functionalized Hppy ligand **14** was synthesized in good yield from 2-(4-hydroxyphenyl)pyridine (**13**) and glycoside **11** *via* an *in situ* halogen exchange of **11** using the Finkelstein reaction followed by an S_N2 reaction. Cyclometallating ligand 14 was characterized by ^1H NMR, ^{13}C NMR and IR spectroscopies, LC-ESI mass spectrometry and elemental analysis.

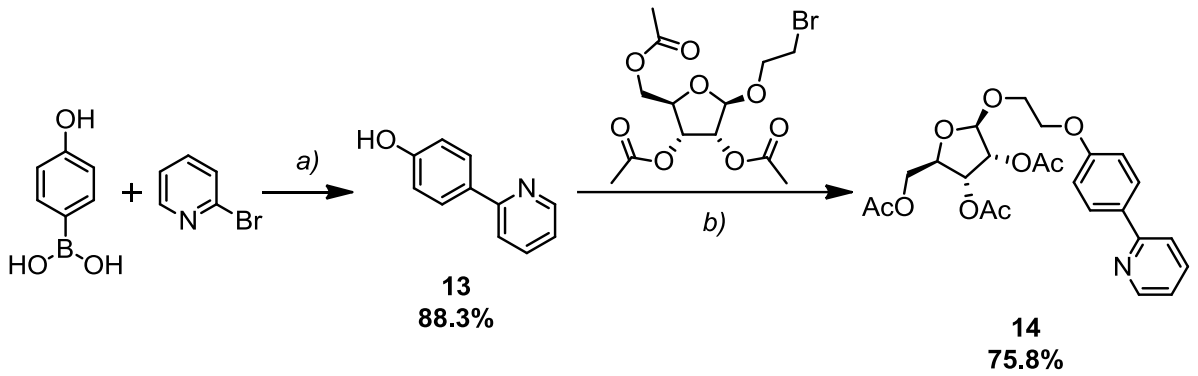

Scheme 24 Synthetic route to glycosylated phenylpyridine ligand **14**. Reaction conditions: *a)* $Pd(OAc)_2$, K_3PO_4, ethylene glycol, 80 °C, 2 h; *b)* K_2CO_3, KI, DMF, 75 °C, overnight, N_2.

2.2. Synthesis of $[Ir(C^N)_2Cl]_2$ dimer

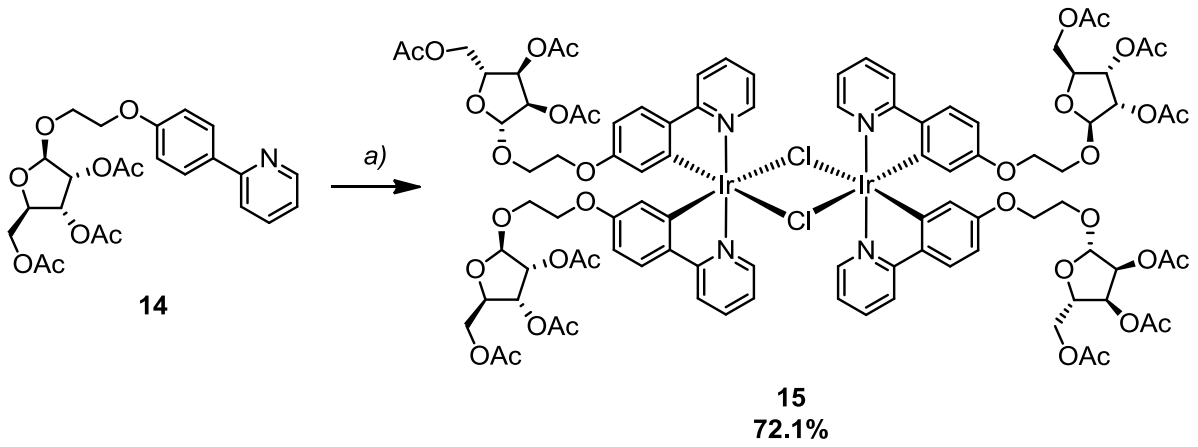

Scheme 25 Synthetic pathway to iridium dimer **15**. Reaction conditions: *a)* $[Ir(cod)Cl]_2$, 2-ethoxyethanol, 130 °C, 2 d.

With the glycosylated cyclometallating ligand **14** in hand, two different routes to obtain iridium dimer **15** were tested: using $IrCl_3 \cdot xH_2O$ in 2-ethoxyethanol/H_2O (3:1)[100,101] or $[Ir(cod)Cl]_2$ in 2-ethoxyethanol (Scheme 25).[102] For both methods, the ligand was dissolved in solvent, iridium source added and the mixture heated at reflux overnight. In the case of

$IrCl_3 \cdot xH_2O$ as starting material, no cyclometallation occurred, as determined by ^1H NMR spectroscopy (Fig. 65). However, starting ligand **14** was not recovered either, suggesting a degradation reaction of the ligand. When cyclometallation takes place, the NMR signal of the proton *ortho* to the Ir–C bond is shifted upfield in a distinctive and significant manner. This is seen for the product of the reaction with $[Ir(cod)Cl]_2$ (bottom spectrum, Fig. 65). Negligible impurities were observed in the ^1H NMR spectrum of dimer **15**, which was therefore used for subsequent transformations without purification.

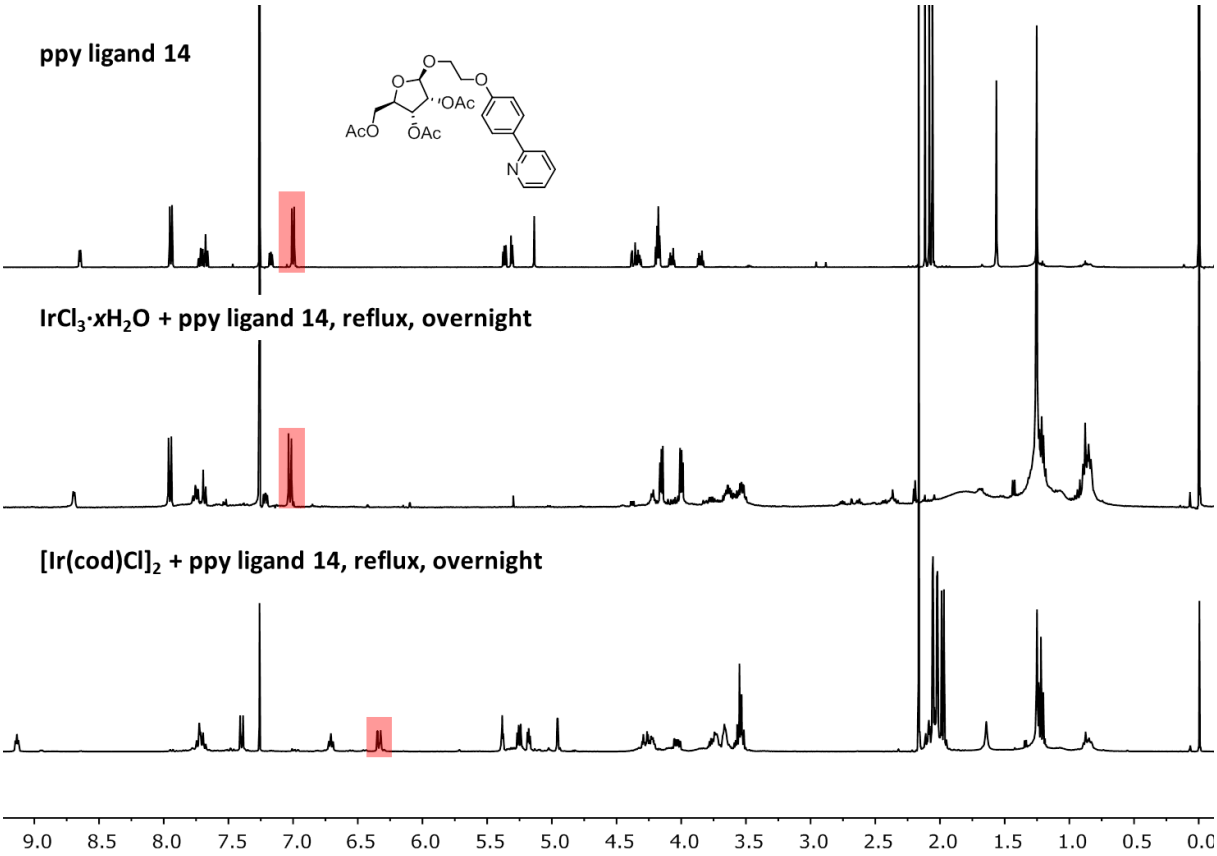

Fig. 65 ^1H NMR spectra of ligand **14** (top) and products of the reactions of ligand **14** with $IrCl_3 \cdot xH_2O$ (middle) and $[Ir(cod)Cl]_2$ (bottom) in $CDCl_3$. The proton in *ortho* position to the Ir–C bond is marked in red; upon cyclometallation, a significant upfield shift takes place (bottom spectrum). Scale: δ/ppm.

2.3. Synthesis of $[Ir(C^N)_2(N^N)][PF_6]$ complexes

Treatment of iridium dimer $[Ir(ppy)_2Cl]_2$ with bpy glycoside **12** under reflux conditions in MeOH followed by anion exchange with an excess of solid NH_4PF_6 led to acetyl-protected complex **16**. Deprotection was performed with sodium methoxide in MeOH and subsequent neutralization with acidic DOWEX 50WX4 resin, according to a procedure described in the literature.[209] Deprotected glycosyl complex **17** was obtained as the $[PF_6]^-$ salt in good yield and was fully characterized (Scheme 26).

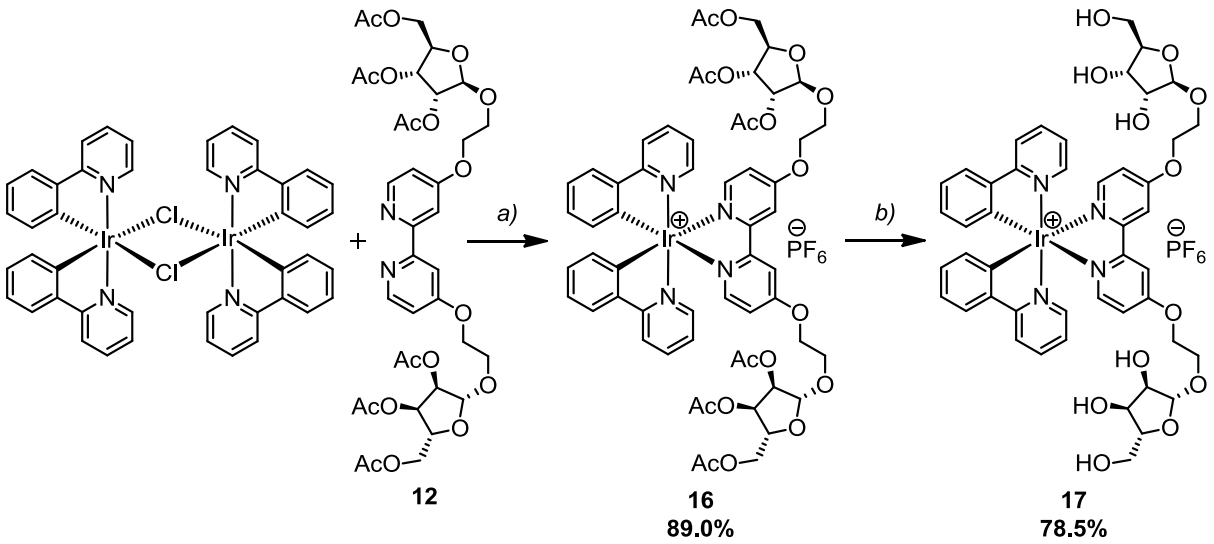

Scheme 26 Synthetic route to iridium complex **17**. Reaction conditions: *a)* MeOH, reflux, overnight, then NH_4PF_6; *b)* NaOMe, MeOH, room temperature, 4.5 h, then DOWEX 50WX4.

In order to enhance the solubility in H_2O, the chloride salt analogue of complex **17** was prepared. In the first step, $[Ir(ppy)_2Cl]_2$ was again reacted with glycosylated ligand **12**, this time without anion metathesis (Scheme 27). This gave protected complex **18** in excellent yield, which was fully characterized by ^1H NMR, ^{13}C NMR and IR spectroscopies, ESI mass spectrometry and elemental analysis. Subsequent deprotection should be carried out analogously to the reaction described for complex **17**.

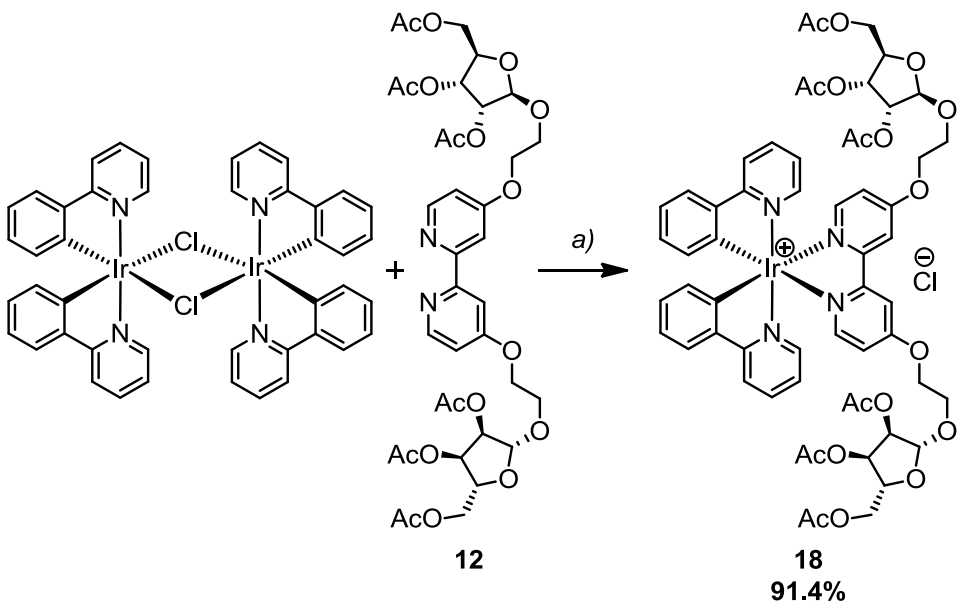

Scheme 27 Synthesis of iridium complex **18**. Reaction conditions: *a)* MeOH, reflux, overnight.

Starting from glycosylated dimer **15**, complex **19** was obtained in excellent yield from the reflux reaction with bpy in MeOH (Scheme 28). This reaction should be repeated on a larger scale and then deprotection carried out according to the procedure described for complex **17**. This appears to be the first report of an iridium complex of the type $[Ir(C\text{^}N)_2(N\text{^}N)]^+$ containing sugar substituents on the cyclometallating ligand, rather than the ancillary ligand.

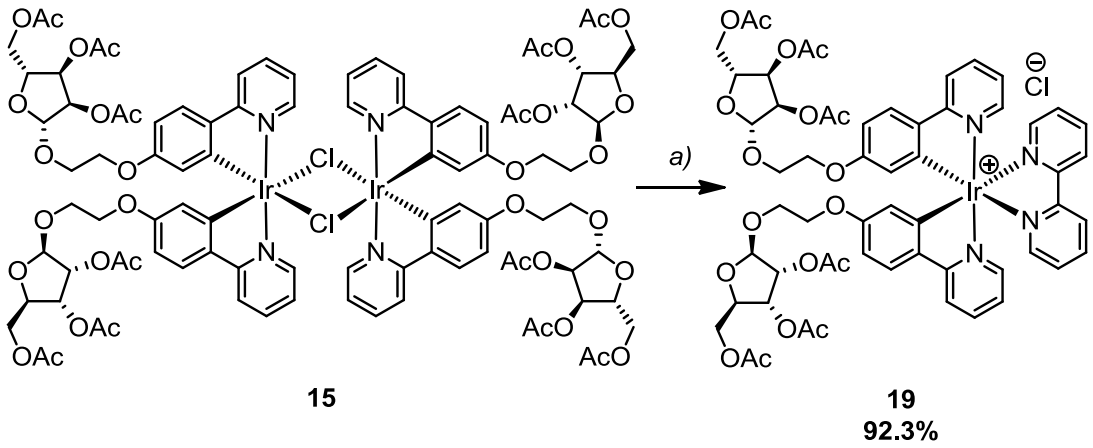

Scheme 28 Synthetic route to iridium complex **19**. Reaction conditions: *a)* bpy, MeOH, reflux, overnight.

2.4. Addition of phenylboronic acid to complex 17

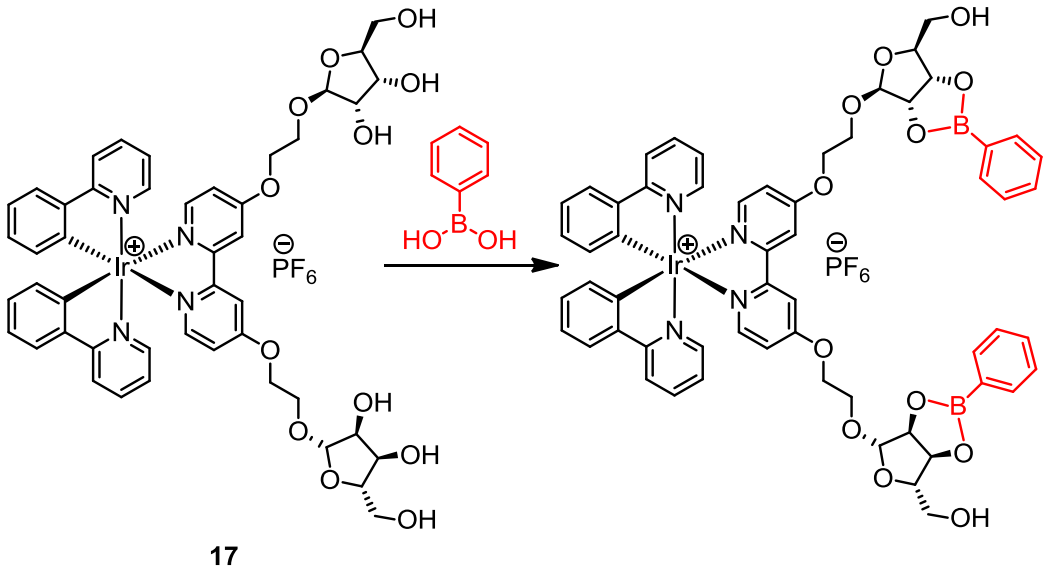

Scheme 29 Addition of phenylboronic acid to deprotected glycosyl complex **17**, leading to binding of the boronic acid to the *cis*-diol of the furanose unit (phenylboronic acid part shown in red).

Boronic acids easily condense with a *cis*-diol moiety of sugars in the fashion shown in Scheme 29.[220] To investigate whether this reaction also takes place with deprotected iridium complex **17**, an excess of solid phenylboronic acid was added to the NMR tube containing complex **17** dissolved in DMSO-d_6. By integration of the obtained ^{1}H NMR spectra taken before and after the addition (Fig. 66), it was possible to show that ester formation indeed occurs. Going from the top to bottom spectrum, the signals of four OH protons disappear, in accordance with the reaction shown in Scheme 29. Photographs were taken of the NMR tube under 366 nm UV light irradiation before and after the addition of phenylboronic acid (Fig. 66). No emission colour change is visible by eye.

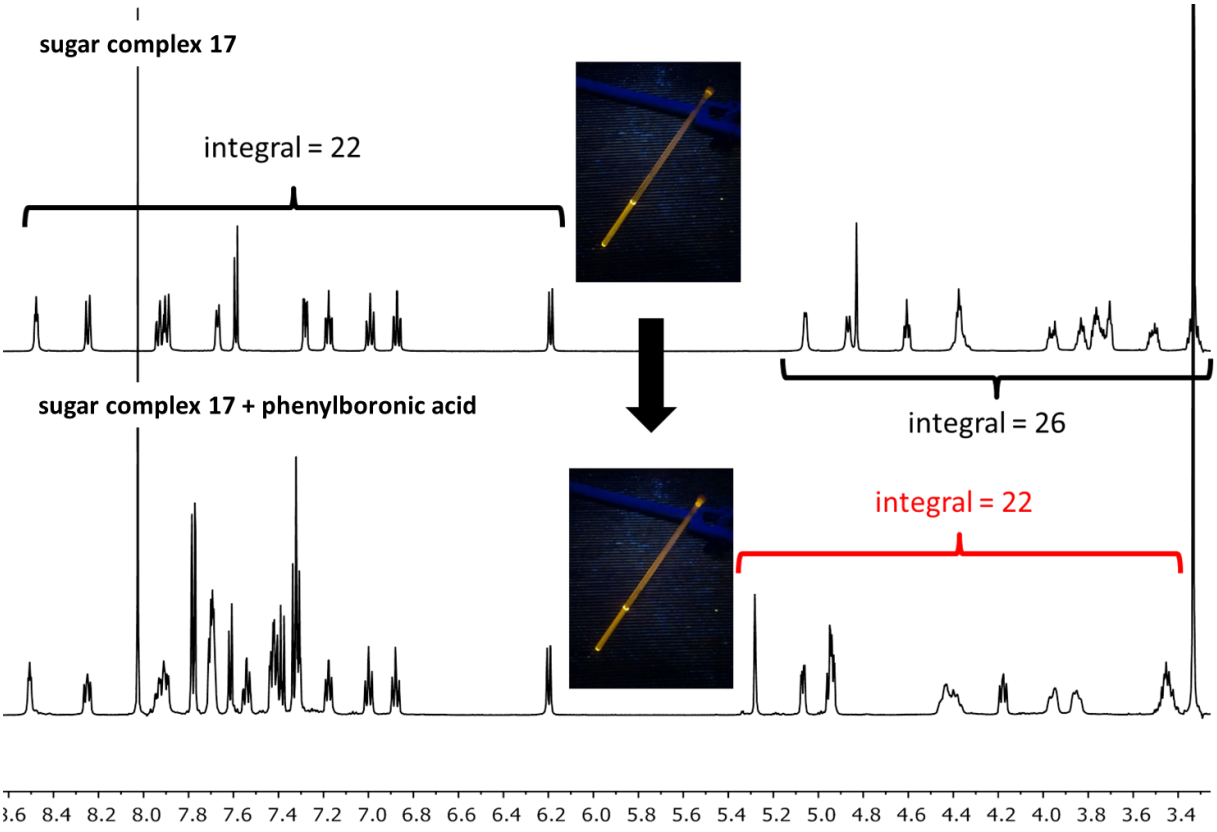

Fig. 66 500 MHz ^{1}H NMR spectra of glycosyl complex **17** in DMSO-d_6 before (top) and after (bottom) the addition of phenylboronic acid to the NMR tube. Due to binding of the phenylboronic acid to the furanose moieties, four proton signals in the alkyl region disappear. The photographs of the NMR tube under 366 nm light irradiation before (top) and after (bottom) the addition of phenylboronic acid show that no emission colour change is visible by eye.

3. Conclusions and Outlook

The synthesis of iridium(III) complexes containing glycosyl moieties either on the ancillary or on the cyclometallating ligand is reported. First, a complex containing ribose-functionalizations on the bpy ancillary ligand was prepared as the $[PF_6]^-$ salt and deprotected to give the free hydroxyl groups. The ribose unit attached to the ligands of the iridium complex readily allows late stage modifications, which can be useful in many fields in which iridium complexes are used. As a proof-of-principle, it was shown that condensation of phenylboronic acid to the *cis*-diol domains of the ribose takes place. As many diverse boronic acids are commercially available, this transformation can be a powerful tool for derivatisation of iridium complexes. Furthermore, the OH group at C-5 position stays unprotected, which allows this position to act as a linker (*e.g.* for the addition of a second iridium complex) or allows transformation into the azide for click chemistry. To improve the solubility in aqueous media, the analogous chloride salt of the complex was prepared and should be deprotected in the next step. Synthesis of the iridium dimer containing glycosylated ppy cyclometallating ligands was followed by cleavage of the chlorido-bridged dimer with bpy to give the corresponding complex, which needs to be deprotected in the next step. This is the first example of an iridium complex containing glycosyl moieties on the cyclometallating, rather than the ancillary ligand.

In the future, scaling up of the reactions will need to be carried out in order to allow for complete characterization and investigation of the photophysical and electrochemical properties.

4. Experimental

4.1. General

$[Ir(cod)Cl]_2$[128] and $[Ir(ppy)_2Cl]_2$[101] were synthesized according to literature procedures. 4,4'-Dihydroxy-2,2'-bipyridine was obtained from Dr. Steffen Müller.

4.2. Brominated ribofuranose 11

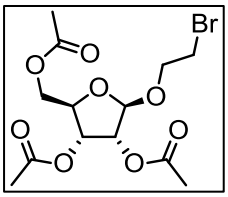

β-D-Ribofuranose 1,2,3,5-tetraacetate (**10**) (986 mg, 3.10 mmol) was dissolved in dry CH_3CN (5 mL) under N_2 atmosphere and a solution of $SnCl_4$ (370 µL, 824 mg, 3.16 mmol) in dry CH_2Cl_2 (3 mL) was added dropwise. The solution was stirred for 15 min at room temperature, then a solution of 2-bromoethanol (220 µL, 387 mg, 3.1 mmol) in dry CH_3CN (5 mL) was added dropwise during 1 h and the mixture was stirred for another 30 min at room temperature. Saturated aq. $NaHCO_3$ solution was added to the mixture at 0 °C, the resulting suspension was filtered over Celite and washed with hot $CHCl_3$ (300 mL). The combined filtrates were washed with H_2O (200 mL) and brine (200 mL), dried over Na_2SO_4 and the solvent was removed under reduced pressure. The crude product was purified by column chromatography (SiO_2, CH_2Cl_2–1% MeOH). The mixed fractions were combined and again purified by column chromatography (SiO_2, cyclohexane/EtOAc 2:1). The pure fractions were combined to yield ribofuranose **11** as colourless oil (455 mg, 1.19 mmol, 38.3%). ^{1}H NMR (400 MHz, $CDCl_3$) δ/ppm 5.34 (dd, J = 7.0, 4.7 Hz, 1H), 5.28 (d, J = 4.8 Hz, 1H), 5.06 (s, 1H), 4.37–4.28 (m, 2H), 4.22–4.10 (m, 1H), 4.01 (dt, J = 10.9, 6.1 Hz, 1H), 3.77 (dt, J = 10.9, 6.3 Hz, 1H), 3.52–3.40 (m, 2H), 2.12 (s, 3H), 2.10 (s, 3H), 2.06 (s, 3H).

4.3. Glycosylated bpy ligand 12

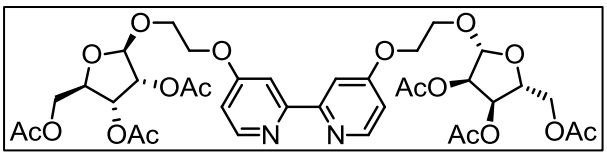

4,4'-Dihydroxy-2,2'-bipyridine (24.6 mg, 130 µmol) and K_2CO_3 (110 mg, 796 µmol) were suspended in dry DMF (2 mL) under N_2 atmosphere and heated at 75 °C for 45 min. A solution of ribofuranose **11** (99.7 mg, 260 µmol) in dry DMF (2 mL) and KI (45.0 mg, 271 µmol) were added and the mixture was stirred overnight. The mixture was let to cool to room temperature and the solvent was evaporated under reduced pressure. The residue was suspended in H_2O and extracted with $CHCl_3$ (3 × 20 mL). The combined organic layers were dried over Na_2SO_4 and the solvent was removed under reduced pressure. The crude product was purified by column chromatography (SiO_2, CH_2Cl_2–8% MeOH) to yield ligand **12** as a colourless solid (66.2 mg, 84.0 µmol, 64.0%). ^{1}H NMR (400 MHz, $CDCl_3$) δ/ppm 8.47 (d, J = 5.7 Hz, 2H), 7.97 (d, J = 2.5 Hz, 2H), 6.87 (dd, J = 5.7, 2.6 Hz, 2H), 5.35 (dd, J = 6.5, 4.9 Hz, 2H), 5.31–5.28 (m, 2H), 5.13 (s, 2H), 4.40–4.27 (overlapping m, 8H), 4.22–4.14 (m, 2H), 4.13–4.05 (m, 2H), 3.91–

3.83 (m, 2H), 2.11 (s, 6H), 2.08 (s, 6H), 2.06 (s, 6H). ^{1}H NMR spectroscopic data matched those reported in the literature.[217]

4.4. 2-(4-Hydroxyphenyl)pyridine (13)

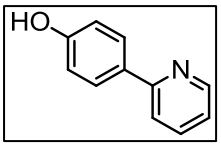

$Pd(OAc)_2$ (4.43 mg, 19.7 µmol), 4-hydroxyphenylboronic acid (405 mg, 2.94 mmol) and K_3PO_4 (825 mg, 3.89 mmol) were suspended in ethylene glycol (12 mL). 2-bromopyridine (190 µL, 314 mg, 1.98 mmol) was added and the mixture was heated at 80 °C for 2 h, after which the mixture was let to cool to room temperature. The mixture was poured into H_2O (100 mL) and brine (100 mL) and the resulting suspension was stirred for 30 min at room temperature. The mixture was filtered. The filtrate was extracted with CH_2Cl_2 (2 × 200 mL) and the combined organic layers were dried over Na_2SO_4. The solid which was collected by filtration was washed with H_2O and redissolved with CH_2Cl_2. The solutions were combined and the solvent was removed under reduced pressure. The residue was purified by column chromatography (SiO_2, cyclohexane/EtOAc 1:1) to yield 2-(4-hydroxyphenyl)pyridine (**13**) as an off-white solid (300 mg, 1.75 mmol, 88.3%). ^{1}H NMR (400 MHz, $CDCl_3$) δ/ppm 8.64 (ddd, J = 4.9, 1.9, 1.0 Hz, 1H), 7.89–7.82 (m, 2H), 7.73 (ddd, J = 8.0, 7.4, 1.8 Hz, 1H), 7.66 (dt, J = 8.0, 1.1 Hz, 1H), 7.19 (ddd, J = 7.4, 4.9, 1.2 Hz, 1H), 6.92–6.84 (m, 2H), 6.15 (s, 1H). ^{1}H NMR spectroscopic data matched those reported in the literature.[219]

4.5. Glycosylated ppy ligand 14

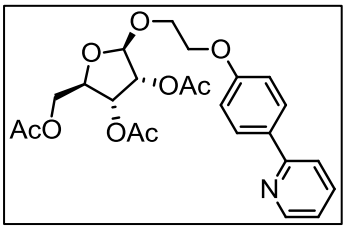

2-(4-Hydroxyphenyl)pyridine (**13**) (44.5 mg, 260 µmol) and K_2CO_3 (109 mg, 785 µmol) were suspended in dry DMF (2 mL) under N_2 atmosphere and heated at 75 °C for 45 min. A solution of glycoside **11** (101 mg, 263 µmol) in dry DMF (2 mL) was added and the mixture was stirred for 2 h at 75 °C. KI (43.4 mg, 261 µmol) was added and the mixture was stirred overnight at 75 °C. The mixture was let to cool to room temperature and the solvent was evaporated under reduced pressure. The residue was suspended in H_2O and extracted with $CHCl_3$ (3 × 20 mL). The combined organic layers were dried over Na_2SO_4 and the solvent was removed under reduced pressure. The crude product was purified by column chromatography (SiO_2, EtOAc/cyclohexane 1:1) to yield ligand **14** as brownish oil (93.3 mg, 197 µmol, 75.8%). ^{1}H NMR (500 MHz, $CDCl_3$) δ/ppm 8.64 (ddd, J = 4.9, 1.9, 1.0 Hz, 1H), 7.97–7.91 (m, 2H), 7.71 (ddd, J = 8.1, 7.3, 1.8 Hz, 1H),

7.66 (dt, *J* = 8.1, 1.2 Hz, 1H), 7.17 (ddd, *J* = 7.2, 4.8, 1.3 Hz, 1H), 7.02–6.97 (m, 2H), 5.36 (dd, *J* = 6.7, 4.9 Hz, 1H), 5.31 (dd, *J* = 4.9, 0.9 Hz, 1H), 5.13 (d, *J* = 0.9 Hz, 1H), 4.39–4.30 (m, 2H), 4.21–4.14 (m, 3H), 4.07 (dt, *J* = 11.1, 4.5 Hz, 1H), 3.85 (dt, *J* = 11.0, 4.8 Hz, 1H), 2.11 (s, 3H), 2.08 (s, 3H), 2.05 (s, 3H). $^{13}C\{^{1}H\}$ NMR (126 MHz, $CDCl_3$) δ/ppm 170.8, 169.80, 169.75, 159.6, 157.2, 149.7, 136.8, 132.5, 128.3, 121.6, 120.0, 114.9, 105.6, 78.9, 74.9, 71.7, 67.1, 66.5, 64.9, 21.0, 20.8, 20.7. IR (solid, $\tilde{\nu}$/cm^{-1}) 2935 (w), 1743 (s), 1607 (w), 1587 (w), 1564 (w), 1515 (w), 1467 (m), 1436 (m), 1369 (m), 1216 (s), 1178 (m), 1094 (s), 1043 (s), 988 (m), 961 (m), 925 (m), 899 (m), 841 (m), 781 (s), 744 (w), 719 (w), 638 (w), 604 (m), 555 (w), 498 (w). LC-ESI-MS *m/z* 474.2 $[M+H]^+$ (calc. 474.2). Found C 60.18, H 5.84, N 2.88; $C_{24}H_{27}NO_9 \cdot 0.5H_2O$ requires C 59.74, H 5.84, N 2.90%.

4.6. Iridium dimer 15

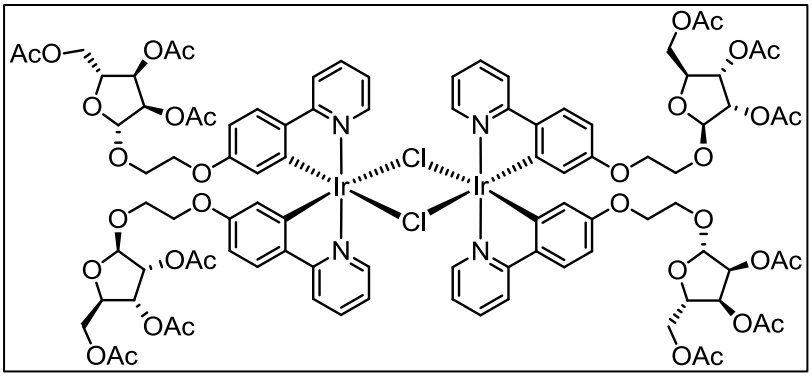

Glycosylated ligand **14** (30.0 mg, 63.4 µmol) and $[Ir(cod)Cl]_2$ (10.6 mg, 158 µmol) were suspended in 2-ethoxyethanol in a microwave vial, sealed and heated at 130 °C for 2 d. The mixture was let to cool to room temperature and a few drops of H_2O were added. The resulting precipitate was filtered off and washed with EtOH. The solid was redissolved with CH_2Cl_2 and the solvent was removed under reduced pressure to yield dimer **15** as an orange solid (13.4 mg, 6.0 µmol, 72.1%).

4.7. Protected ribose complex 16

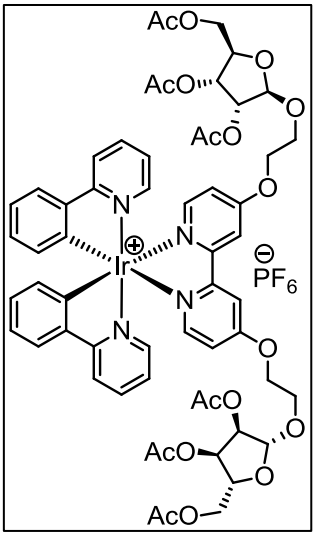

$[Ir(ppy)_2Cl]_2$ (42.3 mg, 39.5 µmol) and ligand **12** (62.4 mg, 78.7 µmol) were suspended in MeOH (5 mL) and heated at reflux overnight. The suspension was let to cool to room temperature, filtered through Celite®, washed with MeOH and the filtrate was concentrated under reduced pressure. The residue was dissolved in little MeOH, an excess of solid NH_4PF_6 was added and the mixture was stirred at room temperature for 15 min. H_2O was added until precipitation was observed and the suspension was stirred for another 15 min at room temperature. The precipitate was filtered off, washed with H_2O and MeOH and redissolved with CH_2Cl_2. The solvent was removed under reduced pressure. The residue was purified by column chromatography (SiO_2, CH_2Cl_2–2% MeOH changing to CH_2Cl_2–4% MeOH) to yield complex **16** as a yellow solid (101 mg, 70.0 µmol, 89.0%). ^{1}H NMR (250 MHz, CD_3CN) δ/ppm 8.13–7.98 (m, 4H), 7.90–7.74 (m, 4H), 7.72 (d, J = 6.4 Hz, 2H), 7.70–7.62 (m, 2H), 7.10–6.96 (m, 6H), 6.89 (td, J = 7.4, 1.4 Hz, 2H), 6.27 (dd, J = 7.6, 1.3 Hz, 2H), 5.21–5.11 (m, 4H), 5.11–5.05 (m, 2H), 4.39–4.22 (m, 8H), 4.16–3.98 (m, 4H), 3.84 (dt, J = 11.7, 4.4 Hz, 2H), 2.05 (s, 3H), 2.05 (s, 3H), 2.00 (s, 6H), 1.98 (s, 3H), 1.96 (s, 3H).

4.8. Deprotected ribose complex 17

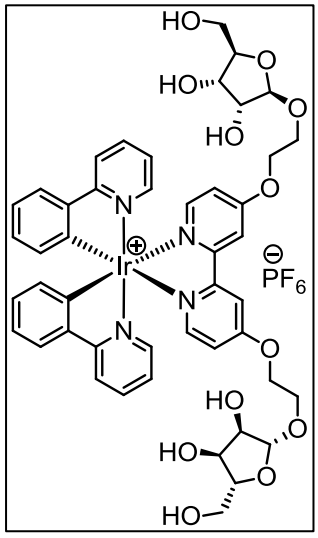

NaOMe (3.28 mg, 59.5 µmol) was added to a solution of complex **16** (85.9 mg, 59.7 µmol) in MeOH (7 mL). The mixture was stirred at room temperature for 4.5 h. DOWEX 50WX4 (washed subsequently with H_2O, 1 M HCl, H_2O and MeOH) was added to neutralize the mixture. The DOWEX was removed by filtration and the filtrate was concentrated under reduced pressure. The residue was suspended in CH_3CN, filtered over Celite® and the filtrate was concentrated under reduced pressure to yield complex **17** as a yellow solid (55.6 mg, 47.0 µmol, 78.5%). ^{1}H NMR (500 MHz, dmso-d_6) δ/ppm 8.51–8.44 (m, 2H), 8.25 (dt, J = 8.5, 1.0 Hz, 2H), 7.97–7.85 (m, 4H), 7.70–7.62 (m, 2H), 7.59 (d, J = 6.4 Hz, 2H), 7.28 (dd, J = 6.5, 2.6 Hz, 2H), 7.18 (ddd, J = 7.4, 5.8, 1.4 Hz, 2H), 6.99 (td, J = 7.5, 1.2 Hz, 2H), 6.87 (td, J = 7.4, 1.3 Hz, 2H), 6.19 (dd, J = 7.6, 1.2 Hz, 2H), 5.06 (dd, J = 4.5, 1.7 Hz, 2H), 4.87 (d, J = 6.7 Hz,

2H), 4.83 (t, *J* = 1.1 Hz, 2H), 4.61 (td, *J* = 5.7, 1.3 Hz, 2H), 4.42–4.31 (m, 4H), 3.96 (ddd, *J* = 11.7, 5.4, 3.2 Hz, 2H), 3.83 (ddd, *J* = 11.2, 6.5, 4.8 Hz, 2H), 3.80–3.67 (m, 6H), 3.51 (ddt, *J* = 11.7, 5.6, 3.7 Hz, 2H), 3.33 (s, 2H). IR (solid, $\tilde{\nu}$/cm^{-1}) 3373 (w), 2927 (w), 1608 (m), 1583 (w), 1558 (w), 1478 (m), 1439 (m), 1420 (m), 1330 (m), 1315 (m), 1268 (m), 1250 (m), 1222 (m), 1165 (w), 1098 (m), 1030 (s), 949 (m), 831 (s), 757 (s), 738 (s), 669 (m), 630 (m), 556 (s). ESI-MS *m/z* 1041.6 $[M-PF_6]^+$ (calc. 1041.3). Found C 43.53, H 4.34, N 4.13; $C_{46}H_{48}F_6IrN_4O_{12}P\cdot 0.5H_2O$ requires C 43.60, H 4.53, N 4.42%.

4.9. Protected ribose complex 18

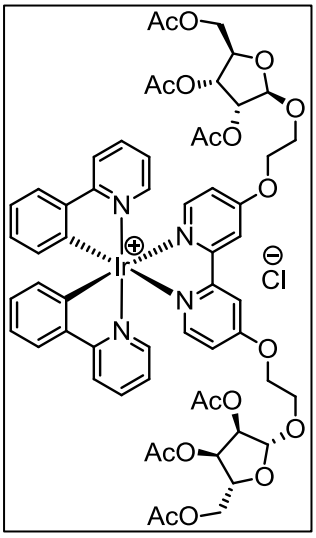

$[Ir(ppy)_2Cl]_2$ (44.6 mg, 41.6 µmol) and ligand **12** (65.7 mg, 82.9 µmol) were suspended in MeOH (5 mL) and heated at reflux overnight. The suspension was let to cool to room temperature, filtered through cotton, washed with MeOH and the filtrate was concentrated under reduced pressure. The crude product was purified by column chromatography (SiO_2, CH_2Cl_2–10% MeOH) to yield complex **18** as a yellow powder (101 mg, 76.0 µmol, 91.4%). ^{1}H NMR (500 MHz, CD_3CN) δ/ppm 8.31 (s, 2H), 8.05 (dt, *J* = 8.2, 1.0 Hz, 2H), 7.86–7.80 (m, 2H), 7.78 (dd, *J* = 8.0, 1.3 Hz, 2H), 7.70 (d, *J* = 6.4 Hz, 2H), 7.69–7.67 (m, 2H), 7.05 (ddd, *J* = 7.4, 5.8, 1.4 Hz, 2H), 7.00 (td, *J* = 6.9, 1.9 Hz, 4H), 6.88 (td, *J* = 7.4, 1.3 Hz, 2H), 6.27 (dd, *J* = 7.6, 1.2 Hz, 2H), 5.17 (dd, *J* = 6.5, 4.7 Hz, 2H), 5.14–5.09 (m, 4H), 4.50–4.40 (m, 4H), 4.31–4.25 (m, 4H), 4.12–4.07 (m, 2H), 4.07–4.00 (m, 2H), 3.87–3.80 (m, 2H), 2.05 (s, 3H), 2.04 (s, 3H), 2.00 (s, 6H), 1.98 (s, 3H), 1.97 (s, 3H). ^{13}C{^{1}H} NMR (126 MHz, CD_3CN) δ/ppm 171.50, 171.49, 170.8, 170.64, 170.63, 168.4, 168.0, 158.4, 152.2, 151.8, 150.0, 145.1, 139.2, 132.5, 131.2, 125.7, 124.3, 123.2, 120.6, 115.4, 112.81, 112.79, 106.01, 105.97, 79.4, 75.1, 72.6, 69.8, 66.5, 66.4, 65.60, 65.57, 21.0, 20.73, 20.66. IR (solid, $\tilde{\nu}$/cm^{-1}) 2935 (w), 1740 (s), 1607 (s), 1583 (w), 1556 (w), 1478 (m), 1437 (m), 1369 (m), 1337 (w), 1218 (s), 1164 (m), 1036 (s), 961 (m), 897 (m), 796 (w), 761 (s), 738 (s), 669 (m), 630 (m), 603 (m). ESI-MS *m/z* 1293.8 $[M-PF_6]^+$ (calc. 1293.4). Found C 50.76, H 4.90, N 4.24; $C_{58}H_{60}ClIrN_4O_{18}\cdot 2H_2O$ requires C 51.04, H 4.73, N 4.11%.

4.10. Protected ribose complex 19

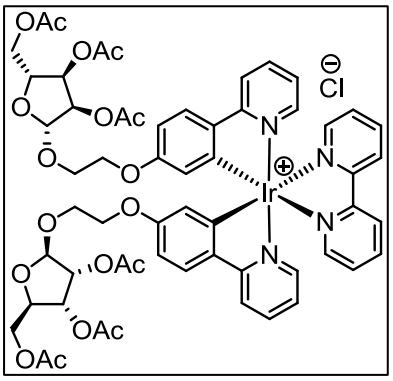

Dimer **15** (13.4 mg, 5.71 µmol) and bpy (1.78 mg, 11.4 µmol) were suspended in MeOH (2 mL) and heated at reflux overnight. The solution was let to cool to room temperature, filtered through cotton, washed with MeOH and the filtrate was concentrated under reduced pressure. The crude product was purified by column chromatography (SiO_2, CH_2Cl_2–10% MeOH changing to CH_2Cl_2–20% MeOH) to yield complex **19** as a yellow solid (14.0 mg, 11.0 µmol, 92.3%). ^{1}H NMR (500 MHz, CD_3CN) δ/ppm 8.59 (d, J = 8.2 Hz, 2H), 8.13 (td, J = 7.9, 1.6 Hz, 2H), 8.07–8.01 (m, 2H), 7.93 (dt, J = 8.3, 0.9 Hz, 2H), 7.81–7.72 (m, 4H), 7.51 (ddd, J = 7.7, 5.6, 1.1 Hz, 4H), 6.93 (dddd, J = 7.4, 5.9, 2.3, 1.4 Hz, 2H), 6.64 (ddd, J = 8.6, 2.6, 0.8 Hz, 2H), 5.72 (dd, J = 2.5, 1.1 Hz, 2H), 5.15 (ddd, J = 6.9, 4.9, 2.3 Hz, 2H), 5.09 (dd, J = 4.9, 0.9 Hz, 2H), 5.00 (d, J = 1.0 Hz, 2H), 4.29–4.20 (m, 4H), 4.04–3.97 (m, 2H), 3.94–3.80 (m, 4H), 3.68–3.59 (m, 2H), 2.05 (s, 3H), 2.04 (s, 3H), 2.00 (s, 3H), 2.00 (s, 3H), 1.96 (s, 3H), 1.94 (s, 3H).

CONCLUSIONS AND OUTLOOK

Sulfur-functionalizations were introduced to the cyclometallating and ancillary ligands of iridium(III) complexes to achieve emission colour tuning over the whole visible region, from blue to red.

By placing thioether and sulfone substituents on the cyclometallating ligands it was possible to obtain yellow and green emitters. This highlights the potential of electron-withdrawing sulfone groups to replace the widely used fluorine substituents in iridium complexes to reach blue-shifted emission. Different alkyl substituents on the sulfur moieties were investigated; these had no or negligible influences on photoluminescence maxima and electrochemical properties. High solution quantum yields of 64 and 74% were observed for complexes containing sulfone-functionalized C^N ligands. The most promising candidates from this series were tested in light-emitting electrochemical cells, resulting in yellow-green electroluminescence. Unfortunately, low luminance levels and device efficiencies were observed, together with short lifetimes of less than 69 min.

In the above described series of complexes, substituents were placed exclusively in 5-position of the cyclometallating ligands, *meta* to the Ir–C bond. Thus, as a next step, the influence of the substitution position on photophysical, electrochemical and device properties was investigated. For this, a series of regioisomeric iridium complexes containing a methylsulfonyl group in 3-, 4- or 5-position of the C^N ligands was prepared. Within this series, the two complexes containing the substituent in *meta* position to the Ir–C bond (3- and 5-position) showed similar properties in terms of quantum yields, excited state lifetimes and structured emission spectra in solution. Substitution in 4-position (*para* to the Ir–C bond) resulted in enhanced quantum yields both in solution (92%) and powder (27%) compared to the other two complexes. Furthermore, a broad, featureless photoluminescence spectrum was observed in solution. This indicates that for the complex containing the sulfone group in 4-position, the charge transfer character of the emissive triplet state is higher than for the complexes containing the substituent in *meta* position to the Ir–C bond. All compounds are green emitters in solution and yellow emitters as powder samples. In LEECs, the 4-substituted

complex yielded the best performance with respect to maximum luminance (940 cd m^{-2}) and efficiency (EQE = 2.6%). However, device stability is limited for all complexes in this series ($t_{1/2} \leq 69$ min).

In order to shift the emission further to the blue, electron-deficient sulfone-functionalized cyclometallating ligands were combined with electron-rich ancillary ligands. Pyrazolylpyridines were chosen as N^N ligands; together, this should lead to a stabilization of the HOMO and destabilization of the LUMO and thus a widening of the energy gap. In fact, the synthesized complexes are green or blue emitters in solution, depending on the substitution position of the methylsulfonyl group. In LEEC devices, all complexes exhibit green electroluminescence, low efficiencies (EQE = 0.2–0.4%) and lifetimes in the order of a few minutes.

The use of ancillary ligands containing benzothiazole units gave complexes with dark orange to deep red photoluminescence (in CH_2Cl_2 solution, thin film and as powder samples) and electroluminescence. Based on the simple benzothiazolylpyridine (btzpy), different functionalizations were introduced to the N^N ligand and the device properties of the corresponding complexes with 2-phenylpyridine (ppy) as cyclometallating ligand investigated. In a second series, different C^N ligands were combined with btzpy. For complex $[Ir(ppy)_2(btzpy)][PF_6]$, excellent device stability was observed when operated under average current densities of both 100 and 700 A m^{-2} ($t_{1/2}$ >1000 h). Addition of a *tert*-butyl group or a pendant phenyl ring on the ancillary ligand leads to complexes with further enhanced lifetimes of over 4500 h. Moreover, luminance and efficiency levels are increased. Both the ppy cyclometallating ligand and the benzothiazole moiety seem to be crucial for long LEEC lifetimes. Replacing either ppy by another C^N ligand or benzothiazole by benzoxazole leads to significantly reduced device stability. The lifetimes reported for this series are by far the longest reported for iridium-based red light emitting electrochemical cells.

It was possible to highlight the potential of sulfone groups to act as an alternative to the widely used fluorine substituents in order to shift the emission to the blue. Whereas blue emission was observed in solution, all complexes showed green electroluminescence in device configuration. The introduction of a second sulfone group on the cyclometallating

ligand might lead to a blue-shift in the electroluminescence maximum. Unfortunately, the LEEC stability of all sulfone-containing complexes was poor, with lifetimes ranging from a few minutes to approximately an hour. This observation leads to the assumption that either the sulfone group is unstable under driving conditions (similar to fluorine substituents) or that instability is an inherent feature of iridium complexes with a large HOMO-LUMO energy gap. To enhance stability, modifications can be made to the ligands; for example, by placing bulky groups or a π-stacking phenyl ring on the ancillary ligand. Another possibility is the introduction of steric hindrance to the cyclometallating ligands, shielding the sulfone group from degradation. Combined with the idea of two sulfone substituents on the C^N ligand, it might be interesting to investigate the effect of connecting these two groups; this goal can be achieved for example by the use of a thianthrene tetraoxide core.

As for the benzothiazole-based red emitters, it might be possible to further enhance LEEC performance by a combination of the beneficial effects of a *tert*-butyl substituent and a pendant phenyl ring on the ancillary ligand. In addition, the use of other cyclometallating ligands might also result in an increased device performance.

Glycosylated iridium complexes are a promising field of research, for they can be applied as phosphorescent labels, sensors, drugs, catalysts, *etc*. By a condensation reaction, ribofuranose-functionalized complexes can be easily modified with boronic acids, making these glycosyl compounds highly versatile intermediates. In the future, the potential of such transformations in addition to the photophysical and electrochemical properties of such iridium(III) complexes will be investigated.

REFERENCES

1 *APEX2, version 2 User Manual*, M86-E01078, Bruker Analytical X-ray Systems, Inc., Madison, WI, 2006.

2 G. M. Sheldrick, *Acta Crystallogr. Sect. A Found. Crystallogr.*, 2008, **A64**, 112–122.

3 P. W. Betteridge, J. P. Carruthers, R. I. Cooper, K. Prout and D. J. Watkin, *J. Appl. Crystallogr.*, 2003, **36**, 1487.

4 M. J. Frisch, G. W. Trucks, H. B. Schlegel, G. E. Scuseria, M. A. Robb, J. R. Cheeseman, G. Scalmani, V. Barone, B. Mennucci, G. A. Petersson, H. Nakatsuji, M. Caricato, X. Li, H. P. Hratchian, A. F. Izmaylov, J. Bloino, G. Zheng, J. L. Sonnenberg, M. Hada, M. Ehara, K. Toyota, R. Fukuda, J. Hasegawa, M. Ishida, T. Nakajima, Y. Honda, O. Kitao, H. Nakai, T. Vreven, J. A. Montgomery, Jr, J. E. Peralta, F. Ogliaro, M. Bearpark, J. J. Heyd, E. Brothers, K. N. Kudin, V. N. Staroverov, R. Kobayashi, J. Normand, K. Raghavachari, A. Rendell, J. C. Burant, S. S. Iyengar, J. Tomasi, M. Cossi, N. Rega, N. J. Millam, M. Klene, J. E. Knox, J. B. Cross, V. Bakken, C. Adamo, J. Jaramillo, R. Gomperts, R. E. Stratmann, O. Yazyev, A. J. Austin, R. Cammi, C. Pomelli, J. W. Ochterski, R. L. Martin, K. Morokuma, V. G. Zakrzewski, G. A. Voth, P. Salvador, J. J. Dannenberg, S. Dapprich, A. D. Daniels, O. Farkas, J. B. Foresman, J. V. Ortiz, J. Cioslowski and D. J. Fox, *Gaussian 09, Revision D.01*, Gaussian, Inc., Wallingford, CT, 2009.

5 A. D. Becke, *J. Chem. Phys.*, 1993, **98**, 5648–5652.

6 C. Lee, W. Yang and R. G. Parr, *Phys. Rev. B*, 1988, **37**, 785–789.

7 M. M. Francl, W. J. Pietro, W. J. Hehre, J. S. Binkley, M. S. Gordon, D. J. DeFrees and J. A. Pople, *J. Chem. Phys.*, 1982, **77**, 3654–3665.

8 P. J. Hay and W. R. Wadt, *J. Chem. Phys.*, 1985, **82**, 299–310.

9 J. Tomasi, B. Mennucci and R. Cammi, *Chem. Rev.*, 2005, **105**, 2999–3093.

10 J. Tomasi and M. Persico, *Chem. Rev.*, 1994, **94**, 2027–2094.

11 C. S. Cramer and D. G. Truhlar, in *Solvent Effects and Chemical Reactivity*, Kluwer, Dordrecht, 1996, pp. 1–80.

12 M. Petersilka, U. J. Gossmann and E. K. U. Gross, *Phys. Rev. Lett.*, 1996, **76**, 1212–1215.

13 M. E. Casida, C. Jamorski, K. C. Casida and D. R. Salahub, *J. Chem. Phys.*, 1998, **108**, 4439–4449.

14 C. Jamorski, M. E. Casida and D. R. Salahub, *J. Chem. Phys.*, 1996, **104**, 5134–5147.

15 *http://www.light2015.org/Home.html*, 05.02.2016.

16 C. E. Housecroft and A. G. Sharpe, *Inorganic Chemistry*, Pearson, Essex, 3rd ed., 2008.

17 P. W. Atkins and J. de Paula, *Physikalische Chemie*, Wiley-VCH, Weinheim, 4th ed., 2006.

18 C. E. Housecroft and E. C. Constable, *Chem. Soc. Rev.*, 2015, **44**, 8386–8398.

19 J. Clayden, N. Greeves, S. Warren and P. Wothers, *Organic Chemistry*, Oxford University Press, Oxford, 1st ed., 2001.

20 N. Armaroli and V. Balzani, *Energy Environ. Sci.*, 2011, **4**, 3193–3222.

21 R. D. Costa, E. Ortí, H. J. Bolink, F. Monti, G. Accorsi and N. Armaroli, *Angew. Chem. Int. Ed.*, 2012, **51**, 8178–8211.

22 *http://www.theskepticsguide.org/humans-seeing-infrared-light-kind-of*, 04.02.2016.

23 *http://www.centennialbulb.org/*, 06.02.2016.

24 M. Krajewski, *IEEE Spectr.*, 2014, **51**, 56–61.

25 *https://commons.wikimedia.org/wiki/File:Livermore_Centennial_Light_Bulb.jpg*, 06.02.2016.

26 E. J. Gago, T. Muneer, M. Knez and H. Köster, *Renew. Sustain. Energy Rev.*, 2015, **41**, 1–13.

27 B. Bowers, *IEEE Spectr.*, 2011, **48**, 44–52.

28 *http://www.tagesanzeiger.ch/leben/rat-und-tipps/Grosses-Lichterlschen-fr-die-Glhbirnen/story/25999013*, 06.02.2016.

29 *http://www.reuters.com/article/us-lightbulbs-env-idUSN2529253520070425*, 06.02.2016.

30 C.-C. Lin, K.-J. Chen, D.-W. Lin, H.-V. Han, W.-C. Lai, J.-J. Huang, T.-C. Lu, S.-J. Chang and H.-C. Kuo, *Top. Appl. Phys.*, 2015, **129**, 337–354.

31 P. Pust, P. J. Schmidt and W. Schnick, *Nat. Mater.*, 2015, **14**, 454–458.

32 *'The Nobel Prize Phys. 2014'. Nobelprize.org. Nobel Media AB 2014. Web. 01.02.2016. <http//www.nobelprize.org/nobel_prizes/physics/laureates/2014/>*.

33 S. Nakamura, *Angew. Chem. Int. Ed.*, 2015, **54**, 7770–7788.

34 H. Amano, *Angew. Chem. Int. Ed.*, 2015, **54**, 7764–7769.

35 I. Akasaki, *Angew. Chem. Int. Ed.*, 2015, **54**, 7750–7763.

36 J. Godlewski and M. Obarowska, *Opto-Electronics Rev.*, 2007, **15**, 179–183.

37 O. Nuyken, S. Jungermann, V. Wiederhirn, E. Bacher and K. Meerholz, *Monatshefte für Chemie - Chem. Mon.*, 2006, **137**, 811–824.

38 A. Bergh, G. Craford, A. Duggal and R. Haitz, *Phys. Today*, 2001, **54**, 42.

39 Q. Pei, G. Yu, C. Zhang, Y. Yang and A. J. Heeger, *Science*, 1995, **269**, 1086–1088.

40 K. M. Maness, R. H. Terrill, T. J. Meyer, R. W. Murray and R. M. Wightman, *J. Am. Chem. Soc.*, 1996, **118**, 10609–10616.

41 J.-K. Lee, D. S. Yoo, E. S. Handy and M. F. Rubner, *Appl. Phys. Lett.*, 1996, **69**, 1686–1688.

42 J.-C. Leprêtre, A. Deronzier and O. Stéphan, *Synth. Met.*, 2002, **131**, 175–183.

43 S. Bernhard, J. A. Barron, P. L. Houston, H. D. Abruña, J. L. Ruglovksy, X. Gao and G. G. Malliaras, *J. Am. Chem. Soc.*, 2002, **124**, 13624–13628.

44 M. Buda, G. Kalyuzhny and A. J. Bard, *J. Am. Chem. Soc.*, 2002, **124**, 6090–6098.

45 H. Rudmann, S. Shimada and M. F. Rubner, *J. Am. Chem. Soc.*, 2002, **124**, 4918–4921.

46 H. Rudmann and M. F. Rubner, *J. Appl. Phys.*, 2001, **90**, 4338–4345.

47 F. G. Gao and A. J. Bard, *J. Am. Chem. Soc.*, 2000, **122**, 7426–7427.

48 C. M. Elliott, F. Pichot, C. J. Bloom and L. S. Rider, *J. Am. Chem. Soc.*, 1998, **120**, 6781–6784.

49 S. Bernhard, X. Gao, G. G. Malliaras and H. D. Abruña, *Adv. Mater.*, 2002, **14**, 433–436.

50 F. G. Gao and A. J. Bard, *Chem. Mater.*, 2002, **14**, 3465–3470.

51 J. D. Slinker, A. A. Gorodetsky, M. S. Lowry, J. Wang, S. Parker, R. Rohl, S. Bernhard and G. G. Malliaras, *J. Am. Chem. Soc.*, 2004, **126**, 2763–2767.

52 M. Lenes, G. Garcia-Belmonte, D. Tordera, A. Pertegás, J. Bisquert and H. J. Bolink, *Adv. Funct. Mater.*, 2011, **21**, 1581–1586.

53 D. Tordera, S. Meier, M. Lenes, R. D. Costa, E. Ortí, W. Sarfert and H. J. Bolink, *Adv. Mater.*, 2012, **24**, 897–900.

54 M. V. Werrett, G. S. Huff, S. Muzzioli, V. Fiorini, S. Zacchini, B. W. Skelton, A. Maggiore, J. M. Malicka, M. Cocchi, K. C. Gordon, S. Stagni and M. Massi, *Dalton Trans.*, 2015, **44**, 8379–8393.

55 O. Moudam, A. C. Tsipis, S. Kommanaboyina, P. N. Horton and S. J. Coles, *RSC Adv.*, 2015, **5**, 95047–95053.

56 N. Armaroli, G. Accorsi, M. Holler, O. Moudam, J.-F. Nierengarten, Z. Zhou, R. T. Wegh and R. Welter, *Adv. Mater.*, 2006, **18**, 1313–1316.

57 R. D. Costa, D. Tordera, E. Ortí, H. J. Bolink, J. Schönle, S. Graber, C. E. Housecroft, E. C. Constable and J. A. Zampese, *J. Mater. Chem.*, 2011, **21**, 16108–16118.

58 S. Keller, E. C. Constable, C. E. Housecroft, M. Neuburger, A. Prescimone, G. Longo, A. Pertegás, M. Sessolo and H. J. Bolink, *Dalton Trans.*, 2014, **43**, 16593–16596.

59 S. Keller, A. Pertegás, G. Longo, L. Martínez, J. Cerdá, J. M. Junquera-Hernández, A. Prescimone, E. C. Constable, C. E. Housecroft, E. Ortí and H. J. Bolink, *J. Mater. Chem. C*, 2016.

60 O. Moudam, A. Kaeser, B. Delavaux-Nicot, C. Duhayon, M. Holler, G. Accorsi, N. Armaroli, I. Séguy, J. Navarro, P. Destruel and J.-F. Nierengarten, *Chem. Commun.*, 2007, 3077–3079.

61 Q. Zhang, Q. Zhou, Y. Cheng, L. Wang, D. Ma, X. Jing and F. Wang, *Adv. Funct. Mater.*, 2006, **16**, 1203–1208.

62 A. Pertegás, D. Tordera, J. J. Serrano-Pérez, E. Ortí and H. J. Bolink, *J. Am. Chem. Soc.*, 2013, **135**, 18008–18011.

63 M. Y. Wong, G. J. Hedley, G. Xie, L. S. Kölln, I. D. W. Samuel, A. Pertegás, H. J. Bolink and E. Zysman-Colman, *Chem. Mater.*, 2015, **27**, 6535–6542.

64 M. S. Lowry and S. Bernhard, *Chem. Eur. J.*, 2006, **12**, 7970–7977.

65 Y. You and S. Y. Park, *Dalton Trans.*, 2009, **9226**, 1267.

66 R. D. Costa, E. Ortí and H. J. Bolink, *Pure Appl. Chem.*, 2011, 1.

67 C. Ulbricht, B. Beyer, C. Friebe, A. Winter and U. S. Schubert, *Adv. Mater.*, 2009, **21**, 4418–4441.

68 L. Flamigni, A. Barbieri, C. Sabatini, B. Ventura and F. Barigelletti, *Top. Curr. Chem.*, 2007, **281**, 143–203.

69 E. Zysman-Colman, J. D. Slinker, J. B. Parker, G. G. Malharas and S. Bernhard, *Chem. Mater.*, 2008, **20**, 388–396.

70 S. Graber, K. Doyle, M. Neuburger, C. E. Housecroft, E. C. Constable, R. D. Costa, E. Ortí, D. Repetto and H. J. Bolink, *J. Am. Chem. Soc.*, 2008, **130**, 14944–14945.

71 H. J. Bolink, E. Coronado, R. D. Costa, E. Ortí, M. Sessolo, S. Graber, K. Doyle, M. Neuburger, C. E. Housecroft and E. C. Constable, *Adv. Mater.*, 2008, **20**, 3910–3913.

72 R. D. Costa, E. Ortí, H. J. Bolink, S. Graber, C. E. Housecroft and E. C. Constable, *Adv. Funct. Mater.*, 2010, **20**, 1511–1520.

73 A. M. Bünzli, E. C. Constable, C. E. Housecroft, A. Prescimone, J. A. Zampese, G. Longo, L. Gil-Escrig, A. Pertegás, E. Ortí and H. J. Bolink, *Chem. Sci.*, 2015, **6**, 2843–2852.

74 R. D. Costa, E. Ortí, H. J. Bolink, S. Graber, C. E. Housecroft, M. Neuburger, S. Schaffner and E. C. Constable, *Chem. Commun.*, 2009, 2029–2031.

75 H.-C. Su, H.-F. Chen, F.-C. Fang, C.-C. Liu, C.-C. Wu, K.-T. Wong, Y.-H. Liu and S.-M. Peng, *J. Am. Chem. Soc.*, 2008, **130**, 3413–3419.

76 L. He, J. Qiao, L. Duan, G. Dong, D. Zhang, L. Wang and Y. Qiu, *Adv. Funct. Mater.*, 2009, **19**, 2950–2960.

77 H.-C. Su, H.-F. Chen, Y.-C. Shen, C.-T. Liao and K.-T. Wong, *J. Mater. Chem.*, 2011, **21**, 9653–9660.

78 L. He, L. Duan, J. Qiao, R. Wang, P. Wei, L. Wang and Y. Qiu, *Adv. Funct. Mater.*, 2008, **18**, 2123–2131.

79 F. De Angelis, S. Fantacci, N. Evans, C. Klein, S. M. Zakeeruddin, J.-E. Moser, K. Kalyanasundaram, H. J. Bolink, M. Grätzel and M. K. Nazeeruddin, *Inorg. Chem.*, 2007, **46**, 5989–6001.

80 E. Baranoff, H. J. Bolink, E. C. Constable, M. Delgado, D. Häussinger, C. E. Housecroft, M. K. Nazeeruddin, M. Neuburger, E. Ortí, G. E. Schneider, D. Tordera, R. M. Walliser and J. A. Zampese, *Dalton Trans.*, 2013, **42**, 1073–1087.

81 S. Schmidbauer, A. Hohenleutner and B. König, *Adv. Mater.*, 2013, **25**, 2114–2129.

82 D. Tordera, J. J. Serrano-Pérez, A. Pertegás, E. Ortí, H. J. Bolink, E. Baranoff, M. K. Nazeeruddin and J. Frey, *Chem. Mater.*, 2013, **25**, 3391–3397.

83 C. Hansch, A. Leo and R. W. Taft, *Chem. Rev.*, 1991, **91**, 165–195.

84 D. H. McDaniel and H. C. Brown, *J. Org. Chem.*, 1958, **23**, 420–427.

85 M. Tavasli, S. Bettington, I. F. Perepichka, A. S. Batsanov, M. R. Bryce, C. Rothe and A. P. Monkman, *Eur. J. Inorg. Chem.*, 2007, 4808–4814.

86 G. Zhou, C.-L. Ho, W.-Y. Wong, Q. Wang, D. Ma, L. Wang, Z. Lin, T. B. Marder and A. Beeby, *Adv. Funct. Mater.*, 2008, **18**, 499–511.

87 G. Zhou, X. Yang, W.-Y. Wong, Q. Wang, S. Suo, D. Ma, J. Feng and L. Wang, *ChemPhysChem*, 2011, **12**, 2836–2843.

88 X. Xu, X. Yang, J. Dang, G. Zhou, Y. Wu, H. Li and W.-Y. Wong, *Chem. Commun.*, 2014, **50**, 2473–2476.

89 J. Zhao, Y. Yu, X. Yang, X. Yan, H. Zhang, X. Xu, G. Zhou, Z. Wu, Y. Ren and W.-Y. Wong, *ACS Appl. Mater. Interfaces*, 2015, **7**, 24703–24714.

90 R. Ragni, E. Orselli, G. S. Kottas, O. H. Omar, F. Babudri, A. Pedone, F. Naso, G. M. Farinola and L. De Cola, *Chem. Eur. J.*, 2009, **15**, 136–148.

91 C. Fan, Y. Li, C. Yang, H. Wu, J. Qin and Y. Cao, *Chem. Mater.*, 2012, **24**, 4581–4587.

92 Y. Hisamatsu and S. Aoki, *Eur. J. Inorg. Chem.*, 2011, 5360–5369.

93 D. Tordera, A. M. Bünzli, A. Pertegás, J. M. Junquera-Hernández, E. C. Constable, J. a Zampese, C. E. Housecroft, E. Ortí and H. J. Bolink, *Chem. Eur. J.*, 2013, **19**, 8597–609.

94 G. E. Schneider, H. J. Bolink, E. C. Constable, C. D. Ertl, C. E. Housecroft, A. Pertegás, J. A. Zampese, A. Kanitz, F. Kessler and S. B. Meier, *Dalton Trans.*, 2014, **43**, 1961–1964.

95 E. C. Constable, C. D. Ertl, C. E. Housecroft and J. A. Zampese, *Dalton Trans.*, 2014, **43**, 5343–5356.

96 C. Liu, Q. Ni, P. Hu and J. Qiu, *Org. Biomol. Chem.*, 2011, **9**, 1054–60.

97 Y. Harrak, G. Casula, J. Basset, G. Rosell, S. Plescia, D. Raffa, M. G. Cusimano, R. Pouplana and M. D. Pujol, *J. Med. Chem.*, 2010, **53**, 6560–6571.

98 S. Clavier, O. Rist, S. Hansen, L.-O. Gerlach, T. Högberg and J. Bergman, *Org. Biomol. Chem.*, 2003, **1**, 4248–53.

99 A. B. Charette, C. Berthelette and D. St-Martin, *Tetrahedron Lett.*, 2001, **42**, 5149–5153.

100 F. O. Garces, K. A. King and R. J. Watts, *Inorg. Chem.*, 1988, **27**, 3464–3471.

101 S. Sprouse, K. A. King, P. J. Spellane and R. J. Watts, *J. Am. Chem. Soc.*, 1984, **106**, 6647–6653.

102 E. Baranoff, B. F. E. Curchod, J. Frey, R. Scopelliti, F. Kessler, I. Tavernelli, U. Rothlisberger, M. Grätzel and M. K. Nazeeruddin, *Inorg. Chem.*, 2012, **51**, 215–224.

103 R. D. Costa, E. Ortí, D. Tordera, A. Pertegás, H. J. Bolink, S. Graber, C. E. Housecroft, L. Sachno, M. Neuburger and E. C. Constable, *Adv. Energy Mater.*, 2011, **1**, 282–290.

104 F. Neve, A. Crispini, S. Campagna and S. Serroni, *Inorg. Chem.*, 1999, **38**, 2250–2258.

105 F. A. M. Rudolph, A. L. Fuller, A. M. Z. Slawin, M. Bühl, R. A. Aitken and J. D. Woollins, *J. Chem. Crystallogr.*, 2010, **40**, 253–265.

106 C. Glidewell, W. T. A. Harrison, J. N. Low, J. G. Sime and J. L. Wardell, *Acta Crystallogr. Sect. B*, 2001, **57**, 190–200.

107 S. Evariste, M. Sandroni, T. W. Rees, C. Roldán-Carmona, L. Gil-Escrig, H. J. Bolink, E. Baranoff and E. Zysman-Colman, *J. Mater. Chem. C*, 2014, **2**, 5793.

108 H. J. Bolink, E. Coronado, R. D. Costa, N. Lardiés and E. Ortí, *Inorg. Chem.*, 2008, **47**, 9149–9151.

109 H.-C. Su, F.-C. Fang, T.-Y. Hwu, H.-H. Hsieh, H.-F. Chen, G.-H. Lee, S.-M. Peng, K.-T. Wong and C.-C. Wu, *Adv. Funct. Mater.*, 2007, **17**, 1019–1027.

110 M. S. Lowry, J. I. Goldsmith, J. D. Slinker, R. Rohl, R. A. Pascal, G. G. Malliaras and S. Bernhard, *Chem. Mater.*, 2005, **17**, 5712–5719.

111 M. Marigo, N. Marsich and E. Farnetti, *J. Mol. Catal. A Chem.*, 2002, **187**, 169–177.

112 N. M. Shavaleev, F. Monti, R. D. Costa, R. Scopelliti, H. J. Bolink, E. Ortí, G. Accorsi, N. Armaroli, E. Baranoff, M. Grätzel and M. K. Nazeeruddin, *Inorg. Chem.*, 2012, **51**, 2263–2271.

113 N. M. Shavaleev, G. Xie, S. Varghese, D. B. Cordes, A. M. Z. Slawin, C. Momblona, E. Ortí, H. J. Bolink, I. D. W. Samuel and E. Zysman-Colman, *Inorg. Chem.*, 2015, **54**, 5907–5914.

114 D. L. Davies, M. P. Lowe, K. S. Ryder, K. Singh and S. Singh, *Dalton Trans.*, 2011, **40**, 1028–1030.

115 J. Nishida, H. Echizen, T. Iwata and Y. Yamashita, *Chem. Lett.*, 2005, **34**, 1378–1379.

116 V. V. Grushin, N. Herron, D. D. LeCloux, W. J. Marshall, V. A. Petrov and Y. Wang, *Chem. Commun.*, 2001, 1494–1495.

117 T.-H. Kwon, H. S. Cho, M. K. Kim, J.-W. Kim, J.-J. Kim, K. H. Lee, S. J. Park, I.-S. Shin, H. Kim, D. M. Shin, Y. K. Chung and J.-I. Hong, *Organometallics*, 2005, **24**, 1578–1585.

118 Q.-L. Xu, C.-C. Wang, T.-Y. Li, M.-Y. Teng, S. Zhang, Y.-M. Jing, X. Yang, W.-N. Li, C. Lin, Y.-X. Zheng, J.-L. Zuo and X.-Z. You, *Inorg. Chem.*, 2013, **52**, 4916–4925.

119 G. Sarada, J. Yoon, W. Cho, M. Cho, D. W. Cho, S. O. Kang, Y. Nam, J. Y. Lee and S.-H. Jin, *J. Mater. Chem. C*, 2016, **4**, 113–120.

120 B. J. Coe, M. Helliwell, J. Raftery, S. Sánchez, M. K. Peers and N. S. Scrutton, *Dalton Trans.*, 2015, **44**, 20392–20405.

121 H. A. Bronstein, C. E. Finlayson, K. R. Kirov, R. H. Friend and C. K. Williams, *Organometallics*, 2008, **27**, 2980–2989.

122 N. Ishida, T. Moriya, T. Goya and M. Murakami, *J. Org. Chem.*, 2010, **75**, 8709–8712.

123 L. Niu, H. Yang, D. Yang and H. Fu, *Adv. Synth. Catal.*, 2012, **354**, 2211–2217.

124 C. Glidewell, W. T. A. Harrison, J. N. Low, J. G. Sime and J. L. Wardell, *Acta Crystallogr. Sect. B Struct. Sci.*, 2001, **57**, 190–200.

125 N. M. Shavaleev, R. Scopelliti, M. Grätzel, M. K. Nazeeruddin, A. Pertegás, C. Roldán-Carmona, D. Tordera and H. J. Bolink, *J. Mater. Chem. C*, 2013, **1**, 2241–2248.

126 C. D. Ertl, J. Cerdá, J. M. Junquera-Hernández, A. Pertegás, H. J. Bolink, E. C. Constable, M. Neuburger, E. Ortí and C. E. Housecroft, *RSC Adv.*, 2015, **5**, 42815–42827.

127 E. C. Constable, C. D. Ertl, C. E. Housecroft and J. A. Zampese, *Dalton Trans.*, 2014, **43**, 5343–5356.

128 M. Marigo, N. Marsich and E. Farnetti, *J. Mol. Catal. A Chem.*, 2002, **187**, 169–177.

129 C. O'Brien, M. Y. Wong, D. B. Cordes, A. M. Z. Slawin and E. Zysman-Colman, *Organometallics*, 2015, **34**, 13–22.

130 J. Xu, G. Cheng, D. Su, Y. Liu, X. Wang and Y. Hu, *Chem. Eur. J.*, 2009, **15**, 13105–13110.

131 M. Mydlak, C. Bizzarri, D. Hartmann, W. Sarfert, G. Schmid and L. De Cola, *Adv. Funct. Mater.*, 2010, **20**, 1812–1820.

132 N. M. Shavaleev, R. Scopelliti, E. Baranoff, M. Grätzel and M. K. Nazeeruddin, *Inorg. Chim. Acta*, 2012, **383**, 316–319.

133 A. B. Tamayo, S. Garon, T. Sajoto, P. I. Djurovich, I. M. Tsyba, R. Bau and M. E. Thompson, *Inorg. Chem.*, 2005, **44**, 8723–8732.

134 S. Ladouceur, K. N. Swanick, S. Gallagher-Duval, Z. Ding and E. Zysman-Colman, *Eur. J. Inorg. Chem.*, 2013, 5329–5343.

135 M. K. Nazeeruddin, R. T. Wegh, Z. Zhou, C. Klein, Q. Wang, F. De Angelis, S. Fantacci and M. Grätzel, *Inorg. Chem.*, 2006, **45**, 9245–9250.

136 C. S. Chin, M.-S. Eum, S. Y. Kim, C. Kim and S. K. Kang, *Eur. J. Inorg. Chem.*, 2007, 372–375.

137 B. Chen, Y. Li, W. Yang, W. Luo and H. Wu, *Org. Electron.*, 2011, **12**, 766–773.

138 C. D. Sunesh, G. Mathai and Y. Choe, *Org. Electron.*, 2014, **15**, 667–674.

139 F. Zhang, D. Ma, L. Duan, J. Qiao, G. Dong, L. Wang and Y. Qiu, *Inorg. Chem.*, 2014, **53**, 6596–6606.

140 S. B. Meier, W. Sarfert, J. M. Junquera-Hernández, M. Delgado, D. Tordera, E. Ortí, H. J. Bolink, F. Kessler, R. Scopelliti, M. Grätzel, M. K. Nazeeruddin and E. Baranoff, *J. Mater. Chem. C*, 2013, **1**, 58–68.

141 T. Hu, L. Duan, J. Qiao, L. He, D. Zhang, R. Wang, L. Wang and Y. Qiu, *Org. Electron.*, 2012, **13**, 1948–1955.

142 F. Monti, A. Baschieri, I. Gualandi, J. J. Serrano-Pérez, J. M. Junquera-Hernández, D. Tonelli, A. Mazzanti, S. Muzzioli, S. Stagni, C. Roldán-Carmona, A. Pertegás, H. J. Bolink, E. Ortí, L. Sambri and N. Armaroli, *Inorg. Chem.*, 2014, **53**, 7709–7721.

143 L. He, L. Duan, J. Qiao, D. Zhang, G. Dong, L. Wang and Y. Qiu, *Org. Electron.*, 2009, **10**, 152–157.

144 L. He, L. Duan, J. Qiao, D. Zhang, L. Wang and Y. Qiu, *Appl. Phys. A*, 2010, **100**, 1035–1040.

145 L. He, L. Duan, J. Qiao, D. Zhang, L. Wang and Y. Qiu, *Chem. Commun.*, 2011, **47**, 6467–6469.

146 L. He, L. Duan, J. Qiao, D. Zhang, L. Wang and Y. Qiu, *Org. Electron.*, 2010, **11**, 1185–1191.

147 T. Hu, L. Duan, J. Qiao, L. He, D. Zhang, L. Wang and Y. Qiu, *Synth. Met.*, 2013, **163**, 33–37.

148 N. M. Shavaleev, R. Scopelliti, M. Grätzel and M. K. Nazeeruddin, *Inorg. Chim. Acta*, 2013, **404**, 210–214.

149 H. Zhang, Q. Cai and D. Ma, *J. Org. Chem.*, 2005, **70**, 5164–5173.

150 Y.-C. Teo, F.-F. Yong and S. Sim, *Tetrahedron*, 2013, **69**, 7279–7284.

151 H.-Y. Liu, Z.-T. Yu, Y.-J. Yuan, T. Yu and Z.-G. Zou, *Tetrahedron*, 2010, **66**, 9141–9144.

152 A. Baschieri, S. Muzzioli, V. Fiorini, E. Matteucci, M. Massi, L. Sambri and S. Stagni, *Organometallics*, 2014, **33**, 6154–6164.

153 F. Monti, M. G. I. La Placa, N. Armaroli, R. Scopelliti, M. Grätzel, M. K. Nazeeruddin and F. Kessler, *Inorg. Chem.*, 2015, **54**, 3031–3042.

154 P. Pla, J. M. Junquera-Hernández, H. J. Bolink and E. Ortí, *Dalton Trans.*, 2015.

155 J. Wang, S. Tang, A. Sandström and L. Edman, *ACS Appl. Mater. Interfaces*, 2015, **7**, 2784–2789.

156 W.-L. Jia, Y.-F. Hu, J. Gao and S. Wang, *Dalton Trans.*, 2006, 1721–1728.

157 A. Breivogel, M. Park, D. Lee, S. Klassen, A. Kühnle, C. Lee, K. Char and K. Heinze, *Eur. J. Inorg. Chem.*, 2014, 288–295.

158 P. Dreyse, B. Loeb, M. Soto-Arriaza, D. Tordera, E. Ortí, J. J. Serrano-Pérez and H. J. Bolink, *Dalton Trans.*, 2013, **42**, 15502–15513.

159 H. J. Bolink, L. Cappelli, E. Coronado and P. Gaviña, *Inorg. Chem.*, 2005, **44**, 5966–5968.

160 H. J. Bolink, E. Coronado, R. D. Costa, P. Gaviña, E. Ortí and S. Tatay, *Inorg. Chem.*, 2009, **48**, 3907–3909.

161 J. L. Rodríguez-Redondo, R. D. Costa, E. Ortí, A. Sastre-Santos, H. J. Bolink and F. Fernández-Lázaro, *Dalton Trans.*, 2009, 9787–9793.

162 H.-F. Chen, K.-T. Wong, Y.-H. Liu, Y. Wang, Y.-M. Cheng, M.-W. Chung, P.-T. Chou and H.-C. Su, *J. Mater. Chem.*, 2011, **21**, 768–774.

163 E. C. Constable, C. E. Housecroft, G. E. Schneider, J. A. Zampese, H. J. Bolink, A. Pertegás and C. Roldan-Carmona, *Dalton Trans.*, 2014, **43**, 4653–4667.

164 J. Zhang, L. Zhou, H. A. Al-Attar, K. Shao, L. Wang, D. Zhu, Z. Su, M. R. Bryce and A. P. Monkman, *Adv. Funct. Mater.*, 2013, **23**, 4667–4677.

165 K. Hasan, A. K. Bansal, I. D. W. Samuel, C. Roldán-Carmona, H. J. Bolink and E. Zysman-Colman, *Sci. Rep.*, 2015, **5**, 12325.

166 W.-J. Xu, S.-J. Liu, T.-C. Ma, Q. Zhao, A. Pertegás, D. Tordera, H. J. Bolink, S.-H. Ye, X.-M. Liu, S. Sun and W. Huang, *J. Mater. Chem.*, 2011, **21**, 13999–14007.

167 R. D. Costa, F. J. Céspedes-Guirao, H. J. Bolink, Á. Sastre-Santos, E. Ortí and J. Gierschner, *J. Phys. Chem. C*, 2009, **113**, 19292–19297.

168 R. D. Costa, F. J. Céspedes-Guirao, E. Ortí, H. J. Bolink, J. Gierschner, F. Fernández-Lázaro and A. Sastre-Santos, *Chem. Commun.*, 2009, 3886–3888.

169 C.-T. Liao, H.-F. Chen, H.-C. Su and K.-T. Wong, *Phys. Chem. Chem. Phys.*, 2012, **14**, 1262–1269.

170 Y.-J. Yuan, Z.-T. Yu, X.-Y. Chen, J.-Y. Zhang and Z.-G. Zou, *Chem. Eur. J.*, 2011, **17**, 12891–12895.

171 K. K.-W. Lo, C.-K. Li and J. S.-Y. Lau, *Organometallics*, 2005, **24**, 4594–4601.

172 K. K.-W. Lo, S.-K. Leung and C.-Y. Pan, *Inorg. Chim. Acta*, 2012, **380**, 343–349.

173 C. K. Choudhary, R. K. Choudhary and L. K. Mishra, *J. Indian Chem. Soc.*, 2002, **79**, 761–762.

174 C. Richardson, F. R. Keene and P. J. Steel, *Aust. J. Chem.*, 2008, **61**, 183–188.

175 F. Gärtner, D. Cozzula, S. Losse, A. Boddien, G. Anilkumar, H. Junge, T. Schulz, N. Marquet, A. Spannenberg, S. Gladiali and M. Beller, *Chem. Eur. J.*, 2011, **17**, 6998–7006.

176 C. Rai and J. B. Braunwarth, *J. Org. Chem.*, 1961, **26**, 3434–3436.

177 L. J. Carlson, J. Welby, K. A. Zebrowski, M. M. Wilk, R. Giroux, N. Ciancio, J. M. Tanski, A. Bradley and L. A. Tyler, *Inorg. Chim. Acta*, 2011, **365**, 159–166.

178 H.-Q. Do, R. M. Kashif Khan and O. Daugulis, *J. Am. Chem. Soc.*, 2008, **130**, 15185–15192.

179 L. Vandromme, H.-U. Reißig, S. Gröper and J. P. Rabe, *Eur. J. Org. Chem.*, 2008, **2008**, 2049–2055.

180 F.-F. Zhuo, W.-W. Xie, Y.-X. Yang, L. Zhang, P. Wang, R. Yuan and C.-S. Da, *J. Org. Chem.*, 2013, **78**, 3243–3249.

181 F. Brunner, *Synthesis and Investigation of Cyclometalated Ruthenium Complexes with Various Anchoring Groups for use in p-type Dye-Sensitized Solar Cells*, Master Thesis, University of Basel, 2015.

182 A. A. Rachford, R. Ziessel, T. Bura, P. Retailleau and F. N. Castellano, *Inorg. Chem.*, 2010, **49**, 3730–3736.

183 M. Lepeltier, F. Dumur, J. Marrot, E. Contal, D. Bertin, D. Gigmes and C. R. Mayer, *Dalton Trans.*, 2013, **42**, 4479–86.

184 L. Donato, P. Abel and E. Zysman-Colman, *Dalton Trans.*, 2013, **42**, 8402–8412.

185 F. Riblet, G. Novitchi, R. Scopelliti, L. Helm, A. Gulea and A. E. Merbach, *Inorg. Chem.*, 2010, **49**, 4194–4211.

186 J. C. Bailar, *J. Inorg. Nucl. Chem.*, 1958, **8**, 165–175.

187 A. Rodger and B. F. G. Johnson, *Inorg. Chem.*, 1988, **27**, 3062–3064.

188 A. L. Spek, *Acta Crystallogr. Sect. D*, 2009, **65**, 148–155.

189 Q. Zhao, S. Liu, M. Shi, C. Wang, M. Yu, L. Li, F. Li, T. Yi and C. Huang, *Inorg. Chem.*, 2006, **45**, 6152–6160.

190 S.-J. Liu, Q. Zhao, Q.-L. Fan and W. Huang, *Eur. J. Inorg. Chem.*, 2008, 2177–2185.

191 Z. Li, P. Cui, C. Wang, S. Kilina and W. Sun, *J. Phys. Chem. C*, 2014, **118**, 28764–28775.

192 Y. Wu, H. Jing, Z. Dong, Q. Zhao, H. Wu and F. Li, *Inorg. Chem.*, 2011, **50**, 7412–7420.

193 J. H. Vella, A. Parthasarathy and K. S. Schanze, *J. Phys. Chem. A*, 2013, **117**, 7818–7822.

194 F. Gärtner, S. Denurra, S. Losse, A. Neubauer, A. Boddien, A. Gopinathan, A. Spannenberg, H. Junge, S. Lochbrunner, M. Blug, S. Hoch, J. Busse, S. Gladiali and M. Beller, *Chem. Eur. J.*, 2012, **18**, 3220–3225.

195 E. C. Constable, M. Neuburger, P. Rösel, G. E. Schneider, J. A. Zampese, C. E. Housecroft, F. Monti, N. Armaroli, R. D. Costa and E. Ortí, *Inorg. Chem.*, 2013, **52**, 885–897.

196 Y. Hong, J. W. Y. Lam and B. Z. Tang, *Chem. Soc. Rev.*, 2011, **40**, 5361–5388.

197 Q. Zhao, L. Li, F. Li, M. Yu, Z. Liu, T. Yi and C. Huang, *Chem. Commun.*, 2008, 685–687.

198 Y. You, H. S. Huh, K. S. Kim, S. W. Lee, D. Kim and S. Y. Park, *Chem. Commun.*, 2008, 3998–4000.

199 K. Huang, H. Wu, M. Shi, F. Li, T. Yi and C. Huang, *Chem. Commun.*, 2009, **2**, 1243–1245.

200 A. J. Howarth, R. Patia, D. L. Davies, F. Lelj, M. O. Wolf and K. Singh, *Eur. J. Inorg. Chem.*, 2014, 3657–3664.

201 L. Vandromme, H.-U. Reißig, S. Gröper and J. P. Rabe, *Eur. J. Org. Chem.*, 2008, 2049–2055.

202 M. Zhu, K. Fujita and R. Yamaguchi, *Chem. Commun.*, 2011, **47**, 12876–12878.

203 M. Peters and R. Breinbauer, *Tetrahedron Lett.*, 2010, **51**, 6622–6625.

204 S. O. Ojwach, G. Westman and J. Darkwa, *Polyhedron*, 2007, **26**, 5544–5552.

205 M. Wu, X. Hu, J. Liu, Y. Liao and G.-J. Deng, *Org. Lett.*, 2012, **14**, 2722–2725.

206 S. M. Khake, V. Soni, R. G. Gonnade and B. Punji, *Dalton Trans.*, 2014, **43**, 16084–16096.

207 D. Toummini, A. Tlili, J. Bergès, F. Ouazzani and M. Taillefer, *Chem. Eur. J.*, 2014, **20**, 14619–14623.

208 A. Singh, K. Teegardin, M. Kelly, K. S. Prasad, S. Krishnan and J. D. Weaver, *J. Organomet. Chem.*, 2015, **776**, 51–59.

209 S. Mandal, R. Das, P. Gupta and B. Mukhopadhyay, *Tetrahedron Lett.*, 2012, **53**, 3915–3918.

210 A. Maity, J.-S. Choi, T. S. Teets, N. Deligonul, A. J. Berdis and T. G. Gray, *Chem. Eur. J.*, 2013, **19**, 15924–15932.

211 H.-W. Liu, K. Y. Zhang, W. H.-T. Law and K. K.-W. Lo, *Organometallics*, 2010, **29**, 3474–3476.

212 W. H.-T. Law, L. C.-C. Lee, M.-W. Louie, H.-W. Liu, T. W.-H. Ang and K. K.-W. Lo, *Inorg. Chem.*, 2013, **52**, 13029–13041.

213 T. Nishioka, T. Shibata and I. Kinoshita, *Organometallics*, 2007, **26**, 1126–1128.

214 T. Shibata, H. Hashimoto, I. Kinoshita, S. Yano and T. Nishioka, *Dalton Trans.*, 2011, **40**, 4826–4829.

215 O. Pàmies, M. Diéguez, G. Net, A. Ruiz and C. Claver, *J. Chem. Soc. Dalt. Trans.*, 1999, 3439–3444.

216 M.-J. Li, P. Jiao, M. Lin, W. He, G.-N. Chen and X. Chen, *Analyst*, 2011, **136**, 205–210.

217 E. C. Constable, R. Frantz, C. E. Housecroft, J. Lacour and A. Mahmood, *Inorg. Chem.*, 2004, **43**, 4817–4819.

218 E. C. Constable, C. E. Housecroft and A. Mahmood, *Carbohydr. Res.*, 2008, **343**, 2567–2575.

219 J. S. Ward, J. M. Lynam, J. W. B. Moir, D. E. Sanin, A. P. Mountford and I. J. S. Fairlamb, *Dalton Trans.*, 2012, **41**, 10514–10517.

220 S. Mundwiler, *Metal complexes of biomolecules: Supramolecular chemistry of 2,2':6',2''-terpyridine bound peptides, carbohydrates and phospholipids*, PhD Thesis, University of Basel, 2000.